

Numerical Modelling of Organic Contaminant Reaction and Transport in Bed-Sediments

A THESIS PRESENTED BY

Jason Go

To

THE DEPARTMENT OF CIVIL, ENVIRONMENTAL AND GEOMATIC ENGINEERING
IN PARTIAL FULFILMENT OF THE REQUIREMENTS
FOR THE DEGREE OF

DOCTOR OF PHILOSOPHY IN ENVIRONMENTAL ENGINEERING

UNIVERSITY COLLEGE LONDON

2008

UMI Number: U591485

All rights reserved

INFORMATION TO ALL USERS

The quality of this reproduction is dependent upon the quality of the copy submitted.

In the unlikely event that the author did not send a complete manuscript and there are missing pages, these will be noted. Also, if material had to be removed, a note will indicate the deletion.



UMI U591485

Published by ProQuest LLC 2013. Copyright in the Dissertation held by the Author.
Microform Edition © ProQuest LLC.

All rights reserved. This work is protected against
unauthorized copying under Title 17, United States Code.



ProQuest LLC
789 East Eisenhower Parkway
P.O. Box 1346
Ann Arbor, MI 48106-1346

I, **Jason Go**, confirm that the work presented in this thesis is my own. Where information has been derived from other sources, I confirm that this has been indicated in the thesis.

ABSTRACT

Reactive transport modelling of contaminants in the environment is being increasingly relied upon for a wide range of tasks associated with risk-based decision-making, such as interpretation of historical contamination data, optimisation of attenuation and remediation methods, and monitoring of changes resulting from an implemented remediation scheme. However, in the area of contaminant fate and behaviour in bed-sediments, reactive transport modelling has until now stopped short of integration of various mechanistic models to a single modelling environment that would allow a cohesive understanding and prediction of contaminant profiles. This study has developed CoReTranS, a predictive modelling environment that simulates one-dimensional organic contaminant reaction and transport in bed-sediments, using an object-oriented modelling approach. The CoReTranS model has been verified and benchmarked by comparing numerical results of simplified problems with their analytical solutions. The following simulations were undertaken to validate the CoReTranS model:

1. Simulation of the dataset from a diffusion-controlled laboratory experiment for the transport and distribution of selected trace level organic contaminants in a riverine environment gave new numerical results to improve on predicted modelling approach.
2. Simulation of the dataset from a study of marsh sediments contaminated with petroleum-derived hydrocarbons from Wild Harbour, West Falmouth, MA and Kitimat Arm, Douglas Channel, British Columbia resulted in an excellent agreement between the numerical results of the transport model in CoReTranS and the numerical results and data of the original study.

The CoReTranS model was also used to interpret results from the following field studies in order to explain key processes that controlled the fate and transport of PAHs and PCBs in bed-sediments:

1. Simulation of the dataset from Kitimat fjord system near Kitimat, British Columbia, wherein PAHs in sediments were purported to be derived from atmospheric particle emissions, wastewater discharges and accidental spillages from a nearby aluminium smelter provided a better understanding of the post-depositional reactive transport of PAHs in the fjord system.
2. Simulation of the dataset from a study on the natural recovery of PCB-contaminated sediments at the Sangamo-Weston/Twelvemile Creek/Lake Hartwell Superfund Site in the US showed that it would take nearly 30 years to achieve the 1 mg/kg clean-up goal for total PCB in the chosen transect sites, and 20 years more than the predicted time in the original study.

The CoReTrans model was also used to predict the effect of capping contaminated sediments as a remedial strategy. Results from the various simulation scenarios using the CoReTrans model showed that sediment capping as a remedial strategy in managing contaminated sediments can effectively reduce contaminant flux to the overlying water through interaction with the sediment cap matrix and by increasing the dissolved contaminants' transport lengths (i.e., cap thickness).

Comparing the results obtained from laboratory experiments or field monitoring studies of bed-sediment systems with different accumulation, degradation and release mechanisms, with the results from the CoReTrans model was critical in identifying the key processes that drive the fate and transport of organic contaminants in bed-sediments. The information derived from the use of the CoReTrans model highlighted recommendations to guide future experiments, field monitoring and model extension which include other relevant transport mechanisms such as colloid-enhanced transport, rate-limited reaction processes and the effect of sediment consolidation to contaminant fate and transport. This information will further enable practical application of such information by engineers to site-specific risk assessment and remediation, as well as continued research and technology development.

ACKNOWLEDGEMENTS

This work was supported by funds from the Dorothy Hodgkin Postgraduate Award scheme and Natural Environment Research Council, UK

The past three years or so have been such a remarkable experience for me. I am tremendously grateful to Julia Stegemann for providing me with the opportunity to investigate reactive transport phenomena in bed-sediments and for the excellent supervision I have received. I would also like to thank Graham Roberts for all the support and interesting discussion that helped shape this manuscript. And to Ian Allan who acted as my external supervisor, thanks for all the input you gave into making this thesis what it is now.

The validation aspect of this work would not be possible without the datasets that were kindly shared to me by colleagues in the scientific community. To Helen White for the PAH dataset, to Victor Magar for the PCB dataset, and to Ian Allan for the lindane dataset, I owe my deepest gratitude.

I would also like to thank Danny Reible and his research staff, especially David Lampert for hosting me during my two-month fellowship at the University of Texas at Austin and for the collaborative work on sediment capping.

Special thanks are owed to all the people that kept me sane and grounded while doing this work. To Tristan, David, Aiduan, Ricky, Crystal, Julia, Sarah and the rest of my UCL mates, thanks for all the drinks, nuts, crisps and stories shared at pubs. To Joana, Moniq, Toto, Bong, Richard, Jetty and the rest of my fellow ex-pats, thanks for always reminding me a glimpse of home – *salamat!*

This work would not be possible without the love and support of my family.

To A.S.M Dillon, *my baby...*

Table of Contents

Chapter One	Introduction	1
1.1	Contaminated sediments	1
1.2	Contaminant fate and behaviour in sediments	3
1.3	Numerical modelling of organic contaminant reaction and transport in bed-sediments using CoReTranS	5
Chapter Two	Organic contaminant fate and transport processes in bed-sediments – a review	9
2.1	Introduction	9
2.2	Contaminant of concern	10
2.2.2	Polycyclic aromatic hydrocarbons	10
2.2.3	Polychlorinated organics	11
2.2.4	Pharmaceutical compounds	11
2.3	Analysis of fate and transport processes in bed-sediments	12
2.3.1	Molecular diffusion	12
2.3.2	Advection	16
2.3.3	Bioturbation	18
2.3.3.1	<i>Overview</i>	19
2.3.3.2	<i>Biodiffusion models</i>	21
2.3.3.3	<i>Non-local exchange models</i>	25
2.3.4	Sorption	28
2.3.4.1	<i>Overview</i>	28
2.3.4.2	<i>Mechanisms of slow sorption</i>	34
2.3.4.3	<i>Sorption to colloids</i>	38
2.3.5	Degradation	39
2.3.5.1	<i>Overview</i>	39
2.3.5.2	<i>Sorption/desorption-limited contaminant bioavailability</i>	41
2.3.5.3	<i>Biofilms</i>	42
2.3.6	Sediment deposition and resuspension	44
2.4	Modelling approaches	45
2.4.1	Analytical approach	45
2.4.2	Numerical approach	47
2.5	Reactive transport modelling environment	48
2.6	Challenges in modelling reactive transport of contaminants in bed-sediments	50

Chapter Three	CoReTranS: an object-oriented modelling environment for organic contaminant reactive transport in bed-sediments	52
3.1	Introduction	52
3.2	CoReTranS modelling environment	54
3.2.1	Object-oriented approach	54
3.2.2	Java performance	56
	Development of the three tier structure for the CoReTranS	
3.2.3	modelling environment	58
3.2.3.1	<i>CoReTranS graphical user interface</i>	59
3.2.3.2	<i>CoReTranS problem domain</i>	65
3.2.3.3	<i>CoReTranS database</i>	71
3.3	CoReTranS model: application to a real dataset	72
Chapter Four	CoReTranS model verification – Reactive transport models and analytical solutions	75
4.1	Introduction	75
4.2	Assessment of model refinement	76
4.2.1	Overview	76
4.2.2	Linear correlation coefficient	77
4.2.3	Mean of residual errors	77
4.2.4	Root mean of squared residual errors	78
4.2.5	Normal probability plots of residual errors	78
4.3	CoReTranS predictions vs. analytical solutions	79
4.3.1	Overview	79
4.3.2	Model contaminant	80
4.3.3	Model parameters	80
4.3.4	Representative elementary volume	82
4.3.5	Diffusion model	82
4.3.5.1	<i>Model formulation and approach</i>	82
4.3.5.2	<i>Effect of contaminant sorption on the diffusion model</i>	86
4.3.5.3	<i>Effect of a constant flux boundary condition on the diffusion model</i>	86
4.3.5.4	<i>Effect of contaminant degradation on the diffusion model</i>	88
4.3.6	Diffusion-advection model	90
4.3.6.1	<i>Model formulation and approach</i>	90
4.3.6.2	<i>Effect of varying the advective velocity</i>	93
4.3.6.3	<i>Effect of contaminant degradation on the diffusion-advection model</i>	94
4.4	Conclusions of model verification	97
Chapter Five	CoReTranS model validation – Interpretation of laboratory experimental study results using the CoReTranS model	99
5.1	Introduction	99
5.2	CoReTranS simulation	100
5.2.1	Background of the study	100

5.2.1	Model contaminant	101
5.2.3	Model formulation and approach	102
5.2.3.1	<i>Scope</i>	102
5.2.3.2	<i>Conceptual model</i>	102
5.2.3.3	<i>Reactive transport model formulation</i>	103
5.4	Model validation	105
5.4.1	Diffusion model	105
5.4.1.1	<i>Approach</i>	105
5.4.1.2	<i>Results</i>	106
5.4.1.3	<i>Discussion</i>	106
5.4.2	Diffusion-sorption model	107
5.4.2.1	<i>Approach</i>	107
5.4.2.2	<i>Results</i>	108
5.4.2.3	<i>Discussion</i>	109
5.4.3	Diffusion-sorption-degradation model	112
5.4.3.1	<i>Approach</i>	112
5.4.3.2	<i>Results</i>	112
5.4.3.3	<i>Discussion</i>	113
5.4.4	Diffusion-sorption-bioturbation model	114
5.4.4.1	<i>Approach</i>	114
5.4.4.2	<i>Results</i>	114
5.4.4.3	<i>Discussion</i>	115
	Conclusions of model validation using laboratory experimental study results and recommendations for future works	116
5.5		
Chapter Six CoReTranS model validation – Interpretation of field study results from PAH-contaminated sites using the CoReTranS model		118
6.1	Introduction	118
6.2	PAHs in West Harbour, West Falmouth, MA	119
6.2.1	Background of the study	119
6.2.2	Model contaminant	120
6.2.3	Model formulation and approach	121
6.2.3.1	<i>Scope</i>	121
6.2.3.2	<i>Conceptual model</i>	121
6.2.3.3	<i>Reactive transport model formulation</i>	122
6.2.4	Model validation	124
6.2.4.1	<i>Approach</i>	124
6.2.4.2	<i>Results</i>	124
6.2.4.3	<i>Discussion</i>	127
6.3	PAHs in Kitimat Arm, Douglas Harbour, British Columbia	128
6.3.1	Background of the study	128
6.3.2	Model contaminant	129
6.3.3	Model formulation and approach	131
6.3.3.1	<i>Scope</i>	131
6.3.3.2	<i>Conceptual model</i>	131

6.3.3.3	<i>Reactive transport model formulation</i>	132
6.3.4	Model validation	134
6.3.4.1	<i>Approach</i>	134
6.3.4.2	<i>Results</i>	136
6.3.4.3	<i>Discussion</i>	136
	Conclusions of model validation using field study results and	
6.4	recommendations for further work	139

Chapter Seven Predicting PCB distribution in Lake Hartwell sediments and the effects of monitored natural recovery using the CoReTrans model 141

7.1	Introduction	141
7.2	PCBs in Lake Hartwell, Pickens County, SC	142
7.2.1	Background of the study	142
7.2.2	Model contaminant	144
7.2.3	Model formulation and approach	145
7.2.3.1	<i>Scope</i>	145
7.2.3.2	<i>Conceptual model</i>	145
7.2.3.3	<i>Reactive transport model formulation</i>	146
7.2.4	Model simulation: Predicting PCB distribution in Lake Hartwell sediments	149
7.2.4.1	<i>Approach</i>	149
7.2.4.2	<i>Results</i>	149
7.2.4.3	<i>Discussion</i>	149
7.2.5	Model simulation: Predicting natural recovery rates for PCB-contaminated sediments in Lake Hartwell	159
7.2.5.1	<i>Approach</i>	159
7.2.5.2	<i>Results</i>	159
7.2.5.3	<i>Discussion</i>	161
	Conclusions for model predictions of PCB distribution and natural recovery in Lake Hartwell sediments and	
7.3	recommendations for future investigations	162

Chapter Eight Predicting the effects of capping contaminated sediments using the CoReTrans model 164

8.1	Introduction	166
8.2	Fate and transport models for sediment cap systems	169
8.3	Simulation of contaminant reactive transport in capped sediment systems	169
8.3.1	Model contaminant	169
8.3.2	Model simulations	169
8.3.2.1	<i>Approach</i>	169
8.3.2.2	<i>Results</i>	175
8.3.2.3	<i>Discussion</i>	178
	Predicting contaminant fate and transport in sand capped	
8.4	systems amended with sorbent materials	179
8.4.1	<i>Approach</i>	179

8.4.2	Results and discussion	181
8.5	Conclusions for model prediction of the effects of capping in contaminated sediments	186
Chapter Nine Summary, Conclusions and Recommendations		188
9.1	Summary	188
9.2	Conclusions	197
9.3	Recommendations	200
References		204
Appendix		
A	Program code for the CoReTranS numerical solver	235
B	Program code for the CoReTranS GUI	245
C	Program code for database access	289
D	Program code for loading data into the CoReTranS GUI	292
E	Program code for saving a data file	293
F	Program code to storing contaminant data	294
G	Program code for catching exceptions	296
H	Text file template for input data to a simulation run.	297
I	Sample summary file (summary.dat) generated after a simulation run.	299

Nomenclature

a_K, b_K	fitting parameters for the linear free energy relationship
a_P, b_P	fitting parameters for the power law expression of porosity
b	solute-surface interaction energy-related parameter
C	contaminant concentration in pore water
C_o	pore water concentration constant
C_W	contaminant concentration in the overlying water
D	molecular diffusion coefficient
D_B	effective diffusion coefficient due to biological transport
D_{bio}	diffusion coefficient at the bioturbation layer
D_{cap}	diffusion coefficient at the capped layer
D_{eff}	effective diffusion coefficient
d_p	mean diameter of the sediment grain
D_{TOT}	total effective diffusion coefficient
D_α	hydrodynamic dispersion coefficient
D_{bio}^{pw}	pore water biodiffusion coefficient
D_{bio}^p	sediment particle biodiffusion coefficient
E	characteristic free energy of adsorption
F_O	prescribed contaminant dlux
f_{OC}	fraction of organic carbon
g	gravitational acceleration
h	prescribed sediment depth
h_{bio}	depth of the bioturbated layer
h_c	hydraulic conductivity of sediment
h_{cap}	depth of sediment cap
$h_{channel}$	depth of the channel
J	contaminant flux
J_A	advective flux
J_{bio}	contaminant flux due to local biological transport
J_D	contaminant flux due to dispersion
J_{film}	contaminant flux across biofilms
J_{phys}	diffusive flux of contaminant
k	sediment permeability
K	sorption isotherm slope
$K(x,t)$	sediment-removal rate constant

$K(x,x',t)$	exchange function for the non-local exchange model
k_b	soluble release mass transfer coefficient
K_D	linear partitioning coefficient
K_F	Freundlich capacity factor
K_{F-OC}	organic carbon-normalised Freundlich capacity factor
k_o	zero-order reaction rate constant
K_{OC}	organic carbon-normalised sorption coefficient
K_{OW}	octanol-water partitioning coefficient
$K_S(x,t)$	sediment-removal rate constant
M	mean of residual error
m	number of discrete reactive sorption domains
m_{PDM}	fitting parameter for the PDM sorption model
MW	molecular weight of contaminant
n	Manning's constant
N	total number of observations or measurements
N_C	number of compounds used for the linear free energy relationship
n_F	Freundlich linearity parameter
P	hydraulic head
q	contaminant mass sorbed into the sediment
Q^o	maximum sorption capacity constant
r	linear correlation coefficient
R	retardation factor
R_{bio}	non-local transport via the sink/source term
r_D	radial distance from the particle centre
R_G	ideal gas constant
r_H	hydraulic radius
RMS	root mean of squared residual errors
R_N	net sediment mixing rate
R_{reac}	chemical reactions via the sink/source term
$\sum R_{reac/bio}$	additional sink/source term
r_{SW}	sediment-to-water ratio
S	solubility of contaminant
S_c	Schmidt number
T	absolute temperature
t	simulation time
$t_{1/2}$	half-life
u	mass averaged advective velocity

v	advective velocity
V	molar volume of contaminant
V_o	maximum volume of sorbed contaminant per unit mass of sediment
V_s	molar volume of water
v_x	velocity of the river
w	velocity of solids either due to burial, compaction or biological process
x	sediment depth
X_L	mass fraction of the sorbed phase exhibiting linear behaviour
X_{NL}	mass fraction of the sorbed phase exhibiting non-linear behaviour
X_{obs}	actual or observed value
$\overline{X_{obs}}$	mean of actual or observed value
X_{pred}	predicted value
$\overline{X_{pred}}$	mean of predicted values
α	empirical attenuation constant for porosity calculations
β	water boundary layer resistance coefficient
Δx	finite depth interval
ε	adsorption potential
η	mass transfer coefficient
θ^2	tortuosity factor
λ	degradation rate constant
μ	dynamic viscosity of pore water
ν_w	kinematic viscosity of water
ρ	pore water density
ρ_B	sediment bulk density
ρ_S	bulk density of sorbent material
ρ_o	contaminant density
τ	duration of contaminant input at sediment-water interface
φ	sediment porosity
φ_∞	porosity at infinite depth
φ_o	porosity value at the interface
Γ	contaminant flux due to a reaction or a prescribed flux
Φ	association parameter of contaminant in pore water

Abbreviations

DDT	Dichlorodiphenyltrichloroethane
DOC	Dissolved organic carbon
DRM	Distributed reactivity model
DSA	Diffusion-sorption-advection model
DSAD	Diffusion-sorption-advection-degradation model
DSD	Diffusion-sorption-degradation model
EPS	Extracellular polymeric substance
GUI	Graphical user interface
HOC	Hydrophobic organic contaminant
HSACM	High surface area carbonaceous material
I/O	Input/output
JDBC	Java database connectivity
LFER	Linear free energy relationship
MNR	Monitored natural recovery
MOC	Micro-organic contaminants
MTBE	Methyl- <i>tert</i> -butyl-ether
O/C	Oxygen-carbon atomic ratio
OCP	Organochlorine pesticides
ODE	Ordinary differential equation
OO	Object-oriented
PAH	Polycyclic aromatic hydrocarbon
PCB	Polychlorinated biphenyl
PCOP	Polychlorinated organic compound
PDE	Partial differential equation
PDM	Polanyi-Dubinin-Manes model
PPCP	Pharmaceuticals and personal care product
REV	Representative elementary volume
SOM	Sediment organic matter
TCB	2,2',4,4'-tetrachlorobiphenyl

List of Tables

Table	Title	Page
2-1	Five parameterisations for porosity as a function of depth	13
2-2	LFERs for organic contaminants: slopes and intercepts of equation 3-13	29
2-3	Summary of sorption-retarded diffusion models	36
3-1	Constitutive equations embedded in the CoReTranS modelling environment	69
4-1	Model parameters used in simulating the three test case scenarios using CoReTranS in comparison with existing analytical solutions	81
5-1	Summary of information taken from Allan (2002)	102
5-2	Model parameters and boundary conditions used in simulating laboratory-scale data taken from Allan <i>et al.</i> (2002; 2004)	105
5-3	Evaluation of goodness of fit between the predicted profiles from the second scenario and the actual profiles from Allan's experiment (2002; 2004)	108
5-4	Evaluation of goodness of fit between the predicted profiles from the third scenario and the actual profiles from Allan's experiment (2002; 2004)	112
6-1	Summary of information taken from White <i>et al.</i> (2005)	121
6-2	Model parameters used in simulating field-scale data for the naphthalene species taken from White <i>et al.</i> (2005)	123
6-3	Evaluation of goodness of fit between the DSA model in CoReTranS and actual profile for all six contaminants	127
6-4	Summary of information taken from Simpson <i>et al.</i> (1998)	131
6-5	Model parameters used in simulating the field-scale data for the aluminium smelter-derived PAHs in Kitimat, British Columbia	134
7-1	Summary of information taken from Simpson <i>et al.</i> (1998)	145
7-2	Model parameters used in simulating the field-scale data for the PCB-contaminated sediments in Lake Hartwell	147
7-3	Physico-chemical properties of selected PCBs used in simulating the field-scale data for the PCB-contaminated sediments in Lake Hartwell	148
7-4	Evaluation of goodness of fit between the CoReTranS model and actual profile for the model contaminants	149

7-5	Estimated time to achieve sediment clean-up goals set by the Superfund Record of Decision at Lake Hartwell (US Environmental Protection Agency, 1994)	161
8-1	Parameters used in model simulations for a capped system	173
8-2	Additional parameters used in model simulations	180
8-3	Phenanthrene concentration at the sand cap-sorbent layer interface	184

List of Figures

Figure	Title	Page
2-1	Contaminant reactive transport processes in bed-sediments	10
2-2	An illustration of various benthic organisms and how they enhance contaminant fate and transport in bed-sediments	19
2-3	Schematic diagram of sediment column with three active biological layers 1, 2, 3 and an underlying homogeneous layer 4	20
2-4	Schematic illustration of <i>intrapphase</i> and <i>interphase</i> mixing	22
2-5	A schematic diagram of vertically orientated irrigated cylindrical burrow structures representing a bioturbated layer of functional micro-environment overlying an unburrowed sediment layer and the resulting pore water concentration profile	24
2-6	A schematic diagram of a complex burrow structure representing a spatially averaged non-local exchange transport of contaminants within the bioturbated layer and the resulting pore water concentration profile	27
2-7	Schematic diagram of the three types of diffusion process where contaminant molecule traverse through a stagnant film at the surface, meso-pores and micro-pores, and within the particle and penetrable solid phase of the particle	35
3-1	Schematic diagram of CoReTranS three-tier structure	58
3-2	CoReTranS graphical user interface	60
3-3	Selecting reactive transport mechanisms to model	60
3-4	Loading or saving data file from the CoReTranS GUI	61
3-5	Model parameters can be estimated or plugged in as user-defined values	61
3-6	Selection of the initial conditions for the model	62
3-7	Selection of the boundary conditions for the model	62
3-8	Selection of contaminant species to model	63
3-9	Adding contaminant species to the CoReTranS database through the GUI	63
3-10	An example of (a) a pore water concentration profile of a modelled contaminant; (b) pore water concentration profile of contaminants in table format, and; (c) summary of model simulation displayed in the GUI	64
3-11	Display of error messages	64
3-12	A diagram of the various building blocks as objects in the CoReTranS modelling environment	65
4-1	Model simulation steps in CoReTranS	79

4-2	Molecular structure of naphthalene and its chemical properties	80
4-3	Contaminant flux through the REV	82
4-4	Pore water concentration-depth profile for naphthalene subject to diffusive transport alone	84
4-5	Sigmoidal distribution patterns of the vertically aligned contaminant front over time in relation to a Gaussian distribution	85
4-6	Pore water concentration-depth profile for naphthalene subject to diffusive transport with mass transfer at the sediment-water interface	87
4-7	Effect of first-order degradation reaction to the pore water concentration-depth profile for naphthalene subject to diffusive transport ($R = 1$)	90
4-8	Pore water concentration-depth profile for naphthalene subject to diffusive-advective transport	92
4-9	Pore water concentration-depth profile for naphthalene subject to diffusive-advective transport ($R = 9$) with varying advective velocities	94
4-10	Effect of first-order degradation reaction to the pore water concentration-depth profile for naphthalene subject to diffusive-advective transport ($R = 9$)	96
5-1	Molecular structure of lindane and its chemical properties	101
5-2	Actual and predicted pore water concentration-depth profiles of lindane in channels 1 and 2 where contaminant distribution was assumed to be controlled with a diffusive transport only	107
5-3	Actual and predicted pore water concentration-depth profiles of lindane in channels 1 and 2 using a constant K_D	109
5-4	Actual and predicted pore water concentration-depth profiles of lindane in channels 1 and 2 using a depth-dependent K_D	111
5-5	Actual and predicted pore water concentration-depth profiles of lindane in channels 1 and 2 where contaminant distribution was assumed to be controlled with a retarded diffusion mechanism using a range of constant K_D 's	113
5-6	Actual and predicted pore water concentration-depth profiles of lindane in channels 1 and 2 for the diffusion-sorption-bioturbation model	115
6-1	Map of the area where the barge Florida sunk.	119
6-2	Molecular structure of phenanthrene and its chemical properties	120
6-3	Pore water concentration-depth profile of the naphthalene species as simulated in CoReTranS in comparison with White's actual data and previous model	125

6-4	Pore water concentration-depth profile of the phenanthrene species as simulated in CoReTranS in comparison with White's actual data and previous model	126
6-5	Map of Kitimat Arm fjord system where sediment samples were taken	129
6-6	Molecular structure of fluoranthene and its chemical properties	129
6-7	Molecular structure of benzofluoranthene and its chemical properties	130
6-8	Molecular structure of pyrene and its chemical properties	130
6-9	Vertical distribution of (a) pyrene, (b) benzofluoranthene, and (c) fluoranthene	132
6-10	Actual and predicted concentration-depth profiles of (a) pyrene, (b) benzofluoranthene, and (c) fluoranthene	135
6-11	Analysis of residual errors between predicted and actual profiles for (a) pyrene, (b) benzofluoranthene, and (c) fluoranthene	136
6-12	Concentration-depth profiles for fluoranthene using various sedimentation rates, w	137
6-13	Actual and predicted concentration-depth profiles for fluoranthene for a diffusion-advection-degradation model scenario using various sedimentation rates, w	139
7-1	Map of the Lake Hartwell Superfund site where the samples were taken.	143
7-2	Molecular structure of a PCB congener where the numbers represent the sites and convention used in naming the congener	144
7-3	Pore water concentration-depth profiles for PCB1, PCB110 and total PCB from T-IA and T-IB transect locations as simulated in CoReTranS in comparison with the actual data	150
7-4	Analysis of residual errors between predicted and actual profiles for PCB1, PCB110 and total PCB in both transect locations T-IA and T-IB	151
7-5	Predicted pore water concentration-depth profile of PCB1 at the transect T-IA site using 5 selected values for τ in comparison with the actual data	153
7-6	Predicted pore water concentration-depth profiles for total PCB1 at transect T-IA and T-IB sites using $\tau = 33$ years in comparison with the actual data	154
7-7	Analysis of residual errors between predicted and actual profiles for total PCB in both transect locations T-IA and T-IB using $\tau = 33$ years	155

7-8	Pore water concentration-depth profile of PCB1 at the transect T-IA site as simulated in CoReTranS using τ between 32 and 33 years and $w = 3 \text{ g cm}^{-2} \text{ y}^{-1}$ in comparison with the actual data	156
7-9	Predicted pore water concentration-depth profiles for total PCB1 at transect T-IA and T-IB sites using $\tau = 33$ years and $w = 3 \text{ g cm}^{-2} \text{ y}^{-1}$ in comparison with the actual data	157
7-10	Analysis of residual errors between predicted and actual profiles for total PCB in both transect locations T-IA and T-IB using $\tau = 33$ years and $w = 3 \text{ g cm}^{-2} \text{ y}^{-1}$	158
7-11	Time series predictions of natural recovery rates for PCB1 from T-IA, $\tau = 33$ years and $w = 3 \text{ g cm}^{-2} \text{ y}^{-1}$	159
7-12	Time series predictions of natural recovery rates for total PCB from T-IA and T-IB, sites $\tau = 33$ years and $w = 3 \text{ g cm}^{-2} \text{ y}^{-1}$	160
8-1	Depiction of a layered sediment cap system	166
8-2a	Pore water concentration profiles of phenanthrene over a 30 cm sediment cap based on (a) Diffusion model, (b) Diffusion – Degradation model was modelled using analytical approach and numerical approach	176
8-2b	Pore water concentration profiles of phenanthrene over a 30 cm sediment cap based on (c) Diffusion – Advection model, and (d) Diffusion – Advection – Degradation model was modelled using analytical approach and numerical approach	177
8-3	Depiction of a sand cap system amended with a sorbent layer	179
8-4a	Pore water concentration profiles of phenanthrene over a 30 cm sediment cap based on (a) Diffusion model, (b) Diffusion – Degradation model, over 100 years simulation time	182
8-4b	Pore water concentration profiles of phenanthrene over a 30 cm sediment cap based on (c) Diffusion – Advection model, and (d) Diffusion – Advection – Degradation, over 100 years simulation time	183
8-5	Pore water concentration of phenanthrene at the interface between the sand cap and the sorbent amended layer for the all four scenarios: (1) Diffusion model, (2) Diffusion – Degradation model, (3) Diffusion – Advection model, and (4) Diffusion – Advection – Degradation model over time.	185

CHAPTER ONE

Introduction

1.1 Contaminated sediments

Contamination of sediments in natural and artificial waters results from a variety of human activities, including mining, industrialisation, urbanisation and agriculture, sometimes through discharge of waste streams, but also through wash-off and erosion of contaminants that have been applied to or accumulated on land. Deposition zones for sediments include canals, streams, rivers, floodplains, wetlands, lakes, estuaries and the ocean. Thus, contaminated sediments are ubiquitous, including (with examples from the UK): metals from mining (Hudson-Edwards *et al.*, 1997; Lord and Morgan, 2003; Merrington and Alloway, 1994; Pirrie *et al.*, 2003; Young, 1997) and urban (Charlesworth and Foster, 1999; Foster *et al.*, 1991; Jennifer and John, 1994) sources, radionuclides from nuclear fuel reprocessing (Assinder *et al.*, 1997; MacKenzie *et al.*, 1999) as well as organotin anti-fouling agents from the shipping industry (Dowson *et al.*, 1996; Harino *et al.*, 2003; Scrimshaw *et al.*, 2005), organic compounds, e.g., polychlorinated biphenyls (Edgar *et al.*, 2003; Harrad *et al.*, 1994; Owens *et al.*, 2001; Tyler and Millward, 1996; Zhou *et al.*, 1999) once used in transformer oil and polyaromatic hydrocarbons (PAHs) (King *et al.*, 2004; Law *et al.*, 2002; Woodhead *et al.*, 1999; Zhou *et al.*, 1999; Zhou *et al.*, 1998) from combustion processes, and phosphorus from detergents and fertilisers (Pretty *et al.*, 2003). There is also increasing concern with contamination of water and sediments by micro-organic contaminants (MOCs), e.g., pesticides washed from agricultural land,

Chapter 1

aqueous film-forming agents, flame retardants, and steroid hormones (Holthaus *et al.*, 2002; Johnson *et al.*, 1998; Thomas *et al.*, 2001), pharmaceuticals and personal care products present in effluent from sewage treatment plants, etc. (Long *et al.*, 1998; Warren *et al.*, 2003). The overall quantity of contaminated sediment in the UK has not been estimated (Power, 2002), but data gathered in the USA reveal the possible scale of the problem in industrialised nations; the US Environmental Protection Agency estimates that 20% of National Priority contaminated sites include a problem with contaminated bed-sediments (US Environmental Protection Agency, 2005b), while the US National Sediment Quality Survey (US Environmental Protection Agency, 1997a) estimates that 6-12% of bed-sediments underlying inland surface waters are contaminated with a selection from 97 different chemicals to an extent that adverse effects on aquatic life are probable.

Accumulation of even trace quantities of contaminants in bed-sediments not only poses a direct threat to the ecological function of the benthic community (Barcelo and Petrovic, 2007; Calmano *et al.*, 1996; Fleming *et al.*, 2006; Hylland, 2006; NRC, 1997), which is a point of entry to the food chain, leading to bioaccumulation in higher organisms, but accumulated contaminants may also be released into the water column for redistribution in the ecosystem over time. The connection between sediment quality and water quality is of particular concern in relation to the recent European Water Framework Directive (2000/60/EC), which requires that “good ecological status” of surface waters be maintained. In many jurisdictions, this will be defined on the basis of ecological assessment and classification system developed as part of the implementation strategies of the Water Framework Directive (Devlin *et al.*, 2007). While quantitative assessment of the immediate ecological effects of contaminated sediments is a contentious issue, the risks posed over time are even more difficult to assess. **Since both effects and risks are related to contaminant concentrations, a predictive model of concentrations in bed-sediments and overlying water can provide a way forward for site-specific risk assessment over the short-, medium- and long-term, and for developing appropriate and cost-effective prevention, mitigation and remediation strategies.** Moreover, data derived from this model can eventually be integrated in the Information Technology (IT) Architecture Environment (Usländer, 2005) proposed for the Water Framework Directive. Until now, development of reactive transport models for bed-

sediments has been limited, compared to that of models in other reactive transport disciplines such as contaminant hydrogeology and early diagenesis.

1.2 Contaminant fate and behaviour in sediments

The fate and behaviour of contaminants in sediments is controlled by a combination of physical, chemical and biological factors. Several studies of hydrophobic organic contaminants have demonstrated that these substances strongly associate with natural sediments (Aller, 2001; Schaffner *et al.*, 1997; Wu and Gschwend, 1986). Due to their large surface area-to-volume ratio and organic matter content (Cornelissen *et al.*, 2005; Golding *et al.*, 2005; Huang *et al.*, 2003), sediment particles are ideal sorption sites for most of these substances. Contaminated sediment particles are transported and distributed over the underlying bed by hydrological flow or turbulent mixing due to episodic events (e.g., storms, tidal mixing). Fine-grained particles are readily dispersed while coarser particles are agglomerated either through biological interaction or physical coagulation. In time, aggregates settle on the sediment-water interface forming loosely consolidated surficial deposits with high water content which become increasingly consolidated over time. Subsequent re-suspension of this loose, highly permeable sediment layer may occur as a result of episodic events or human activities (e.g., dredging).

Chemical and biological changes occurring within the bed sediment are likewise known to affect the fate and transport of contaminants. The sediment-water interface acts as a boundary between the oxic overlying water of neutral pH and the generally anoxic, and therefore often more acidic, sediment column. pH and Eh gradients result in reduction/precipitation of trace metals as sulfides and decreased microbial degradation of organic matter with depth. Moreover, high concentrations of nutrients and organic matter near the sediment-water interface draw a diversity of deposit and filter-feeding organisms. The actions of these benthic fauna significantly alter contaminant transport pathways and sediment erodibility (Eggleton and Thomas, 2004).

Chapter 1

Reactive transport modelling has long been used in the analysis of complex interactions between processes occurring in sediment systems (Goldberg and Koide, 1962; Harper *et al.*, 1999; e.g., Meysman *et al.*, 2003c; Thibodeaux *et al.*, 2001) leading to a gradual development of fundamental principles in sediment biogeochemistry. The emergence of these contaminant reactive transport models in aquatic bed-sediments was paved by the field of early diagenesis (Boudreau, 1997). Various 1-dimensional numerical models such as OMEXDIA (Soetaert *et al.*, 1996b), STEADYSED (Wang and Van Cappellen, 1996) and CANDI (Boudreau, 1996a) provided effective tools for understanding primary biogeochemical processes in bed-sediments. Meysman *et al.* (2003c) recently developed MEDIA, an object-oriented modelling environment where users can construct multiple diagenetic models from a toolbox of functional modules to simulate experimental or field scenarios. Sediment diagenetic models, however, generally apply to cycling of nutrients and transformation of limited inorganic species and bulk organic matter within the topmost layer of the aquatic sediments following deposition from the overlying water and do not apply to the fate and transport of organic contaminants through the lower depths of the bed-sediment. Modelling of hydrophobic organic contaminant fate and transport in aquatic sediments has also been initiated in several studies. Most of these studies typically involve parameterisations of available concentration-depth profiles using analytical solutions of the reactive transport equations (e.g., Koelmans *et al.*, 2000; Formica *et al.*, 1988; Valsaraj and Sojitra, 1997). Allan *et al.* (2004) developed a 1-dimensional numerical model that simulates diffusion-sorption-degradation (DSD)-controlled reactive transport of MOCs in the sediment pore water and the entire bed-sediments. Key parameters were optimised by comparing the generated concentration-depth profile to observations from diffusion-controlled experiments. Several versions of the DSD model were written to gain insight into various sorption and degradation scenarios.

Over the past quarter century, reactive transport models of contaminant fate and behaviour in sediments have dynamically evolved from analytical models of basic phenomena to numerical representations of complex interactions (Allan and Stegemann, 2007; Allan *et al.*, 2005; Boudreau, 1997b; Daniels *et al.*, 1998; Meysman *et al.*, 2003c; Soetaert *et al.*, 1996b). With recent significant increases in computational power and capability, reactive transport codes can now potentially accommodate

complex phenomena previously unaccounted for in legacy models (e.g., early FORTRAN models). For example, understanding of the diffusive transport of organic contaminants has progressed from a simple Fickian process (Goldberg and Koide, 1962) to a spatially-explicit transport mechanism affected by sediment physical (Boudreau, 1996b) and organic matter content heterogeneity (Chiou *et al.*, 2000; Kleineidam *et al.*, 2002; LeBouef and Weber Jr., 1997; Weber *et al.*, 1992; Xia and Pignatello, 2001). The presence of a diverse benthic community and its contribution to the fate and transport of organic contaminants in bed-sediments has been investigated as well (Aller, 1980; Meysman *et al.*, 2003a; Reible *et al.*, 1996; Thibodeaux *et al.*, 2001). These studies have certainly contributed to the theoretical foundation of reactive transport modelling. **However, the question of whether existing knowledge of the various in-bed processes is sufficient to model contaminant fate and transport in bed-sediments or not still remains unanswered.**

1.3 Numerical modelling of organic contaminant reaction and transport in bed-sediments using CoReTranS

The main aim of this thesis was to develop a numerical model for organic Contaminant Reaction and Transport in layered bed-Sediments (**CoReTranS**) that enables prediction of concentration-depth profiles in bed-sediments on the basis of input information about the contaminants and site. The CoReTranS model can be used to facilitate assessment and comparison of the effectiveness of remediation alternatives for organic contaminants (e.g., monitored natural attenuation, sediment capping) by estimating the vertical distribution of contaminants along sediment cores, fate and transport parameters and engineering design criteria (e.g., recovery rates, time to approach steady-state conditions). The CoReTranS model also aims to complement environmental monitoring plans and address knowledge gaps that exist in site-specific empirical information (e.g., site characterisation plan in its initial stages). By identifying the fate and transport processes and parameters that control contaminant distribution in bed-sediments, the reactive transport model can guide field and experimental studies and make tangible contributions to the growing understanding of contaminant fate and transport in bed-sediments.

Chapter 1

The CoReTranS model code was benchmarked against the analytical solutions of simplified reactive transport models. The numerical model was validated and subsequently used to interpret the results of important individual experiments and field monitoring studies from existing literature. Limitations of the CoReTranS model and recommendations to guide further experiments and monitoring projects work were also identified based on the simulation results. Because of the complexity of the phenomena involved, the present work solely focused on organic contaminants, but was intended to be amenable to future extension to inorganic species.

The contribution of this work is demonstrated through new findings in relation to the individual experiments and field studies presented in this thesis. Specific insights into post-depositional fate and transport of organic contaminants in lake sediments were obtained by comparing the results of these field studies with the numerical results from the CoReTranS model. Key parameters such as effective diffusivity of contaminants and sediment accumulation rates were shown to possibly account for the predicted contaminant concentrations in bed-sediments. Further, the ability to predict the fate and transport of organic contaminants both in natural and capped bed-sediment systems was demonstrated using the CoReTranS model.

The current understanding of organic contaminant fate and transport processes in bed-sediments is critically surveyed in Chapter [2], highlighting various areas of reactive transport modelling theory for further investigations. The chapter also explores challenges faced by scientist and engineers in developing and applying validated numerical models to better understand the fate and transport of organic contaminants in bed-sediments.

Chapter [3] describes development of the CoReTranS modelling environment using the object-oriented approach. The chapter also explains the three-tier structure of the modelling environment, the mathematical procedure used for the numerical solution of the resulting model equations in CoReTranS. A summary of all the constitutive equations that can be used in the modelling environment is presented at

Chapter 1

the end of the chapter. A general guideline on the application of the CoReTranS model to laboratory and field dataset is also outlined at the end of the chapter.

The CoReTranS model code is verified and benchmarked in Chapter [4] by comparing the numerical results of simplified problems with their analytical solutions. Diffusion, diffusion-advection models and their derivatives were used in verifying the CoReTranS model. Various modes of assessment for model refinement are also discussed in the chapter.

In Chapter [5], the CoReTranS model is validated by simulating a dataset from a laboratory experiment aimed at identifying key processes and critical parameters that control the fate and transport of lindane in a simulated riverine environment. Improved model scenarios were used to better understand the fate and transport of lindane in the bed-sediment.

Datasets from studies of sediments contaminated with petroleum-derived hydrocarbons from Wild Harbour, West Falmouth, MA and from Kitimat, British Columbia were simulated and interpreted using the CoReTranS model to investigate the post-depositional distribution of PAHs at the contaminated site, the simulation results of which are presented in Chapter [6].

In Chapter [7], a dataset derived from field monitoring studies for PCBs in Lake Hartwell was simulated and interpreted using the CoReTranS model in order to explain key processes that controlled the fate and transport of these contaminants in surface waters and assess the natural recovery of PCB-contaminated sediments. The natural recovery rates for PCB-contaminated sediments and the time to achieve clean-up goals were also predicted and presented in the chapter.

Predicting the effects of capping contaminated sediments as a remedial option to manage contaminated sediments with examples of the application of each scenario to simulation of different transport and reaction mechanisms in a sand cap and demonstration of numerical approach for modelling a sorptive cap using the CoReTranS model is discussed in Chapter [8]. Simulation results from the CoReTranS model is also compared with a steady state model developed,

Chapter 1

highlighting key points of each modelling approach as well as knowledge gaps. Results presented in this thesis and the recommendations to guide future field investigations are summarised in Chapter [9].

CHAPTER TWO

Organic contaminant fate and transport processes in bed-sediments – a review

2.1 Introduction

Aquatic sediments, suspended or settled to the bed, act initially as sinks, and ultimately as sources, for contaminants released from a variety of natural and anthropogenic activities. The fate and transport of these contaminated sediments generally define the overall pattern of chemical contaminant distribution within the aquatic ecosystem. In-bed fate and transport processes (i.e., no net movement of sediments), as illustrated in Figure 2-1, include contaminant diffusion through pore water and transport of dissolved contaminants by advection, physical, chemical and biological reactions, and sediment mixing as a result of biological activities and periodic events at the benthic layer (i.e., surficial layer at the sediment-water interface). A quantitative description of these processes that determine contaminant fate and behaviour in bed-sediments facilitates the development of a predictive model of the system that can be used to identify and evaluate appropriate strategies for attenuation, mitigation or remediation of contaminated sediments. Extensive reviews have already been done on each of these mechanisms separately (e.g., Allan and Stegemann, 2007; Pignatello and Xing, 1996; Warren *et al.*, 2003). This chapter, hence, simply intends to summarise recent developments for each transport mechanism and reaction process as well as to highlight areas for further investigation.

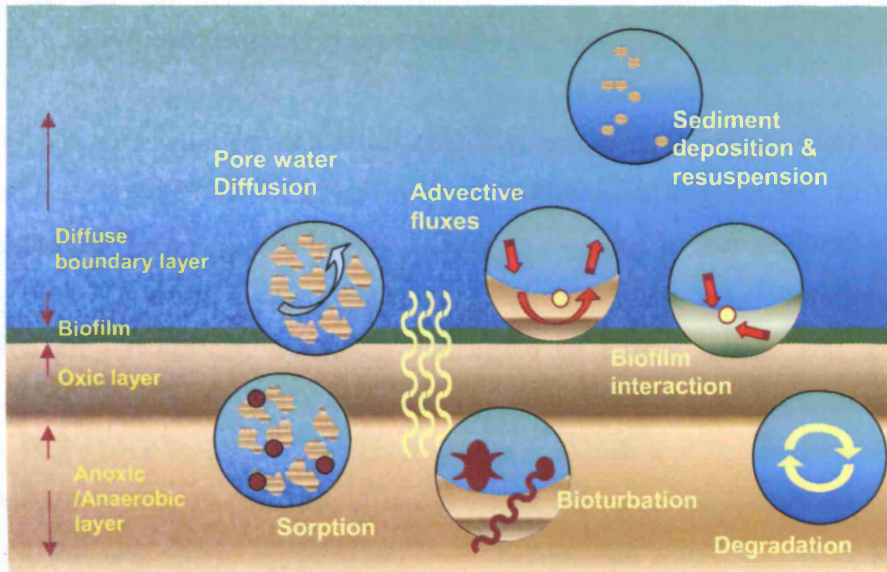


Figure 2-1. Contaminant reactive transport processes in bed-sediments

2.2 Contaminants of concern

2.2.1 Polycyclic aromatic hydrocarbons

PAHs are ubiquitous sediment pollutants due to their chemical stability and legacy of production throughout the past century (Brenner *et al.*, 2002; Youngblood and Blumer, 1975). Many are known to cause mutagenic and carcinogenic effects (White, 1986). PAHs are primarily formed during incomplete combustion of fuels such as coal, oil, diesel and wood. Due to their hydrophobicity and strong affinity to organic matter, PAHs often end up in aquatic sediments through direct spill, atmospheric deposition or urban road runoff. They may also be produced as natural products of transformations from precursors formed as a result of diagenetic processes in sediments. PAH-contaminated sediments are widely documented (e.g., King *et al.*, 2004; Liu *et al.*, 2005; Naf *et al.*, 1994; Simpson *et al.*, 1998a; Wild and Jones, 1995).

2.2.2 Polychlorinated organic compounds

Polychlorinated organic compounds (PCOCs) are among the most widely studied contaminants, particularly PCBs and organochlorine pesticides (OCPs). PCBs are high-molecular weight polychlorinated organic compounds that tend to exhibit strong hydrophobicity, low mobility and low degradation rates. They strongly partition onto sediments, are readily assimilated by aquatic animals and tend to biomagnify in the food chain (Barnthouse *et al.*, 2003; Brenner *et al.*, 2004; Jones *et al.*, 1995). PCBs have been shown to cause cancer in animals and significant ecological and human health effects, such as neurotoxicity, reproductive and developmental toxicity, immune system suppression, liver damage, skin irritation, and endocrine disruption (Agency for Toxic Substances and Disease Registry, 1995; US Environmental Protection Agency, 1996).

Pesticides, on the other hand, are chlorinated hydrocarbons that have been found to pollute most aquatic ecosystems worldwide, and virtually every lake, river and stream in the US (US Geological Survey, 2007). Examples of chlorinated pesticides include aldrin, dieldrin, dichlorodiphenyltrichloroethane (DDT), heptachlor, lindane, and chlordane. They are also known to bioaccumulate in aquatic organisms and biomagnify in the food chain (Hornsby *et al.*, 1995; Sancho *et al.*, 1998). Due to their known toxicity and persistence in the environment, PCOCs are included in the list of priority pollutants in most countries and thus their use is either banned or restricted.

2.2.3 Pharmaceutical compounds

The incidence and fate of PPCPs in surface waters is rapidly becoming a thriving research area. This new class of pollutants and their occurrence in aquatic ecosystems has been investigated in several studies (e.g., Carlsson *et al.*, 2006; Kummerer, 2004; Ternes, 1998). Indiscriminate use and disposal, and continuous discharge of PPCPs and their metabolites to sewage, have resulted in measurable steady-state concentrations despite their relatively short environmental half-lives, prompting Hernando *et al.* (2006) to described PPCPs as “pseudo-persistent.” Although the fate

and behaviour of these contaminants in aquatic sediments are still poorly understood (az-Cruz *et al.*, 2003; Cunningham *et al.*, 2006), they may play a role in decline of biodiversity and produce adverse effects and ecological changes (Loffler *et al.*, 2005) due to the similarity in physico-chemical behaviour they display with other deleterious sediment contaminants. For example, triclosan was shown to affect biomass production of the algae *Scenedesmus subspicatus* with an EC_{50} of $1.4 \mu\text{g/L}$ (Orvos *et al.*, 2002), diclofenac resulted in liver cell damage of rainbow trout *Oncorhynchus mykiss* with a lowest observed effect concentration of $1 \mu\text{g/L}$ ³⁰ (Triebkorn *et al.*, 2004), and carbamazepine decreased emergence of the midge larva *Chironomus riparius* at sediment concentrations $> 70 \mu\text{g/kg}$ (Oetken *et al.*, 2005). Further, Ying *et al.* (2002) showed that estrogenic steroids are typically hydrophobic organic compounds with low volatility and thus their persistence in bed-sediments is expected to be controlled by sorption on sediment, to the possible detriment of bed-sediment quality. The Environment Agency has issued a position statement calling for more research aimed at understanding and quantifying the fate and transport of PPCPs in surface waters (Environmental Agency Wales, 2004).

2.3 Analysis of fate and transport processes in bed-sediments

2.3.1 Molecular diffusion

Contaminant molecules are in continuous random motion. This results in net movement in pore water from a region of high concentration to low concentration, i.e., diffusion. Diffusive transport of contaminants within the bed sediment becomes significant when physical or biotic sediment mixing and pore water advection is negligible.

The magnitude of the contaminant flux J ($\text{g/m}^2\text{-s}$) is quantified using Fick's law (Crank, 1975) and the rate of contaminant concentration change within the sediment pore water in the x direction and time t is quantified as,

$$J = -\phi(x) D_{eff} \frac{\partial C}{\partial x} \quad \text{Eq. 2-1}$$

where C is the pore water concentration of the contaminant (g/m^3), $\phi(x)$ is the sediment porosity as a function of sediment depth x , and D_{eff} is the effective diffusion coefficient (cm^2/s).

Porosity is typically modelled based on an assumption of steady state compaction. This implies that porosity is not incorporated into the model equation (equation 2-1) as a differential quantity but is assumed invariant with time. Five parameterisations presented in Table 2-1 are typically used for approximating porosity values.

Table 2-1. Five parameterisations for porosity as a function of depth.

Porosity type	Porosity function
Constant	$\phi(x) = \phi_o$
Linear	$\phi(x) = \phi_\infty + (\phi_o - \phi_\infty) \left[1 - \frac{x}{h} \right]$
Exponential	$\phi(x) = \phi_\infty + (\phi_o - \phi_\infty) \exp\left[-\frac{x}{h} \right]$
Inverse exponential	$\phi(x) = \frac{\phi_o \phi_\infty}{\phi_\infty + (\phi_o - \phi_\infty) \exp\left[-\frac{x}{h} \right]}$
Power	$\phi(x) = a_p h \exp(-b_p)$

All these empirical correlations, except for the power expression, are functions of four parameters: the porosity value at the sediment-water interface (ϕ_o), the porosity at infinite depth (ϕ_∞), and the sediment depth (h). The power law expression uses two fitting parameters (a_p and b_p) that are supplied *a priori*. The exponential relation decreasing with depth is the most commonly used correlation for the calculation of porosity values (Soetaert *et al.*, 1996). Recent additions to parameterize porosity are presented in papers by Boudreau and Bennett (1999), where they developed an

Chapter 2

inverse exponential correlation, and Allan *et al.* (2004), where they demonstrated the applicability of a power law equation to their porosity-depth profiles. The evaluation of sediment porosity necessitates careful site characterisation, as this parameter is included in all the terms of the governing equation and therefore an erroneous porosity value would result in over/under-predictions of contaminant distribution in bed-sediments.

D_{eff} is typically a magnitude or two less than the molecular diffusion coefficient, D (i.e., measured in pure aqueous solution), due to sediment porosity and tortuosity. Sediment tortuosity essentially accounts for the convoluted path that diffusing contaminant molecules follow within the bed-sediment porosity. The tortuosity factor θ^2 is used to calculate the effective diffusion coefficient. A constitutive relationship similar to that proposed by Millington and Quirk (1961) is often used to estimate D_{eff} :

$$D_{eff} = D \varphi(x)^{4/3} \quad \text{Eq. 2-2}$$

Boudreau (1996), however, advocated use of the Modified Weissberg equation, as it fitted the data from various marine and lacustrine sediments the best (i.e., R^2 value of 0.65). The tortuosity factor θ^2 , approximated using the modified Weissberg equation is given by,

$$\theta^2 = 1 - \ln[\varphi(x)^2] \quad \text{Eq. 2-3}$$

In the absence of actual measurements, D for contaminants dissolved in water can be estimated using empirical equations such as Stokes-Einstein or contaminant molar volume-based equations (Niesner and Heintz, 2000; van der Wielen *et al.*, 1997) including those developed by Wilke-Chang (Chang and Wilke, 1955), Reddy-Doraiswamy (Reddy and Doraiswamy, 1967) and Hayduk-Laudie (Hayduk and Laurie, 1974). The Stokes-Einstein equation is given by,

$$D = \frac{k_{Boltzman} T}{6\pi\mu_w r_{HOC}} \quad \text{Eq. 2-4}$$

Chapter 2

where $k_{Boltzman}$ is the Boltzman constant ($1.38 \times 10^{-23} \text{ m}^2 \text{ kg/s}^2\text{-K}$), T is absolute temperature (K), μ_w is the viscosity of water (cP) and r_{HOC} is the radius of contaminant particle (m). Although the Stokes-Einstein equation may be accurate, it is only valid for spherical molecules (McClung and Kivelson, 1968).

In this work, the molecular diffusion coefficient was estimated using one of the three aforementioned empirical equations: Wilke-Chang (equation 2-5), Reddy-Doraiswamy (equation 2-6) and Hayduk-Laudie (equation 2-7), or specified as a user-defined parameter (i.e., constant). Among these three empirical correlations, the Wilke-Chang equation is widely used (Li and Carr, 1997; Niesner and Heintz, 2000; van der Wielen *et al.*, 1997). Since Hayduk-Laudie and Reddy-Doraiswamy are similar forms of the Wilke-Chang equation, their use in estimating the molecular diffusivities of organic contaminants is therefore suitable. These empirical equations are given by:

$$D = 7.4 \times 10^{-8} \frac{T(\Phi MW)^{0.5}}{\mu V^{0.6}} \quad \text{Eq. 2-5}$$

$$D = 10 \times 10^{-8} \frac{TMW^{0.5}}{\mu V^{1/3} V_s^{1/3}} \quad \text{Eq. 2-6}$$

$$D = 13.26 \times 10^{-5} \mu^{-1.14} V^{-0.589} \quad \text{Eq. 2-7}$$

where T is the absolute temperature (K), V is the contaminant's molar volume ($\text{cm}^3 \text{ mol}^{-1}$), μ , the viscosity of water (cP), and MW , V_s , Φ are molecular weight (g/mol), molar volume and association parameter (i.e., with a typical value of 2.6 for water) of the contaminant species in pore water, respectively. All of these correlations are based on inherent molar volumes of the contaminants, approximated using the Le Bas method (LeBas, 1915). A study made by Sastri *et al.* (1996) on molar volumes of 163 liquids at normal boiling point demonstrated the efficacy of the Le Bas method in estimating V .

The viscosity of water is estimated in the CoReTranS model as a built-in function of the absolute temperature and is expressed as (Yaws, 1999):

$$\log_{10} \mu = -10.2158 + \frac{1.7925 \times 10^{-3}}{T} + 1.773 \times 10^{-2} T - 1.2631 \times 10^{-5} T^2 \quad \text{Eq. 2-8}$$

Integrating all these parameters in a single equation (equation 2-9) results in a one-dimensional diffusion process within the sediment column to and from the homogeneous overlying water:

$$\frac{\partial[\phi(x)C]}{\partial t} = \frac{\partial}{\partial x} \left(\frac{\phi(x)D}{\theta^2} \frac{\partial C}{\partial x} \right) = \frac{\partial}{\partial x} \left(\frac{\phi(x)D}{1 - \ln[\phi(x)^2]} \frac{\partial C}{\partial x} \right) \quad \text{Eq. 2-9}$$

2.3.2 Advection

Contaminant transport by advection in bed-sediments can be caused by burial, compaction and/or hydrological flow (Boudreau, 1997). Waves and tidal flows are likewise known to induce advective transport in permeable sediments for estuarine and marine environments (Huettel and Webster, 2001). Pore water advection due to burial results from the movement of the sediment-water interface relative to the pore water. Expulsion of pore water caused by the compaction of the bed-sediment also affects contaminant distribution (Berner, 1980). Hydrological flows, on the other hand, may either be attributed to pressure or density gradients (e.g., thermal-, haline-convection).

The advective flux, J_A , for a 1-D model is quantified as,

$$J_A = u\phi(x)C \quad \text{Eq. 2-10}$$

where the mass averaged advective velocity, u (cm/s), of the pressure-driven flow is further described by Darcy's equation (equation 2-11) (Bear, 1972; Darcy, 1856). That is,

$$u = \frac{k}{\varphi\mu} \left(\frac{\partial P}{\partial x} - \rho g \right) \quad \text{Eq. 2-11}$$

where k is the sediment permeability (m^2), μ is the dynamic viscosity of the pore water (cP), $\partial P/\partial x$ is the spatial gradient for pressure (Pa/m), and ρ is the water density (kg/m^3) and g , the gravitational acceleration ($9.8 \text{ m}/\text{s}^2$). Assuming hydrostatic equilibrium (i.e., $\partial u/\partial x = 0$) along the sediment column, a second order differential equation is obtained for the pressure gradient. The permeability value can be estimated using various empirical equations reviewed by Boudreau (1997), among which, the most widely used is the Carman-Kozeny equation (Bear, 1972):

$$k = \frac{d_p^2}{180} \left(\frac{\varphi^3}{(1-\varphi)^2} \right) \quad \text{Eq. 2-12}$$

where d_p is the mean diameter of the sediment grain (m). It should be noted, however, that these permeability equations assume no organic matter within the interstitial spaces of the particle aggregates and that the grain diameter and sediment porosity are fairly uniform (Boudreau, 1997; Huettel and Webster, 2001). The challenge, then, is to estimate sediment permeability values, knowing that sediment columns through which are contaminants distributed contain natural organic matter, and have a porosity that decreases with depth.

For the CoReTranS model, u is either plugged into the equation as a user-defined value taken directly from seepage metre readings or approximated using Darcy's law, where the hydraulic head measured from pore pressure gradient readings and the sediment permeability can be plugged in. The sediment permeability can also be approximated using the hydraulic conductivity h_c which can be plugged in as a user-defined parameter. That is,

$$k = \frac{h_c \mu}{\rho g} \quad \text{Eq. 2-13}$$

where k is the sediment permeability, g is acceleration due to gravity, ρ and μ are the density and viscosity of the pore water, respectively.

Hydrological flow creates lateral mixing known as dispersion within the sediments. This type of mixing is generally given a description according to Fick's first law, where the contaminant flux due to dispersion (J_D) is given by:

$$J_D = -\phi(x)D_\alpha \frac{\partial C}{\partial x} \quad \text{Eq. 2-14}$$

The hydrodynamic dispersion coefficient D_α is a function of the pore water velocity (Rutgers van der Loeff, 1981; Webster and Taylor, 1992). The importance of transport by dispersion/advection relative to molecular diffusion can be estimated using a dimensionless parameter called the hydrological Peclet number (Boudreau, 1997). For Peclet numbers below 1, dispersion/advection may be neglected. In contrast, when sediment permeability values exceed 10^{-12} m^2 , transport across the sediment-water interface is chiefly driven by advective flow of contaminated pore water (Huettel *et al.*, 2003).

2.3.3 Bioturbation

2.3.3.1 Overview. It has long been recognised that the presence of a diverse benthic community impacts sediment geochemistry and contaminant fate and transport. Macrobenthos, meiofauna, and microzoobenthos pullulating in bed-sediments enhance the transport of both sediment particles and contaminants through a variety of biological activities such as feeding, burrowing, excavation and respiration, as illustrated in Figure 2-2 (Aller, 1982; Aller and Aller, 1992; Aller and Aller, 1998). The resulting biological reworking of the sediment network is generally called bioturbation (Aller, 1982; Berner, 1980).

Over the past few decades, various models have been developed to describe biogenic transport in aquatic ecosystems. For example, Aller (2001) used four conceptualisations for bioturbation: biogenic diffusion (e.g., Boudreau, 1986a; Matisoff and Wang, 1998), biogenic advection (e.g., Hammond *et al.*, 1985; Huettel *et al.*, 1998), non-local exchange models and functional geometric analogues of an

average micro-environment. It was noted, however, that the attempt to define the complexity and dynamics of sediment biota through these models failed to completely fit observed data. Other techniques used to quantify bioturbation include: random walks (Choi *et al.*, 2002; Wheatcroft *et al.*, 1990), stochastic modelling (Boudreau, 1986a; Boudreau, 1986b), finite difference methods (Francois *et al.*, 1997; Soetaert *et al.*, 1996a) and Markov chain theory (Shull, 2001; Trauth, 1998).



Figure 2-2. An illustration of various benthic organisms and how they enhance contaminant fate and transport in bed-sediments (taken from Rhoads (1974)).

Boudreau (1986b) originally conceptualised a criterion to distinguish *local* biological transport processes from *non-local* ones. A transport or reaction process was categorically described by Boudreau (1986b; 1997) as *local* if it depends on the parameters evaluated at a specified point. For example, the diffusive flux J is a local process because D_{eff} and C are evaluated at a single point x . In the same way, advection and most reaction kinetics are considered as local processes. Further, a

moving particle subjected to a local transport process is required to travel through all adjacent points from one position to another. A *non-local* process, in contrast, involves parameters evaluated at more than one point and allows transport of material from one position to another without travelling through the intervening points.

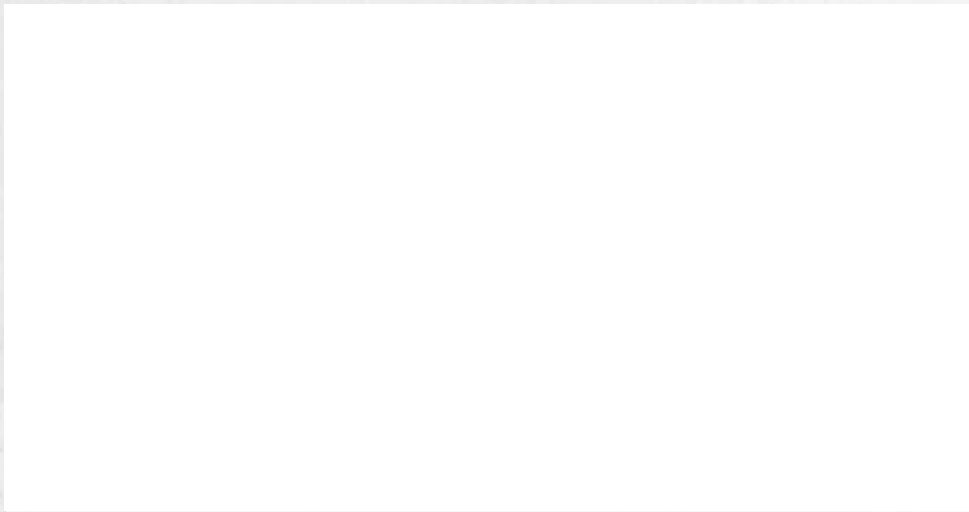


Figure 2-3. Schematic diagram of sediment column with three active biological layers 1, 2, 3 and an underlying homogeneous layer 4 (i.e., no mixing). Displacement of particles from layer 2 to 1 or from layer 3 to 2 is described as a local process while transport of particles between non-adjacent layers (e.g., layer 3 to 1) is a non-local process. (Adapted from Boudreau and Imboden (1987).

Meysman *et al.* (2003) recently proposed a more general framework to classify existing bioturbation models using the “locality” criterion providing quantitative basis to decide whether a biological transport model is described as local or non-local. The following criteria were derived (see Meysman *et al.* (2003) for the derivations):

1. **Frequency criterion.** For a non-local process, bioturbation events (i.e., burrowing, feeding, etc.) must be sufficiently frequent as compared to mixing time of the tracer introduced into the system under consideration.

2. ***Symmetry criterion.*** For a local process, the sediment displacement must be random in direction and time. However, the directional randomness requires an equal probability of a particle moving in either direction (i.e., up or down).
3. ***Length criterion.*** For a local process, the sediment displacement must occur under a sufficiently small scale (i.e., the average distance through which a particle is displaced during a bioturbation event should be smaller than that of a tracer introduced into the system under consideration).

From this view, two bioturbation formalisms emerged: local biodiffusion models and non-local exchange models.

2.3.3.2 Biodiffusion models. Goldberg and Koide (1962), in a pioneering attempt to model bioturbational flux, used a Fickian diffusion analogy to provide a quantitative description of biologically-induced transport phenomena. With subsequent modifications done by Guinasso and Schink (1975) and Berner (1980), the biodiffusion model has been widely accepted and applied in diagenetic models (Boudreau, 1986a; Soetaert *et al.*, 1996b; Wang and Van Cappellen, 1996).

Moreover, bioturbation as local transport is given the Fickian formulation to describe the biological mixing of sediment and pore water as a diffusive process (Berner, 1980; Boudreau, 1986a; Goldberg and Koide, 1962). Boudreau (1986a, 1986b) clearly made a distinction between the types of biological mixing: *intrapphase* and *interphase* mixing. The difference between *intrapphase* and *interphase* mixing is illustrated as follows:

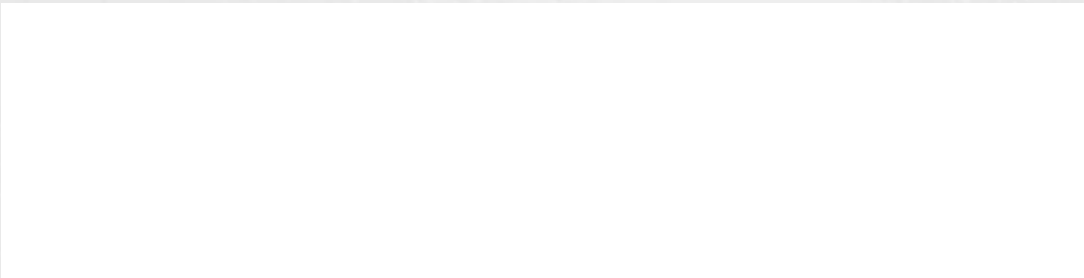


Figure 2-4. Schematic illustration of *intraphase* and *interphase* mixing. In *intraphase* mixing, the number of particles remains unchanged for both upper and lower region (i.e., constant porosity). In *interphase* mixing, the volume fraction of solids is homogenised. Adapted from Muslow *et al.*(1998).

Intraphase mixing characterises contaminant distribution as a result of biological mixing of sediment and pore water without changing the porosity profile of the sediment bed. The biodiffusive flux J_{bio} describing this formalism is expressed as

$$J_{\text{bio}} = -D_{\text{bio}}^{\text{pw}} \frac{\partial[\varphi(x)C]}{\partial x} \quad \text{Eq. 2-15}$$

where $D_{\text{bio}}^{\text{pw}}$ is the pore water biodiffusion coefficient (cm^2/s). The effect of biological mixing of sediment and pore water on contaminant distribution and how this type of mixing influences the bed-sediment's porosity profile is referred to as *interphase mixing*. It is given as

$$J_{\text{bio}} = -\varphi(x) D_B \frac{\partial C}{\partial x} \quad \text{Eq. 2-16}$$

where D_B is the effective diffusion coefficient due to biological transport (e.g., mixing of sediment and pore water by macrofauna) (Aller and Yingst, 1985), meiofauna (Aller and Aller, 1992) and macrozoobenthos (Glud and Fenchel, 1999)). The paper of Meysman *et al.* (2005), however, proved that *interphase* mixing is the correct biodiffusion model under the assumption of steady-state porosity.

Chapter 2

Average values of D_{bio}^{pw} for both reactive and non-reactive contaminants near the sediment-water interface are typically three to ten times larger than those predicted by molecular diffusion (Aller and Yingst, 1985; Devol and Christensen, 1993; Forster *et al.*, 1995; Tahey *et al.*, 1994). Thoms *et al.* (1995) presented a summary of observed bioturbation depths and biodiffusion coefficients collated from numerous studies with a variety of animals in both fresh and salt waters throughout the world. D_{bio}^{pw} , however, is a difficult parameter to predict in advance as no equation has hitherto been developed to approximate this parameter. This parameter can, thus, be plugged into the CoReTranS model as a user-defined value.

The constitutive 3-D equation (equation 2-17) proposed by Aller (1980) defines an average functional micro-environment which is basically assumed as a vertically orientated, irrigated, cylindrical burrow structure (Figure 2-5). That is,

$$\frac{\partial C}{\partial t} = D_{bio}^{pw} \frac{\partial^2 C}{\partial x^2} + \frac{D_{bio}^{pw}}{r} \left(\frac{\partial}{\partial r} r \frac{\partial C}{\partial r} \right) + \sum R \quad \text{Eq. 2-17}$$

where r is the radial distance from the centre of the burrow axis (m). Boudreau's (1984) study on bromine tracers showed, however, that bioturbation-induced contaminant fluxes predicted using the simplest form of the cylindrical model (equation 2-17) were no different when modelled using a mass transfer term with a constant transfer coefficient to describe the bioturbated layer. Moreover, the application of the cylindrical model is limited due to the complexity of representing burrowing patterns as a function of sediment depth.

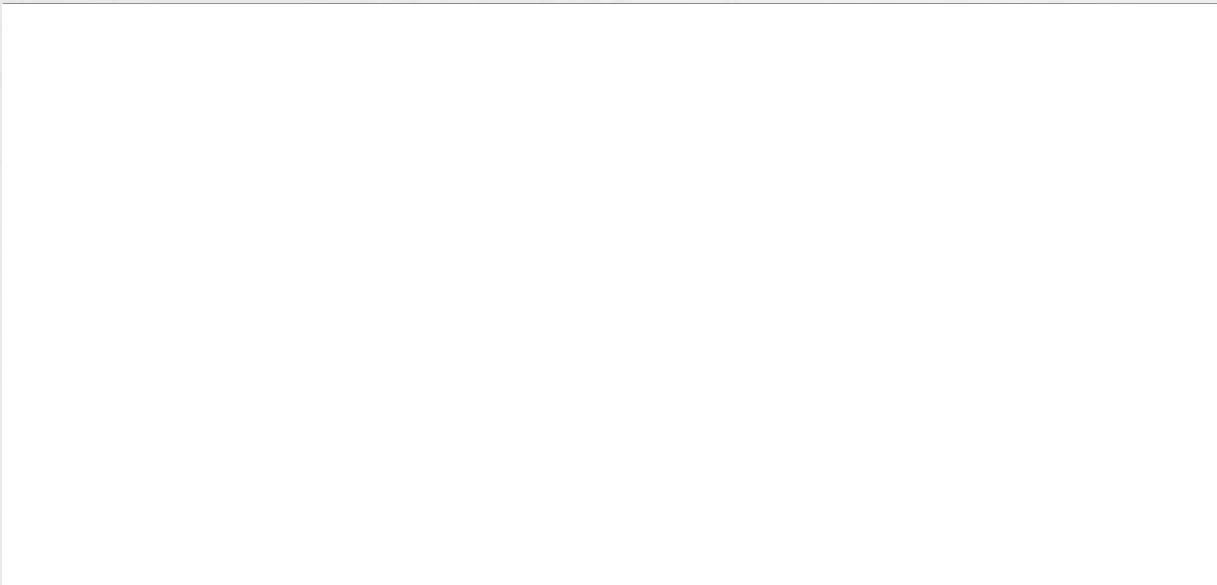


Figure 2-5. A schematic diagram of vertically orientated, irrigated, cylindrical burrow structures representing a bioturbated layer of functional micro-environment overlying an unburrowed sediment layer (adapted from Aller (2001)) and the resulting pore water concentration profile.

Numerous studies done over the years have shown that biogenic diffusion increases both contaminant fluxes and transport in the sediment-water column. For example, Sandnes *et al.* (2000) found biogenic particle reworking rates to be nine times greater than rates predicted using molecular diffusion alone. Reible *et al.* (1996) also found that contaminant fluxes from sediments increased due to tubificid oligochaete bioturbation-induced transport. Distribution of HOCs was also altered near the sediment-water interface as a result of macrofauna communities in a study conducted by Schaffner *et al.* (1997). Moreover, Thibodeaux *et al.* (2001) showed that bioturbation-driven soluble fraction transport for HOCs from bed sediment is faster than molecular diffusion, supporting the hypothesis that the controlling mechanisms for the observed behaviour are bioturbation, chemical desorption of contaminants to the sediment-water interface, followed by transport to the overlying water column.

Although the biodiffusion model has proven to be a significant modelling tool in predicting bioturbational effects, it still fails at some point to fit data observed in bioturbation studies. For instance, Ewald *et al.* (1997) found that the increased accumulation of 2,2',4,4'-tetrachlorobiphenyl (TCB) in sediments could be explained by a simple sorption-retarded diffusion model without including bioturbation. The

results were likewise echoed by Jönsson *et al.* (2000) in his study of PCB distribution in Baltic Sea sediments. Further, the luminophore experiment conducted by Mermillon-Blondin, *et al.* (2005) showed that the transport of hydrocarbon and heavy metals was not affected by biodiffusion.

The validity of the Fickian bioturbation model was critically examined by Boudreau (1986a; 1986b), Boudreau and Imboden (1987), Wheatcroft, *et al.* (1990), and recently, by Meysman, *et al.* (2003). From these studies, the biodiffusion model, in order to be considered local transport, essentially requires that sediment mixing should be (1) random relative to the spatial and temporal scales of the processes modelled (i.e., symmetry criterion); and (2) small-scaled relative to any sampling distribution (i.e., length criterion). Meysman *et al.* (2003), thus, deduced that the local biodiffusion formalism is a special case of a more inclusive formalism, the non-local exchange formalism.

In the CoReTranS model, contaminant transport as a result of bioturbation can thus be modelled as diffusion mechanism, where the diffusion coefficient is plugged in as a user-defined parameter.

2.3.3.3 Non-local exchange models. Biodiffusion models, despite their compelling simplicity and wide applicability, are still unable to mechanistically describe all effects of benthic fauna on contaminant transport. Complex internal geometric boundaries and time-dependent biogenic activity patterns were not realistically simulated by biodiffusion models. This gap eventually resulted in the second bioturbation formalism, called non-local exchange models (Boudreau, 1986b). As discussed further below, non-local transport is typically modelled as an additional sink/source term in general diagenetic models via either an irrigation formulation (Aller, 1980; Aller and Aller, 1998) or an integro-differential formalism (Boudreau, 1986b). The non-local bioirrigation model, originally derived from the cylindrical model (Eq. 2-17), simulates mass transfer across the tube walls due to molecular diffusion (Figure 2-1). The 1-D analogue of the surficial transport due to bioirrigation is given by:

$$\frac{\partial C}{\partial t} = \eta(C_w - C) \quad \text{Eq. 2-18}$$

where η is the mass transfer coefficient (1/s) and C_w is the contaminant concentration in the overlying water (g/m^3). In these models, the mass transfer coefficient is estimated a priori. Thibodeaux and Bierman (2003) recently proposed an empirical equation (equation 2-19) to evaluate the mass transfer coefficient, at the same time taking into account the effect of a sorption-retarded diffusion transport mechanism. The theoretical model distinctly defines the bioturbation effects on the bed side from the water boundary layer. That is,

$$\eta = \frac{1}{\beta + \frac{h_{bio}}{D_{bio}^{pw} K_{oc} f_{oc} \rho_B}} \quad \text{Eq. 2-19}$$

where η and β are the soluble release mass transfer coefficient and water boundary layer resistance coefficient (m/s), respectively, h_{bio} is the depth of the bioturbated layer (m), f_{oc} is the mass fraction of organic carbon in the sediment matrix and K_{oc} is the organic carbon normalised partition coefficient of the contaminant (L/kg). It is expected that less contaminant is released to the overlying water when this equation is used, due to contaminant partitioning to the organic matter in the sediment. Koretsky, *et al.* (2002), on the other hand, used a stochastic approach in quantifying bioirrigation. 3-D burrow networks of worms, shrimp and crabs were created to simulate burrow-network distribution in sediment zones using ecological parameters, such as depth-dependent burrow surface areas and radial diffusive length scales. Assessment of contaminant concentrations along the cylindrical burrow depth is planned in future investigations.

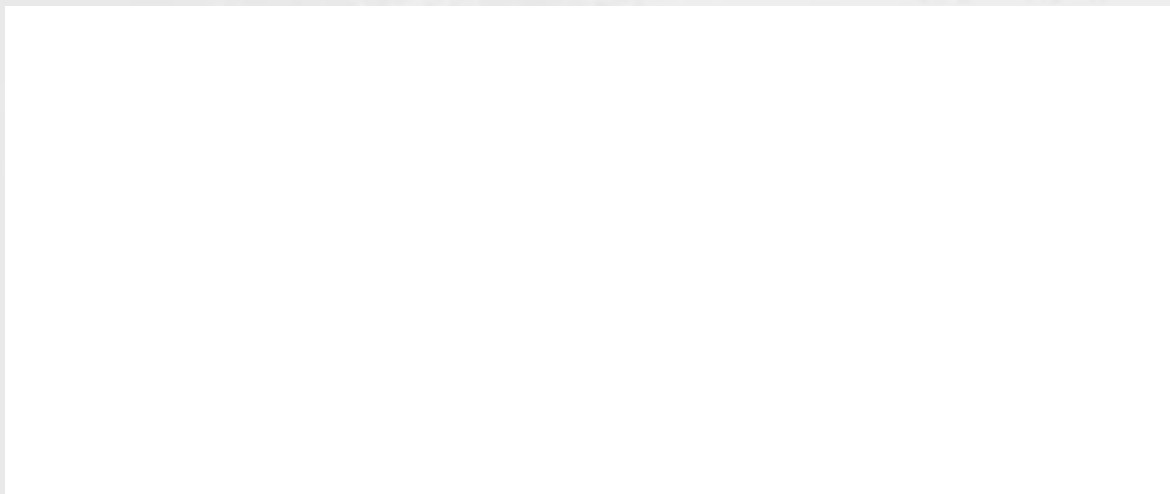


Figure 2-6. A schematic diagram of a complex burrow structure representing a spatially averaged non-local exchange transport of contaminants within the bioturbated layer and the resulting pore water concentration profile (adapted from Aller (2001)).

The second non-local transport formalism essentially accounts for the biogenic transport of solid sediment grains, which is not considered in the biorrigation model. A non-local exchange function in the form of an integro-differential equation (equation 2-20) was developed by Boudreau (1986b) to model the effect of head-down deposit feeding organisms in the bioturbated layer, emulating a conveyor-belt type mechanism. The exchange function was developed using stochastic principles in modelling particle displacement (Gardiner, 1985), which resulted in:

$$\frac{\partial C}{\partial t} = \int_0^L \phi K(x:x',t) C(x',t) dx' - \phi C(x,t) \int_0^L K(x':x,t) dx' \quad \text{Eq. 2-20}$$

where the exchange function $K(x:x',t)$ is evaluated from points (i.e., sediment depth) x to x' along the sediment layer.

Non-local exchange models are seldom used in bioturbation studies (Boudreau, 1986b; Boudreau and Imboden, 1987; Francois *et al.*, 1997; Francois *et al.*, 2001; Shull, 2001; Soetaert *et al.*, 1996b), presumably due to the complicated numerical solution required by integro-differential equations.

As such, a thorough understanding of the coupling of bioturbational activities with other contaminant fate and transport mechanisms in bed-sediments is needed. Further investigations should be done to assess bioturbational mechanisms using both chemical and ecological parameters. Moreover, studies of the depth-dependence of these modelling parameters, temporal variations of contaminant concentration within the burrow, and spatial distribution of burrow networks in the bed sediment should be pursued. In the CoReTranS model, the non-local exchange model was simulated using the simple irrigation formula (equation 2-18).

2.3.4 Sorption

2.3.4.1 Overview. HOCs are often immobilised within the solid matrix (i.e., organoclay fraction of the sediment) due to physical entrapment or electrostatic forces. This process is generally called *sorption* in reactive transport modelling terminology (Karickhoff *et al.*, 1979; Pignatello and Xing, 1996; Zheng and Bennett, 1995). When the contaminants are dissolved back to the pore water phase, this process is referred as *desorption*. When sorption is sufficiently fast and reversible, a local equilibrium at the sediment-pore water interface can be assumed (Rubin, 1983). Under the local equilibrium assumption, the change in contaminant concentration in pore water is instantly accompanied by a change in the sorbed concentration q in sediments. That is,

$$\frac{\partial q}{\partial t} = \frac{\partial q}{\partial C} \frac{\partial C}{\partial t} = \rho_B K \frac{\partial C}{\partial t} \quad \text{Eq. 2-21}$$

where q is the contaminant concentration on the solid phase (g/kg), K represents the slope of the sorption isotherm and ρ_B is the bulk dry density.

The sorption-desorption equilibrium is generally described using a linear partitioning model (equation 2-24) where the sediment organic matter is envisaged as a gel-like phase with relatively homogenous and amorphous structure (Chiou *et al.*,

Chapter 2

1979; Karickhoff *et al.*, 1979). The linear partitioning model has a single parameter, the partitioning coefficient K_D , defined as

$$K_D = \frac{q}{C} \quad \text{Eq. 2-22}$$

Further, K_D (L/kg) can be estimated from the relation

$$K_D = f_{OC} K_{OC} \quad \text{Eq. 2-23}$$

K_{OC} is estimated using a compound class-specific linear free energy relationship (LFER), based on the correlation between the contaminant's organic matter sorption coefficient and its octanol-water partition coefficient. That is,

$$\log K_{OC} = a_K \log K_{OW} + b_K \quad \text{Eq. 2-24}$$

Table 2-2 presents the slopes a_K and intercept b_K from equation 2-24 for the classes of contaminants used in this study.

Table 2-2. LFERs for organic contaminants: slopes and intercepts of equation 2-21

Contaminant	a_K	b_K	R^2 ^a	N_C ^b	References
PCB	0.74	0.15	0.96	32	(Sabljić <i>et al.</i> , 1995)
PAH	0.98	-0.32	0.98	14	(Chiou <i>et al.</i> , 1998)
Wide variety, mostly pesticides	0.54	1.377	0.74	45	(Kenaga and Goring, 1980)

^a correlation coefficient for the regression equation. ^b number of compounds used for LFER

The strong correlation observed between the organic carbon-normalised partition coefficient (K_{OC}) and contaminant octanol-water partition coefficient (K_{OW}) plus the simplicity of the linear model structure, have made it widely utilised in the field of fate and transport modelling.

Several works on sorption phenomena have shown, however, that the linear model is often inadequate as it underpredicts actual sorbed contaminant concentrations especially at low total dissolved concentrations of contaminants (e.g., Chiou *et al.*, 2000; Karapanagioti *et al.*, 2000; Klaneidam *et al.*, 1999; Xia and Ball, 1999; Xing and Pignatello, 1997). Nonlinear sorption behaviour is typically modelled using either a Langmuir (equation 2-25) or Freundlich isotherm (equation 2-26), (Schwarzenbach *et al.*, 1993; Weber Jr. and DiGiano, 1996), given by:

$$q = \frac{Q^o bC}{1 + bC} \quad \text{Eq. 2-25}$$

$$q = K_F C^{n_F} \quad \text{Eq. 2-26}$$

where Q^o is the maximum sorption capacity constant (g/kg), b is the solute-surface interaction energy-related parameter, K_F is the Freundlich capacity factor and n_F is the linearity parameter. The Langmuir isotherm model is based on the concept of a limited sorption capacity of the sediments, where the total sorption sites exhibiting the same free energy become saturated. The Freundlich model, on the other hand, assumes that there exist various types of sorption sites in abundance exhibiting different sorption free energies.

Sorption nonlinearity is generally explained using the concept of sediment organic matter (SOM) heterogeneity where organic matter is assumed to consist of an amorphous, rubbery, 'soft carbon' phase that exhibits relatively fast sorption (i.e., linear) and a relatively condensed, glassy, 'hard carbon' phase that exhibits slow sorption (i.e., non-linear) (Huang *et al.*, 2003; Pignatello and Xing, 1996; Weber *et al.*, 1992; Xing and Pignatello, 1997). The obvious analogy to this conception is a well-structured synthetic polymer. SOM was found to mostly comprise of humic substances with molecular weights ranging from hundreds to hundred thousands Daltons (Stevenson, 1994). The observed physicochemical properties of SOM similar to those of synthetic organic polymers include: matrix swelling due to solubilisation of hydrophobic organic compounds (Huang and Weber Jr., 1998; LeBouef and Weber Jr., 1997; Nkedi-Kizza *et al.*, 1989; Pignatello and Xing, 1996; Young and

Weber Jr., 1995) and glass transition temperature (LeBouef and Weber Jr., 2000a; LeBouef and Weber Jr., 2000b; Young and Weber Jr., 1995). Consistent with the SOM-polymer analogy, dual-mode sorption models for polymeric substances (Berens, 1978) were developed for SOM. For example, Brusseau *et al.* (1991) used a bicontinuum model based on first-order mass transfer to quantitatively define intra-organic diffusion as a rate-limiting process. In this model, sorption is predicted to occur in two domains: instantaneous and rate-limited. The model was treated as an intra-organic diffusion process by relating the calculated mass-transfer constant to a diffusion coefficient for polymers. Fundamentally, however, the first-order mass transfer model still represents an approximation of the diffusion process and thus could not fit experimental data as well as a diffusion model (Wu and Gschwend, 1986; Wu and Gschwend, 1988). The permeant/polymer model by Carroll *et al.* (1994) likewise used the bimodality of HOC desorption from sediments to predict diffusion rates.

Weber *et al.* (1992) changed the sorption modelling approach by conceptualising the Distributed Reactivity Model (DRM), a multiple reaction sorption phenomenon based on an improved conceptualisation of SOM heterogeneity. The model's basic premise is that the linear sorption behaviour is described as single partitioning into the rubbery phase of SOM while the nonlinear component is treated as a set of multiple reactions involving site energy heterogeneity (i.e., Freundlich-type isotherm). The overall sorption isotherm developed to describe the dual-mode sorptive property of SOM is given as,

$$q = X_L K_{D,L} C + \sum_{i=1}^m X_{NL}^i K_F^i C^{n_{F^i}} \quad \text{Eq. 2-27}$$

where X represents the mass fractions of the sorbed phase exhibiting linear (L) and nonlinear (NL) properties and m , the number of discrete reactive sorption domains, is given a value of either 1 or 2.

A simplification of the DRM resulted in the Dual Reactive Domain Model, also termed the Dual-Mode Model, (Huang and Weber Jr., 1997; LeBouef and Weber Jr., 1997; Xing and Pignatello, 1997):

$$q_T = q_L + q_{NL} = K_{D,L} + \frac{Q^{\circ}bC}{1+bC} \quad \text{Eq. 2-28}$$

where q_T is the total contaminant concentration on the solid phase. The simplified model assumes that the glassy polymer phase represents a limited sorption site with homogeneous surface energies, thus manifesting Langmuir-type behaviour.

In addition, the organic carbon-normalised sorption partition coefficient and Freundlich capacity parameter for a contaminant concentration of 1 $\mu\text{g/L}$ have been shown to correlate with the oxygen-carbon (O/C) atomic ratio of the SOM (i.e., a measure of its chemical polarity) (Grathwohl, 1990; Huang and Weber Jr., 1997; Karapanagioti *et al.*, 2000; Kleineidam *et al.*, 1999). By definition, the lower the O/C atomic ratio of the SOM, the more heterogeneous and complex the organic matrix becomes, thus increasing the nonlinear sorption capacity (Chiou *et al.*, 2000; Huang and Weber Jr., 1997). The O/C ratio dependence of sorption nonlinearity, however, has not been adequately explored in the literature. Moreover, SOM fractions such as kerogen and black carbon, detected on soil and sediment samples, were found to further exhibit non-linear partitioning phenomena (Accardi-Dey and Gschwend, 2002; Chiou *et al.*, 2000; Cornelissen and Gustafsson, 2005; Lohmann *et al.*, 2005; Song *et al.*, 2002).

Sorption onto these SOM fractions, often described as high surface area carbonaceous material (HSACM) (Chiou and Kile, 1998), shows significant deviations from the existing sorption models discussed above, prompting new modelling approaches to describe uptake of HOCs, especially at low concentrations on natural sorbents. A recent modelling approach, based on the Polanyi adsorption theory, showed that there exists an adsorption potential ε (J/mol) defined as,

$$\varepsilon = R_G T \ln (S / C) \quad \text{Eq. 2-29}$$

where S is the solubility of the solute (g/m^3) at temperature T (K) and R_G is the ideal gas constant (8.314 L/mol-K). The theory postulates that there is a fixed adsorption site on the particle surface where adsorption takes place. Two notable concepts were

introduced in this model: (1) solubility-normalised equilibrium concentration of solute; and (2) Polanyi-based adsorption over Langmuir-type as a ‘pore-filling’ mechanism within the micro-porous solid (Xia and Ball, 1999). The first concept addresses reported inconsistencies of concentration-dependent nonlinear isotherm coefficients (e.g., Freundlich) (Carmo *et al.*, 2000; Chiou *et al.*, 2000; Crittenden *et al.*, 1999). The second concept explains the need for a better model to quantify the effect of micro-porosity within the sorbent particle as the use of Langmuir-type model often results in exceeding values of adsorption capacity (Chiou and Kile, 1998; Xing and Pignatello, 1997). The pore-filling mechanism for the micro-porous solid is described by the Polanyi-Dubinin-Manes (PDM) model (Manes, 1998) (equation 2-30). That is,

$$q = V_o \rho_o \exp \left[\frac{-R_G T \left(\ln \frac{S}{C} \right)}{E} \right]^{m_{PDM}} \quad \text{Eq. 2-30}$$

where V_o is the maximum volume of sorbed contaminant per unit mass of sediment (m^3/kg), ρ_o , the contaminant density (kg/m^3), m_{PDM} , a fitting parameter, and E , the characteristic free energy of adsorption calculated from the vapour phase adsorption theory. Xia and Ball (1999; 2000) were the first to model sorption of organic compounds on natural sorbents using a combination of linear partitioning isotherm and nonlinear PDM isotherm. Kleineidam *et al.* (2002) modified the isotherm equation by incorporating a fraction of organic matter available for partitioning. That is,

$$q = V_o \rho_o \exp \left[\frac{-R_G T \left(\ln \frac{S}{C} \right)}{E} \right]^{m_{PDM}} + f_{OC} K_D C \quad \text{Eq. 2-31}$$

The parameter f_{OC} is estimated using the method proposed by Gustafsson and Gschwend (1998) while K_D is predicted using published correlations between K_{OC} and K_{OW} . The PDM model certainly showed that adsorption as a ‘pore-filling’

mechanism significantly contributes to the nonlinear sorption behaviour of HOCs both in single solute and binary solute sorption experiments (Yong *et al.*, 2004). Xia *et al.* (2001) later showed, however, that the Polanyi-based approach still failed to explain hysteresis and gave diverse values of volumetric pore capacity. Further to this, the model has been shown to contain too many parameters to be optimised and thus, may pose too much uncertainty (Ran *et al.*, 2004; Xia and Ball, 2000). On a positive note though, the PDM model is still in its early stage of conception and thus could be fully developed as further investigations ensue. As such, the PDM model was not used in predicting the effect of sorption on fate and transport of organic contaminants simulated in this study.

While sorption-desorption equilibrium is considered in this section, it is important to note that the equilibrium assumption is not always appropriate to describe sorption. When the sorption process is not fast compared with the contact time between contaminant and sediment, sorption is aptly characterised as a rate-limited reaction process (Bahr, 1989; Bouchard *et al.*, 1988; Valocchi, 1988). Several mathematical kinetic models for sorption including first-order and multiple first-order rate laws have been incorporated in reactive transport models showing goodness of fit with actual data (e.g., Miller and Pedit, 1992; Pedit and Miller, 1994; Weber *et al.*, 1991). Fit to a particular model, however, does not represent proof of mechanism. Further, sorption is often kinetically hysteretic, meaning that the rate by which contaminants are adsorbed onto the sediment particle are relatively faster than the rate by which they are desorbed back into the pore water. Several studies have investigated the cause of sorption-desorption hysteresis but this phenomena remains poorly understood and therefore, difficult to model (Braida *et al.*, 2003; Miller and Pedit, 1992; Weber *et al.*, 1998).

In the succeeding sections, the probable mechanisms for sorption as a rate-limited reaction process are discussed as well as the effect of sorption on contaminant fate and transport in natural systems.

2.3.4.2 Mechanisms of slow sorption. Over the years, a number of mechanisms have been proposed to explain sorption of contaminants onto sediment particles as a rate-limited (i.e., slow) reaction process (Daniels *et al.*, 1998; Huang *et al.*, 2003;

Pignatello and Xing, 1996; Weber *et al.*, 1992). From these studies, slow sorption may be either due to high activation energy of sorption bonds or retardation of contaminant diffusion to sorption sites. Adsorption of neutral organic compounds to flat and rigid surfaces, however, is typically unactivated due to control by weak molecular interactions (e.g., van der Waal's forces, dipole-dipole, etc.) and is therefore instantaneous (Adamson, 1976). Thus, most studies attribute slow sorption of HOCs to some form of retarded diffusion.

As presented in Figure 2-7, in order for diffusing contaminant molecules to reach all potential sorption sites, they must traverse (1) through a stagnant layer at the surface of the particle (surface diffusion), (2) pores within the sediment particle (pore diffusion), and (3) penetrable solid phases (matrix diffusion). However, diffusion through a stagnant film at the surface of the particle was shown to be insignificant compared to the other two diffusion mechanisms (Miller and Pedit, 1992; Miller and Weber Jr., 1988; Weber Jr. and Miller, 1988). Models developed to account for slow sorption via retarded diffusion phenomena can thus be categorised as intra-organic (matrix) diffusion or intra-particle (pore) diffusion models. A number of these models are summarised in Table 2-3.



Figure 2-7. Schematic diagram of the three types of diffusion processes where contaminant molecules traverse through a stagnant film at the surface (A), mesopores (B) and micro-pores (C), and within the particle and penetrable solid phase (D) of the particle (adapted from Pignatello and Xing (1996)).

Table 2-3. Summary of sorption-retarded diffusion models

Model	Assumptions	Limitations
Bicontinuum intra-organic diffusion model based on 1 st order mass transfer (Brusseau <i>et al.</i> , 1991)	Sorption is predicted to occur in two domains: instantaneous and slow process	Use of first-order mass transfer as an estimate to the diffusion coefficient
Permeant/Polymer diffusion model (Carroll <i>et al.</i> , 1994)	Diffusion in two organic phases within the sorbent matrix	Use of Permachor equations to estimate diffusion coefficient
Distributed Reactivity Model (McGinley <i>et al.</i> , 1993; Weber Jr. and Huang, 1996; Weber <i>et al.</i> , 1992; Young and Weber Jr., 1995)	Linear partitioning occurs in the rubbery phase of OM while the nonlinear sorption occurs in the glassy phase.	SOM heterogeneity is not fully investigated yet.
Dual Reactive Domain Model (Huang and Weber Jr., 1997; LeBouef and Weber Jr., 1997; Xing and Pignatello, 1997)	glassy polymer phase represents a limited sorption site with homogeneous surface energies, thus manifesting Langmuir-type behaviour	Sorption mechanism is not fully elucidated
Polanyi-Dubinin-Manes Model (Kleineidam <i>et al.</i> , 2002; Xia and Ball, 1999; Xia and Ball, 2000; Xia and Pignatello, 2001)	Combined adsorption and linear partitioning sorption mechanisms	Extensive use of fitting parameters
Intraparticle (pore) diffusion model (Wu and Gschwend, 1986)	Diffusion through sediment pores is slow and is therefore rate-limiting	May produce erroneous conclusions when extrapolated to actual data
Two-compartment diffusion model (Ball and Roberts, 1991; Pignatello <i>et al.</i> , 1993)	Instantaneous sorption equilibrium followed by pore diffusion	Need for a second fitting parameter
Dual-intra-aggregate porosity model (Farrell and Reinhard, 1994)	Considers both meso- and micro-pore sizes	Erroneous conclusion may be drawn when micropore adsorption is significant
Two-domain radial diffusion model (Shor <i>et al.</i> , 2003b)	Weighted linear combination of fast and slow diffusive process	Use of a single representative diffusion coefficient

The intra-particle diffusion model assumes that the diffusion process is retarded by adsorption of contaminant molecules to pore walls which may or may not be coated with organic matter (Pignatello and Xing, 1996; Wu and Gschwend, 1986). Pore diffusion models have been mostly described using Fick's second law in spherical coordinates,

$$\frac{\partial C}{\partial t} = \frac{D_{eff}}{r_D^2} \frac{\partial}{\partial r} \left(r_D^2 \frac{\partial C}{\partial r} \right) \quad \text{Eq. 2-32}$$

where r_D is the radial distance from the particle centre (m). The effective intra-particle diffusion coefficient, D_{eff} , is corrected for retardation by sorption within intraparticle porosity using a partitioning coefficient, K_D .

Several variations of pore diffusion models have been developed to explain various sorption behaviours. For example, Wu and Gschwend (1986) modelled a radial diffusive penetration of HOCs to natural sediments and soils using an experimentally fitted effective diffusion coefficient parameter. The model, however, was only tested over a small range of concentrations from laboratory experiments and thus may produce erroneous conclusions when used to predict actual data. Ball and Roberts (1991) introduced a two-compartment diffusion model which assumes an instantaneous equilibrium followed by pore diffusion mechanism. The data were fitted more accurately than those obtained from shorter term experiments using two fitting parameters. However, the model predictions among various size fractions were still not consistent. In addition, a dual-intra-aggregate porosity model was also developed to account for the effect of porosity structures (i.e., meso- and micro-porosity) (Farrell and Reinhard, 1994). Linear and nonlinear sorption behaviours were modelled separately using diffusion coefficient-sorption isotherm relations. For the nonlinear behaviour, the Freundlich isotherm model was used. That is,

$$D_{eff} = \frac{D}{1 + \frac{\rho_B}{\phi} [K_F n_F C^{n_F-1}]} \quad \text{Eq. 2-33}$$

Nonetheless, the validity of a representative D_{eff} based on homogeneous pore distribution remains in question. Recently, Shor *et al.*, (2003b) modelled desorption kinetics of field-aged PAHs from sediments using a two-domain radial diffusion model where a weighted linear combination of fast and slow diffusive processes is used. The model, however, did not produce good results for less hydrophobic PAHs and sediments with lower organic matter content.

In this study, contaminant sorption can be modelled using either a single isotherm (linear, Freundlich or Langmuir) or combinations of these isotherms.

2.3.4.3 Sorption to colloids. Colloids in subsurface systems have long been recognised to impact contaminant transport either due to partitioning or sorption phenomena (McCarthy and Zachara, 1989). Colloidal particles, typically 1 to 10 nm in size, can easily absorb contaminants due to their large specific surface areas filled with numerous reactive sites. Humic substances, metal oxides, extracellular polymeric substances from biotic populations, and other dissolved organic carbon (DOC) mostly comprise these colloidal particles. Colloids have been shown to increase the rates of geochemical cycling of trace metals in aquatic systems (Gueguen and Dominik, 2003; e.g., Wells *et al.*, 2000; Wen *et al.*, 1999) and contaminant transport and persistence in soils and aquifers (e.g., Ryan and Elimelech, 1996; Shimizu *et al.*, 1998). In aquatic sediments, colloidal particles likewise affect the distribution of hydrophobic organic contaminants. For instance, Tye, *et al.* (1996) quantitatively described colloid effects on hexachlorobenzene adsorption and partitioning. The study revealed that the measured partition coefficients and adsorption rates depend on the colloidal concentration in pore waters and amount of organic matter in sediments. Colloidal- and dissolved organic matter from protozoan grazers have also been shown to control PCB speciation in sediments (Kujawinski *et al.*, 2001). Lower HOC bioavailabilities and slow desorption process have likewise been attributed to colloidal particles resulting from the condensation of organic matter in aquatic sediments (Galle *et al.*, 2005).

Modelling colloid-enhanced contaminant transport requires judicious differentiation between colloidal organic matter and DOC. Several models based on the three-phase partitioning theory for HOC among the sediment particle, colloidal phase, and DOC have been developed for porous media assuming colloidal interaction with contaminants at equilibrium. For example, Abdel-Salam and Chrysikopoulos (1995) predicted contaminant transport based on concentrations in colloidal particles using a modified Freundlich, reversible equilibrium, sorption equation. Using their model, the mobility of contaminants can either be increased or decreased by colloidal concentrations. Recently, Bekhit and Hassan (2005) developed a two-dimensional contaminant transport model in porous media to investigate the different interactions between colloids, contaminants, and porous media under homogeneous conditions. The model showed that the effective retardation factor can be increased under certain combinations of sorption/desorption rates and partitioning coefficients. The underlying significance of colloids in contaminant transport is certainly important, thus the need to further study colloidal characteristics and their effect on contaminant mobility. Most of the recent findings on colloidal transport however remain untested in a wide range of field applications. These demonstrations can be facilitated by a fully integrated reactive transport model.

2.3.5 Degradation

2.3.5.1 Overview. Degradation of organic contaminants in bed-sediments can be chemically and/or biologically mediated. Chemical degradation pathways include hydrolysis, reduction-oxidation (redox) processes and photochemical reactions (Leenheer, 1991). Favourable geochemical and hydrological conditions such as pH changes and elevated oxidant-reductant concentrations (e.g., O₂, Fe(II, III), Mn(II, IV), OH radicals) basically drive the abiotic degradation of HOCs. For example, in a study conducted by Klupinski *et al.* (2004) on pentachloronitrobenzenes, a class of fungicide originally thought to degrade biologically, the contaminant was observed to undergo reduction via a surface-association process in the presence of Fe(II) and goethite. Abiotic degradation was likewise shown for fluoroquinolone antibacterial agents via oxidative transformation by manganese oxide in sediment studies (Zhang and Huang, 2005) and photolytic degradation in aqueous experiments (Fasani *et al.*, 2001). Biotic degradation, on the other hand, is primarily due to the diverse and

dynamic microbial population in the aquatic ecosystem. Microorganisms could metabolise or co-metabolise substrates such as HOCs, which do not even yield much energy, under various redox conditions (i.e., aerobic, anaerobic, sulphate-reducing or methanogenic bacteria). For example, Tixier *et al.* (2003) quantified removal rates of six pharmaceutical contaminants in surface water at real environmental conditions via biodegradation and phototransformation while Tang *et al.* (2005) showed that phenanthrene in undisturbed-sediments is degraded under anaerobic conditions. Further, Massias *et al.* (2003) showed that linear and isoprenoid acyclic petroleum hydrocarbons can be biodegraded below the bioturbated zone under anoxic conditions after 6 to 24 months of incubation. Biodegradation of methyl-*tert*-butyl-ether (MTBE) under a range of anaerobic terminal electron-accepting conditions (SO_4 , Fe(III), Mn(IV), NO_3 , O_2) resulted in decreased *tert*-butyl alcohol concentration, a toxic co-contaminant, and increased mineralization of MTBE to CO_2 in the absence of methanogenic activity (Bradley *et al.*, 2001).

The impact of organic contaminant degradation on fate and transport in bed-sediments is typically predicted using a first-order kinetic rate law. That is,

$$\frac{dC}{dt} = \lambda C \quad \text{Eq. 2-34}$$

where λ is the degradation rate constant (1/s). Degradation curves from a study on biodegradation of aromatic amines done by Bornick *et al.* (2001) were logarithmic. Similarly, biodegradation kinetics of two phenoxy acid herbicides in groundwater and sediments at low concentration followed first-order rate laws (Torang *et al.*, 2003). Concentrations of pesticide contaminant and its five degradation products were likewise simulated assuming first order kinetics and irreversible degradation (Gonzales *et al.*, 2001). Recently, Allan *et al.* (2004) used two distinct degradation rates for the oxic/anoxic regions to model transport and distribution of lindane and simazine in river bed-sediments. The inclusion of the first-order equation in general reactive transport models typically approximates both abiotic and biotic degradation where the degradation constant estimates may not be constant with time nor sediment depth. Thus, in this study, contaminant degradation is modelled using a first-order kinetic rate law.

Over the years, several issues regarding the significance of biodegradation have emerged in connection with fate and transport of contaminants and their subsequent remediation. These include bioavailability and contaminant sorption to both sediment and colloidal particles in the benthic layer. The following sections discuss these relevant issues.

2.3.5.2 Sorption/desorption-limited contaminant bioavailability. The extent of microbial degradation in bed-sediments is highly dependent on the amount of contaminant available to biological organisms, or what is typically called the contaminant's bioavailability. Several definitions of bioavailability (Ehlers and Luthy, 2003; European Center for Ecotoxicology and Toxicology of Chemicals (ECETOC), 2002; National Research Council, 2002) have been proposed but no authoritative definition has yet been agreed upon, presumably due to the emerging status of the concept's regulatory acceptance as well as the lack of a standard quantitative methodology to evaluate bioavailability.

The bioavailability of hydrophobic organic contaminants in sediments is influenced by several factors including sorption/desorption phenomena, microbial characteristics, chemical variation, and environmental conditions, either independently occurring or in combination (Alexander, 2000). Insufficient oxygen supply is postulated to hinder HOC degradation in a field study conducted by Madsen *et al.* (1996). It is likewise known that a certain concentration threshold for HOCs needs to be reached before significant biodegradation occurs (Bosma *et al.*, 1997). Previous studies have also hypothesised that contaminant dissolution is necessary for biodegradation (Manilal and Alexander, 1991; Volkering *et al.*, 1992). In these cases, it is postulated that the amount of dissolved contaminant available for biodegradation is highly dependent on desorption of contaminants from either organic matter or intra-particle compartments within sediments grains. Desorption rates in turn are mainly controlled by absorption of HOCs and sorption-limited mass transfer from sediment to water (e.g., pore water, overlying water) (Manilal and Alexander, 1991; Nam and Alexander, 1998). For instance, Shor *et al.* (2003a) showed that intra-aggregate mass transport limitations (i.e., micro-, meso-porosity) influenced biodegradation rates the most. Biodegradation rates were predicted using a two-

domain intra-aggregate mass transport model (Shor *et al.*, 2003b), where the fast-diffusion regime essentially dictates the rate of biodegradation. On the other hand, Woo *et al.* (2001) examined models without sorbed-phase degradation and found that they were insufficient to describe the biodegradation process. Their study used a non-steady state model that simulates the interaction between sorption and biodegradation, showing that microorganisms attached to the surface of the particles are able to degrade desorbing chemicals faster. Further, microbial properties and the knowledge to manipulate them play a most important role in contaminant degradation. Calvillo and Alexander (1996) proposed three mechanisms for microbial contaminant utilisation, which include sorbed-phase degradation, production of natural surfactants and physical acquisition of the substrate. The adaptive capability of microorganisms also influences contaminant biodegradation (Haack and Bekins, 2000). The addition of surfactants, either to enhance biodegradation or stimulate contaminant mobilisation, has also received attention from previous studies (Kim and Weber Jr., 2003; e.g., Schmitt, 1992). Understanding the interplay between bioavailability and the factors that affect it is crucial, not only in reactive transport modelling but also in the remediation of contaminated areas.

2.3.5.3 Biofilms. Biofilms are ubiquitous. From plaques in teeth to vast mats in aquatic beds, these organism-containing slime layers are well-structured microbial communities with high levels of organisation and coordinated functionalities. The application of advanced technologies such as fluorescence microscopy (FM) and confocal scanning laser microscopy (CSLM) have significantly revealed biofilm heterogeneity (Lawrence *et al.*, 1991). Once viewed as a flat impermeable layer, biofilms are now visualised as elaborate 3-D patches of cell clusters embedded in a dense extracellular polymeric substance (EPS) matrix with void spaces serving as water channels (Davey and O'toole, 2000). The EPS matrix serves many functions including protection, attachment, and microbial growth (Decho, 1990; Nguyen and Schiller, 1989). The formation of microcolonies within the biofilm, either single-species populations or mixed bacterial assemblages, is highly dependent on key environmental parameters, namely physicochemical properties of surfaces and interfaces, nutrient availability and hydrodynamics. Romani and Sabater (2000) further suggested that ionic content of the water and chlorophyll *a* concentration in biofilms both stimulate extracellular enzyme activity in streams. These bacterial

communities have long been recognised to produce and degrade organic matter including pollutants, cycle nutrients and assimilate metals (de Brouwer *et al.*, 2002; Flemming, 1995; Rocher *et al.*, 2004; White, 1995). For instance, Schorer and Eisele (1997) detected varying concentrations of selected heavy metals (e.g., Cu, Zn, Pb), PAHs and PCBs sorbed in aquatic biofilms and sediment particles. Sorbed contaminant concentrations in sediments were shown to be significantly influenced by biofilm conditions. Wide ranges of butyltin concentrations, presumably from antifouling paints of ships, barges and other fishing vessels, were also observed in biofilms along the west coast of India (Bhosle *et al.*, 2004). PCB degradation was also significant in recently discovered microbial consortia capable of dehalorespiration in biofilms (Abraham *et al.*, 2002).

Transport of contaminants across biofilms is typically diffusive in nature, although advection has been known to occur as well, due to voids within the structure (de Beer *et al.*, 1994b; de Beer *et al.*, 1994a). Sorption is likewise significant in the fate and transport of contaminants in biofilms (Allan *et al.*, 2005; Headley *et al.*, 1998). These mass-transfer mechanisms essentially control microbial activity and therefore contaminant degradation in biofilms. For example, de Beer and Kuhl (2001) modelled contaminant flux (J_{film}) across biofilms as

$$J_{film} = k_o \sqrt{\frac{2D_{eff}C}{k_o}} \quad \text{Eq. 2-35}$$

where k_o is the zero-order reaction rate constant ($\text{g}/\text{m}^3\text{-s}$). The model assumes partial penetration (i.e., contaminant is partially consumed before penetrating the base of the biofilm) and low microbial conversion (Boudreau and Westrich, 1984), hence the zero-order approach. A biodegradation model adapted from trickling filters was also used to predict degradation of linear alkylbenzene sulphonate (LAS) in a riverine system (Boeije *et al.*, 2000). The model considered contaminant degradation from both bulk water and biofilm. The seemingly simple empirical equation describing contaminant transport in biofilms conceals the complexity of the underlying mechanisms.

2.3.6 Sediment deposition and resuspension

Contaminant remobilisation from bed-sediments to overlying water may be facilitated by natural or anthropogenic activities in aquatic environments. Bioturbation and episodic events such as storms, tidal currents and seasonal flooding can result in large sediment disturbances. Human activities such as dredging operations and contaminated waste disposals are known to cause massive sediment mixing. These disturbances subsequently lead to changes in physical and chemical sediment properties (Eggleton and Thomas, 2004). For example, anoxic sediments become exposed to oxic conditions, thereby accelerating contaminant degradation (Simpson *et al.*, 1998b; Wainright and Hopkinson, 1997). Lin *et al.* (2003) further showed that the change in oxic state affects diffusive flux of contaminants across the sediment-water interface. Contaminant redistribution in sediment particles, both in place and suspended, is also influenced by these resuspension events. Latimer, *et al.* (1999), using a particle entrainment simulator, predicted increased HOC concentrations in both resuspended particles and the overlying water. Dissolution of PAH was increased by a factor of three while linear partitioning to sediments, up to a factor of two. Ko and Baker (1995) on the other hand, showed that sediment resuspension over short time scales (e.g., hours, days) impacts HOC distribution in the water column. For longer time scales, HOC partitioning to sediment particles and burial control the distribution of these contaminants. Various models were developed to account for the effect of sediment resuspension and deposition on fate and transport of contaminants. Boudreau and Imboden (1987), using a burrow-and-fill mixing model, gave a non-local exchange transport description for the net sediment mixing rate, R_N . That is,

$$R_N = -K_S(x,t)[(1-\phi)q - (1-\phi(0))C_o] \quad \text{Eq. 2-36}$$

where the sediment-removal rate constant $K_S(x,t)$ is assumed to be equal to the sediment-filling rate (Jørgensen and Boudreau, 2001). Sherwood *et al.* (2002) on the other hand, integrated sediment deposition and contaminant loss from sediment resuspension by wave action in a one-dimensional advection-diffusion equation. In Sherwood's model, sediment deposition was simulated as an advection process using estimated burial velocities. Models incorporating wave and tidal effects on sediment

resuspension have been developed as well (Kuhrts *et al.*, 2004; e.g., Wang *et al.*, 2005). However, the full impact of sediment deposition and resuspension on contaminant fate and transport is still uncertain as a cohesive and effective predictive model is yet to be developed. Thus, in this study, sediment deposition is integrated into the CoReTranS model as a simple advective mechanism.

2.4 Modelling approaches

2.4.1 Analytical approach

Analytical models are extensively applied in understanding contaminant transport mechanisms and predicting solute transport in conjunction with column experiments. They use exact solutions of the model equation describing the fate and transport of contaminants which are often simplified in order to produce such solutions. They are often used as a starting point in describing contaminant migration before moving on to more sophisticated numerical models (Liu and Ball, 1998). Alternatively, they provide useful tools for validating numerical approaches.

Analytical models also afford a fast and computationally efficient approach in assessing contaminant migration. With the aid of a spreadsheet, numerous parameter correlations (e.g., C/C_0) and variations can be determined rapidly. In addition, techniques for uncertainty analysis (e.g., Monte-Carlo) can be easily applied to these models where the analytical model is used as an “approximation” (e.g., Monte-Carlo probabilistic index) to a more detailed model in a simulation.

Analytical models however are characteristically applicable only to simple contaminant transport systems due to the need to produce exact solutions. Spatial and temporal variability (e.g., nonlinear sorption mechanisms) cannot often be accommodated as the resulting transport equation becomes too difficult to solve. Moreover, the use of simplifying assumptions requires detailed arguments to support the modelling approach adopted. In most cases, though, assumptions leading to the use of superposition principles have been accepted (Liu *et al.*, 1998) where problems with similar linear boundary conditions are resolved into simpler sub-problems, the

individual solution of which are summed up for the overall solution of the problem. Van Genuchten and Alves (1982) have compiled a list of available analytical models for the one dimensional convective-dispersive transport of a single chemical constituent under transient fluid flow conditions.

Laplace transformation is often the method of choice in deriving the analytical solution for a one-dimensional multi-layered contaminant transport system (Carslaw and Jaeger, 1959; Leij and Genuchten, 1995). Leij and van Genuchten (1995) have derived an approximate analytical solution for solute transport in two-layer systems using a Laplace transform assuming a constant boundary and initial conditions. The binomial theorem was then used to cast the solution back in the real time domain. Alternatively, adjoint solution techniques and finite integral transforms (Mikhailov and Özisik, 1984) can be used to derive the exact solution of advection-diffusion equations. Complications arise when the concentration for an upper layer follows directly from the concentration predicted at the top of a lower layer (i.e., concentration and flux continuity at interfaces). The governing equation can be simplified by either assuming an unrealistic zero concentration gradient at the interface between the layers (Al-Niami and Rushton, 1979) or a steady-state flow (Kreft, 1981).

2.4.2 Numerical approach

Numerical models for contaminant fate and transport in porous media allow characterisation of more complex processes than analytical models. Complexities such as nonlinear behaviour (e.g., porosity as a function of depth, nonlinear sorption) arising from wide temporal and spatial variations can be accommodated by a numerical approach. For example, diffusive transport of organic contaminants has been progressively modelled from a simple Fickian process (Goldberg and Koide, 1962) to a spatially explicit transport mechanism affected by sediment physical (Allan *et al.*, 2004; Boudreau, 1996) and organic matter content heterogeneity (Chiou *et al.*, 2000; Kleinedam *et al.*, 2002; Xia and Pignatello, 2001). The presence of a diverse benthic community and its contribution to the fate and transport of organic contaminants in bed-sediments has been investigated using numerical modelling

studies as well (Choi *et al.*, 2002; Francois *et al.*, 2001; Meysman *et al.*, 2003). Numerical simulations can also produce unrealistic results especially if model parameters are “fitted” with values outside the typical range found in the literature to reduce relative errors between the numerical results and the actual data.

Numerical models are highly dependent on a robust understanding of the contaminant problem and the availability of sufficient data for validation. Once the processes affecting contaminant transport are reduced to simplified equations, a wide range of numerical codes and solution techniques are available to solve the resulting equations. The most common approach in numerical modelling is the use of either finite difference or finite element methods (Zheng and Bennett, 1995). In finite difference methods, the transport equations are approximated using grids representing the changes in the property values that describe the model system. A finite element method, in contrast, uses a mesh of elements, typically triangular or quadrilateral in shape, to represent the spatial domain. The variation in property values across each model element is approximated by polynomial functions.

2.5 Reactive transport modelling environment

Model codes built using a traditional procedural programming style are often hard to modify or extend. Modified models written in this style, once applied to simulation scenarios other than that for which they were originally intended, often result in oversimplifications and diminished predictive capability (Meysman *et al.*, 2003b). Further, new modelling requirements can not be accommodated in legacy models written in a traditional programming style due to inherent limits in algorithm flexibility and model extensibility. Scientists and engineers with minimal modelling skills are thus forced to cope with this situation, facing steep learning curves when legacy models require complex modifications. More often, a simpler model is produced either analytically, or using electronic spreadsheets. To address these constraints in the modelling practice and make it easier to change aspects of a model without rewriting large portions of the code, modelling environments have been introduced (Argent, 2004; Reed *et al.*, 1999).

Chapter 2

Modelling environments are built using an architecture that offers the benefits of modularity, whereby different configurations of the building blocks (e.g., contaminant species, transport processes, parameters) can be easily assembled to describe complex model systems without rewriting the underlying code and performing subsequent recompilation. Graphical visualisation tools and interactive features can be added to support the dynamic structure of a modelling environment and assist the simulation process.

An effective way of designing and constructing a modelling environment is to use the Object-Oriented (OO) paradigm, which offers structural flexibility and robustness, and code reusability and extensibility (Page-Jones, 2000; Pressman, 2001). Under the OO approach, entities in the system being modelled are represented as 'objects' that have attributes and methods. The attributes store the state of an object, while the methods can be invoked to get an object to carry out tasks. An object is an 'instance' of a class that defines how that particular kind of object is actually implemented in code. A class effectively provides a template that can be used to create as many objects of its particular kind as needed during a simulation.

When a simulation is run, objects are created and communicate by invoking methods on one another. Thus, the resulting model can be viewed as a collection of interacting objects and a particular simulation characterised as a sequence of method invocations between objects. The major advantage of objects is that they can be combined and substituted for each other in very flexible ways when a simulation is run. This allows a simulation to be configured dynamically from a collection of available objects without having to modify the code of the simulation application.

A wide range of modelling environments has been developed for various disciplines in reactive transport modelling. For example, early diagenetic processes can be investigated using MEDIA (Meysman *et al.*, 2003c) where elements, species, parameters and reactions are modelled as objects that users can simply select from a toolbox. Li and Liu (2003) have developed the Interactive Groundwater (IGW) software, a novel 'digital laboratory' for groundwater research, where modellers and students can investigate and visualise groundwater systems. Other environmental modelling environments such as the Ecological Component Library for Parallel

Spatial Simulation (ECLPSS) (Wenderholm, 2005), the Java implementation of the Discrete Event System (JDEVS) (Filippi and Bisgambiglia, 2004), the Interactive Component Modelling System (ICMS) (Reed *et al.*, 1999), the Spatial Modelling Environment (SME) (Voinov *et al.*, 1999), and the Modular Modelling System (MMS) (Leavesley *et al.*, 1996; Leavesley *et al.*, 2002) have been developed to simulate various environmental processes. These modelling environments all incorporate scientifically defensible mechanisms to describe relevant physical, chemical and biological processes in a user-friendly package which share the following desirable features:

- a modelling (or *problem-solving*) environment that provides a virtual problem domain equipped with visualisation and advanced numerical solvers designed for model construction where components are selected from a toolbox or built based on existing templates;
- a suite of graphical user interface (GUI)-based simulation control components that facilitates selection of model scenarios and input/output (I/O) data operations employing text editors for code generation and compilation and/or single button click implementation;
- a computing resource package that provides numerical solutions, optimisation procedures, and statistical analyses;
- a database management system for an easy data retrieval process that is interoperable with the simulation process to optimise modelling functionalities; and
- an efficient documentation system for operational use and maintenance purposes.

2.6 Challenges in modelling reactive transport of contaminants in bed-sediments

With the maturation of the field of reactive transport modelling in bed-sediments, the main challenge is to apply existing mathematical model formulations to actual field systems as interpretative tools for further understanding the complex interactions within the system and enable future predictions of contaminant fate and transport. Reactive transport modelling must also go beyond the simple heuristic function of reactive transport models as defined by Oreskes *et al.* (1994) making them impossible to validate (i.e., a model is never identical with what it models).

The obvious prerequisite to an effective reactive transport model is therefore to ensure that all relevant processes have been adequately captured in the model. Utilising first-principles representation of the fundamental processes occurring in bed-sediments is one approach in developing reactive transport models as 'mechanistic' models. However, due to the underlying complexity of the system, parameterisation and model calibration are sometimes necessary, consequently adding a certain degree of empiricism to the model. 'Empirical' models, in contrast, can potentially capture the fate and transport of contaminants in bed-sediments using extensive data and some calibrated parameters. However, while empirical models guarantee goodness of fit, these modelling approach limits the model application in describing other field systems (e.g., other contaminated sites). Further, the ultimate test in assessing the effectiveness of a particular model, whether mechanistic or empirical, is its ease in using a number of field observations to explain the system.

The field of reactive transport modelling is continuously evolving. Various research groups on the distribution of HOCs in natural bed-sediments have significantly contributed to the pool of knowledge collected over the years. This chapter has reviewed, in some detail, current trends and issues relevant to the mechanistic description of contaminant fate and transport in bed-sediments, highlighting potential areas for future research. Thus, the following key points can be made:

- Understanding fate and transport of HOCs in sediment environment, the resulting impact on the environment and human health is crucial in the

overall framework of environmental protection. Presently, reactive transport modelling offers tremendous support in investigating new conceptual arenas, allowing knowledge gaps in sediment contamination to be addressed through multiple hypothesis testing.

- Individual components of reactive transport modelling have certainly advanced. Mechanistic descriptions of reaction and transport processes in bed-sediments have considerably improved. For example, the once-vague sorption-related processes are slowly becoming mechanistically coherent. The role benthic fauna play in contaminant fate and behaviour is increasingly understood. Moreover, technical development of model codes has reached a new level as programming paradigm shifted from procedural programming to object-oriented approach. The main challenge then is to integrate all this new-found knowledge into a single model embedded in a user-friendly software package where scientists and modellers alike can continue to investigate fate and transport of contaminants in bed-sediments.
- The environmental modelling environment developed to date can easily facilitate integrated modelling applications and further research on fate and transport of HOC in bed-sediments. The use of a problem-solving environment equipped with a graphical user interface will enable selection of simulation scenarios from a well structured database system. Automatic generation of model documentation on the other hand will facilitate an effective feedback mechanism for further model improvements. Reactive transport modelling as an integrated tool will therefore enable identification of critical processes and parameters that control contaminant fate and transport in bed-sediments in order to further guide field and experimental studies.

CHAPTER THREE

CoReTrans: an object-oriented modelling environment for organic contaminant reactive transport in bed-sediments

3.1 Introduction

Early works on reactive transport modelling for aquatic sediment environments were done to investigate early diagenesis, a field that collectively describes all the transformations that occur in the top-most layer of the sediment bed (Berner, 1980). These transformations include a wide range of physical (e.g., diffusion, advection), chemical (e.g., degradation, sorption) and biological (e.g., bioturbation) transport processes. Contaminant distribution within the bed-sediment as well as sediment biogeochemistry is, thus, quantitatively predicted through the application of early diagenetic models.

Early diagenetic models are traditionally developed as abiotic descriptions of contaminant fate and transport in bed-sediments (Berner, 1964; Goldberg and Koide, 1962; Tzur, 1971). The concentration change of contaminants in sediment pore water is derived using mass conservation principles which constitute a particular form of the advection-diffusion equation given by:

$$\frac{\partial(\varphi C)}{\partial t} - \underbrace{\frac{\partial}{\partial x}(J_{\text{phys}})}_{\text{term 1}} + \underbrace{\frac{\partial}{\partial x}(\varphi C u)}_{\text{term 2}} = \underbrace{\sum R_{\text{reac}}}_{\text{term 3}} \quad \text{Eq. 3-1}$$

The concentration change in the whole sediment is given as:

$$\frac{\partial[(1-\varphi)q]}{\partial t} - \underbrace{\frac{\partial}{\partial x}(J_{\text{phys}})}_{\text{term 1}} + \underbrace{\frac{\partial}{\partial x}[(1-\varphi)wq]}_{\text{term 2}} = \underbrace{\sum R_{\text{reac}}}_{\text{term 3}} \quad \text{Eq. 3-2}$$

where q denotes the mass of the contaminant per unit volume of solids (i.e., sediments) and w , the velocity of the solids which can be attributed to burial, compaction or biological processes.

The contaminant distribution is generally defined by the differential physical transport through a diffusive flux J_{phys} (term 1), the bulk transport (term 2) and chemical reactions via the sink/source term $\sum R_{\text{reac}}$ (term 3). This early diagenetic model (equation 3-1) is essentially similar to the advection-diffusion equation typically used to describe reactive transport in the subsurface environment. Both diagenetic models (Domenico and Palciauskas, 1979; Nguyen *et al.*, 1982) and subsurface reactive transport models (Bear, 1972; Bear and Bachmat, 1986; Hassanizadeh and Gray, 1979) were extensively derived using the volume-averaging approach of the general continuum theory (Bachmat and Bear, 1986).

At present, reactive transport models are given both an abiotic and biotic description of contaminant fate and behaviour in order to provide a consistent picture of what transpires in aquatic sediment environment. The inclusion of the biological transport component is deemed important in fully describing fate and transport of contaminants in bed-sediments (Aller, 1980; Goldberg and Koide, 1962; Rhoads, 1974). It is important to note, however, that the “biological extension” to the early diagenetic model is regarded as an empirical addition, as the biological transport terms in the diagenetic equation are not deduced from mechanistic principles. Pioneering attempts to deduce the theoretical underpinning of the biological transport mechanism were presented in papers by Boudreau (1986a; 1986b) and Boudreau and Imboden (1987).

To date, in the area of contaminant fate and behaviour in bed-sediments, reactive transport modelling has until now stopped short of integration of various

mechanistic models to a single modelling environment that would allow a cohesive understanding and prediction of contaminant distributions in bed-sediments. This study, thus, developed CoReTranS, a predictive modelling environment that served as a tool to simulate 1-dimensional (1-D) organic contaminant reaction and transport in bed-sediments. In this chapter, the development and structure of the CoReTranS modelling environment is presented. A general guideline on the application of the CoReTranS model to laboratory and field dataset is outlined at the end of the chapter.

3.2 CoReTranS modelling environment

3.2.1 Object-oriented approach

The object-oriented (OO) approach to information systems development characterises a system (e.g., contaminant fate and transport in bed-sediments) as a collection of “objects” that interact with each other to achieve a common goal (e.g., predict contaminant concentration in sediment pore water) (Bian, 2007; Page-Jones, 2000). The term “object” in computer systems is essentially a model of real-world objects, simulating their respective states and behaviours. For example, a model system which simulates the reactive transport of contaminants in bed-sediments includes contaminant objects, reactive transport objects and concentration profile objects. A contaminant object stores its state in fields or variables such as contaminant name, contaminant type, half-life and molar volume. The contaminant object then demonstrates its behaviour through functions or methods such as getting a contaminant’s half life and setting the value to be used in evaluating the impact of contaminant degradation, which is another object. This illustrates how objects interact with each other – by carrying out their respective methods. OO programming also affords a systematic way of hiding the internal state of the object and requiring all interaction only through the method of the object. This is generally referred to as *encapsulation* which protects data from corruption. Further, objects of the same kind are bundled together as a *class*. A specific object of that class is referred to as an *instance* of the class. When an object is created for a class, the class is said to be “instantiated.”

The advantages of using the OO approach include:

1. **Modularity.** Each object has its own separate and independent source code. A model system can, thus, be systematically built and developed by building one object/source code at a time. This structure makes it easy to maintain the system as well. If a particular code contains problem areas, it can easily be isolated and dealt with.
2. **Extensibility.** Due to the modular structure of OO programming, a model system can easily accommodate new features by just adding more object and source codes to the existing package.
3. **Flexibility.** Objects, once built, can be used and re-used several times over the life cycle of the model system.

OO, hence, is an improvement in application design from previous functional programming approaches. This approach, however, is not without its share of potential disadvantages. Some of them are:

1. It has a steep learning curve, especially for beginners. It often takes years of dedication before abstraction (i.e., representing features without including the background details) becomes second nature.
2. OO codes can be very hard to read, at times. For classes that have inherited attributes from other classes or interfaces (i.e., written as separate codes/file), one may end up threading through codes looking for the method that have been called. This is especially difficult when the outcome of the specific method called can only be determined at runtime (i.e., virtual function). For example, a base class can have a virtual function `getData()` designed to obtain different information. If a subclass needs to call `getData()` to get a certain type of information (e.g. contaminant name), one has to thread through the codes to find which exact version of `getData()` is needed for obtaining the information needed. This non-linear

flow of programming will need good tools for browsing OO codes (e.g., Eclipse, XOTcIIDE).

3. Although the *encapsulation* feature of the OO approach is good from a maintenance standpoint, one can end up with OO codes that may use more memory than would be needed if one knew what an object needs in order to do its job.

As the CoReTranS modelling environment is developed *de novo*, the aforementioned limitations of the OO approach in the design and development of CoReTranS have been properly addressed.

3.2.2 Java performance

The increasing complexity of reactive transport models is driving environmental modellers to use the OO approach. Java, as a pure OO language, offers a suite of desirable features that make it ideal not only for graphical user interfaces (GUI) and other web-centric applications, but for developing extensible and portable modelling environments designed to solve complex problems as well.

First released in 1995 by Sun Microsystems, Java was developed both as an object-oriented programming language and as a platform. The following features demonstrate the suitability of Java in developing CoReTranS:

1. Java is free. The Java 2 Platform Standard Edition, integration libraries, user interface toolkits, deployment tools and a whole wide range of other development tools are available free of charge from the internet.
2. Java is platform-independent. Source codes written in Java are portable (Caromel *et al.*, 1998; Yu and Cox, 1997). This means that the program can be written, compiled, and run on any processor or operating systems.

3. Java is simple. Learning Java is easy, especially for programmers with C or C++ background. To date, the number of scientists and engineers who develop computing applications in Java is increasing (Boisvert *et al.*, 2001). Further, Java is structured in such a way that writing Java programs require fewer lines of codes. As a result, development time can be greatly reduced.
4. Java-based software is easily distributed. With Java Web Start, applications can easily be deployed, used and updated within the internet.

However, the use of Java for numerical computing remains debatable due to its computational performance compared with either C++ or Fortran (e.g., Chandra and Chandra, 2005). In a case study done by Vivanco and Pizzi (2005) on using Java and C++ for the analysis of functional magnetic resonance neuroimages, it has been shown that C++ still outperforms Java. The run-time performance of the Java code is significantly slowed down by its automatic garbage collection feature (i.e., execution of codes momentarily stops to de-allocate used objects). The Java development community is cognizant of Java's limitation and is continually working on improving its performance (Ciernak and Li, 1997; Gu et al., 2000). Sun Microsystem's *Just In Time* compiler, for example, has been designed to facilitate translation of Java byte-codes to machine code at runtime making it competitive with either C++ or Fortran. Thus, Java's numerical computing efficiency heavily relies on the continued development of modern compiler technologies.

In addition, Java's computational efficiency can be vastly improved by writing more efficient algorithms and coding methodologies. Moreira *et al.* (2000), for example, showed that optimising codes written in Java (e.g., creating loops for "null" checks) can achieve at least 80% of the peak performance of a Fortran code using the same benchmarks. With the emergence of more efficient compilers, Java is increasingly relied upon in solving extensive computational problems in science and engineering (Boisvert *et al.*, 2001; Moreira *et al.*, 1998; Moreira *et al.*, 2000).

3.2.3 Development of the three tier structure for the CoReTranS modelling environment

In order to take advantage of the OO approach to application systems development, the CoReTranS modelling environment was designed and developed as a three tier structure (Figure 3-1) application package written in Java and built using Java 2 Platform Standard Edition (J2SE version 1.4.1).

The three tier design requires that all objects created within the modelled system are separated in three categories of classes: GUI classes, problem domain classes, and data access classes. This structure is recently used in some innovative modelling applications in the internet (Cheng and Fen, 2006; Faraj *et al.*, 1999; Kokkonen *et al.*, 2003; la Penna *et al.*, 2006; Li and Liu, 2003). The components of the three tier structure are easily modified with minimal effects on each other. For example, extending the functionalities of the database management system would only require changing the data access classes, keeping both GUI and problem domain classes unchanged. Similarly, adding more buttons and other special graphic elements called widgets to the GUI would only involve altering the GUI classes. The three tier structure, thus, makes the CoReTranS application package easy to maintain. Further, the coupling between classes within each tier is minimised, allowing them to be easily changed without affecting those in another tier, thus making the application more extensible and easier to maintain.

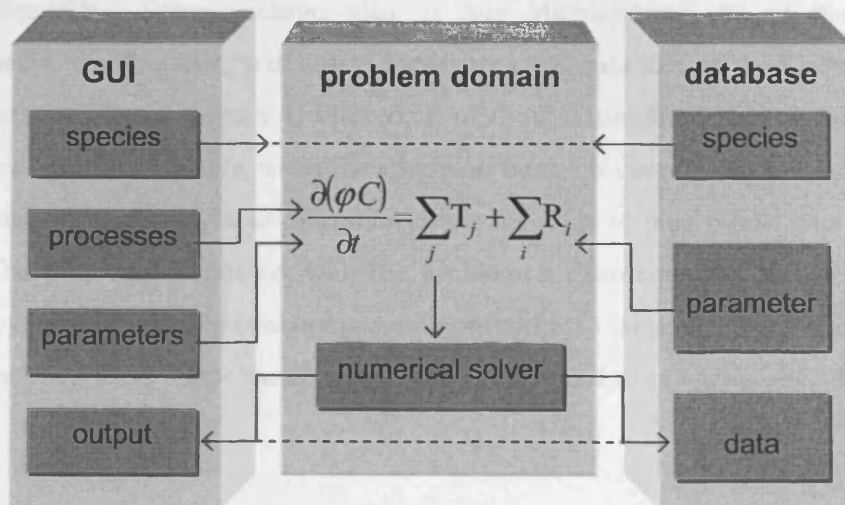


Figure 3-1. Schematic diagram of CoReTranS three-tier structure

The numerical code for the CoReTranS modelling environment was written on Eclipse 3.0, an open source software platform that provides an integrated development environment for application projects. At present, the compilation and deployment of the CoReTranS modelling environment is done through Eclipse 3.0 (i.e., the code is run in Eclipse 3.0) but it will eventually be deployed using the Java Web Start framework from Sun Microsystems where in CoReTranS can be started directly using a web browser from the Internet. The succeeding sections discuss the development of the individual component of the CoReTranS modelling environment.

3.2.3.1 CoReTranS graphical user interface. A GUI is a type of user interface through which humans interact with computers in order to enhance the usability of the underlying logical design of the application. A well designed GUI for reactive transport modelling provides an efficient tool for selecting simulation scenarios, entering data, modifying key parameters, and calibration of the resulting model. In addition to conventional tabular data modes, graphical representation of simulation outputs in exportable formats can also be facilitated through smart-menu structured GUIs. Legacy codes from C, FORTRAN and Pascal have even been integrated as executable files in interactive visual windows with a GUI as its first means of implementation (Friedrich and Karslioglu, 2003).

The CoReTranS GUI (Figure 3-2) was developed and written using the Java Foundation Class Swing package, also by Sun Microsystems. All of the GUI components (e.g., buttons, text fields, frame, etc.) are instances of the CoReTranS GUI classes. When a button is clicked, a method is simultaneously invoked to perform a task. For example, when the advection button is clicked, the advection tab on the right of the main frame becomes visible for users to plug model parameters into. The GUI classes interact with the problem domain and data access classes mostly by passing variables containing a memory address that points to or references an instance of a class. These variables are generally referred to as *reference variables*.

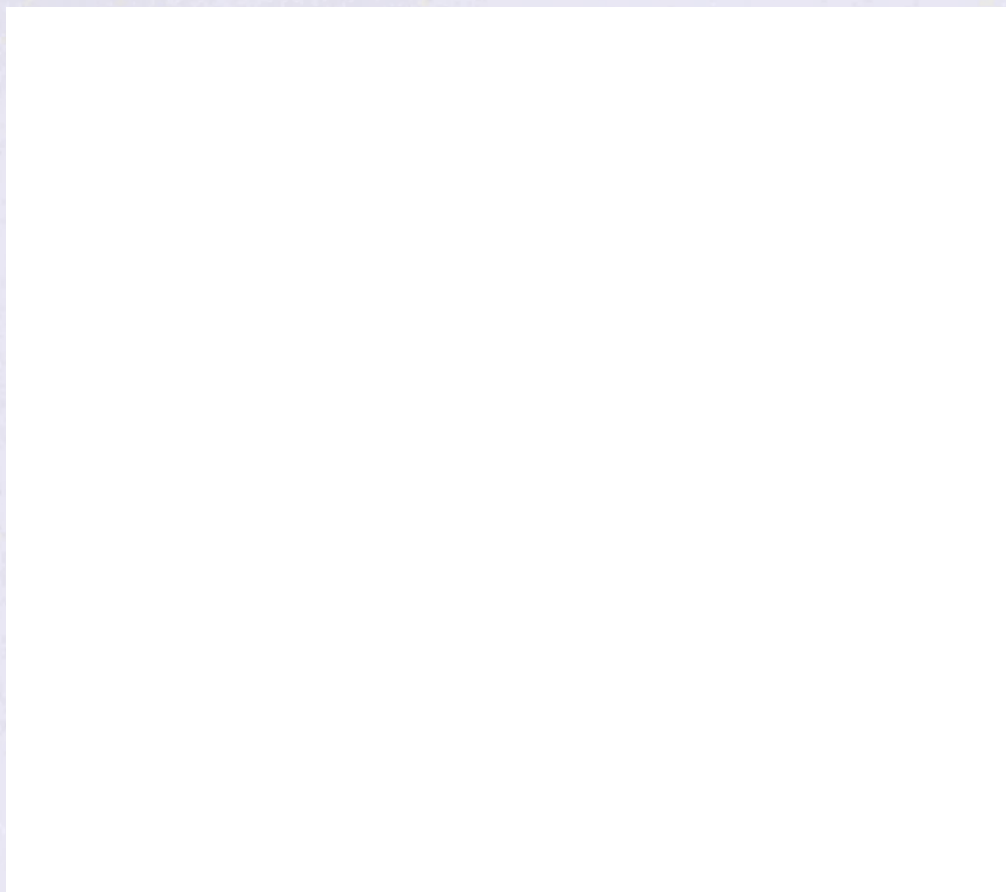


Figure 3-2. CoReTranS graphical user interface

The CoReTranS GUI provides the following integrated functionalities:

1. Construction of reactive transport model scenarios. A model scenario is built by clicking the reactive transport processes buttons on the upper left side of the main frame (Figure 3-3). Once a process button is clicked, a tab on the right side of the frame where model parameters can be estimated or plugged into becomes visible.



Figure 3-3. Selecting reactive transport mechanisms to model

2. Input/Output data operations. The GUI allows users to load and save data files containing parameter values. By clicking the button File on the left top most of the main frame, a file browser window (Figure 3-4) pops out so that users can select a data file in text format that can be loaded or saved.



Figure 3-4. Loading or saving data file from the CoReTranS GUI

3. Estimate model parameters or plug in user-defined values. Model parameters can be estimated by clicking the button representing empirical correlations. User-defined values can also be plugged in the system through labelled text fields.



Figure 3-5. Model parameters can be estimated or plugged in as user-defined values

4. Initial conditions can be selected either as a constant value or expressed as a step function.



Figure 3-6. Selection of the initial conditions for the model

5. Boundary conditions can be chosen as either Dirichlet, Neumann or Robin conditions.



Figure 3-7. Selection of the boundary conditions for the model

6. Selection of contaminant species from the database. A list of contaminant species is displayed on the upper right side of the frame (Figure 3-8). User can scroll down the list to select the contaminant to model.

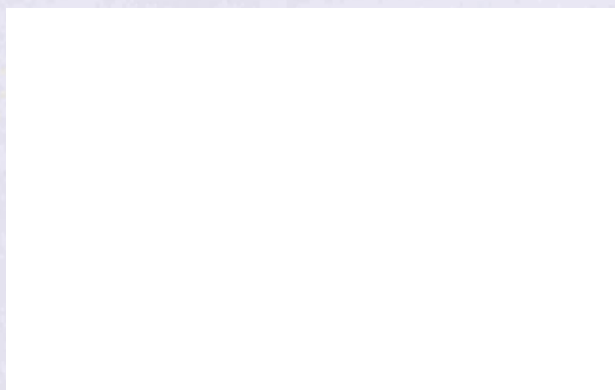


Figure 3-8. Selection of contaminant species to model

7. Amendment of database entries vis-à-vis contaminant chemical and physical properties (e.g., molar volume, half-life, $\text{Log } K_{ow}$). By clicking on the add button below the list of contaminant species, more contaminants can be added to the database.

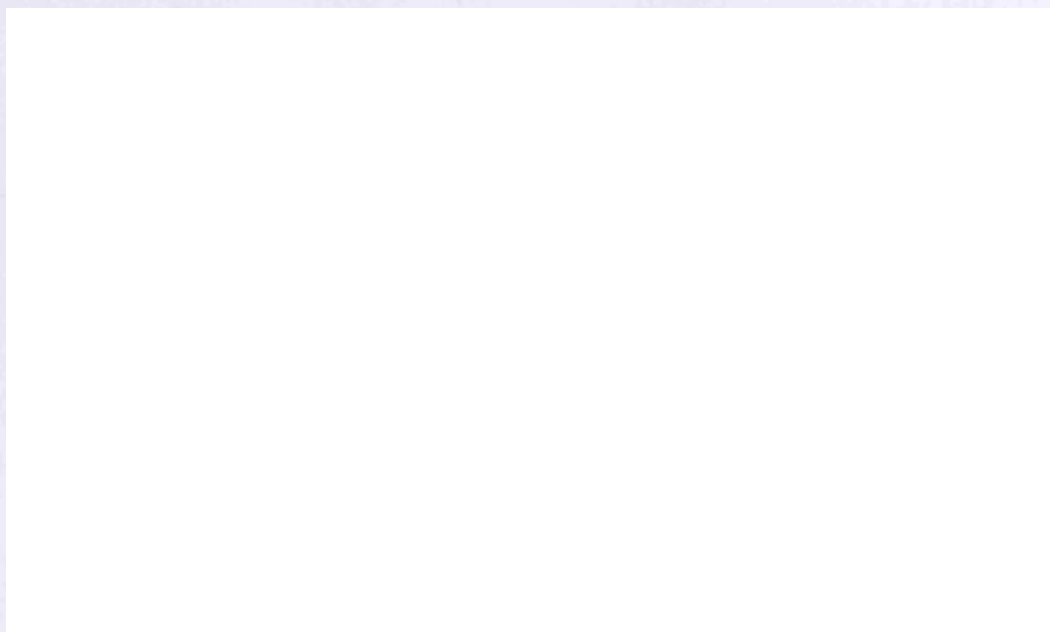


Figure 3-9. Adding contaminant species to the CoReTranS database through the GUI

8. Display of graphical (Figure 3-10a) and tabular representations (Figure 3-10b) of simulation outputs as well as a summary of the model simulation (Figure 3-10c).



Figure 3-10. An example of (a) a pore water concentration profile of a modelled contaminant; (b) pore water concentration profile of contaminants in table format, and; (c) summary of model simulation displayed in the GUI

9. Display of error messages. Pop-up dialogs containing error messages are displayed if the simulation process is done incorrectly.

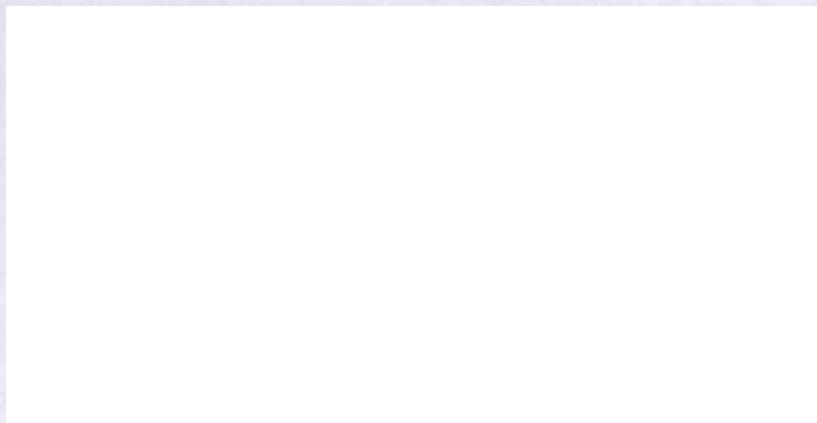


Figure 3-11. Display of error messages

3.2.3.2. CoReTranS problem domain. The problem domain holds the underlying logic of the application design for modelling reactive transport of contaminants in bed-sediments. Within the problem domain of the CoReTranS modelling environment, data representing contaminant species, reactive transport processes, and simulation parameters are passed to objects created during the simulation process (Figure 3-12). The constitutive laws describing the reactive transport of organic contaminants in bed-sediments are integrated as coupled components that users can simply select by a single button-click implementation. The simulation configuration objects, once instantiated, prompt the user to either choose values from the CoReTranS' database or enter their own parametric values, which can then be saved for retrieval and reuse. User-defined parametric values are integrated into the problem domain using simple accessor methods (e.g., getSedimentDepth, setSedimentDepth). This modular structure, thus, enables the application users to build their own reactive transport model using single button-click implementation and execution.

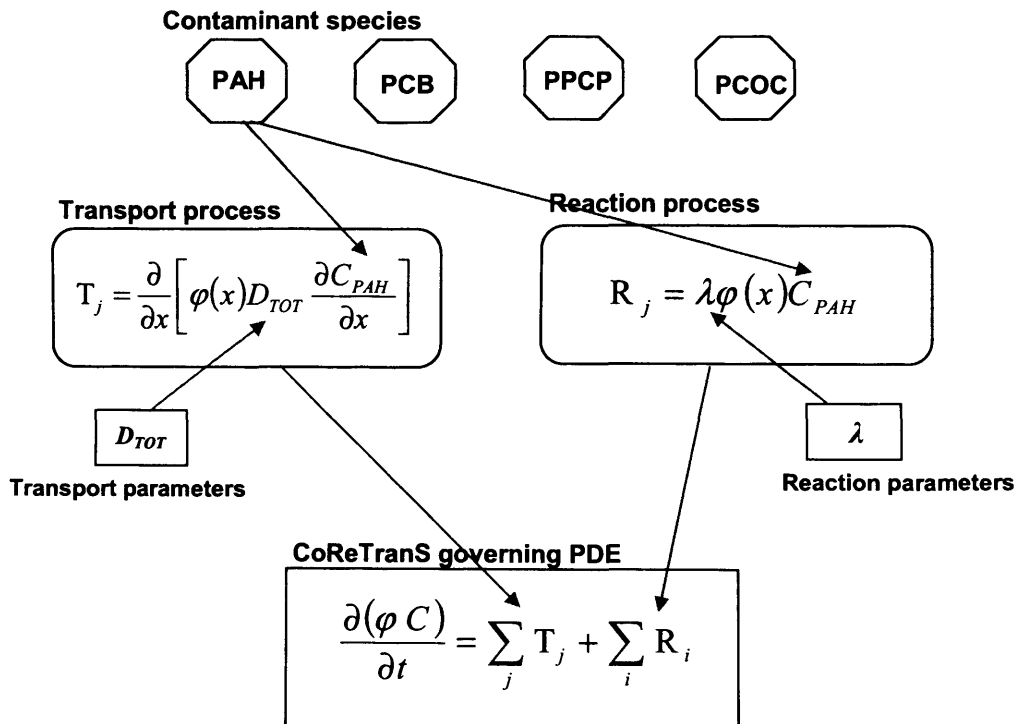


Figure 3-12. A diagram of the various building blocks as objects in the CoReTranS modelling environment

Chapter 3

Essentially, a PDE class that is instantiated during the simulation process represents a variable $C(x,t)$ that varies according to the PDE of the form:

$$\frac{dC}{dt} = f\left\{x, t, C, \frac{dC}{dx}, \frac{d}{dx}\left(D(x)\frac{dC}{dx}\right)\right\} \quad \text{Eq.3-3}$$

Equation 3-3 represents a coupled system of PDEs where $C(x,t)$ is a vector (i.e., an array of computational elements). The numerical approach in solving equation 3-3 involves the approximation of continuous derivatives in the conservative equation along a finite depth interval and is generally referred to as the Finite Difference method.

The first derivative is approximated using either a forward, central or backward differencing formula. The backward difference formula is considered a stable scheme due to its inherent capability of avoiding stiffness (i.e., oscillation of the numerical solution around the exact solution) (Shampine and Gear, 1979). Thus,

$$\frac{\partial C}{\partial x} = \frac{C_i - C_{i-1}}{\Delta x} \quad \text{Eq. 3-4}$$

where Δx denotes the finite depth interval. The second derivative is approximated as:

$$\left.\frac{\partial^2 C}{\partial x^2}\right|_{x_i} = \frac{C_{i+1} - 2C_i + C_{i-1}}{\Delta x^2} \quad \text{Eq. 3-5}$$

Thus, if equations 3-4 and 3-5 are introduced to a simple diffusion-advection model with constant parameters, the resulting equation is given as:

$$\frac{dC}{dt} = D_{eff} \frac{C_{i+1} - 2C_i + C_{i-1}}{\Delta x^2} - u \frac{C_i - C_{i-1}}{\Delta x} \quad \text{Eq. 3-6}$$

which when rearranged yields:

$$\frac{dC}{dt} = \left(\frac{D_{eff}}{\Delta x^2} \right) C_{i+1} - \left(\frac{2D_{eff}}{\Delta x^2} + \frac{u}{\Delta x} \right) C_i + \left(\frac{D_{eff}}{\Delta x^2} - \frac{u}{\Delta x} \right) C_{i-1} \quad \text{Eq. 3-7}$$

The governing PDE is, thus, effectively reduced to a set of ordinary differential equations (ODEs). The boundary conditions, also discretised in space using the finite difference method, are then applied. The set of ODEs is subsequently solved using jDisco, a numerical solver integrated in the CoReTranS application package to solve and simulate customised reactive transport models as combined discrete and continuous events. The jDisco numerical solver was developed by Helsgaun (2001) based on finite element systems and was also written in Java

The mathematical process implemented to solve the PDE is known as the Method of Lines (Byrne and Hindmarsh, 1987; Schiesser, 1991) in which the spatial variable (i.e., x = sediment depth) is discretised while the time variable (i.e., t = time) remains continuous. The spatial mesh consists of a specified number of equidistant points. This data is passed on to the instance of the PDE class, which then splits the PDE equation into a system of ODEs and subsequently solved using the Runge-Kutta-Fehlberg integration method. The design and implementation of the PDE class was based on the Fortran subroutine PDEONE by Sincovec and Madsen (1975).

In cases where the diffusion coefficients in the reactive transport model are functions of depth (i.e., depth-dependent porosity and tortuosity parameters), the diffusion term is approximated using the form (Nogotov, 1978):

$$\frac{\partial}{\partial x} \left[D(x) \frac{\partial C}{\partial x} \right] = \frac{1}{\Delta x} \left[D_{i+1/2} \left(\frac{C_{i+1} - C_i}{\Delta x} \right) - D_{i-1/2} \left(\frac{C_i - C_{i-1}}{\Delta x} \right) \right] \quad \text{Eq.3-8}$$

For the boundary conditions, three general boundary conditions are used: (1) concentration, (2) flux and (3) mixed conditions, also called continuity conditions.

Chapter 3

These boundary conditions are chosen to reflect what transpires at the boundaries of the sediment core being modelled and are derived from well-developed theories (See, for example, Hassanizadeh and Gray, 1989a; Hassanizadeh and Gray, 1989b; Slattery, 1967). Concentration conditions are also known as *Dirichlet* conditions or boundary conditions of the *first kind*. This boundary condition explicitly defines the concentration of the contaminant at the sediment-water interface and at a prescribed sediment depth. Mathematically, this condition is expressed as:

$$C(x,t) = C_0 \quad \text{Eq. 3-9}$$

where C_0 is a known concentration at depth x . A constant concentration boundary condition implies that the sediment layer is in contact with a well-mixed layer (e.g., overlying water column). If C_0 is zero, the layer is characterised as homogeneous.

Contaminant flux conditions represent a statement of mass conservation at the boundaries (Hassanizadeh and Gray, 1989a). This implies that for a certain boundary layer (e.g., sediment-water interface), the contaminant flux that enters this layer (i.e., diffusive- or advective flux) must equal that which exits it (i.e., surface reaction or a prescribed flux). That is,

$$\varphi(x) \left[uC - D_{TOT} \frac{\partial C}{\partial x} \right] = \Gamma \quad \text{Eq. 3-10}$$

where D_{TOT} denotes the total effective diffusion coefficient (i.e., sum of physical and biological diffusion coefficients) and Γ is the contaminant flux either due to a reaction or a prescribed flux.

In cases where advection is negligible and Γ is a prescribed flux F_0 , equation 3-10 is reduced to:

$$-\varphi(x) D_{TOT} \frac{\partial C}{\partial x} = F_0 \quad \text{Eq. 3-11}$$

The negative sign denotes the direction of the diffusive flux. If F_O is equal to zero, this implies that there is no diffusive flux through the boundary and therefore defines the boundary as homogeneous. Equation 3-11 is generally known as the *Neumann* condition or boundary conditions of the *second kind*.

The term Γ can also represent interfacial reactions (e.g., volatilisation or mass transfer). Bioturbational effects, for example, modelled as a non-local exchange process can be simulated as a mixed boundary condition. That is,

$$-\varphi(x)D_{TOT} \frac{\partial C}{\partial t} = \varphi(x)\eta(C - C_w) \quad \text{Eq. 3-12}$$

where the porosity factors on each side of the equation cancel each other. This type of boundary condition is known as *Robin's* condition or boundary condition of the *third kind*.

A summary of all the constitutive equations embedded in the CoReTranS modelling environment is summarised in Table 3-1.

Table 3-1. Constitutive equations embedded in the CoReTranS modelling environment.

	Equation	Description
<i>Reactive transport mechanisms</i>		
Diffusion	$\frac{\partial[\varphi(x)C]}{\partial t} = \frac{\partial}{\partial x} \left[\varphi(x) \frac{D}{\theta^2} \frac{\partial C}{\partial x} \right]$	
Advection	$\frac{\partial[\varphi(x)C]}{\partial t} = -\varphi(x)u \frac{\partial C}{\partial x}$	
Bioturbation	$\frac{\partial[\varphi(x)C]}{\partial t} = \frac{\partial}{\partial x} \left[\varphi(x)D_B \frac{\partial C}{\partial x} \right]$ or $\frac{\partial[\varphi(x)C]}{\partial t} = -\varphi(x)\eta(C - C_w)$	

Chapter 3

Sorption	$\frac{\partial[\varphi(x)C]}{\partial t} = \varphi(x)\rho_B \frac{\partial q}{\partial t}$	
Degradation	$\frac{\partial[\varphi(x)C]}{\partial t} = \varphi(x)\lambda C$	
Model parameters		
Molecular diffusion coefficient	$D = 7.4 \times 10^{-8} \frac{T(\Phi MW)^{0.5}}{\mu V^{0.6}}$	Wilke-Chang
	$D = 10 \times 10^{-8} \frac{TMW^{0.5}}{\mu V^{1/3} V_s^{1/3}}$	Hayduk-Laudie
	$D = 13.26 \times 10^{-5} \mu^{-1.14} V^{-0.589}$	Reddy-Doraiswamy
Mass average advective velocity	$u = \frac{k}{\varphi\mu} \left(\frac{\partial P}{\partial x} - \rho g \right)$	Darcy's equation
Mass transfer coefficient	$\eta = \frac{1}{\frac{1}{\beta} + \frac{h_{bio}}{D_{bio}^{pw} K_{OC} f_{OC} \rho_B}}$	Thibodeux-Bierman
Sorption isotherms	$q = K_D C$	Linear
	$q = \frac{Q^{\circ} b C}{1 + b C}$	Langmuir
	$q = K_F C^{n_F}$	Freundlich
	$q = X_L K_{D,L} C + \sum_{i=1}^m X_{NL}^i K_F^i C^{n_{Fi}}$	Distributed reactivity model
Degradation rate constant	$\lambda = \frac{\ln 2}{t_{1/2}}$	
Porosity	$\varphi(x) = \varphi_o$	Constant
	$\varphi(x) = \varphi_{\infty} + (\varphi_o - \varphi_{\infty}) \left[1 - \frac{x}{h} \right]$	Linear
	$\varphi(x) = \varphi_{\infty} + (\varphi_o - \varphi_{\infty}) \exp \left[-\frac{x}{h} \right]$	Exponential
	$\varphi(x) = \frac{\varphi_o \varphi_{\infty}}{\varphi_{\infty} + (\varphi_o - \varphi_{\infty}) \exp \left[-\frac{x}{h} \right]}$	Inverse exponential
	$\varphi(x) = a_p h \exp(-b_p)$	Power
Tortuosity	$\theta^2 = 1 - \ln[\varphi(x)^2]$	Modified Weissberg equation
Temperature	$\log_{10} \mu = -10.2158 + \frac{1.7925 \times 10^{-3}}{T} + 1.773 \times 10^{-2} T - 1.2631 \times 10^{-5} T^2$	

Sediment permeability	$k = \frac{h_c \mu}{\rho g} \quad \text{or}$ $k = \frac{d_p^2}{180} \left(\frac{\varphi^3}{(1-\varphi)^2} \right)$	
Retardation factor	$R = \varphi(x) + \rho_B K_D$	Linear
	$R = \varphi(x) + \rho_B \left[\frac{Q^o b}{(1+bC)^2} \right]$	Langmuir
	$R = \varphi(x) + \rho_B (n_F K_F C^{n_F-1})$	Freundlich
	$R = \varphi(x) + \rho_B (n_F K_F C^{n_F-1} + K_D)$	Linear-Freundlich
Linear partitioning coefficient	$K_D = f_{OC} K_{OC}$	
Organic carbon-normalised sorption coefficient	$\log K_{OC} = a_K \log K_{OW} + b_K$	Linear free energy relationship
Boundary conditions		
Dirichlet condition	$C(x, t) = C_o$	Concentration
Neumann condition	$\varphi(x) \left[uC - D_{TOT} \frac{\partial C}{\partial x} \right] = \Gamma$	Flux
Robin condition	$-\varphi(x) D_{TOT} \frac{\partial C}{\partial t} = \varphi(x) \eta (C - C_w)$	Mixed

3.2.3.3 CoReTranS database. In the OO paradigm, objects are made persistent when instances of their classes as well as their state variables are stored for use and retrieval purposes. A relational database is a key tool in facilitating object persistence in application development. The CoReTranS database was developed using MySQL, a relational database management system, through an interface available on the Information Systems website at UCL. It can be accessed through a set of data access classes employing the JDBC protocol and is currently maintained using the MySQL database server (release 4.0.16) at UCL.

Within the CoReTranS modelling environment, contaminant species are selected using its object-oriented database, where data access classes are invoked to store and

retrieve values for the selected contaminant species and their physical and chemical properties. The methods involved in the data access class include:

1. **Initialise method.** The function of the initialise method is to load the Java Database Connectivity (JDBC) - MySQL driver and create a connection instance that links to the CoReTranS database.
2. **Get data method.** The function of this method is to read the state variables of the contaminant object from a sequential file, create an instance of the contaminant object and store references (e.g., contaminant name, contaminant type, molecular weight, etc.) for those instances into a vector.
3. **Find contaminant method.** The purpose of this method is to find a specified contaminant from a vector list and then retrieve its reference variables.
4. **Add contaminant method.** This method invokes a new instance of the contaminant object being added.
5. **Terminate method.** This method simply invokes the close method for both the statement and connection instances.

3.3 CoReTranS model: application to a real dataset

Reactive transport models are tools for a wide range of tasks associated with risk-based decision-making, such as interpretation of historical contamination data, optimisation of attenuation and remediation methods, and monitoring of changes resulting from an implemented remediation scheme. However, the inappropriate application of these models to real situations due to poor understanding of in-bed fate and transport phenomena or insufficient site-specific data may result in misleading conclusions and recommendations.

The application of the CoReTranS models to real dataset is generally determined by the objective of the study from which the dataset originated, availability of data (i.e., parameters measured in field), and the complexity of the system. Therefore, modelling approaches will vary from one dataset to the next. The general approach in using the CoReTranS model is outlined below.

a. Scoping

This phase involves a critical review of existing information on the contaminated site, the aim and objectives of the study, and the scope of work done on the study. Information derived from the dataset should comprise: (1) known contaminants on site, and (2) physical and chemical characteristics of the bed-sediment. The information from the survey of contaminants present within the contaminated site will then be added to the CoReTranS database which contains all the physical and chemical properties of the specified contaminants. The bed-sediment characteristics that are critical to the modelling study include: sediment depth, bulk density, pore water temperature, porosity, overlying water concentration, organic carbon content, mass transfer coefficient on the sediment-water interface, Darcy velocity, presence of contaminant degrading microorganisms and bioturbating organisms. The scoping phase should identify whether there is a need to further investigate the site, or whether approximation of parameters by using data derived from other studies in the existing literature can be justified.

b. Development of a conceptual model

This phase identifies the critical reaction processes and transport mechanisms that control the fate and transport of contaminants at the contaminated site, and verifies that the identified processes can be translated into mathematical equations.

c. Construction of a reactive transport model

This phase involves the use of the CoReTranS GUI in constructing the chosen reactive transport model to represent the conceptual model. It also requires specification of the boundary conditions and model parameters. Assumptions and simplifications should be carefully justified.

d. Validation

The numerical results from the CoReTranS model should be compared with any field or experimental data in order to validate the reactive transport model and assess whether the reactive process and/or transport mechanisms chosen has represented the system well.

e. Predictions and assessment of results

The results of the model predictions should then be assessed whether they convey new findings or can be used in decision-making with regards to sediment management.

f. Recommendations

The information derived from the use of the CoReTranS model should highlight recommendations to guide future experiments, field monitoring and model extension. This information will further enable practical application of such information by engineers to site-specific risk assessment and remediation, as well as continued research and technology development.

Throughout the use of the CoReTranS model, it is important to note that a modelling study should be a continual process. Both the conceptual model and the reactive transport model should be constantly challenged and updated.

CHAPTER FOUR

CoReTranS model verification - Reactive transport models and analytical solutions

4.1 Introduction

The demand for a better and cohesive understanding of contaminant fate and transport in bed-sediments as required by increasingly stringent environmental policies and standards (Devlin *et al.*, 2007; Fenner *et al.*, 2005; Young, 1997), coupled with the rapid growth of information system technology, has made modelling and simulation tools vital in the overall scheme of sediment management. This research, hence, is aimed to enable assessment and comparison of the effectiveness of remediation alternatives for organic contaminants (e.g., low-cost monitored natural attenuation, with more costly dredging or capping) using the CoReTranS model.

In developing a site-specific reactive transport model scenario, a number of intuitive assumptions and simplifications are required to predict contaminant fate and behaviour in bed-sediments, and how the model should be mathematically represented. The model parameters, either estimated from a limited number of measurements, or using empirical correlations, are not always known with certainty despite numerous measurements or systematic site characterisation. The reactive transport model, hence, needs to be tested against measured values taken from field observations. The confidence that can be placed on the model is therefore dependent on the extent to which the model has been tested and *refined* based on prediction vs.

observed values. Model refinement involves adjustment or refinement of parameter, either manually or through an automated mathematical procedure, based on previous simulation results to improve model prediction of observed conditions whilst making sure that the model parameters remain realistic (i.e., within field tested range values, open literature values, etc.) as oppose to simply fitting the model to the observed values as implied by the term ‘calibration’ (Environmental Agency, 2001a; Environmental Agency, 2001b). In the course of model refinement, the mathematical model is first *verified* to test and confirm the accuracy with which the numerical code (i.e., computer program) was able to represent the model and then *validated* to show the capability of the model in predicting future conditions with sufficient precision.

The terms verification and validation, in the course of modelling studies, are often interchangeably used (Balci, 1995; Oreskes *et al.*, 1994). In this research, model verification is referred to as the process in which a system or problem is accurately transformed into a model specification or into a numerical code and subsequently benchmarked against analytical solutions of simplified reactive transport models. Model validation is defined as the process wherein the refined model is shown to predict actual site conditions with satisfactory accuracy.

In this chapter, The CoReTranS model was verified and benchmarked by comparing numerical simulation results for simplified problems with their analytical solutions.

4.2 Assessment of Model Refinement

4.2.1 Overview

Qualitative assessment of the fit between the predicted outcomes and actual observations comprises the first step in model refinement. This process is typically done using visual comparisons. However, after adjusting the model parameters a more quantitative assessment must be done using statistical measures of goodness of

Chapter 4

fit. The following are some common measures of goodness of fit (Benjamin and Cornell, 1970; Cooley, 1979; Loague and Green, 1991):

4.2.2 Linear correlation coefficient

The linear correlation coefficient, r , is defined as

$$r = \frac{\sum_{i=1}^N (X_{pred} - \overline{X_{pred}})(X_{obs} - \overline{X_{obs}})}{\sqrt{\sum_{i=1}^N (X_{pred} - \overline{X_{pred}})^2} \sqrt{\sum_{i=1}^N (X_{obs} - \overline{X_{obs}})^2}} \quad \text{Eq. 4-1}$$

where X_{pred} is the predicted value, X_{obs} is the actual or observed value and $\overline{X_{pred}}$ and $\overline{X_{obs}}$ are the means of the predicted and actual values, respectively. A linear correlation coefficient near one is indicative of good correlation, whereas a correlation coefficient near zero is indicative of poor correlation. However, it can be shown that if $X_{pred} = (AX_{obs} + B)$ for any non-zero value for A and B , then r is equal to 1. Thus, r , can be insensitive to additive and proportional differences between X_{pred} and X_{obs} . It is therefore necessary to use r in conjunction with measures of error (e.g., mean of residual errors, root mean of squared residual errors) in model refinement (Legates and McCabe Jr., 1999; Willmott, 1981).

4.2.3 Mean of residual errors

The mean of residual errors, M , is defined as

$$M = \frac{1}{N} \sum_{i=1}^N (X_{obs} - X_{pred}) \quad \text{Eq. 4-2}$$

where N is the total number of observations or measurements. The predicted or observed values may be contaminant concentrations in pore water or sediment. A mean value close to zero suggests overall agreement between the predicted and actual

values. The ensuing sign indicates the overall tendency of the model towards over-prediction or under-prediction.

4.2.4 Root mean of squared residual errors

The root mean of squared residual errors, RMS , is defined as

$$RMS = \left[\frac{1}{N} \sum_{i=1}^n (X_{obs} - X_{pred})^2 \right]^{1/2} \quad \text{Eq. 4-3}$$

When comparing mathematical models that use the same dependent variable and the same estimation period, the RMS value goes down as r goes up. Therefore, the model with the highest adjusted r value will have the lowest root mean of squared residual error, and the use of r is justified as co-measures of model validity. However, although RMS is more sensitive than other measures, the squaring process may give disproportionate weight to very large errors. Still, RMS is a generalised measure of standard deviation and is often considered a valid indicator of relative model quality (Cichota *et al.*, 2004; Willmott, 1981).

4.2.4 Normal probability plots of residual errors

Normal probability plots are used to assess whether the residual errors are drawn from a normal distribution or not. If the plotted points are linear and fluctuate in a uniform band around zero, the assumptions made for the model indicates adequate representation of the actual system. Further, distinct curvature or “tailings” within the plot indicates that the residual errors are not normally distributed and might be due to some unaccounted process or unrealistic model parameters used in the simulation.

The normal probability plot is constructed by plotting the sorted values of RMS against the theoretical values from the standard normal distribution (i.e., -1 to 1).

4.3 CoReTranS Predictions vs. Analytical Solutions

4.3.1 Overview

The CoReTranS model was verified and benchmarked by comparing numerical simulation results for simplified problems with their analytical solutions taken from Crank (1975), van Genuchten and Alves (1982), and Choy and Reible (2000). Two distinct reactive transport models were built and modified using the CoReTranS model, the first assumes a diffusion-controlled scenario (i.e., diffusion model) while the second assumes a significant groundwater seepage (i.e., diffusion-advection model ~ 20 and 100 cm y^{-1}). In both of these scenarios, the effect of sorption is shown by increasing the retardation factor, R , to 9. The effect of degradation on contaminant transport was also shown by adding a degradation term to the model equations. Figure 4-1 details the steps involved in simulating all four test models using CoReTranS' GUI:

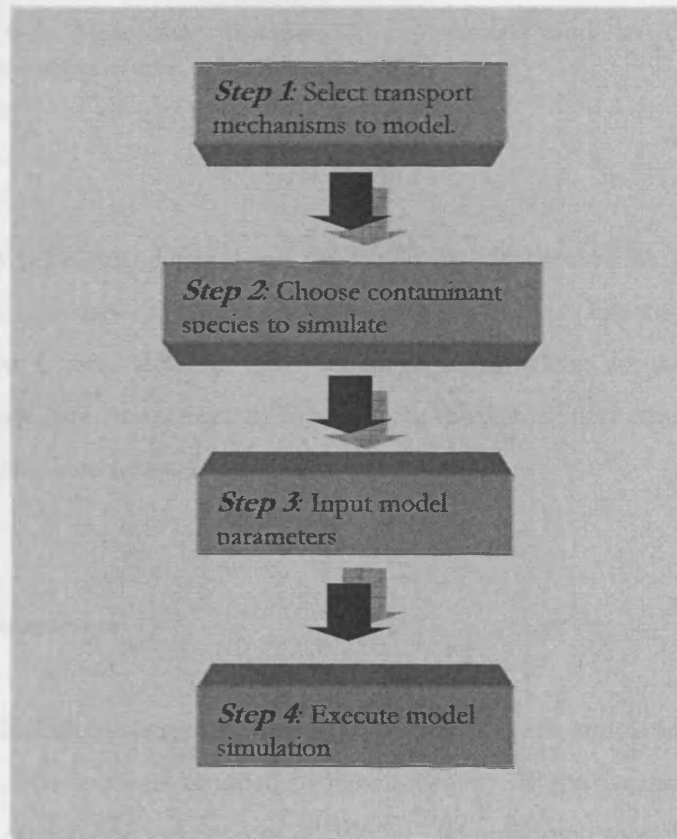
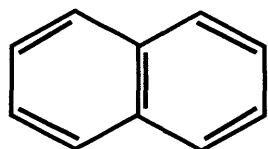


Figure 4-1. Model simulation steps in CoReTranS. Model parameters may be either from a data file or plugged in by the user. The customised model simulation is executed by pressing the “Ready” button at the bottom of the GUI.

4.3.2 Model contaminant

In all test models, naphthalene was chosen as an arbitrary test contaminant. Naphthalene is a volatile, crystalline white solid hydrocarbon, best known as the main component of mothballs. Its molecular structure consists of two fused benzene rings (Figure 4-2). Accordingly, naphthalene is classified as a benzenoid polycyclic aromatic hydrocarbon.



Naphthalene C₁₀H₈
CAS Registry No. 90-20-3
Molecular Weight, 128.19 (g/mol)
Molar Volume, 147.6 (cm³/mol)
Log K_{OW}, 3.37
Half-life, 229.16 (day)

Figure 4-2. Molecular structure of naphthalene and its chemical properties -values as cited in Mackay *et al.*(1997)

Naphthalene is produced from coal tar and is mostly used as an antiseptic and insecticide. The International Agency for Research on Cancer (International Agency for Research on Cancer (IARC), 2002) classifies naphthalene as possible human carcinogen. Acute exposure, either by ingestion or inhalation, may cause cataracts in humans and haemolytic anaemia in children and infants.

4.3.3 Model parameters

A 30 cm sediment column was considered over a 16 week-simulation time for all test cases. The sediment was assumed to have a density of approximately 2.5 kg/L, and an organic carbon fraction content of 0.05%. The governing model equation was numerically discretised to 100 grids.

Chapter 4

The diffusivity of the model contaminant was estimated using the Wilke-Chang empirical correlation at an assumed temperature of 15°C. The sorption mechanism was assumed to follow linear partitioning and K_D was approximated using the organic carbon normalised sorption coefficient (K_{OC}) wherein K_{OC} was further evaluated using LFER. The parameters used in simulating the test models are summarised in Table 4-1.

Table 4-1. Model parameters used in simulating the three test case scenarios using CoReTranS in comparison with existing analytical solutions.

Parameters	Values
Sediment depth, cm	30
Sediment density, kg/L	2.5
Temperature, °C	15
Number of grids	100
Simulation time, t , days	112
Porosity	0.5
Organic carbon fraction (dry mass basis)	0.0005
Mass transfer coefficient, η , cm/day	0.20
Diffusion coefficient, cm ² /day	2.26×10^{-2}
K_D , L/kg	4.8
λ , degradation rate, 1/day	3.02×10^{-3}
Advective velocity, cm/y	20/100

4.3.4 Representative elementary volume

In describing the fate and transport of contaminants in bed-sediments, an appropriate representative elementary volume (REV) that is vertically orientated is

assumed to integrate CoReTranS governing equation (equation 3-4, see Section 3.3) from the microscale to the macroscale (Bachmat and Bear, 1986; Bear, 1972; Hassanizadeh and Gray, 1979). Thus, for the 1-D analysis of contaminant fate and transport, only the contaminant flux along the vertical axis is considered as shown in Figure 4-3.

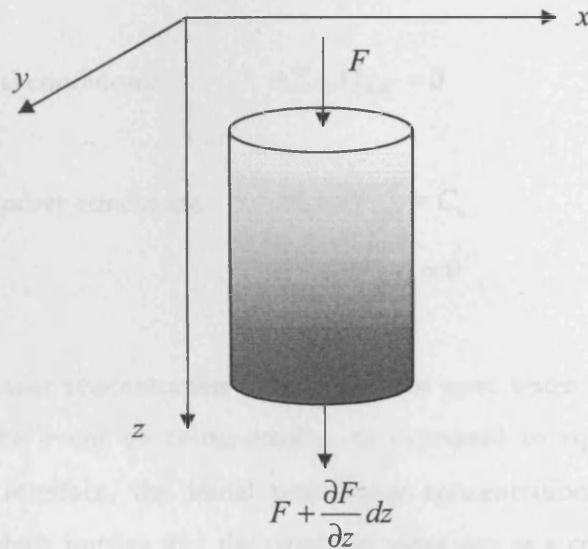


Figure 4-3. Contaminant flux through the REV.

4.3.5 Diffusion model

4.3.5.1 Model formulation and approach. Contaminant transport becomes diffusion-controlled when groundwater seepage is not significant and pore water flow conditions are hydrostatic. The diffusive transport over the vertical length of a sediment column is driven by the difference in dissolved contaminant concentration between the sediment pore water and the water column overlying the sediment bed. For the 1-D transport of dissolved contaminants in pore water through a homogeneous sediment layer (i.e., constant porosity) subject to sorption, the diffusion transport model is expressed as,

Chapter 4

$$\frac{\partial C}{\partial t} = \frac{D_{eff}}{R} \frac{\partial^2 C}{\partial x^2} \quad \text{Eq. 4-4}$$

where R is the linear retardation factor (Table 3-3, see Section 3.3.3). The initial and boundary conditions applied were as follows:

$$\text{Initial conditions:} \quad C(x, t)|_{t=0} = 0 \quad \text{Eq. 4-5}$$

$$\text{Boundary conditions:} \quad C(x, t)|_{x=0} = C_o \quad \text{Eq. 4-6}$$

$$C(x, t)|_{x=30} = 0 \quad \text{Eq. 4-7}$$

The contaminant concentration in the sediment pore water was assumed to be zero prior to the event of contamination as expressed in equation 4-5. At the sediment-water interface, the initial pore water concentration C_o was set to 1 (equation 4-6) which implies that the overlying water acts as a continuous source of contamination. The boundary condition at the 30 cm depth (equation 4-7) assumed that the migration of the contaminant never reached that layer.

The analytical solution to equation 4-8 for the given initial and boundary conditions was given as (Crank, 1975):

$$\frac{C}{C_o} = 1 - \text{erfc} \left[x \sqrt{\frac{R}{4D_{eff}t}} \right] \quad \text{Eq. 4-8}$$

where C/C_o represents the pore water contaminant concentration normalised to the source concentration and is therefore dimensionless. Further, the boundary condition at the 30 cm depth was assumed to be a semi-infinite boundary condition, where the dissolved concentration at the base of an infinite sediment layer will never rise above zero (i.e., the contaminant will never travel an infinite distance). That is,

$$C(x, t)|_{x=\infty} = 0 \quad \text{Eq. 4-9}$$

The assumption for equation 4-9 was made in order to derive an exact solution for equation 4-4 using Laplace transform. The analytical solution for the succeeding model equations were evaluated using the same assumption.

The diffusion model was simulated using CoReTranS and the profiles predicted contaminant concentration in pore water were compared with the analytical solution as shown in Figure 4-4.

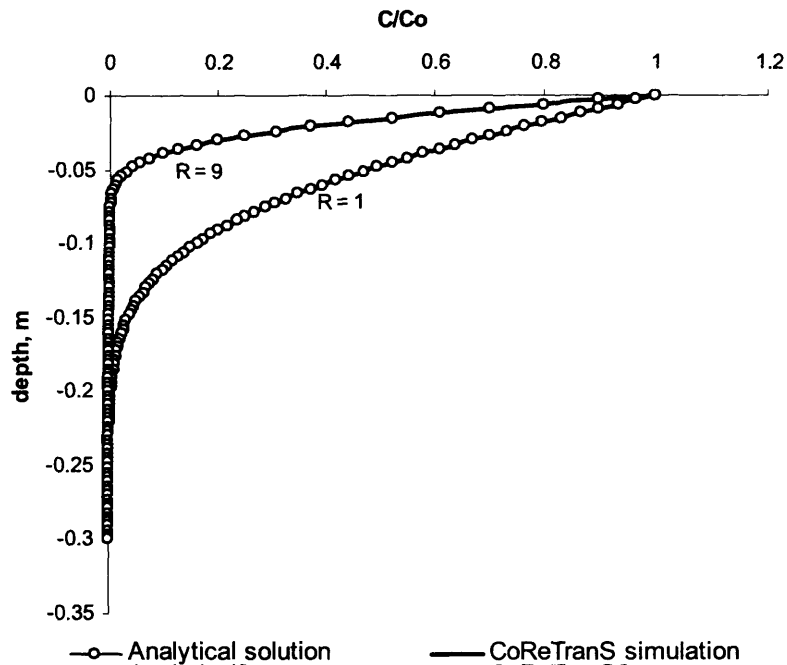


Figure 4-4. Pore water concentration-depth profile for naphthalene subject to diffusive transport alone.

Goodness of fit between pore water concentration profiles from analytical solution and CoReTranS simulation was evaluated. The *RMS* values for the retarded ($R = 9$) and non-retarded ($R = 1$) are 6.92×10^{-4} and 5.70×10^{-3} , respectively. Although minimal, the probable source of error between the predicted profile and the analytical solution lies in the assumption that was made in deriving the exact solution of the diffusion model. The analytical solution was derived assuming zero concentration at infinite depth while the CoReTranS model was numerically

simulated using finite boundaries which imply that at the 30 cm depth the CoReTranS model was forced to take a concentration value of zero. An r value of 1.0 was obtained for both cases showing excellent correlation between the two profiles.

Conceptually, the downward vertical migration of the dissolved contaminant due to diffusion transport is caused by the difference in pore water concentration of the contaminant at the sediment-water interface (equation 4-6) and the background concentration of the sediment column (equation 4-5). At the sediment-water interface, the naphthalene concentration is abruptly changed from C_o to the background concentration in the sediment, set to zero. As diffusion proceeds with time, the abrupt change in concentration will gradually moderate and evolve into an interval. The interval over which the contaminant concentration changes from C_o to the background concentration aligned vertically is called the contaminant front as depicted in Figure 4-5. The spatial distribution of the contaminant concentration follows a sigmoidal distribution related to the Gaussian distribution (e.g., Bear, 1972; Scheidegger, 1954).

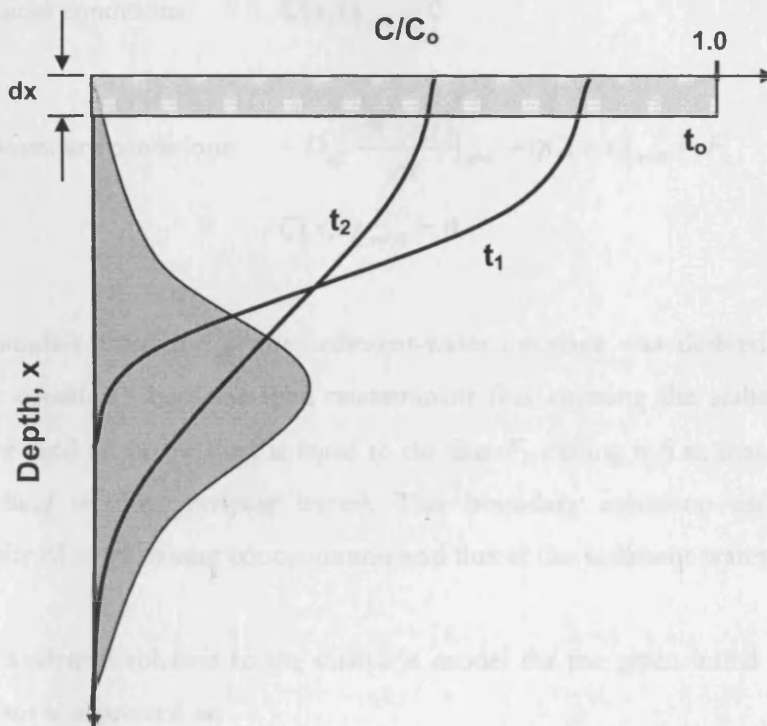


Figure 4-5. Sigmoidal distribution patterns of the vertically aligned contaminant front over time.

4.3.5.2 Effect of contaminant sorption on the diffusion model. For a non-sorbing bed-sediment (i.e., $f_{oc} \sim 0$, $R = 1$), the contaminant front was predicted to be wider and far advanced from the front in a sediment bed with high sorption capacity.

The vertical distribution of naphthalene along the sediment column was heavily influenced by the abundance of organic matter in the sediment bed (i.e., $f_{oc} = 0.5\%$, $R = 9$). As R increased, the contaminant front decreased due to a diminished diffusion coefficient (i.e., D_{eff}/R). Further, the depth of penetration was observed to be far less than in the case of unretarded diffusion (Figure 4-4).

4.3.5.3. Effect of a constant flux boundary condition on the diffusion model.

A constant flux, F_o , at the sediment-water interface was also investigated using the diffusion model. The following initial and boundary conditions were applied:

$$\text{Initial conditions: } C(x, t)|_{t=0} = 0 \quad \text{Eq. 4-10}$$

$$\text{Boundary conditions: } -D_{eff} \frac{dC(x, t)}{dx} \Big|_{x=0} + \eta C(x, t) \Big|_{x=0} = F_o \quad \text{Eq. 4-11}$$

$$C(x, t) \Big|_{x=30} = 0 \quad \text{Eq. 4-12}$$

The boundary condition at the sediment-water interface was derived from a mass balance equation where the total contaminant flux entering the sediment bed (i.e., diffusive- and advective flux) is equal to the flux F_o exiting it (i.e., mass carried away by flushing of the overlying water). This boundary condition essentially states continuity of contaminant concentration and flux at the sediment-water interface.

The analytical solution to the diffusion model for the given initial and boundary conditions is expressed as:

$$\frac{C}{C_o} = \frac{F_o}{\eta} \left[\begin{aligned} & \operatorname{erfc} \left(x \sqrt{\frac{R}{4D_{eff}t}} \right) - \exp \left(\frac{\eta x}{D_{eff}} + \frac{\eta^2 t}{RD_{eff}} \right) \\ & \times \operatorname{erfc} \left(\eta \sqrt{\frac{t}{RD_{eff}}} + x \sqrt{\frac{R}{4D_{eff}t}} \right) \end{aligned} \right] \quad \text{Eq. 4-13}$$

The contaminant pore water concentration profiles derived from the analytical solution (equation 4-13) and that from CoReTranS is shown in Figure 4-6.

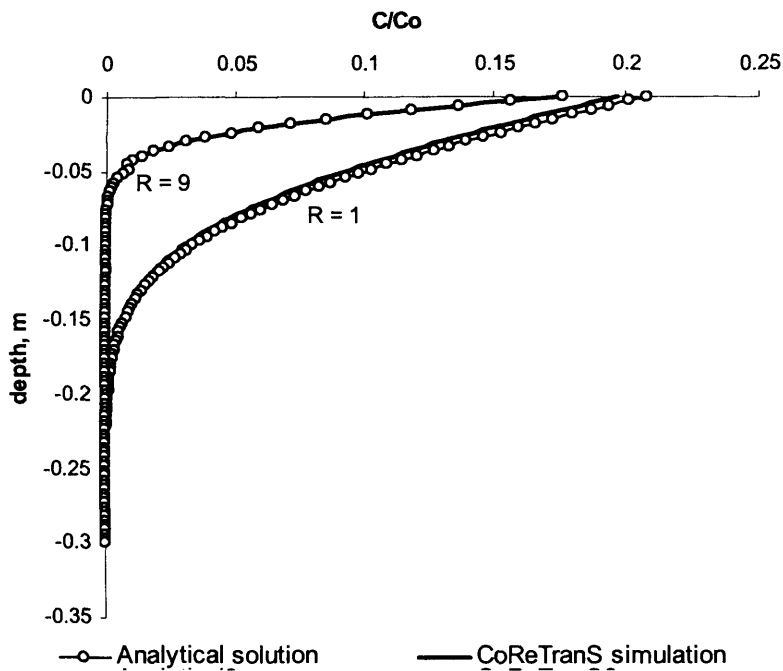


Figure 4-6. Pore water concentration-depth profile for naphthalene subject to diffusive transport with mass transfer at the sediment-water interface.

For the diffusion model, η and F_o were arbitrarily given values of 0.2 cm/day and 50 ng/cm²-day, respectively. In most applications, η is given a range of values from 0.1 to 40 cm/day as a result of calibrating a model to best fit the actual data (Erickson *et al.*, 2005; Lick, 2006; Thibodeaux *et al.*, 2001). In laboratory experiments, η at the sediment-water interface is quantified using gypsum-doubloon wafers (See,

for example, Marshal and Slusher, 1966; Santschi *et al.*, 1991). For contaminant fluxes, Reible *et al.* (1996) demonstrated that under oxic conditions, variations in contaminant fluxes in high-density bioturbated microcosms remained constant at 37 ng/cm²-day for pyrene and 70 ng/cm²-day for phenanthrene.

An *RMS* value of 4.89×10^{-3} was obtained for the non-retarded case while for the retarded diffusion model, the *RMS* was 4.14×10^{-4} . The *r* values for both cases are still 1.0 showing excellent correlation between the profiles from the analytical solution and CoReTranS' simulation. Again, as discussed in the previous section, the source of error between the analytical solution and the predicted profile was the difference in assumed boundary conditions between the analytical approach and CoReTranS simulation. The pore water concentration profiles of the retarded and non-retarded diffusion models for naphthalene with the mass transfer reaction at the sediment water interface are similar in shape but of greater magnitude compared with the profiles generated from the use of a constant contaminant concentration at sediment-water interface. The contaminant concentration at the interface was about 5 times less when a constant contaminant flux occurs at the interface, in contrast with the use of a constant concentration condition, illustrating the effect of the action of burrowing benthic organisms and other bioturbation processes at the sediment-water interface. The bioturbation-induced flux at the interface is thus dependent on the type of organism, its population density, the contaminant and the bed-sediment. For example, *Tubifex tubifex*, a common oligochaete, can produce a flux twice as much as *Lumbricus*, a relatively smaller organism (Fisher *et al.*, 1980).

4.3.5.4 Effect of contaminant degradation on the diffusion model. The effect of an irreversible first-order degradation reaction on the diffusive movement of contaminants in bed-sediments was also investigated. This model scenario is governed by the following equation:

$$R \frac{\partial C}{\partial t} = D_{eff} \frac{\partial^2 C}{\partial x^2} - \lambda RC \quad \text{Eq. 4-14}$$

The initial and boundary conditions are as follows:

$$\text{Initial conditions: } C(x, t)|_{t=0} = 0 \quad \text{Eq. 4-15}$$

$$\text{Boundary conditions: } C(x, t)|_{x=0} = C_o \quad \text{Eq. 4-16}$$

$$C(x, t)|_{x=30} = 0 \quad \text{Eq. 4-17}$$

The analytical solution to equation 4-14 governed by the same initial and boundary conditions is given by (Carslaw and Jaeger, 1959; Danckwerts, 1950):

$$\begin{aligned} \frac{C}{C_o} = \frac{1}{2} \exp \left[-x \sqrt{\frac{\lambda R}{D_{eff}}} \operatorname{erfc} \left(x \sqrt{\frac{R}{4D_{eff}t}} - \sqrt{\lambda t} \right) \right] \\ + \frac{1}{2} \exp \left[x \sqrt{\frac{\lambda R}{D_{eff}}} \operatorname{erfc} \left(x \sqrt{\frac{R}{4D_{eff}t}} + \sqrt{\lambda t} \right) \right] \end{aligned} \quad \text{Eq. 4-18}$$

The diffusion-sorption-degradation model was simulated using CoReTranS and the predicted contaminant concentration in pore water profile was compared with the analytical solution as shown in Figure 4-7.

The *RMS* value for the diffusion- degradation model was 1.60×10^{-2} while for the simple diffusion model, 6.92×10^{-3} . The *r* values for both cases are still 1.0 showing excellent correlation between the profiles from the analytical solution and CoReTranS' simulation. The source of error for the discrepancy between the predicted profiles and the analytical solution is still from the assumed boundary conditions. For the CoReTranS simulation, the contaminant concentration at the 30 cm depth was zero while for the analytical solution, the contaminant concentration at the 30 cm depth was $3.42 \times 10^{-5} \text{ g/m}^3$.

The effect of the degradation term is shown by a very slight shift of the contaminant front to the left. This is indicative of contaminant loss due to decay over time. The impact of the degradation process however was minimal due to the chosen contaminant's low degradation rate in the sediments.

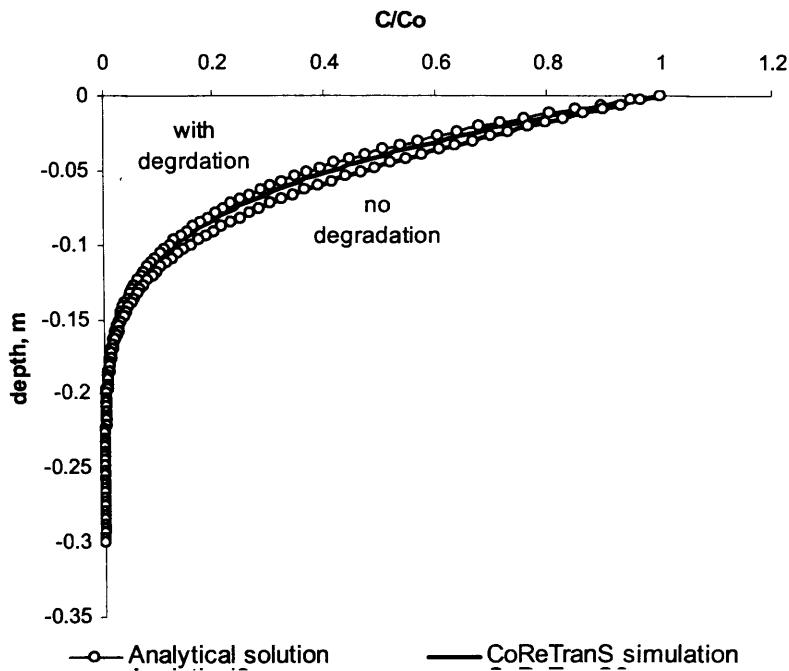


Figure 4-7. Effect of first-order degradation reaction to the pore water concentration-depth profile for naphthalene subject to diffusive transport ($R = 1$).

4.3.6 Diffusion-Advection model

4.3.6.1 Model formulation and approach. In most environmental situations, it is probable that advection may play a role in the vertical migration of contaminants within the bed-sediment. Hydrological flow due to groundwater discharge or surface water seepage can carry dissolved contaminants from the contaminated sediment to the body of water overlying the sediment bed, or vice-versa. As a result, contaminant dissolved in the sediment pore water may be subject to advection in addition to diffusive transport.

The governing equation for a diffusion-advection model describing the vertical transport of contaminants through a homogeneous sediment layer is:

$$\frac{\partial C}{\partial t} = \frac{D_{eff}}{R} \frac{\partial^2 C}{\partial x^2} - \frac{u}{R} \frac{\partial C}{\partial x} \tag{Eq. 4-19}$$

Chapter 4

given the following initial and boundary conditions:

$$\text{Initial conditions: } C(x,t)|_{t=0} = 0 \quad \text{Eq. 4-20}$$

$$\text{Boundary conditions: } C(x,t)|_{x=0} = C_o \quad \text{Eq. 4-21}$$

$$C(x,t)|_{x=30} = 0 \quad \text{Eq. 4-22}$$

The continuous contamination source for this scenario was assumed to be of finite duration (equation 4-19). Examples for this case in surface-water applications wherein solutes are released at a constant, continuous rate for a finite period of time include determining contaminant distribution in multi-layer porous media under conditions of steady-state flow (Liu *et al.*, 1998), environmental behaviour of persistent organics in bed-sediments (Jonkers *et al.*, 2005), and assessment of decay mechanisms for aquatic herbicides (O'Loughlin and Bowmer, 1975). The advective velocities for the cases presented in this model scenario were given values of 20 and 100 cm/year which were arbitrarily chosen to reflect an advection-dominated transport mechanism (i.e., $Pe > 1.0$).

The analytical solution to equation 4-19 for the given initial and boundary conditions is given as (Ogata and Banks, 1961):

$$\frac{C}{C_o} = \frac{1}{2} \left[\operatorname{erfc} \left(\frac{Rx - ut}{\sqrt{4RD_{eff}t}} \right) + \exp \left(\frac{ux}{D_{eff}} \right) \operatorname{erfc} \left(\frac{Rx + ut}{\sqrt{4RD_{eff}t}} \right) \right] \quad \text{Eq. 4-17}$$

The diffusion-advection model is simulated using CoReTranS and the profiles for the predicted contaminant concentration in pore water were compared with the analytical solution as shown in Figure 4-8.

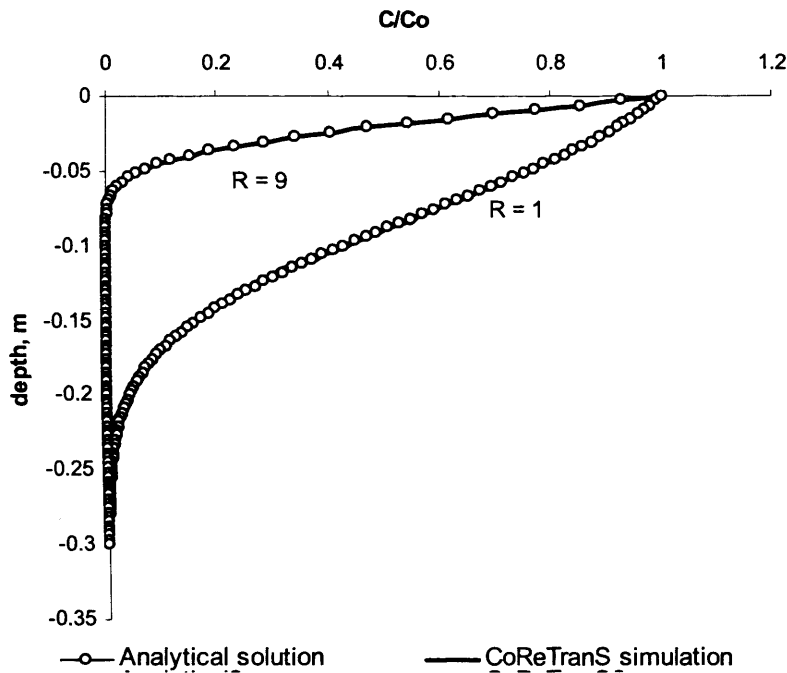


Figure 4-8. Pore water concentration-depth profile for naphthalene subject to diffusive-advective transport.

The *RMS* values for the retarded and non-retarded diffusion-advection model are 2.69×10^{-3} and 4.01×10^{-3} , respectively. Predicted contaminant concentrations approaches zero as sediment depth approaches 30 cm, while for the analytical solution, the contaminant concentration will only approach to zero as sediment depth approaches infinity which essentially makes up the error between the predicted profile and the analytical solution. The overall agreement between the analytical and numerical solutions, however, was shown to be good with an *r* value of 1.0 for both cases, demonstrating good correlation between the analytical solution and the predicted profiles.

As with the diffusion model, the contaminant front at the onset of the diffusive-advective transport process started its movement from the sediment-water interface where the concentration abruptly changed from C_o to zero. The speed of the contaminant front into the sediment is equal to the contaminant's average linear velocity (i.e., u/R). Thus, the centre of the contaminant front within the sediment column will be located at depth ut at any time, t (Figure 4-8). As migration proceeds

with time, the diffusion process will result in the widening of the contaminant front while the advection process will produce a further downward movement of the contaminant front.

Further, the presence of the complementary error function (*erfc*) in the analytical solution to the diffusion-advection model equation is reflective of the sigmoidal distribution of the contaminant concentration. As with the diffusion model, the presence of the retardation factor primarily affects the width of the contaminant front. An increase in R will result in a much narrower contaminant front that lags behind the front of a non-sorbing contaminant.

4.3.6.2 Effect of varying the advective velocity. From the concentration profiles, the diffusive transport of contaminants in bed-sediments coupled with advective flow essentially results in a downward movement of the contaminant front due to advection. The contaminant front moved downward at a speed proportional to the contaminant's average linear advection velocity as shown in Figure 4-9. As the advection velocity is increased, the contaminant front moves further down from the sediment-water interface.

The *RMS* value for the diffusion-sorption-advection model assuming $u = 20$ cm/y was 2.69×10^{-3} while for the diffusion-sorption-advection model assuming $u = 100$ cm/y, 9.99×10^{-3} . The r values for both cases are still 1.0 showing excellent correlation between the profiles from the analytical solution and CoReTrans' simulation. The source of error for the discrepancy between predicted profiles and the analytical solution is still from the assumed boundary conditions for both modelling approaches.

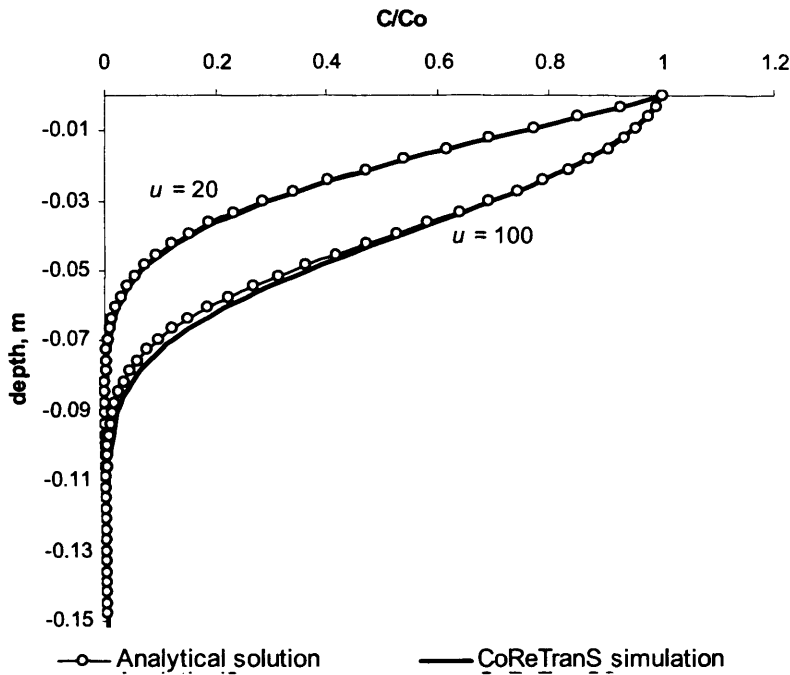


Figure 4-9. Pore water concentration-depth profile for naphthalene subject to diffusive-advective transport ($R = 9$) with varying advective velocities.

4.3.6.3 Effect of contaminant degradation on the diffusion-advection model. Just as in the diffusion model, the effect of an irreversible first-order degradation reaction on the diffusive-advective transport of contaminants in bed-sediments is investigated. The model scenario described herein is governed by the following equation:

$$\frac{\partial C}{\partial t} = \frac{D_{eff}}{R} \frac{\partial^2 C}{\partial x^2} - \frac{u}{R} \frac{\partial C}{\partial x} - \lambda RC \quad \text{Eq. 4-23}$$

subject to the following initial and boundary conditions:

Initial conditions: $C(x, t)|_{t=0} = 0$ Eq. 4-24

Chapter 4

$$\text{Boundary conditions: } C(x, t)|_{x=0} = C_o \quad \text{Eq. 4-25}$$

$$C(x, t)|_{x=30} = 0 \quad \text{Eq. 4-26}$$

The analytical solution for equation 4-23 is discussed by Bear (1972) and developed using Laplace transforms by O'Loughlin and Bowmer (1975):

$$\frac{C}{C_o} = \frac{1}{2} \left[\exp\left\{\frac{ux}{2D_{eff}}(1-\zeta)\right\} \operatorname{erfc}\left(\frac{Rx-ut\zeta}{\sqrt{4RD_{eff}t}}\right) + \exp\left\{\frac{ux}{2D_{eff}}(1+\zeta)\right\} \operatorname{erfc}\left(\frac{Rx+ut\zeta}{\sqrt{4RD_{eff}t}}\right) \right] \quad \text{Eq. 4-27}$$

where

$$\zeta = \sqrt{1 + \frac{4\lambda RD}{u^2}} \quad \text{Eq. 4-28}$$

Simplified forms of equation 4-27 are often used in the open literature. For example, Ogata and Banks (1961) stated that omission of the second term in the governing equation can result to a maximum error of 3% for values of $D_{eff}/ux < 0.002$. O'Loughlin and Bowmer (1975) also showed that terms involving $Rx - ut\zeta$ are relatively small compared to the other terms using L'Hospital's theorem.

The diffusion-advection-degradation model is simulated using CoReTranS and the profiles for the predicted contaminant concentration in pore water were compared with the analytical solution as shown in Figure 4-10.

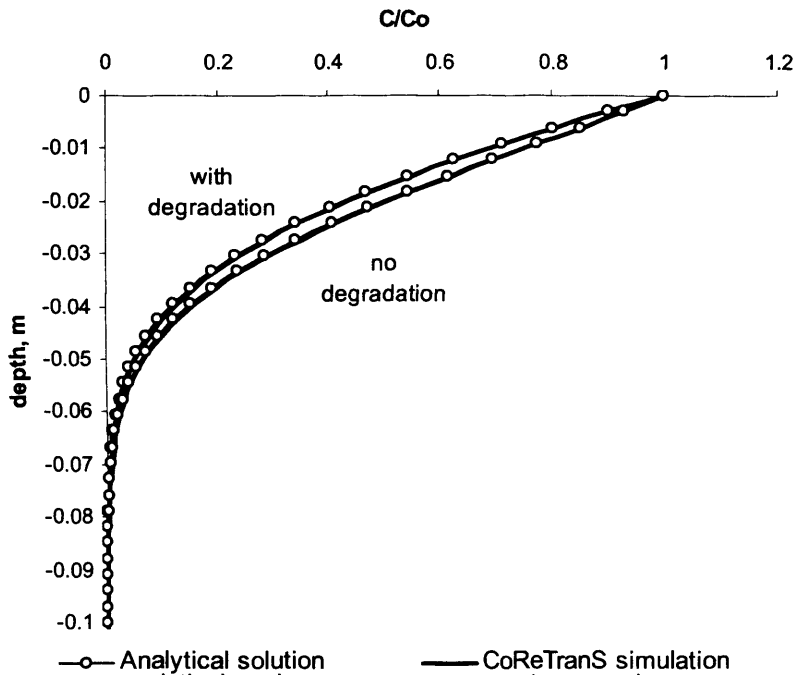


Figure 4-10. Effect of first-order degradation reaction on the pore water concentration-depth profile for naphthalene subject to diffusive-advective transport ($R = 9$).

For the model scenario with degradation, RMS was calculated as 2.39×10^{-3} while for the scenario with no degradation occurring, RMS was calculated as 2.69×10^{-3} . The assumed boundary conditions for the analytical solution and numerical simulation is still the main source of error among the profiles in Figure 4-8. However, the r values for both cases are still 1.0 showing excellent correlation between the profiles from the analytical solution and CoReTranS' simulation.

As predicted in the diffusion model, the effect of contaminant degradation on the diffusive-advective transport of contaminants along the sediment column is shown by a very slight shift of the contaminant front to the left indicating contaminant loss due to decay over time. The impact of the degradation process however was minimal due to the contaminant's high resistance to biological/chemical degradation in the sediments.

4.4 Conclusions of model verification

The CoReTrans model was verified and benchmarked by comparing the numerical simulation results from the two distinct reactive transport models (i.e., diffusion model and diffusion-advection model) and their respective derivatives with their corresponding analytical solutions. Goodness of fit between the predicted profile and the profile quantified from the analytical solution was evaluated using *RMS* and *r* on all model scenarios simulated in this chapter. The *RMS* values obtained from all scenarios ranged from 4.14×10^{-4} to 1.60×10^{-2} . Although minimal, the probable source of error between the predicted profile and the analytical solution lies in the assumption that was made in deriving the exact solution of the diffusion model. Predicted contaminant concentrations approaches zero as sediment depth approaches 30 cm, while for the analytical solution, the contaminant concentration will only approach to zero as sediment depth approaches infinity. Thus, the residual error mostly lies on the base of the sediment column. However, the *r* values for all the profiles were consistently evaluated ($r = 1.0$) which showed excellent correlation between the predicted profiles and the analytical solutions.

On the reactive transport model scenarios, the following concepts were highlighted:

1. The vertical spread of the contaminant front is controlled by diffusion transport caused by the difference in pore water concentration of the contaminant at the sediment-water interface and the background concentration of the sediment column.
2. As migration proceeds with time, the advection process will produce a further downward movement of the contaminant front.
3. Contaminant sorption retards both diffusive and advective transport.
4. The effect of the degradation term is shown by a very slight shift of the contaminant front to the left. This is indicative of contaminant loss due to decay over time. The impact of the degradation process however was minimal due to the chosen contaminant's low degradation rate in the sediments.

Chapter 4

5. The contaminant concentration at the interface was about 5 times less when a constant contaminant flux occurs at the interface, in contrast with the use of a constant concentration condition. This is explained by the action of burrowing benthic organisms and other bioturbation processes at the sediment-water interface.

CHAPTER FIVE

CoReTranS model validation – Interpretation of laboratory experimental study results using the CoReTranS model

5.1 Introduction

Reactive transport modelling is a tool to critically examine the behaviour of contaminated sediment systems. By identifying the fate and transport processes and parameters that control contaminant distribution in bed-sediments, the reactive transport model can guide field and experimental studies and make tangible contributions to the growing understanding of contaminant fate and transport in bed-sediments.

Reactive transport models can be validated using laboratory experiments, where conditions can be more easily controlled and measured than in the field (e.g., spiked initial concentrations, inhibition of microbial growth, etc.). By comparing the simulation results (e.g., contaminant concentration-depth profiles) with the observed data from the experiment, the reactive transport model can be systematically refined in order to predict future contaminant concentrations.

In this chapter, the conditions of a diffusion-controlled experiment for the transport and distribution of selected trace level organic contaminants in a riverine environment as reported in Allan *et al.* (2002; 2004) were simulated using

the CoReTranS model. In order to validate the reactive transport models simulated in CoReTranS, the resulting predictions were compared with the actual data. Key processes and critical parameters that control the fate and transport of contaminants in bed-sediments were identified, highlighting knowledge gaps in order to guide future experimental investigations.

5.2 CoReTranS simulation

5.2.1 Background of the study

Two experimental channels (i.e., channels 1 & 2) that allowed control of water velocity overlying a bed-sediment were developed by Allan (2002) to simulate riverine environmental conditions. Both channels were kept under dark conditions to inhibit photosynthetic activity (i.e., to prevent algal formation). The replicate channels were spiked with 10 mg of lindane in 2 ml acetone. Samples were then collected for analysis. Actual contaminant concentrations in pore water and sediment were determined, and then compared with the profiles generated by a numerically optimised diffusion-sorption-degradation (DSD) model.

Using Fortran 90, Allan *et al.* (2002, 2004) developed a basic 1-dimensional DSD procedural program for the study to calculate diffusion-controlled concentration-depth profiles for micro-organic contaminants in the sediment pore water and the whole sediment bed, based on temporal changes in concentration in the overlying water. The organic matter-normalised linear partitioning coefficient (K_{OC}), linear partitioning coefficient (K_D) and degradation rate constant (λ) were optimised by minimising the *RMS* values between the observed and predicted concentration-depth profiles. The numerical approach of Allan's DSD model allowed temporally and spatially flexible definition of sediment characteristics and processes.

Allan's DSD model was formulated as:

$$\frac{\partial C}{\partial t} = D_{eff} \frac{\partial^2 C}{\partial x^2} - \lambda C \quad \text{Eq. 5-1}$$

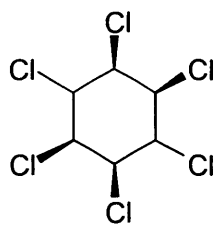
where the effective diffusion coefficient was defined as:

$$D_{eff} = \frac{D}{[1 - \ln(\phi)]^2 [1 + K_D]} \quad \text{Eq. 5-2}$$

The molecular diffusion coefficient D was approximated using the Wilke-Chang empirical correlation and corrected for both retardation and tortuosity effects. The sediment porosity and the linear partitioning coefficient as functions of depth were modelled using an empirical power law equation. An optimised first-order degradation constant completed the set of parameters for Allan's DSD model.

5.2.2 Model contaminant

In all of the scenarios for modelling of the laboratory experiment, lindane was selected from among the micro-organic compounds (permethrin, simazine, nonylphenol) investigated in the original study.



Lindane $C_6H_6Cl_6$
 CAS Registry No. 58-89-9
 Molecular Weight, 290.83 (g/mol)
 Molar Volume, 243.6 (cm³/mol)
 Log K_{ow} , 3.52
 Half-life (*in soil*), 90 (day)

Figure 5-1. Molecular structure of lindane and its chemical properties- values as cited in Mackay *et al.*(1997)

Lindane is an organochlorine insecticide, also called 1,2,3,4,5,6-hexachlorocyclohexane (γ -HCH) and benzene hexachloride (BHC), primarily used in soil treatment, timber protection and treatment for scabies, ticks, and other parasites. Like other agricultural pesticides, lindane is introduced to surface-water environments through run-off, sewage treatment effluents, and industrial

wastewaters. The use of lindane is banned in 52 countries, and it has been proposed to be included in the list of persistent organic pollutants during the Stockholm convention in 2005 (UNEP Persistent Organic Pollutants Review Committee, 2005).

5.2.3 Model formulation and approach

5.2.3.1 Scope. Allan's study (2002; 2004) was aimed at understanding and modelling the various processes that determined the depth distribution of micro-organic contaminants. The dataset mined from Allan's study (2002) is presented in Table 5-1.

Table 5-1. Summary of information taken from Allan (2002).

Lindane mass in spiking solution, μg	10,000
Analysis done	Pore water concentration Whole sediment concentration Overlying water concentration
Sediment sections, mm	10
Experimental measurements	
During experiment	pH and dissolved oxygen profile, temperature, conductivity
After experiment	Major ions, chlorophyll a, EPS, dissolved silicon, sediment particle analysis, porosity profile, organic matter profile

5.2.3.2 Conceptual model. From the observations noted by Allan (2002) in his study, the transport of contaminants was assumed to be mainly diffusion-controlled. Low flow rates (~ 10 cm/s) were used to avoid sediment resuspension. Worm activity was also noted on the sediment-water interface. Changes in contaminant concentration in the overlying water, pore water and whole sediment were measured. As such, a reactive transport model which includes diffusion, sorption, degradation and bioturbation mechanisms may potentially predict the contaminant distribution in sediments.

5.2.3.3 Reactive transport model formulation. In predicting the vertical distribution of lindane using CoReTranS, the following corrections were made to the formulations used in Allan's DSD model:

1. Equation 5-1 is only valid if D_{eff} is a constant parameter. Since the molecular diffusion coefficient was corrected for both retardation and tortuosity effects which were modelled as functions of depth, the governing equation should be expressed as

$$R \frac{\partial C}{\partial t} = \frac{\partial}{\partial x} \left[\phi(x) D_{eff} \frac{\partial C}{\partial x} \right] - \lambda RC \quad \text{Eq. 5-3}$$

where D_{eff} is defined as

$$D_{eff} = \frac{D}{1 - \ln[\phi(x)]^2} \quad \text{Eq. 5-4}$$

2. Sorption, as an additional sink/source term in the governing equation should be dimensionally consistent. Hence, the linear partitioning coefficient (K_D) in equation 5-2 should be replaced by $\rho_B K_D$ and retardation factor should be evaluated as

$$R(x) = \phi(x) + \rho_B K_D(x) \quad \text{Eq. 5-5}$$

3. Thus, solving for the change of contaminant concentration with time, equation 5-3 should be expressed as

$$\frac{\partial C}{\partial t} = \frac{1}{R(x)} \frac{\partial}{\partial x} \left[\phi(x) D_{eff} \frac{\partial C}{\partial x} \right] - \lambda C \quad \text{Eq. 5-6}$$

As described further in the following sections, four model scenarios were considered and simulated in CoReTranS: (1) transport by molecular diffusion only, (2) sorption-retarded diffusive transport using linear partitioning coefficient, K_D , as a function of depth; modelled using a power law equation, (3) sorption-retarded diffusive transport with degradation, and; (4) sorption-retarded diffusive transport with degradation and bioturbation.

For the initial concentration, the bed-sediment was assumed clean prior to spiking of the model contaminants, and C_0 was thus set to zero. The concentration of lindane in the overlying bulk water which was assumed to be uniformly mixed was periodically measured all throughout the experiment using solid-phase extraction. The bulk water concentration of lindane in channel 2 only reached a peak concentration of 117.3 $\mu\text{g/L}$ at the start of the experiment while in channel 1, the bulk water concentration of lindane reached 435.5 $\mu\text{g/L}$. The difference between the nominal concentrations of lindane in both replicate channels may be explained by the incomplete mixing that may have occurred in the second channel. Further, the analytical error may have been attributed to the expected uncertainty associated to the analytical method (i.e., solid-phase extraction) employed in the analysis. Ratola *et al.* (2006) showed that for lindane, a detection limit of 0.097 $\mu\text{g/L}$ corresponded to a precision level of 11.6%, suggesting that the uncertainty associated with the use of solid-phase extraction is inversely correlated to its detection limits (i.e., the lower the detection limit, the higher the uncertainty associated with the results).

In modelling the dataset, the measured bulk water concentration was therefore considered as a boundary condition at the sediment-water interface. The averaged bulk water concentrations from the two replicate channels varied with time and were thus modelled with an exponential correlation, the parameters of which were determined on the basis of a least-square fit. Thus, the boundary condition at the sediment water interface was evaluated as:

$$C(t) = 0.13e^{(-1.1t)} \quad \text{Eq. 5-7}$$

where the *RMS* value was 113.84 $\mu\text{g/L}$.

Zero contaminant flux was assumed at the bottom of the two channels. The parameters used in the CoReTranS simulations, including the porosity profile modelled in Allan's paper, the partition coefficients and degradation rates optimised by Allan's DSD model are presented in Table 5-2.

Goodness of fit between pore water concentration profiles from the CoReTranS simulation using the corrected DSD model and the experimental data from the two replicate channels was evaluated using *RMS* and *r*. The experimental data was taken from eight sediment core sections. Thus, to compare the numerical output with the experimental data, concentration values from the simulation results were averaged based on the length of the individual sediment core sections.

Table 5-2 Model parameters and boundary conditions used in simulating laboratory-scale data taken from Allan *et al.* (2002; 2004)

Parameters	Values
Sediment depth, x , mm	30
Number of grids	100
Simulation time, t , weeks	6
Porosity, $\phi(x)$	$0.69 X^{-0.12 b}$
Organic carbon fraction (dry mass basis), f_{OC}	0.05
Diffusion coefficient, D , cm^2/s	4.64×10^{-6}
Linear partitioning coefficient, K_D , L/kg	21.83
Degradation rate constant, λ , 1/day	5.21×10^{-2}

5.4 Model validation

5.4.1 Diffusion model

5.4.1.1 Approach. The first model simulation was assumed to involve no contaminant degradation and sorption. The porosity profile varied with depth and was thus modelled with a power law equation given as:

$$\varphi(x) = a_p \times \text{depth}^{-b_p} \quad \text{Eq. 5-9}$$

where a_p and b_p were 0.69 and 0.123, respectively, determined on the basis of a least-square fit with *depth* measured in millimetres (Allan *et al.*, 2002; Allan *et al.*, 2004). In the CoReTranS model, the power function for porosity is based on the sediment depth measured in metres; thus, a conversion factor equal to 0.43 was applied to a_p in order to make the units consistent.

5.4.1.2 Results. The pore water concentration-depth profiles of lindane from the two test channels of the experimental dataset from the study were compared to the predicted profiles generated from the model in CoReTranS as shown in Figure 5-2. The *RMS* value was 3.0 $\mu\text{g/L}$ while the *r* value was 0.79.

5.4.1.3 Discussion. The predicted profile was parabolic in shape similar to the actual profile as reflected by a relatively high *r* value, but over-predicted the location of the contaminant concentration peak within the sediment core. The predicted peak concentration of lindane using the diffusion model was only 8% of the actual peak concentration. The computed residuals showed that the predicted contaminant using diffusion model did not fit the actual data. This suggests that concentration gradient (i.e., molecular diffusion) alone is not sufficient to predict the actual contaminant levels in the bed-sediment. Thus, to improve the prediction of the contaminant distribution in the bed-sediment, the retention time of the contaminant in the sediment matrix has to be increased by retarding the diffusive transport of lindane through sorption (i.e., reduced diffusion coefficient, D_{eff}/R).

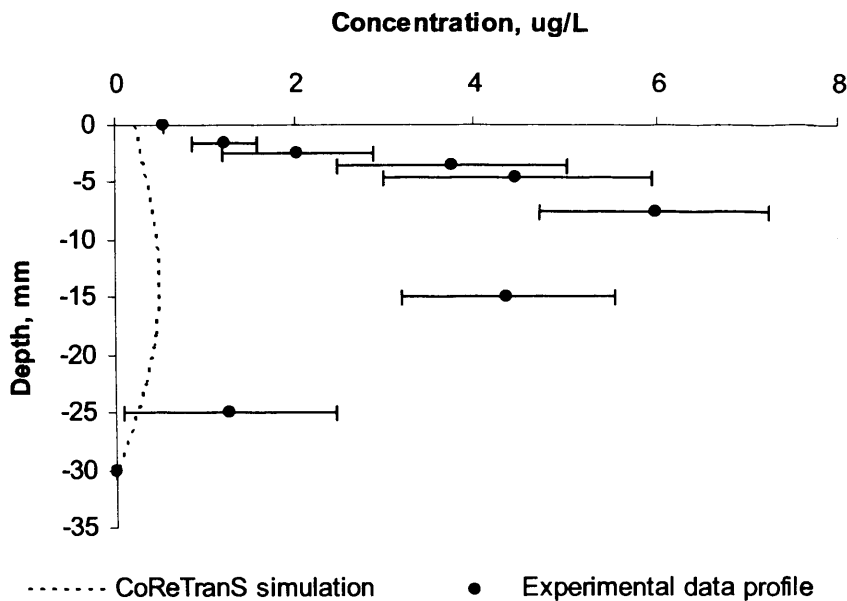


Figure 5-2. Actual and predicted pore water concentration-depth profiles of lindane where contaminant distribution was assumed to be controlled with a diffusive transport only.

5.4.2 Diffusion-sorption model

5.4.2.1 Approach. In this modelling scenario, the vertical distribution of the contaminant was predicted to be controlled by a sorption-retarded diffusive process, where the organic matter-normalised linear partitioning coefficient was assumed to be invariant with time and sediment depth. In CoReTranS, K_D was modelled using the K_{OC} value of lindane reported in the literature.

In Allan's study (2002; 2004), the diffusion-sorption model scenario was simulated by adjusting the organic matter-normalised partitioning coefficient to vary with depth. The organic matter content of the sediment bed was found to be significantly higher in the top layer. The presence of small and light sediment particles in the top layer was shown to possibly account for the variance of the organic matter content in the bed-sediment. Zhou *et al.* (1994) showed that the humic coating on sediment particles is influenced by sediment size (i.e., the smaller the particle, the higher the surface area). Thus, partitioning of the contaminant to the sediments was

hypothesized to decrease with depth. K_D values were calculated for each depth layer in each channel, using the measured whole sediment and pore water concentrations of lindane. A simple power law equation of the form:

$$K_D(x) = 180.94 \times x^{-1.14} \quad \text{Eq. 5-10}$$

was found to fit the range of calculated K_D 's.

The extent of contaminant partitioning and its effect on the diffusive transport of lindane in the sediment was also investigated using various K_D values ranging from 22 L/kg (actual value from literature) down to 1 L/Kg.

5.4.2.2 Results. The pore water concentration-depth profiles of lindane from the two test channels of the experimental dataset from the study were compared to the predicted profiles generated from the diffusion-sorption model in CoReTranS as shown in Figure 5-3. Table 5-3 summarises the *RMS* and *r* values evaluated from the second scenario.

Table 5-3. Evaluation of goodness of fit between the predicted profiles from the second simulation scenario and the actual profile from Allan's experiment (2002; 2004)

K_D (L/kg)	<i>r</i>	<i>RMS</i> , $\mu\text{g/L}$
22	0.51	2.24
15	0.59	2.01
10	0.75	1.59
5	0.94	0.72
3	0.99	0.30
2	0.96	0.58
1	0.83	1.18

The *RMS* and *r* values for the scenario where the linear partitioning coefficient was modelled to vary with depth were 6.08 $\mu\text{g/L}$ and 0.0, respectively.

5.4.2.3 Discussion. As shown in Figure 5-3, the agreement of the predicted profile with the actual data has significantly improved by using the sorption-retarded diffusive transport scenario. The predicted profiles showed a high degree of correlation (e.g., $r \sim 1.0$) when the retardation was decreased by adjusting the K_D values to 3 L/kg.

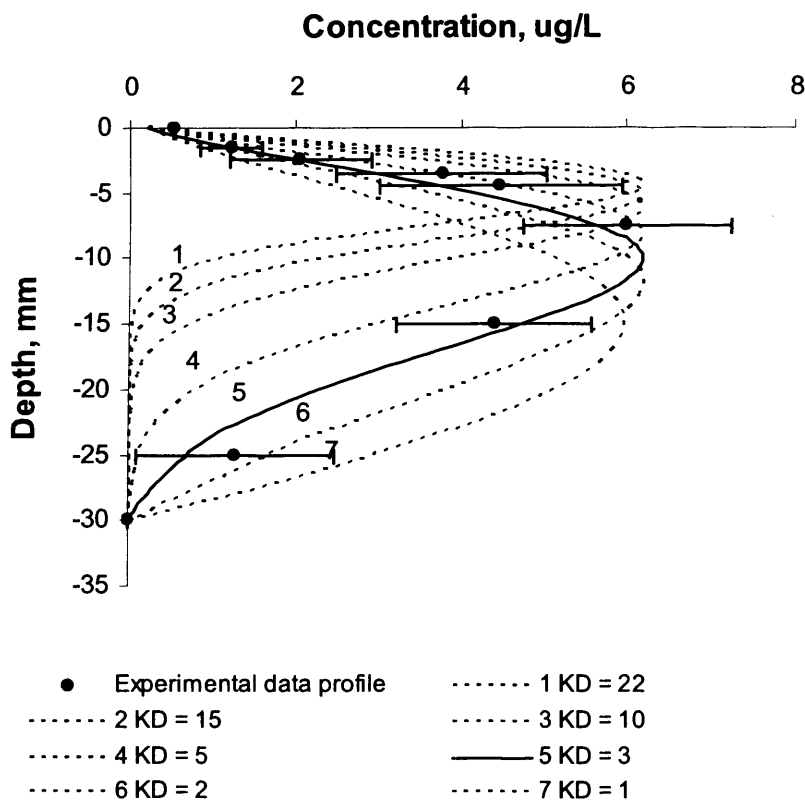


Figure 5-3. Actual and predicted pore water concentration-depth profiles of lindane where contaminant distribution was assumed to be controlled with a sorption-retarded diffusion mechanism using a range of constant K_D 's.

The location of the predicted concentration peak within the sediment core where the linear partitioning coefficient was approximated using the K_{OC} value of lindane reported in the literature may be explained by the set boundary conditions at the sediment-water interface and the extent of contaminant partitioning to the sediment

organic matter. The contaminant concentration at the boundary decreased with time, and as lindane diffused into the bed-sediment, the abrupt change in lindane concentration from C_o to background concentration in the sediment (i.e., zero) coupled with contaminant sorption resulted in contaminant pooling near the interface. Further, lindane diffused significantly less into the lower section of the sediment core due to decreased diffusivity as a result of contaminant partitioning.

The decreasing trend in contaminant partitioning as prediction improves signified less sorption affinity than reported in Allan's study (2002; 2004). The decrease in retardation factor may be explained by the presence of a static or mobile third phase (e.g., colloids, biofilm) which can potentially sequester contaminants from the bulk pore water within the bed-sediment.

Colloidal concentrations were not measured in the original study, and thus no conclusive explanation can be made for the predicted decrease in sorption affinity of the contaminant. Koelmans *et al.* (2000) has also made the same conclusion on the observed decrease in sorption affinity of carbendazim in their microcosm experiment, highlighting a potential gap with regards to the importance of a third phase to the fate and transport of organic contaminants in bed-sediments.

Further, the presence of co-solutes (i.e., permethrin, simazine, nonylphenol) in the experimental channels may have also influenced the contaminant transport predictions. McGinley *et al.* (1993) showed that competitive sorption occurs in a multi-component system, where uptake of organic contaminants by natural sediments is reduced when other organic contaminants are present.

From Allan's modelling approach (2002; 2004), the sorption mechanism was simulated by adjusting the organic matter-normalised partitioning coefficient to vary with depth. Thus, to investigate whether a better agreement between the predicted and actual pore water concentration-depth profiles will result or not, the sorption parameter was adjusted in such a way that enhanced sorption at the top layers is modelled with decreasing sorption capacity along the bed-sediment to allow diffusion of the contaminant to the bottom, as shown in equation 5-10.

Figure 5-4 showed that modelling contaminant partitioning using K_D as a function of depth did not improve the agreement between the predicted and actual profiles. The contaminant concentrations in the first 5 mm were over-predicted by an average of 71%, while the concentrations below the 5 mm depth were under-predicted by an average of 89%. The *RMS* value increased to 6.1 $\mu\text{g/L}$, while the *r* value was almost 0. This scenario suggested that the contaminant was strongly sorbed into the sediment matrix. Thus, to improve the prediction of the contaminant distribution in the bed-sediment, the extent of contaminant partitioning should be decreased. Moreover, the contaminants diffusing through the sediment bed may have undergone decay or flow out of the sediment matrix by mechanical mixing of the upper bed-sediment layer through benthic activity near the sediment water interface, and thus should be included in the model scenario.

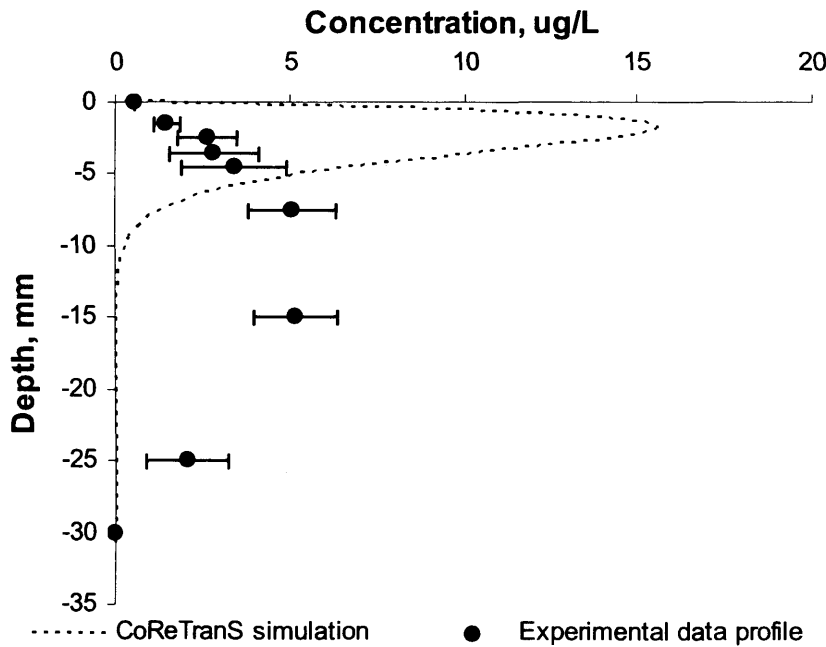


Figure 5-4. Actual and predicted pore water concentration-depth profiles of lindane in using a depth-dependent K_D .

5.4.3 Diffusion-sorption-degradation model

5.4.3.1 Approach. The third CoReTranS simulation of Allan’s experiment (2002; 2004) included a term to describe loss of lindane by degradation, for which, much work has already been done. For example, Kalsch *et al.* (1998) showed that after 91 days, 46.8% of lindane were mineralized in a sediment-water set-up. Aerobic degradation by specific bacterial strains has been demonstrated for lindane (Imai *et al.*, 1991; Nagasawa *et al.*, 1993). Lindane has also been found to degrade under anaerobic conditions (Middeldorp *et al.*, 1996; Singh *et al.*, 2000). Thus, the addition of a degradation mechanism to the model is intuitive.

The average half-life of lindane in soil is 90 days (Mackay *et al.*, 1997) but was found to be 12 days for channel 1 and 15 days for channel 2 in Allan’s study (2002; 2004). The degradation process in CoReTranS was assumed to occur in both pore water and sediment particles, under the local equilibrium assumption.

The sorption mechanism for the third model scenario was still assumed to be linear and constant ($K_D = 3 \text{ L/kg}$).

5.4.3.2 Results. The pore water concentration-depth profiles of lindane from the two test channels of the experimental dataset from the study were compared to the predicted profiles generated from the DSD model in CoReTranS, as shown in Figure 5-5. Table 5-4 summarises the *RMS* and *r* values evaluated from the diffusion-sorption-degradation model scenario.

Table 5-4. Evaluation of goodness of fit between the predicted profiles from the third simulation scenario and the actual profile from Allan’s experiment (2002; 2004)

Scenario	<i>r</i>	<i>RMS</i> , ug/L
use of $t_{1/2} = 12\text{-}15$ days	0.18	2.65
use of $t_{1/2} = 90$ days	0.99	0.87
no degradation	0.99	0.30

5.4.3.3 Discussion. As shown in Figure 5-5, the inclusion of a degradation process in the model equation did not improve the prediction of the pore water concentration profile of lindane. The predicted profiles for the scenario where the contaminant half-life was approximated using the value reported in the literature (i.e., 90 days) showed a high degree of correlation (e.g., $r \sim 1.0$). The residual error, however, increased to more than twice the value from the scenario where there was no degradation involved. Further, the actual contaminant concentrations exceeded the predicted concentrations from the K_D -adjusted scenario ($K_D = 3 \text{ L/kg}$) by an average of 28%.

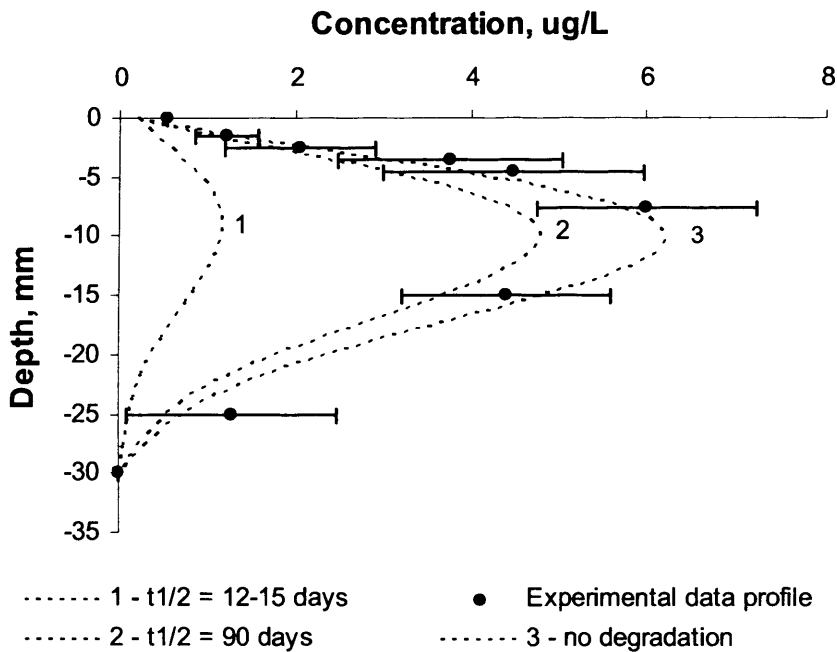


Figure 5-5. Actual and predicted pore water concentration-depth profiles of lindane where contaminant distribution was assumed to be controlled with a sorption-retarded diffusion mechanism using a range of contaminant half-lives ($K_D = 3 \text{ L/kg}$).

The predicted pore water concentration profiles for lindane in both channels were influenced by the extent of contaminant loss through degradation. From Allan's experiment, the reported degradation rates (i.e., $t_{1/2} = 12-15$ days) were significantly higher than the rates reported in literatures ($t_{1/2} \sim 90$ days). The presence of a highly

oxic layer near the sediment-water interface was shown to possibly account for the accelerated degradation in Allan's experiment. It is important to note, however, that the experiment only lasted for 6 weeks, and thus only a fraction of the contaminant present in the bed-sediment may have degraded.

5.4.4 Diffusion-sorption- bioturbation model

5.4.4.1 Approach. In Allan's experiment (2002; 2004), bioturbation activity was observed. A few native *oligochaete* worms were noted for their deposit-feeding activity at the surface. To predict the effect of bioturbation on the fate and transport of lindane in the bed-sediment, a bioturbation mechanism modelled as an exchange function was included in the governing transport equation.

The potential effect of bioturbation on the vertical distribution of lindane in the sediment pore water was investigated using parameters obtained from the open literature. For this particular simulation scenario, the bioturbation process was given the non-local exchange formalism. Thus, the governing equation was expressed as:

$$\frac{\partial C}{\partial t} = \frac{1}{R(x)} \frac{\partial}{\partial x} \left[\phi(x) D_{eff} \frac{\partial C}{\partial x} \right] - \eta(C - C_w) \quad \text{Eq. 5-10}$$

where the effective mass transfer coefficient η was given a value of $6.912 \times 10^{-3} \text{ day}^{-1}$ estimated from the values presented in Wang and Matisoff (1997), and the overlying water concentration C_w was assumed to be the contaminant concentration at the sediment-water interface.

5.4.4.2 Results. From Figure 5-6, the resulting pore water concentration-depth profiles of lindane from the two test channels were compared to the predicted profiles generated from the model incorporating bioturbational effects in CoReTranS. The *RMS* value was $0.44 \mu\text{g/L}$, and the *r* value was 0.99.

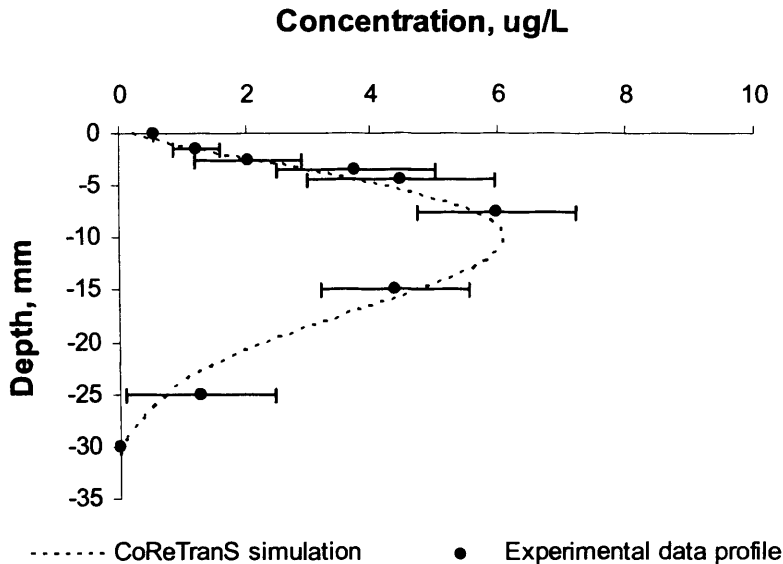


Figure 5-6. Pore water concentration-depth profiles of lindane for the diffusion-sorption -bioturbation model.

5.4.4.3 Discussion. As shown in Figure 5-6, the inclusion of the bioturbation process in the DSD model did not improve the agreement between actual and predicted profiles of lindane. The deviation between the profiles may be caused by other unaccounted phenomenon within the bed-sediment. For example, contaminant sorption to colloids (i.e., as a third phase) may have influenced the decrease in observed K_p values (Chiou *et al.*, 1986; Mitra and Dickhut, 1999). A combination of fast and slow sorption may have also occurred in the system, which is not considered in all of the simulation scenarios. For instance, lindane exhibited both fast and slow partitioning with subsurface fine sand, with the slow fraction about $\frac{3}{4}$ of the total sorbed compound in a study by Pignatello and Xing (1996). In Allan's study (2002; 2004), lindane was observed to reside in the top sections for a longer period compared to the bottom layers, potentially leading to slow partitioning in the top layers.

5.5 Conclusions of model validation using laboratory experimental study results and recommendations for future works

A dataset from a diffusion-controlled experiment for the transport and distribution of selected trace level organic contaminants in an artificial river system was used to validate the CoReTranS model in predicting the fate and transport of the contaminant lindane in bed-sediments. The controlled conditions in place such as spiked initial contaminant concentrations and water flow velocity overlying a finite sediment layer allowed the selection of fate and transport processes which critically influenced the vertical distribution of the contaminant. A DSD model was therefore developed and simulated, the results of which were compared with actual contaminant concentration-depth profiles measured from two replicate channel experiments done by Allan *et al.* (2002; 2004).

In predicting the vertical distribution of lindane using CoReTranS, corrections were made to the formulations used in Allan's DSD model. Thus, four new simulation scenarios (diffusion, diffusion-sorption, diffusion-sorption-degradation and diffusion-sorption-bioturbation models) were developed to better understand the fate and transport of lindane in the experimental bed-sediment. The diffusion-sorption model gave a good agreement after adjusting the sorption capacity (i.e., $K_D = 3 \text{ L/kg}$). No conclusive explanation of the reduced sorption capacity was presented, however, due to lack of data regarding colloidal concentration in the experimental bed-sediment. Further, both contaminant degradation and bioturbational activity in the experimental channels were not predicted to impact the fate and transport of lindane in the bed-sediment. The experiment only lasted for 6 weeks, and thus only a fraction of the contaminant present in the bed-sediment may have degraded. The deviation between the profiles may be caused by other unaccounted phenomenon within the bed-sediment such as contaminant sorption to colloids (i.e., as a third phase) resulting in observed K_D 's which may be actually lower than the true K_D 's.

Therefore, the potential areas for further investigation may be as follows:

1. Evaluation of the mass transfer coefficient to critically examine the effect of bioturbation using the native *oligochaete* worms in Allan's experimental set-up;
2. Analysis of the bioturbation flux of contaminant using a local bio-diffusion parameter;
3. Investigation of the effect of colloids present in different pore water concentrations; and
4. Investigation of slow/fast sorption phenomenon.

CHAPTER SIX

CoReTranS model validation – Interpretation of field study results from PAH-contaminated sites using the CoReTranS model

6.1 Introduction

Polycyclic aromatic hydrocarbons (PAHs) are ubiquitous contaminants in sedimentary environments (Blumer, 1976; Brenner *et al.*, 2002; 1975). Over the past centuries, anthropogenic activity, primarily through fossil fuel combustion, has contributed to the general increase of PAHs in surface waters (Hites *et al.*, 1977). These anthropogenic inputs were mostly from atmospheric deposition to the surrounding surface water due to industrial discharges such as that from smelting plants (Naf *et al.*, 1994; Simpson *et al.*, 1998a; Thrane, 1987) or oil spillages in open waters (Peacock *et al.*, 2007; Reddy *et al.*, 2002a; Reddy and Quinn, 2001).

The persistence of PAHs in sedimentary environments is mainly attributable to their hydrophobic nature and low water solubility, as well as their toxicity to potential degrading organisms. Their presence in natural sediments is of great concern due to their mutagenic and carcinogenic effects (White, 1986), environmental persistence, and their potential to bioaccumulate in aquatic species (Mitra *et al.*, 2000; Roper *et al.*, 1997). As such, PAHs are listed as priority environmental contaminants by the United States and the European Community (Wild and Jones, 1995).

In this chapter, datasets derived from two field monitoring studies for PAHs (Simpson *et al.*, 1998; White *et al.*, 2005) were simulated using the CoReTranS model. The dataset from the study made by White *et al.*, (2005) was used to validate the CoReTranS model by comparing the numerical results with the actual field data and the results from a numerical model developed by White. The CoReTranS model was then applied to the dataset from Simpson's study (1998) in order to explain key processes that controlled the fate and transport of PAHs in bed-sediments. Recommendations to guide future field investigations were made based on the simulation results.

6.2 PAHs in West Harbour, West Falmouth, MA

6.2.1 Background of the study

From the study earlier made by Reddy *et al.* (2002a) on the persistence of petroleum-derived hydrocarbons in marsh sediments from Wild Harbour, West Falmouth, MA (see Figure 6-1), it was shown that the concentration levels of a complex mixture of petroleum at the 6 – 28 cm depth remained unchanged over the span of 30 years since the No. 2 fuel oil spill from the barge *Florida* occurred in 1969, indicating an absence of chemical or biological degradation.

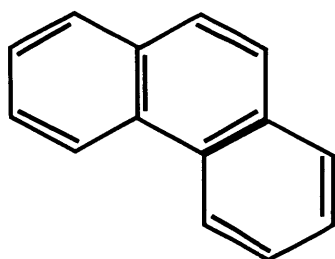


Figure 6-1. Map of the area where the barge Florida sank. (taken from Reddy (2002)).

White et al. (2005) collected a 15-cm diameter sediment core from the intertidal marsh sediments at the M-1 station (see Figure 6-1) in August 2000. The sediment core was sectioned at 2-cm intervals and analysed for total petroleum hydrocarbon content. The sediment samples collected at the site were observed to be heterogeneous due to the presence of channels through which the spilled oil penetrated and the widespread *Spartina alterniflora* root systems.

6.2.2 Model contaminant

In simulating White's dataset, the naphthalene species (C1-, C2-, C3-N) and the phenanthrene species (C1-, C2-, C3-P) were selected from among the 36 target PAHs analysed in the original study. This species grouping is based on the number of alkyl homologues for both naphthalene and phenanthrene. For the C1 species, the alkylated compounds contain only one carbon group (i.e., methyl group). For the C2 species, two carbon groups (i.e., dimethyl or ethyl group) are attached to the parent compound; while for the C3 species, three carbon groups (i.e., trimethyl, methylethyl, or propyl group). The molecular structure of phenanthrene is shown in Figure 6-2, while for naphthalene, see Figure 4-2 (section 4.3.1) for its structure and properties.



Phenanthrene $C_{14}H_{10}$
CAS Registry No. 85-01-8
Molecular Weight, 178.2 (g/mol)
Molar Volume, 199 (cm³/mol)
Log K_{ow} , 4.57
Half-life, 708.33 (day)

Figure 6-2. Molecular structure of phenanthrene and its chemical properties -values as cited in Mackay et al.(1997)

Phenanthrene, like most PAHs is produced from coal tar and is used to make dyes, plastics, pesticides, explosives, and pharmaceuticals. It has also been used to make cholesterol and steroids. Sufficient information exists to classify phenanthrene

as a carcinogenic substance (Agency for Toxic Substances and Disease Registry (ATSDR), 1990).

6.2.3 Model formulation and approach

6.2.3.1 Scope. White *et al.* (2005) investigated the abundance and persistence of PAHs in the Wild Harbour marsh sediments in order to assess whether diffusion and sorption are the prevailing processes that control the vertical distribution of PAHs at the contaminated site. White's study (2005) examined the dominant reactive transport processes that controlled the vertical distribution of PAHs through a simple post-depositional transport model built to assess the effects of sediment-water partitioning and molecular diffusion on the post-depositional transport of PAHs. The dataset mined from White's study (2005) is presented in Table 6-1.

Table 6-1. Summary of information taken from White *et al.* (2005).

Analysis done	Total contaminant concentration in bulk sediment
Sediment sections, cm	15
Field measurements	Radioactive decay of ^{210}Pb , ^{214}Pb , ^{137}Cs , Total organic carbon, moisture content (solid-to-water ratio), porosity profile

6.2.3.2 Conceptual model. From the observed downcore profiles of the PAHs, the peak width (i.e., measured at the base of the peak) can be explained by the contaminants' diffusivities in the bed-sediment. The modelling approach previously developed by Reisser (1997) to investigate alkylbenzenesulfonates as potential molecular markers in lake sediments was used by White *et al.* (2005) to predict PAH distribution at the site.

6.2.3.3 Reactive transport model formulation. The governing equation used by White *et al.* (2005) was,

$$\phi \frac{\partial C}{\partial t} = \frac{\partial}{\partial x} \left(\phi D_{eff} \frac{\partial C}{\partial x} \right) - \frac{\partial}{\partial x} (\phi w C) \quad \text{Eq. 6-1}$$

where w is the velocity of burial of particles below the sediment-water interface and set to 0.35 cm y^{-1} . This parameter was based on sediment accumulation rates measured from ^{210}Pb profiles. The effective diffusion coefficient was evaluated as

$$D_{eff} = \frac{D}{\theta^2(1 + r_{SW}K_D)} \quad \text{Eq. 6-2}$$

where the tortuosity factor θ^2 was given a value of 2.27 and the sediment-to-water ratio r_{SW} was set to 0.28 g ml^{-1} . The molecular diffusion coefficient was estimated using the Hayduk-Laudie empirical correlation. The governing equation was then solved using the Crank-Nicolson implicit method (Crank, 1975).

Using the CoReTranS modelling environment, the governing equation (equation 6-1) was simulated as a diffusion-sorption-advection (DSA) model, where the effective diffusion coefficients of the contaminant species were estimated using the Hayduk-Laudie correlation. The retardation factor was evaluated using a linear sorption mechanism, where the bulk density was estimated from the sediment-to-water ratio r_{SW} and the average sediment porosity (i.e., $r_{SW} = \rho_B / \phi$). The tortuosity factor was estimated using modified Weissberg equation.

The model was simulated over a 30 cm sediment depth and 31 year period. The model parameters used to simulate the governing model equation are presented in Table 6-2 for both the naphthalene species (C1-, C2-, C3-N) and the phenanthrene species (C1-, C2-, C3-P).

Table 6-2. Model parameters used in simulating field-scale data for the naphthalene and phenanthrene species taken from White *et al.* (2005)

Parameters	C1 - N	C2 - N	C3 - N	C1 - P	C2 - P	C3 - P
Sediment depth, cm	30	30	30	30	30	30
Number of grids	100	100	100	100	100	100
Simulation time, weeks	1612	1612	1612	1612	1612	1612
Porosity (v/v)	0.44	0.44	0.44	0.44	0.44	0.44
Organic carbon fraction (dry mass basis)	0.1	0.1	0.1	0.1	0.1	0.1
Diffusion coefficient, cm ² /s	5.70 x10 ⁻⁶	5.30 x10 ⁻⁶	5.00 x10 ⁻⁶	4.90 x10 ⁻⁶	4.60 x10 ⁻⁶	4.40 x10 ⁻⁶
log K_{ow} , L/kg	3.94	4.15	4.36	4.99	5.20	5.40
K_D , L/kg	350	560	900	3720	5970	9380
Pore water velocity, cm/y	0.35	0.35	0.35	0.35	0.35	0.35

Moreover, no significant contaminant loss due to biodegradation was observed to occur today as shown in a study done by Slater *et al.* (2005), and thus degradation was assumed as a non-controlling mechanism for the vertical distribution of PAHs at the site. Bioturbational effects was also assumed negligible, considering the probable decimation of the macrobenthic population as an after-effect of the oil spill (Krebs and Burns, 1977; Wheatcroft and Martin, 1996).

An initial unit concentration was set at a depth of 6 cm from the sediment-water interface as no actual initial concentration was available from the study. The contaminant was assumed to penetrate approximately 6 cm of the sediment bed when the oil was spilled based on the measured peak width of the contaminant profile at its highest concentration. The initial and boundary conditions for this model scenario were given as:

$$\begin{array}{lll} \text{Initial conditions:} & C(x,t)|_{t=0} = 1 & 0 < x \leq 6 \text{ cm} \\ & = 0 & x > 6 \text{ cm} \end{array} \quad \text{Eq. 6-3}$$

$$\text{Boundary conditions:} \quad C(x,t)|_{x=0} = 0 \quad \text{Eq. 6-4}$$

$$C(x,t)|_{x=30} = 0 \quad \text{Eq. 6-5}$$

6.2.4 Model validation

6.2.4.1 Approach. Six contaminant concentration-depth profiles from CoReTranS as shown in Figure 6-3 and Figure 6-4 were compared with the PAHs downcore profiles and the numerical model profiles from the published literature. The contaminant concentrations were placed in a single scale of variation (i.e., 0 to 1) by normalising the concentration values to their maxima.

Goodness of fit between the concentration profiles from the CoReTranS simulation using the DSA model and experimental data was evaluated using *RMS* and *r*. The experimental data was taken from 16 sediment core sections. Therefore, the concentration values from the simulation results were averaged based on the length of the individual sediment core sections in order to compare the numerical output with the experimental data. Simulation results from White's numerical model in CoReTranS were also compared with the DSA model results using *RMS* and *r*.

6.2.4.2 Results. Table 6-3 summarises the *RMS* and *r* values evaluated from comparing the predicted pore water concentration-depth profiles using the DSA model in CoReTranS with the actual profiles. An excellent agreement (*r* = 1.0, *RMS* = 0) was achieved between simulation results of the DSA model in CoReTranS and White's numerical profiles.

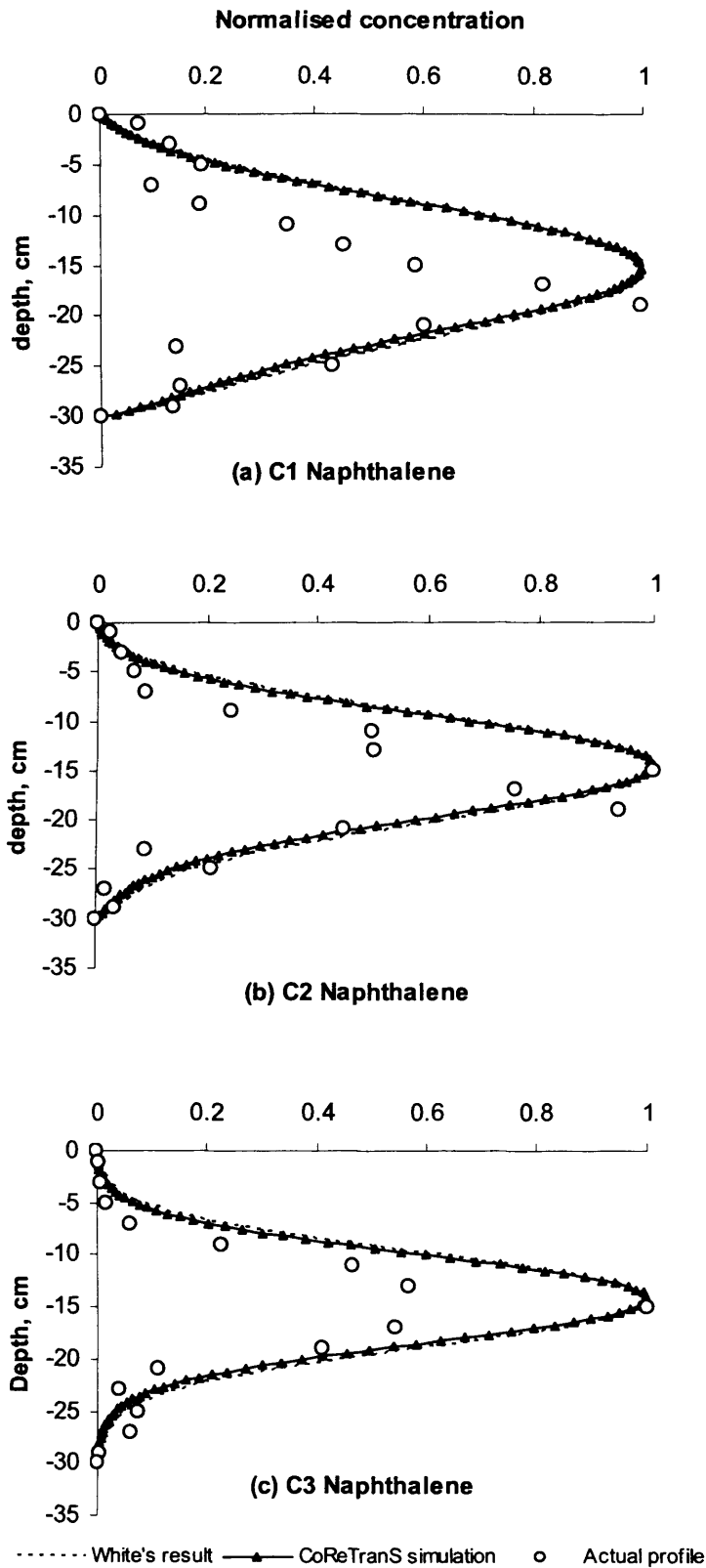


Figure 6-3. Contaminant concentration-depth profile of the naphthalene species as simulated in CoReTranS in comparison with White's actual data and previous model.

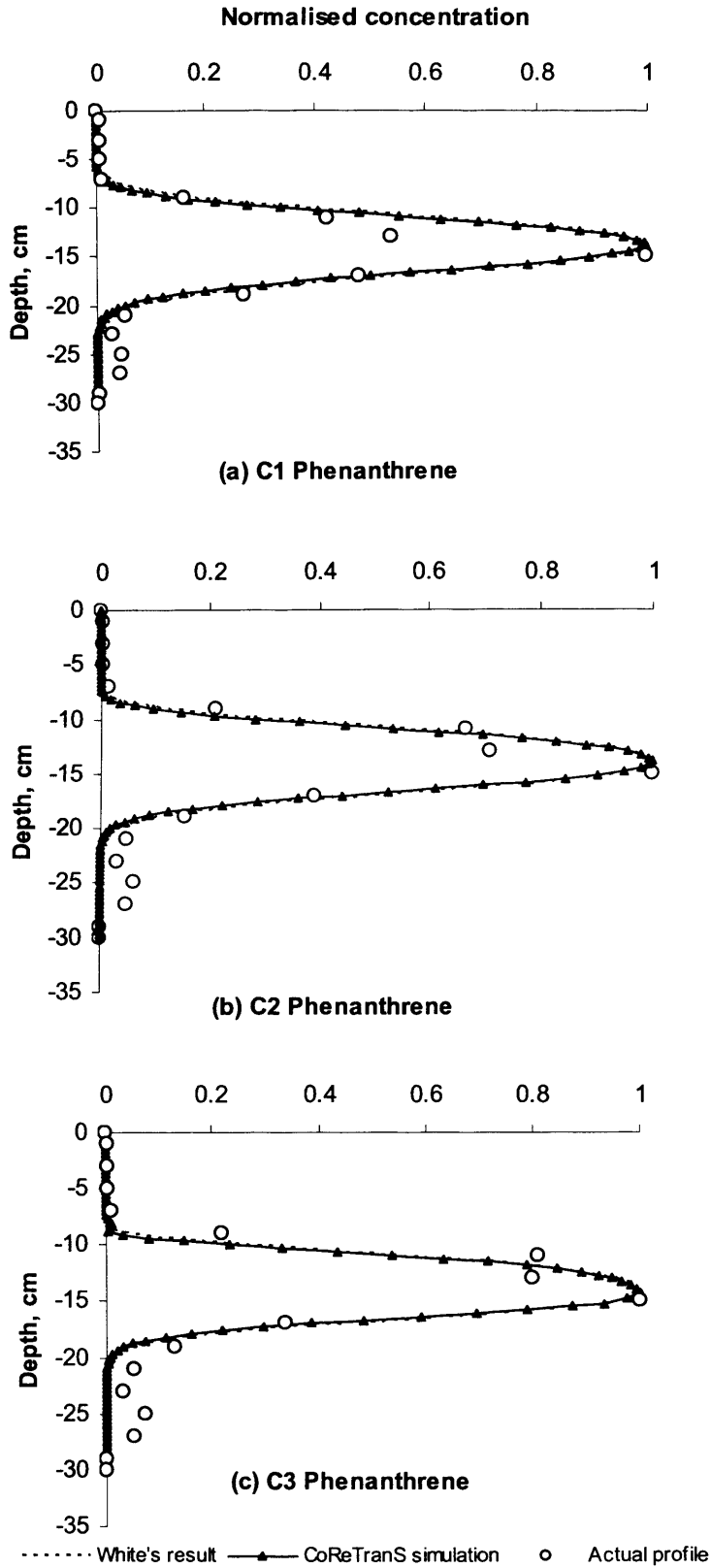


Figure 6-4. Contaminant concentration-depth profile of the phenanthrene species as simulated in CoReTranS in comparison with White's actual data and previous model.

Table 6-3. Evaluation of goodness of fit between the DSA model in CoReTranS and actual profile for all six contaminants.

Contaminant	<i>RMS</i>	<i>r</i>
C1 - naphthalene	0.28	0.73
C2 - naphthalene	0.23	0.99
C3 - naphthalene	0.18	0.99
C1 - phenanthrene	0.17	0.99
C2 - phenanthrene	0.11	1.0
C3 - phenanthrene	0.10	1.0

6.2.4.3 Discussion. For C1- and C2-naphthalene, the predicted profiles showed broad asymmetric distributions that were over-predicted by the model in the 5 – 20 cm depth. The predicted concentrations of C1- and C2-naphthalene in the upper 5 cm can be attributed to the contaminant’s diffusivities (i.e., 0.81 and 0.47 cm²/yr, respectively) exceeding the burial velocity (0.35 cm/yr). Contaminant loss either due to surface evaporation or biodegradation activity of oil-resistant microbial species may possibly cause the failure to correctly predict the contaminant distribution.

For C3-naphthalene, the predicted profile was narrower and more symmetric as compared to the profiles for C1- and C2-naphthalene. The C3-naphthalene profile was better approximated by the model and thus showed to be a more diffusion-controlled scenario.

For the phenanthrene species, much narrower peaks resulted in the predicted profiles due to their relatively higher diffusion coefficients and more hydrophobic nature. The overall agreement between the predicted and actual profiles was also better than that of the naphthalene species.

Goodness of fit of the simulation profiles can further be improved by evaluating and extending the original model to incorporate more processes such as bioturbation and degradation. Thus, the following may be potential areas for further research:

1. Evaluation of the mass transfer coefficient to critically examine the effect of contaminant loss due to bioturbation activity of macrobenthic organisms in marsh sediments.
2. Analysis of colloidal concentrations along the marsh sediment cores to see if partitioning to a third phase can improve the prediction of contaminant distribution.
3. Analysis of the intermittent effect of tides on the model parameters (i.e., functions of time)
4. Analysis of the effect of the marsh grass *Spartina alterniflora* that grow at the site and penetrate the upper sediment on the contaminant uptake loss (See, for example, Watts *et al.*, 2006).

6.3 PAHs in Kitimat Arm, Douglas Harbour, British Columbia

6.3.1 Background of the study

In an earlier study done by Cretney *et al.* (1983) in the Kitimat fjord system near Kitimat, British Columbia, elevated levels of PAHs were found in sediments purported to be derived from atmospheric particle emissions, wastewater discharges, and accidental spillages from a nearby aluminium smelter. Simpson *et al.* (1998; 1996) further examined the variations in PAH composition in size-fractionated sediments and depth-fractionated sediments collected from a Canadian fjord.

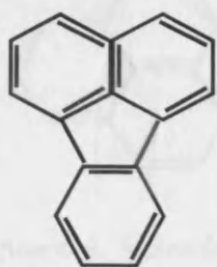
Kitimat Arm (see Figure 6-5) has three major industries: an aluminium smelter, a pulp mill, and a methanol producing plant, all believed to be major contributors to the decline of water and sediment quality in Kitimat Arm and Douglas Channel. A 9-cm sediment core was collected from Gilyotees Inlet (Figure 6-5). The sample was subsectioned at 5-cm intervals and analysed for unsubstituted PAHs and selected alkylated PAH homologues.



Figure 6-5. Map of Kitimat Arm fjord system where sediment samples were taken (taken from Simpson et al (1998)).

6.3.2 Model contaminant

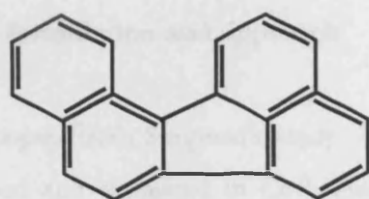
In all of the scenarios for modelling of the Kitimat fjord dataset, fluoranthene (Figure 6-6), benzo[a]fluoranthene (Figure 6-7) and pyrene (Figure 6-8) were selected from among the unsubstituted PAHs and alkylated PAH homologues analysed from 5-cm sections of sediments core collected at the contaminated site.



Fluoranthene $C_{16}H_{10}$
CAS Registry No. 206-44-0
Molecular Weight, 202.26 (g/mol)
Molar Volume, 217 (cm³/mol)
Log K_{OW} , 5.22
Half-life, 2291.67 (day)

Figure 6-6. Molecular structure of fluoranthene and its chemical properties- values as cited in Mackay *et al.*(1997)

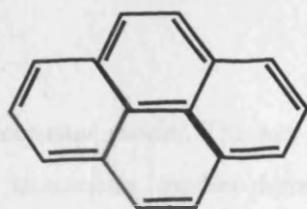
Fluoranthene is a product of combustion of organic matter, and is present in fossil fuel products. It is also used as a constituent of coal tar and petroleum derived asphalt primarily as lining material in water pipes and storage tanks. Fluoranthene is one of the U.S. Environmental Protection Agency's 16 priority pollutant PAHs and is considered carcinogenic (Agency for Toxic Substances and Disease Registry, 2005).



Benzofluoranthene $C_{20}H_{12}$
CAS Registry No. 206-44-0
Molecular Weight, 252.0 (g/mol)
Molar Volume, 268.9 (cm^3/mol)
Log K_{OW} , 5.8
Half-life, 2291.67 (day)

Figure 6-7. Molecular structure of benzofluoranthene and its chemical properties- *values as cited in Mackay et al.(1997)*

Benzofluoranthene, like most PAHs, is found in fossil fuels and occurs ubiquitously in products of incomplete combustion. However, there is no commercial production or known use of this compound. The U.S. Environmental Protection Agency ranked benzofluoranthene as one of the most hazardous compounds (i.e., among the worst 10%) to the environment (Agency for Toxic Substances and Disease Registry, 2005; US Environmental Protection Agency, 2000).



Pyrene $C_{16}H_{10}$
CAS Registry No. 129-00-0
Molecular Weight, 202.25 (g/mol)
Molar Volume, 214 (cm^3/mol)
Log K_{OW} , 5.18
Half-life, 2291.67 (day)

Figure 6-8. Molecular structure of pyrene and its chemical properties- *values as cited in Mackay et al.(1997)*

Pyrene is formed during incomplete combustion of organic material and can be isolated from coal tar. It is used commercially to manufacture dyes, pesticides, pharmaceutical products, and plastics. Pyrene is also included in the U.S. Environmental Protection Agency's list of 16 priority pollutant PAHs, and is considered a human carcinogen (Agency for Toxic Substances and Disease Registry, 2005).

6.3.3 Model formulation and approach

6.3.3.1 Scope. From Simpson's study (1998), a reactive transport model scenario was developed and simulated in CoReTranS to determine the key processes that controlled the vertical distribution of PAHs at the Kitimat fjord site. No previous numerical model was developed for Simpson's study (1998), and thus the findings shown in the preceding sections were mostly presumptive. The dataset mined from Simpson's study (1998) is presented in Table 6-4.

Table 6-4. Summary of information taken from Simpson *et al.* (1998).

Analysis done	Total contaminant concentration in bulk sediment
Sediment sections, cm	9
Field measurements	Sediment particle size fractions, total organic carbon

6.3.3.2 Conceptual model. The key processes controlling the post-depositional distribution of aluminium smelter-derived PAHs in the marine sediments were deduced from the sediment core samples collected on site. The vertical distribution of fluoranthene, benzofluoranthene and pyrene are presented in Figure 6-9.

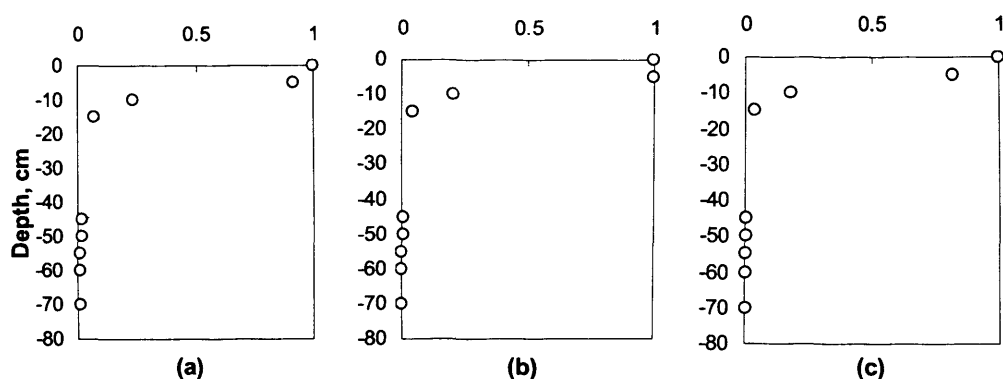


Figure 6-9. Vertical distribution of (a) pyrene, (b) benzofluoranthene, and (c) fluoranthene. All concentrations are normalised to their respective maximum concentrations.

From Figure 6-9, PAH concentrations were highest at the sediment water interface, and decreased significantly with sediment depth. Contaminant concentrations remained relatively constant below the 40 cm depth. Accordingly, the downcore profiles of PAH suggest diffusive transport of contaminants from a continuous contamination source at the sediment water interface, i.e., presumably there is an ongoing local input. The dramatic decrease of PAH concentration with depth implies retarded diffusive movement due to low diffusion coefficients and partitioning to the sediment matrix. And the vertical movement of the contaminant front at the top segments of the sediment core (i.e., 0 – 10 cm depth) indicates inclusion of an advective process to the model scenario.

6.3.3.3 Reactive transport model formulation. The model was developed in CoReTranS as a DSA scenario governed by the equation,

$$\phi \frac{\partial C}{\partial t} = \frac{\partial}{\partial x} \left(\phi D_{eff} \frac{\partial C}{\partial x} \right) - \frac{\partial}{\partial x} (\phi w C) \quad \text{Eq. 6-6}$$

where w is the velocity of burial of particles below the sediment-water interface (i.e., sediment accumulation rate). This parameter was given values ranging from 0.25 to 0.5 cm y^{-1} by Simpson *et al.* (1998).

The effective diffusion coefficient was evaluated as

$$D_{eff} = \frac{D}{\theta^2 \left(1 + \frac{\rho_B}{\phi} K_D \right)} \quad \text{Eq. 6-7}$$

where the tortuosity factor θ^2 was estimated using the modified Weissberg correlation while the molecular diffusion coefficient was estimated using the Wilke-Chang empirical correlation. K_D was modelled using the K_{OC} values of the selected PAHs from the database and the given organic carbon fraction.

Sediment porosity and bulk density were not measured in Simpson's study (1998). Hence, this gap within the initial site-characterisation phase could have potentially benefitted from the CoReTranS model. As such, the sediment porosity was given a value of 0.86 based on the study done on the collected sediments cores at the British Columbia fjords by Bornhold and Prior (1989). The value given for the porosity parameter also falls within the estimated 0.85 – 0.95 porosity range values based on a study done by Sugai (1990) on evaluating sedimentation rates in 2 southeast Alaskan fjords. The British Columbia and Alaska coastline share common fjord features, that is, both are considered high latitude fjords and are typically subjected to episodic sediment deposition. The sediment bulk density was estimated at 1.6 g/cm³ (Bornhold and Prior, 1989). A summary of model parameters and their values are presented in Table 6-5.

Initial and boundary conditions for this model scenario were given as:

Initial conditions: $C(x, t)|_{t=0} = 0$ Eq. 6-8

Boundary conditions: $C(x, t)|_{x=0} = 1$ Eq. 6-9

$C(x, t)|_{x=70} = 0$ Eq. 6-10

Chapter 6

Table 6-5. Model parameters used in simulating the field-scale data for the aluminium smelter-derived PAHs in Kitimat, British Columbia

Parameters	Fluoranthene	Benzofluoranthene	Pyrene
Sediment depth, x , cm	70	70	70
Number of grids	100	100	100
Simulation time, t , weeks	2288	2288	2288
Porosity, ϕ	0.86	0.86	0.86
Organic carbon fraction (dry mass basis), f_{OC}	0.01	0.01	0.01
Diffusion coefficient, D , cm ² /s	4.95×10^{-6}	4.36×10^{-6}	5.0×10^{-6}
Octanol-water partitioning constant, $\log K_{ow}$, L/kg	5.22	5.80	5.18
Linear partitioning constant, K_D , L/kg	624.60	2312.06	570.69
Sediment accumulation rate, w , cm/y	0.15	0.15	0.15

6.3.4 Model validation

6.3.4.1 Approach. The vertical distribution of the contaminants in the Kitimat fjord site was analysed by comparing the actual field data to the numerical results of the DSA model (equation 6-6) simulated in CoReTranS. The concentration-depth profiles of pyrene, benzofluoranthene, and fluoranthene are presented in Figure 6-10.

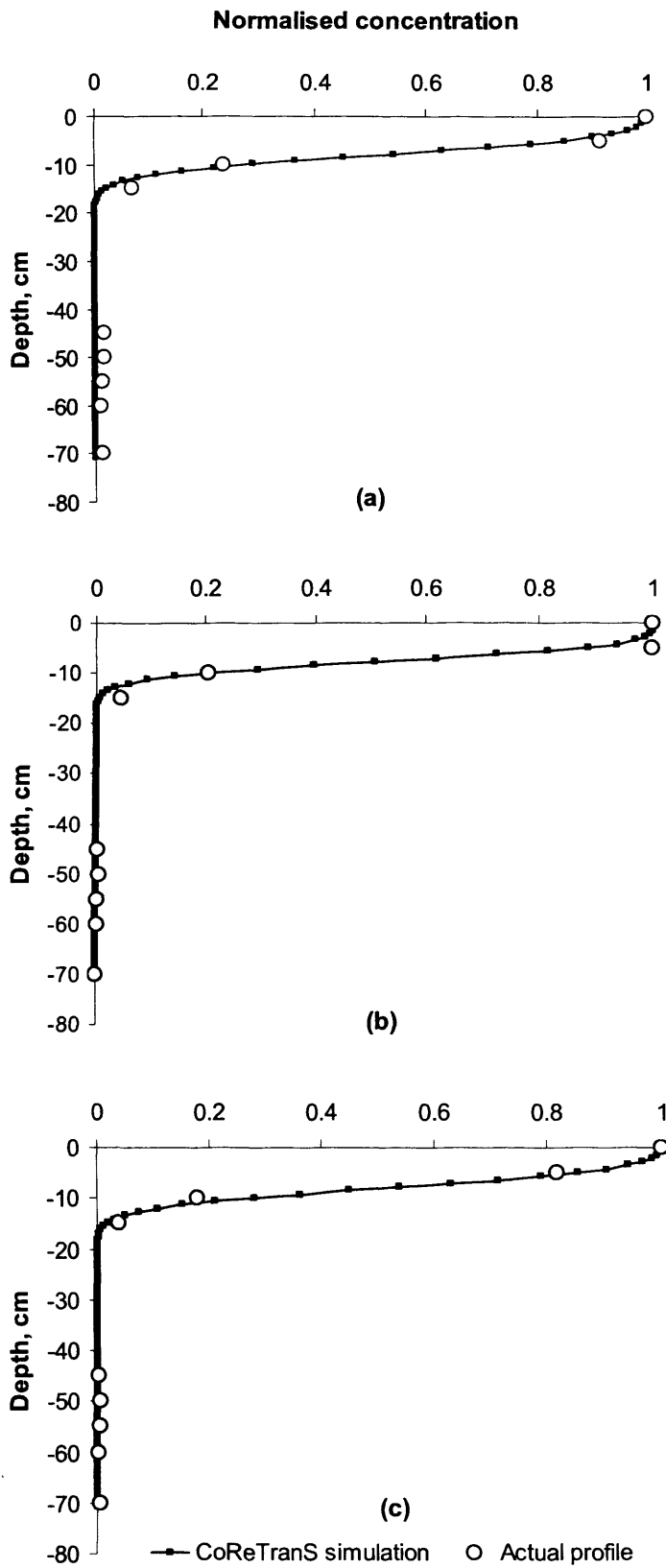


Figure 6-10. Actual and predicted concentration-depth profiles of (a) pyrene, (b) benzofluoranthene, and (c) fluoranthene. All concentrations are normalised to their maximum concentration.

6.3.4.2 Results. The total concentration-depth profiles of the selected contaminants from the Kitimat dataset were compared to the predicted profiles generated from CoReTranS as shown in Figure 6-10. The *RMS* values for pyrene, fluoranthene and benzofluoranthene were 0.08, 0.10 and 0.08, respectively. A good overall agreement was observed (i.e., $r = 0.98$) between CoReTranS' simulation results and the downcore profiles from Kitimat sediments.

6.3.4.3 Discussion. From Figure 6-10, the CoReTranS model predicted the dramatic decrease of the selected PAH concentrations with depth and the vertical movement of the contaminant front at 0 – 10 cm depth. The former can be attributed to low diffusion coefficients and partitioning of the contaminants to the sediment matrix, while the latter may be explained by an assumed advective mechanism in place. The relatively high PAH concentration near the sediment surface was indicative of the downward migration pattern of the contaminant front through episodic sediment deposition. Moreover, the absence of a subsurface maxima on the downcore PAH concentration profiles show that sediment contamination is still controlled by ongoing local inputs, presumably from the nearby aluminium smelter. To further check for systematic error in the simulation process, residual errors between the predicted and actual profiles were analysed as shown in Figure 6-11.

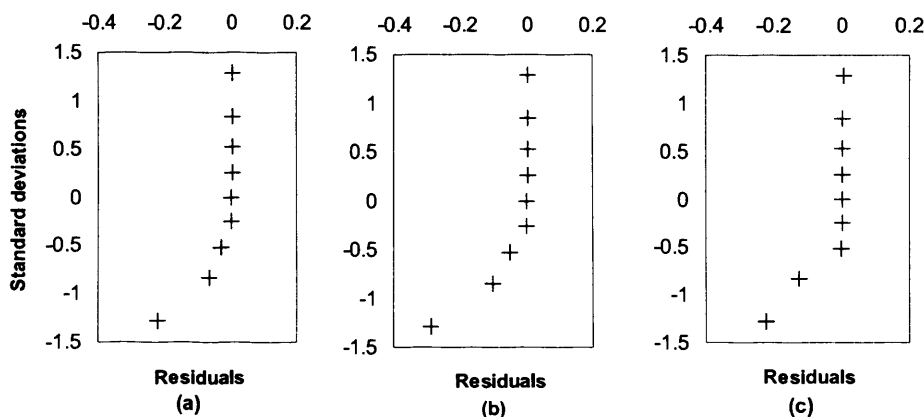


Figure 6-11. Analysis of residual errors between predicted and actual profiles for (a) pyrene, (b) benzofluoranthene, and (c) fluoranthene.

From Figure 6-11, the normal distribution of residuals for all three contaminants produced distinct “tailings” on one end of the distribution plot. These residuals coincided with the contaminant concentrations in the 5 – 15 cm depth section of the sediment cores. The asymmetric distribution of the residuals was indicative of an inadequate representation of the actual system (Ljung, 1987; Soderstrom and Stoica, 1989) probably due to some unaccounted mechanisms that occurred in the past or unrealistic model parameters used in the simulation.

The sediment accumulation rate was one of the model parameters that was approximated with a range of values from the study done by Simpson (1998) as the sediment cores were not dated. The study posited that the increase in PAH concentration between the 20 and 45 cm depth range which coincided with the start of operations at the nearby aluminium smelter plant in 1954 gave an estimate of the sediment accumulation rate between 0.25 - 0.5 cm/y, assuming no sediment compaction and biological mixing occurred in the sediment. Thus, this parameter was calibrated using the model equation (equation 6-6). From Figure 6-12, the sedimentation rate increased with the width of the contaminant peak near the sediment surface. The sedimentation rate that gave the best fit for the downcore profiles of the selected PAHs was 0.15 cm y⁻¹.

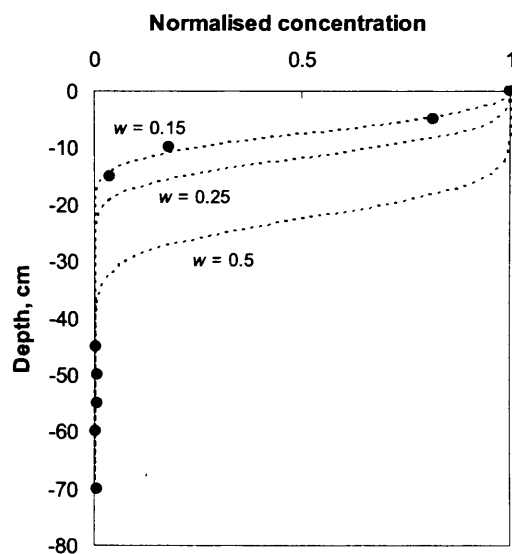


Figure 6-12. Concentration-depth profiles for fluoranthene using various sediment accumulation rates, w . All concentrations are normalised to their maximum concentration.

The two mechanisms that were not included in the model, but may potentially influence the distribution of PAHs were bioturbation and degradation. Contaminant loss due to bioturbation was initially assumed negligible due to lack of bioturbational evidence (e.g., lacking burrows and other distinctive features) on site as reported by Hay (2005) in his study of a fjord system in British Columbia. The assumption can be further explained by anoxic basins that are typically found in fjord environments which offer the potential for examining historic contamination unaffected by bioturbation activity (Syvitski *et al.*, 1987; Syvitski and Shaw, 1995). However, as seen from the results of the residual analysis done on the profiles, the discrepancy between the actual and predicted concentrations lie on the top sections of the bed-sediment where bioturbational activities are most likely to occur. Therefore, bioturbational activity of macro- and micro-benthos at the Kitimat site must be investigated. The mass transfer coefficient should be evaluated in order to critically examine the effect of contaminant loss due to bioturbation activity

To assess whether degradation is a controlling factor in the vertical distribution of PAHs in marine sediments at the contaminated site, the degradation mechanism was added to the simulation scenario. The governing equation was given as,

$$\phi \frac{\partial C}{\partial t} = \frac{\partial}{\partial x} \left(\phi D_{eff} \frac{\partial C}{\partial x} \right) - \frac{\partial}{\partial x} (\phi w C) - \lambda (\phi C + \rho_b K C) \quad \text{Eq. 6-11}$$

where the degradation rate constant λ was estimated using the theoretical half-lives of the selected PAHs taken from CoReTranS' database. From Figure 6-13, it is evident that adding a degradation mechanism to the reactive transport model overly predicted contaminant loss particularly in the top layer of the bed-sediment. This may be explained either by limited contaminant bioavailability or enhanced resistance to biodegradation due to anoxic conditions in fjord sediments.

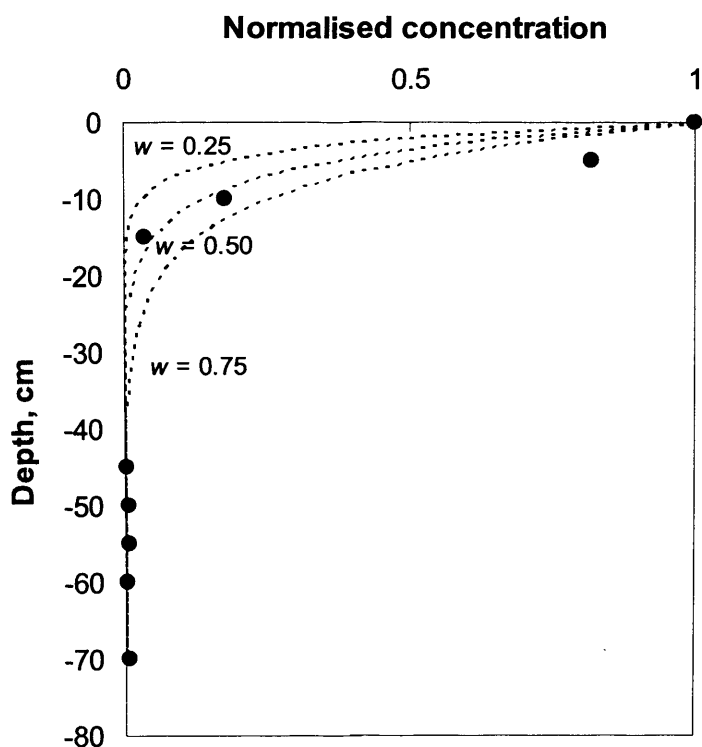


Figure 6-13. Actual and predicted concentration-depth profiles for fluoranthene for a diffusion-advection-degradation model scenario using various sedimentation rates, w . All concentrations are normalised to their maximum concentration.

6.4 Conclusions of model validation using field study results and recommendations for further work

The widespread distribution of PAHs in bed-sediments, just like other hydrophobic organic contaminants, is controlled by diffusive-advective processes as well as post-depositional weathering and biodegradation. This hypothesis was tested using site-specific reactive transport models developed for the marsh sediments contaminated with petroleum-derived hydrocarbons from Wild Harbour, West Falmouth, MA; and for marine sediments near Kitimat, British Columbia. An existing numerical model developed for the Wild Harbour sediments allowed the

Chapter 6

validation of the CoReTranS model by comparing the resulting predictions with the actual data as well as outputs from the numerical model developed by the study.

From the simulations done on the PAH distribution in these contaminated sites, the following may be potential areas for further research:

1. Determine accurate sediment accumulation rates using either ^{210}Pb or ^{137}Cs geochronological studies to examine the effect of sediment deposition on the vertical distribution of PAHs at the contaminated site.
2. Evaluate physico-chemical characteristics of the contaminated sediments to determine exact porosity values and anoxic/oxic conditions.
3. Evaluate the mass transfer coefficient to critically examine the effect of contaminant loss due to bioturbation activity of macrobenthic organisms on the contaminated sediments.
4. Analyse colloidal concentrations in pore water to see if partitioning to a third phase can improve the prediction of contaminant distribution.

CHAPTER SEVEN

Predicting PCB distribution in Lake Hartwell sediments and the effects of monitored natural recovery using the CoReTrans model

7.1 Introduction

Monitored natural recovery (MNR) is a remedial strategy that generally relies on in-bed fate and transport processes to contain, reduce or remove contaminants in bed-sediments (US Environmental Protection Agency, 2005a). The prevailing mechanisms that affect MNR include physical containment of contaminants through sediment burial and sediment mixing, reduction of contaminant mobility and bioavailability through sorption, contaminant transformation through biodegradation, and reduction of contaminant concentration through dispersion of contaminated sediments and/or pore water to the overlying water column. In order to reduce the risk posed by contaminated sediments, burial or mixing of contaminated sediments with clean sediments (i.e., natural capping) is often suggested to augment MNR, since some persistent contaminants are not easily degraded and contaminant dispersion may impact downstream loading. It is important to note however that MNR is a relatively slow process, and its usefulness as a remedial option is subject to several factors such as sufficient rates of sediment deposition and contaminant degradation, reduction of contaminant source, and development of an effective monitoring plan and evaluation methods.

Reactive transport models can complement environmental monitoring plans and address knowledge gaps that exist in site-specific empirical information. This includes:

1. identifying gaps within the site characterisation plan in its initial stages;
2. identifying the fate and transport processes that control the spatial distribution of contaminants at the site; and
3. predicting future contaminant distribution and natural recovery rates.

As monitoring progresses, information gathered from reactive transport models can be compared to measured data from the site, to help assess clean-up progress of MNR.

In this chapter, a dataset derived from field monitoring studies for PCBs was simulated using the CoReTranS model in order to explain key processes that controlled the fate and transport of these contaminants in surface waters and assess the remediation of PCB-contaminated sediments using MNR. Recommendations to guide future field investigations were made based on the simulation results.

7.2 PCBs in Lake Hartwell, Pickens County, SC

7.2.1 Background of the study

From the studies done on the persistence and distribution of PCBs at the Sangamo-Weston/Twelvemile Creek/Lake Hartwell Superfund Site (Lake Hartwell), Pickens County, SC (e.g., Brenner *et al.*, 2004; Dunnivant *et al.*, 1989; Sivey and Lee, 2007), the reservoir was shown to be significantly contaminated with PCBs discharged from a capacitor manufacturing plant at Sangamo-Weston, SC from 1955 to 1977, when PCB use was terminated at the plant. The capacitor manufacturing plant, however, remained in operation until 1987, when the business was sold (US Environmental Protection Agency - Region 4, 2005).

In 2001, sediment cores were sampled from Lake Hartwell (see Figure 7-1). The sediment samples were subsectioned at 5-cm intervals and analysed for 107 PCB congeners, ^{210}Pb and ^{137}Cs . From Brenner's study (2004), the total PCB concentration at the sediment-water interface at sampled locations around Lake Hartwell in 2001 exceeded the EPA clean-up requirement of 1.0 mg/kg, suggesting that resident biota are exposed to high levels of concentration consequently increasing the potential for bioaccumulation.

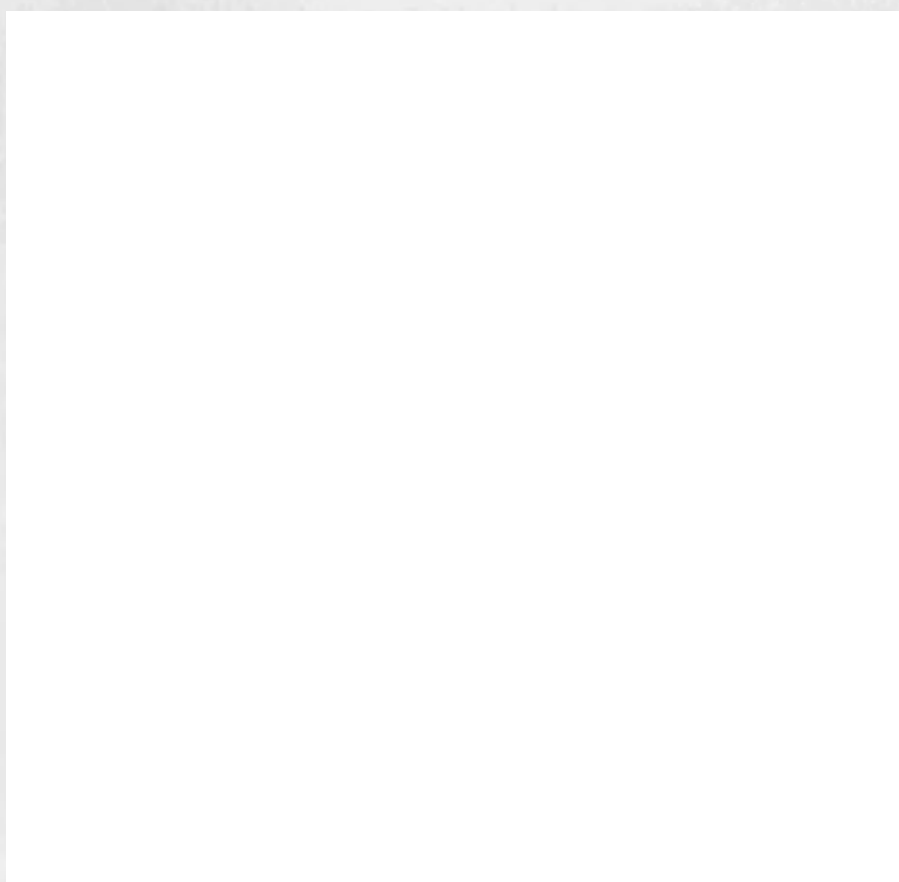


Figure 7-1. Map of the Lake Hartwell Superfund site where the samples were taken. (taken from Brenner et al (2004)).

Further, Brenner, *et al.* (2004) showed that by combining sediment concentration profiles and age dating results, information regarding the range of time anticipated to achieve the 1.0 mg/kg clean-up goal estimated can be quantified. Thus, the sediment recovery rates for Lake Hartwell were estimated by fitting logarithmic regressions

using the concentration-depth profiles of the contaminants and the results of the age dating analysis. However, it was noted in Brenner's study that an inherent challenge exists when the prediction of recovery rates are not based on scientifically defensible transport mechanisms of PCB fate and transport on site, but on simple extrapolation of historical data trends.

7.2.2 Model contaminant

In simulating Brenner's dataset, 2-chlorobiphenyl (PCB1) and 2,3,3',4',6-pentachlorobiphenyl (PCB110) were selected from among the 107 PCB congeners analysed in the original study due to their relative abundance in comparison with other PCB congeners. PCBs are organic compounds, whose hydrogen atoms of the biphenyl skeleton (see Figure 7-2) are substituted to various degrees by chlorine atoms. A PCB molecule can therefore contain a range of 1-10 chlorine atoms, and 209 PCB congeners may, thus, theoretically exist. For PCB1, 3 possible isomers exist while for PCB110, 46 combinations (i.e., placement of the chlorine atoms) make up the number of possible isomers.

Figure 7-2. Molecular structure of a PCB congener where the numbers represent the sites and convention used in naming the congener -adapted from US Environmental Agency (1983).

PCBs fall within the group of toxic and hazardous substances, whose adverse effects on living organisms can take effect even in relatively low concentrations (Agency for Toxic Substances and Disease Registry, 1995).

7.2.3 Model formulation and approach

7.2.3.1 Scope. PCB contamination of Lake Hartwell sediments was primarily due to discharges from the nearby capacitor plant. The dataset mined from Brenner's study (2004) is presented in Table 7-1.

Table 7-1. Summary of information taken from Brenner *et al.* (2004).

Analysis done	Total contaminant concentration in bulk sediment
Sediment sections, cm	20
Field measurements	Moisture content, dry weight of sample, total organic carbon

7.2.3.2 Conceptual model. The migration of PCB to the bed-sediment was hypothesized to be a result of the following individual (or combination of) mechanisms:

1. contaminant diffusion from the overlying water;
2. contaminant sorption to suspended sediments that will eventually deposit at the sediment-water interface; and/or
3. pooling of PCB as a dense non-aqueous phase liquid at the top section of the bed-sediments.

Of the three scenarios, the likelihood of the PCB pooling at the interface to occur was low due to lack of evidence regarding the existence of PCB pool at the site. Deposition of contaminated sediments and its impact on the fate and transport of contaminants in bed-sediments is one of the limitations of the CoReTranS model. Therefore, the migration of PCB to the bed-sediment was assumed to be due to contaminant diffusion from the overlying water. Brenner's dataset was simulated using the CoReTranS model in order to assess whether deposition, diffusion,

sorption and degradation are the prevailing processes that controlled the vertical distribution of PCBs at the contaminated site.

From Brenner's study, sediment cores from 10 transect locations during the spring of 2000 and 2001, were sampled in order to analyse and establish the concentration profiles of the 107 PCB congeners, quantify sedimentation rates, and predict rates of sediment recovery. From this dataset, data from two transect locations (T-IA and T-IB) which had the lowest sediment accumulation rates were simulated using the CoReTranS model. T-1A and T-1B were collected from shore to shore as oppose to sediments collected solely from deeper portions of the reservoir, to better understand the sediment deposition trends at the site.

Concentration profiles from collected sediment cores showed an increase in PCB concentration with depth, reaching a maximum, and then gradually decreased with depth. This profile is indicative of undisturbed sediment due to an initial contamination from a point source (i.e., manufacturing plant) over a finite duration and then reduction of PCB input (i.e., termination of PCB use within the plant). The reduction of PCBs in Lake Hartwell may be therefore hypothetically facilitated by MNR (i.e., via combined deposition, biodegradation, sorption and diffusion processes) given sufficient time.

7.2.3.3 Reactive transport model formulation. The governing model equation was simulated in CoReTranS as a diffusion-sorption-advection-degradation (DSAD) model and given as:

$$\phi \frac{\partial C}{\partial t} = \frac{\partial}{\partial x} \left(\phi D_{eff} \frac{\partial C}{\partial x} \right) - \frac{\partial}{\partial x} (\phi w C) - \lambda (\phi C + \rho_B K C) \quad \text{Eq. 7-1}$$

where w is the velocity of burial of particles below the sediment-water interface (i.e., sediment accumulation rate) estimated using the ^{210}Pb and ^{137}Cs profiles from the study done by Brenner *et al.* (2004), and given the values of 2.02 and 2.21 g/(cm² yr) for sediment cores T-IA and T-IB, respectively. The degradation rate constant λ was

Chapter 7

estimated using the theoretical half-lives of the selected PCBs taken from CoReTranS database. The effective diffusion coefficient was evaluated as:

$$D_{eff} = \frac{D}{\theta^2 \left(1 + \frac{\rho_B}{\phi} K_D \right)} \quad \text{Eq. 7-2}$$

where the tortuosity factor θ^2 was estimated using the modified Weissberg correlation while the molecular diffusion coefficient was estimated using the Wilke-Chang empirical correlation. K_D was modelled using the K_{OC} values of the selected PCBs from the database and the given organic carbon fraction. The sediment bulk density was estimated at 2.6 g cm^{-3} (Farley *et al.*, 1994). A summary of model parameters and their values are presented in Table 7-2. The physico-chemical properties of PCB1 and PCB110, used as model parameters are presented in Table 7-3. The parameters used for the simulation of total PCB are also shown; these were based on average values of parameters for the 107 PCB congeners analysed.

Table 7-2. Model parameters used in simulating the field-scale data for the PCB-contaminated sediments in Lake Hartwell

Parameters	T-IA	T-IB
Sediment depth, cm	100	100
Number of grids	100	100
Simulation time, weeks	2392	2392
Porosity (v/v)	0.52	0.49
Organic carbon fraction (dry mass basis)	0.02	0.02
Sedimentation rate, g/(cm ² y)	2.02	2.21

Table 7-3. Physico-chemical properties of selected PCBs used in simulating the field-scale data for the PCB-contaminated sediments in Lake Hartwell.

Parameters	PCB1	PCB110	Total PCB	
			T-IA	T-IB
CAS Registry No.	2051-60-7	38380-03-9	-	-
Solubility S , g/cm ³	5.5	4.0 x10 ⁻³	1.3	1.3
Molar volume, mol/cm ³	205.5	289.1	237.7	323.0
Diffusion coefficient, cm ² /s	2.22 x10 ⁻⁶	1.81 x10 ⁻⁶	2.0 x10 ⁻⁶	1.61 x10 ⁻⁶
log K_{ow} , L/kg	4.3	6.3	5.2	5.2
Degradation rate, 1/day	9.79 x10 ⁻⁴	3.02 x10 ⁻⁴	5.69 x10 ⁻⁴	5.51 x10 ⁻⁴

The initial and boundary conditions for this model scenario were given as:

$$\text{Initial conditions: } C(x, t)|_{t=0} = 0 \quad \text{Eq. 7-3}$$

$$\text{Boundary conditions: } \begin{matrix} C(x, t)|_{x=0} = S & 0 \leq t \leq \tau \\ = 0 & t < \tau \end{matrix} \quad \text{Eq. 7-4}$$

$$C(x, t)|_{x=70} = 0 \quad \text{Eq. 7-5}$$

The contaminant concentration at the sediment-water interface as shown in equation 7-4 is estimated using the contaminant's solubility S on the assumption that Lake Hartwell was heavily contaminated and thus, fully saturated with PCB discharged from the nearby capacitor manufacturing plant at Sangamo-Weston, SC from 1955 until 1977 (US Environmental Protection Agency - Region 4, 2005). The duration of PCB input at the sediment-water interface, τ , was initially estimated at 22 years commensurate with PCB use at the plant.

7.2.4 Model validation: Predicting PCB distribution in Lake Hartwell sediments

7.2.4.1. Approach. Contaminant concentration-depth profiles for PCB1, PCB110 and total PCB from both transect locations (T-1A and T-1B) generated from CoReTranS as shown in Figure 7-3 were compared with the PCB sediment core profiles sampled in 2001. Contaminant concentrations were placed in a single scale of variation (i.e., 0 to 1) by normalising the concentration values to their maximum.

7.2.4.2 Results. Table 7-4 summarises the *RMS* and *r* values evaluated from comparing the predicted contaminant concentration-depth profiles from the CoReTranS simulations with the actual profiles.

Table 7-4. Evaluation of goodness of fit between the CoReTranS model and actual profile for the model contaminants.

Contaminant	<i>RMS</i>	<i>r</i>
T-1A location		
PCB1	0.18	0.85
PCB110	0.45	0.11
Total PCB	0.28	0.48
T-1B location		
PCB1	0.19	0.84
PCB110	0.49	(-0.06)
Total PCB	0.28	0.57

7.2.4.3 Discussion. The predicted profiles showed narrow peak widths similar to the actual profiles suggesting that a retarded diffusion mechanism was one of the controlling mechanisms. For PCB1 and Total PCB, both top and bottom sections of the sediment cores were accurately predicted by the CoReTranS model indicating that the assumed boundary condition at the sediment-water interface (equation 7-4) was correct. For PCB110, however, the profile was poorly predicted by the model

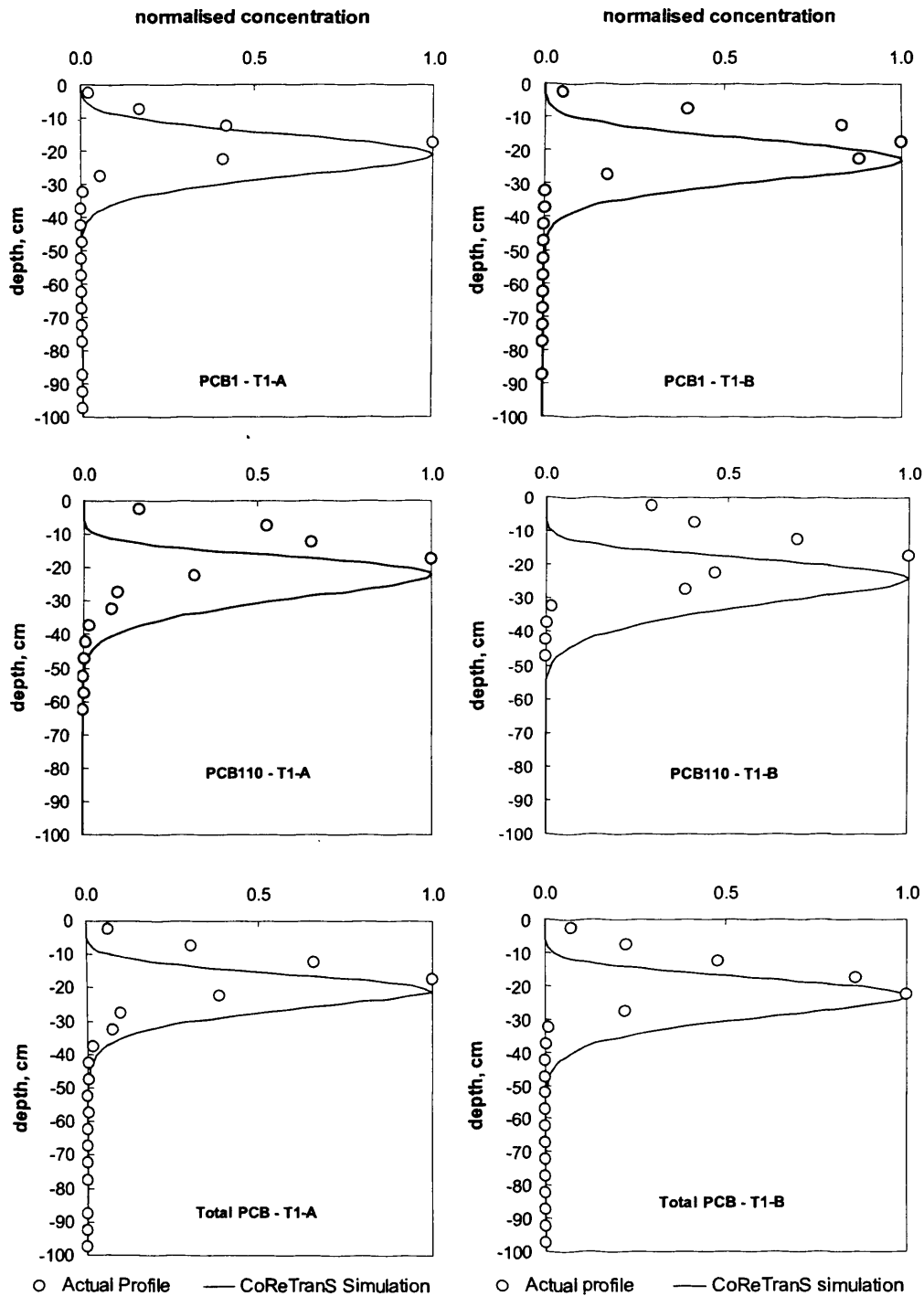


Figure 7-3. Concentration-depth profiles for PCB1, PCB110 and total PCB from T-1A and T-1B transect locations as simulated in CoReTranS in comparison with the actual data.

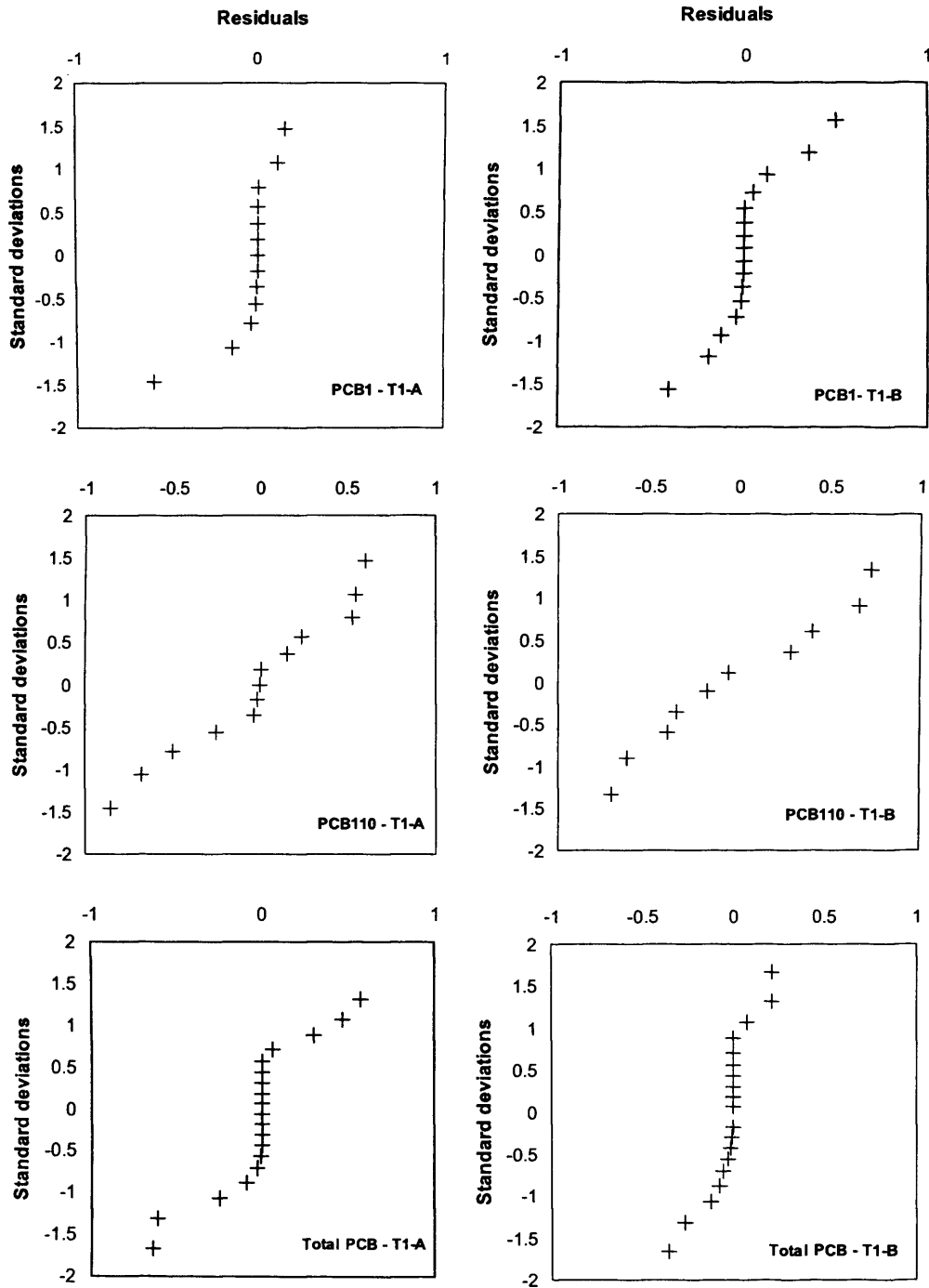


Figure 7-4. Analysis of residual errors between predicted and actual profiles for PCB1, PCB110 and total PCB in both transect locations T-1A and T-1B.

suggesting that critical model parameters may need to be identified and refined. To further check for systematic error in the simulation process, residual errors between the predicted and actual profiles were analysed as shown in Figure 7-4.

From Figure 7-4, the probability distribution of residuals for the selected contaminants produced distinct “tailings” on both ends of the distribution plot. These residuals coincided with the contaminant peak concentrations in the 10 – 25 cm depth section of the sediment cores. The asymmetric distribution of the residuals was indicative of systematic error presumably due to unrealistic model parameters used in the simulation, or some unaccounted-for mechanisms that occurred in the past such as contaminated sediment resuspension/deposition due to bioturbation events.

Further, the predicted contaminant peaks did not match the contaminant peaks from the actual profiles which suggests that sedimentation rates estimated by Brenner *et al.* (2004) did not fully capture the non-uniform historical sediment deposition at Lake Hartwell based on sediment dating, possibly due to sediment heterogeneity on site. In their study, Brenner *et al.* (2004) used an unconventional approach in dating the Lake Hartwell sediments which involved removal of segments within the sediment core with high sand contents, and thus probably did not produce accurate sedimentation rates.

The predicted contaminant peak concentration for PCB1 after the application of the assumed boundary condition at the sediment-water interface (equation 7-4) was 24.42 $\mu\text{g/g}$ which is considerably below the actual measured peak concentration of 1,979 $\mu\text{g/g}$ at transect T-IA site. The peak concentration for total PCB from transect T-IA site were likewise under-predicted, having a predicted peak concentration of 1,136 $\mu\text{g/g}$ as compared to the actual peak concentration of 19,274 $\mu\text{g/g}$. This suggests that PCB flux onto the bed-sediments at the site may have continued well beyond 22 years after PCB use was terminated at the Sangamo-Weston, SC plant in 1977. To test this hypothesis, the duration of PCB flux (i.e., as continuous source) into the sediment-water interface was investigated in CoReTranS using various values of τ : 27, 32, 33, 33.25, 34 years. The concentration-depth profiles of PCB1 at the

transect T-IA site using 5 selected finite time durations for the boundary conditions at the sediment-water interface is presented in Figure 7-5.

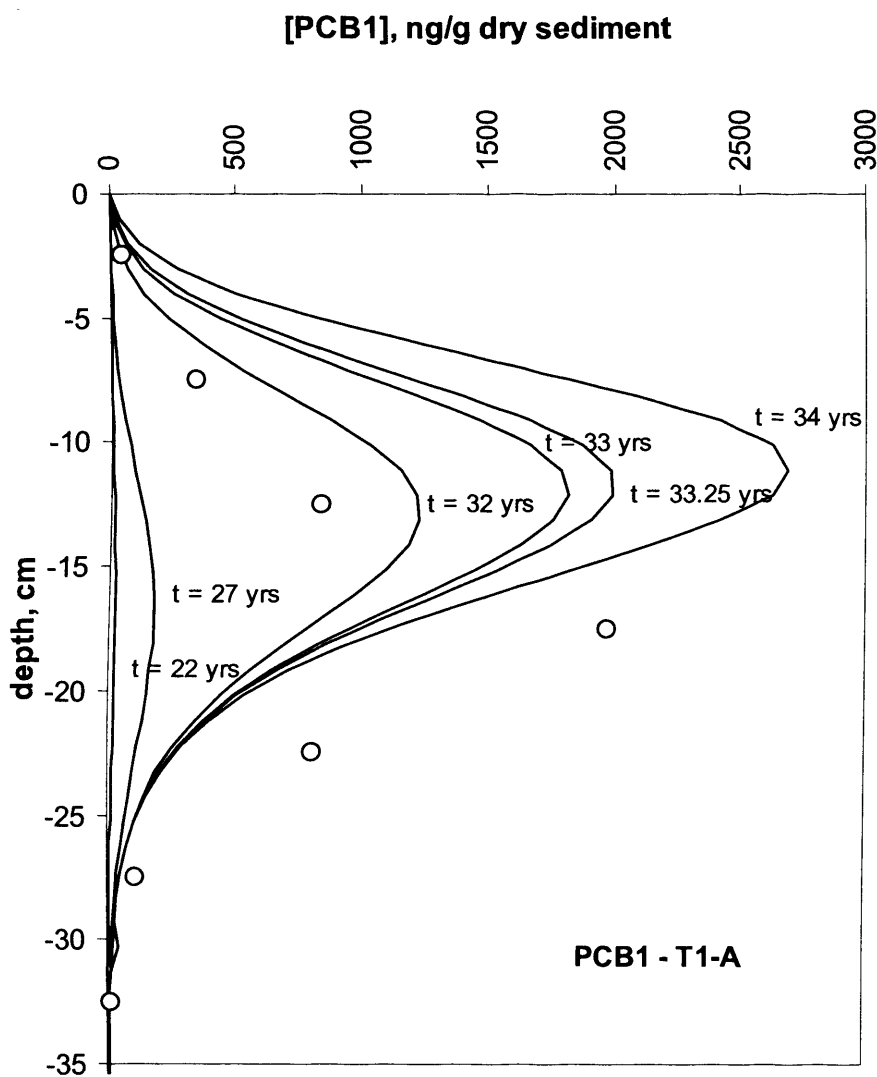


Figure 7-5. Predicted concentration-depth profile of PCB1 (solid line) at the transect T-IA site using 5 selected values for τ in comparison with the actual data (o).

The concentration-depth profiles of total PCB at transect T-IA and T-IB sites using $\tau = 33$ years for the boundary conditions at the sediment-water interface is presented in Figure 7-6.

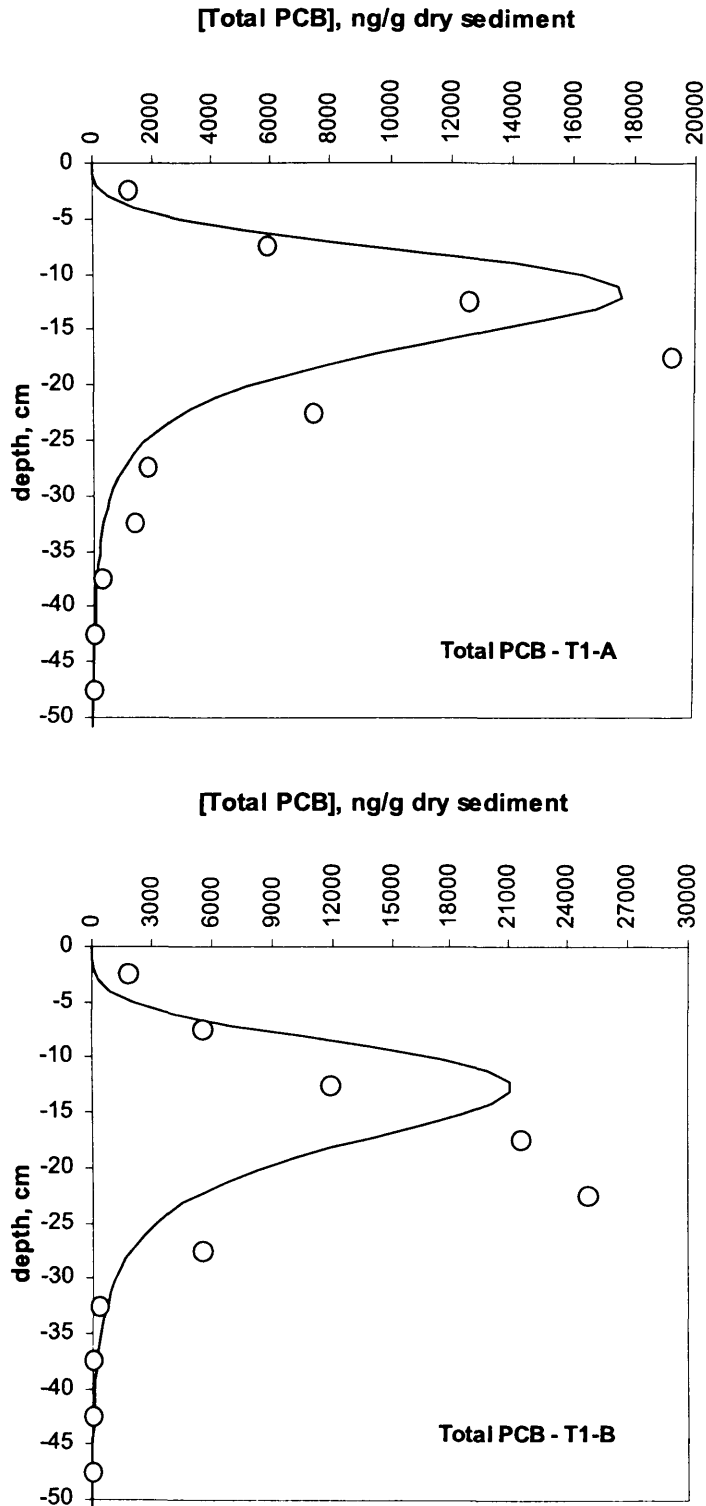


Figure 7-6. Predicted concentration-depth profiles for total PCB1 (solid line) at transect T-1A and T-1B sites using $\tau = 33$ years in comparison with the actual data (o).

The RMS values for the predicted profiles shown in Figure 7-6 were 0.18 for the total PCB at transect T-1A, and 0.13 for the total PCB at transect T-1B. An improved overall agreement between the predicted and actual profiles was also shown with r values of 0.95 and 0.90 for the total PCB at transects T-1A and T-1B, respectively. Further, residual errors between the predicted and actual profiles using $\tau = 33$ years for the boundary conditions at the sediment-water interface were analysed. As shown in Figure 7-7, the tailings of the residual error distributions suggest an uncalibrated model parameter, or an unaccounted-for mechanism used in the simulation of the dataset.

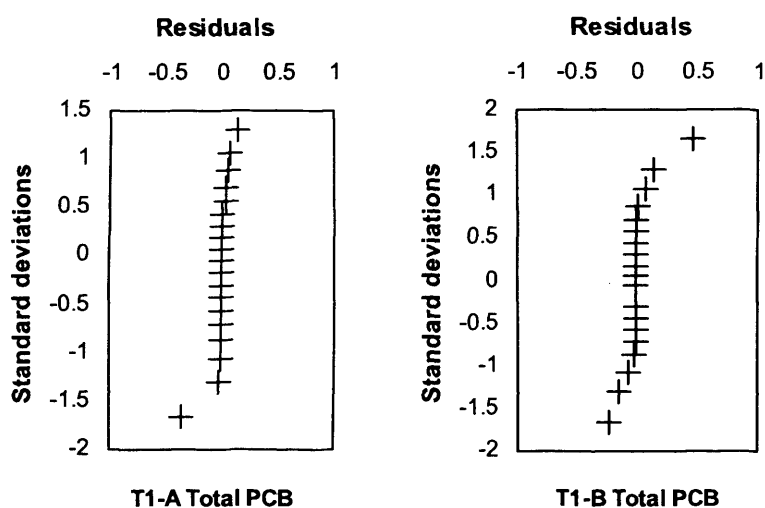


Figure 7-7. Analysis of residual errors between predicted and actual profiles for total PCB in both transect locations T-1A and T-1B using $\tau = 33$ years.

From Figures 7-5 and 7-6, the predicted contaminant peak concentrations of PCB1 and total PCB at both transect locations fell within the τ range of 32 – 34 years, which is about 10 – 12 years of continuous contamination after PCB use at the site was terminated concomitant with the closure of the plant in 1987. The predicted contaminant peaks, however, were closer to the sediment-water interface as compared to the actual profile which indicates that the vertical contaminant

distribution is sensitive to both contaminant loading over finite duration, τ and sedimentation rates. To test this hypothesis, the model was refined using τ between 32 – 33 years, and sedimentation rate of $3.0 \text{ g}/(\text{cm}^2 \text{ y})$ for PCB1 at transect location T-IA and total PCB from both locations. The predicted concentration-depth profiles from the calibrated model are shown in Figure 7-8 for PCB1 at transect T-IA, and Figure 7-8 for total PCB at transect T-IA and T-IB sites.

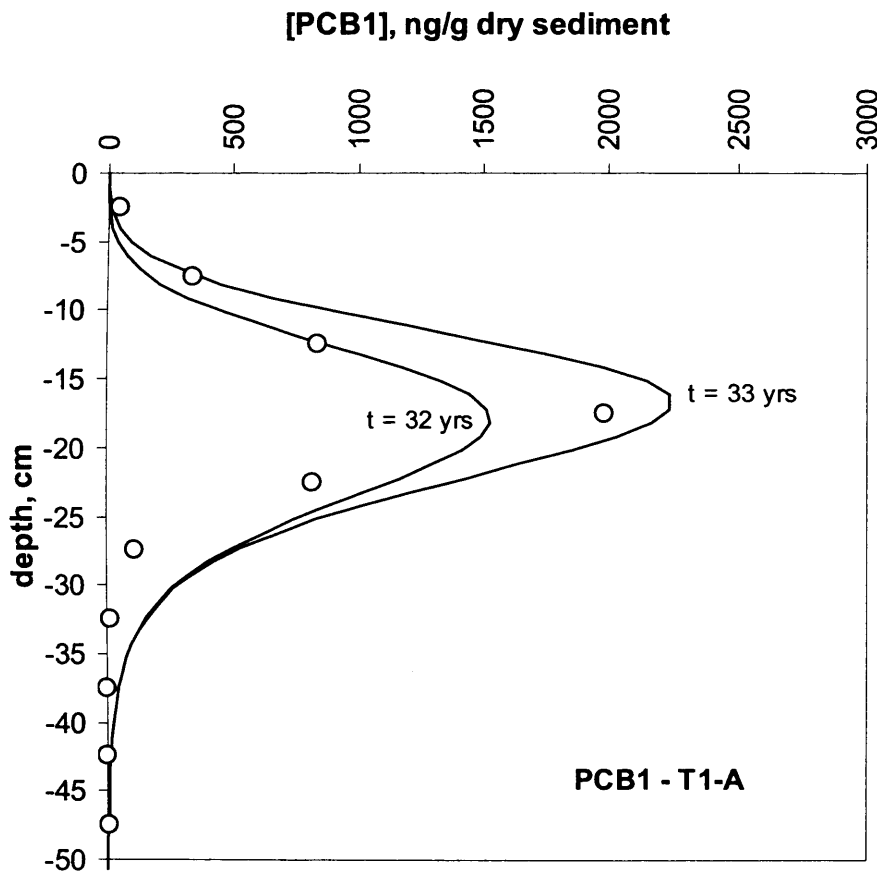


Figure 7-8. Concentration-depth profile of PCB1 (solid line) at the transect T-IA site as simulated in CoReTranS using τ between 32 and 33 years and $w = 3 \text{ g}/(\text{cm}^2 \text{ y})$ in comparison with the actual data (\circ).

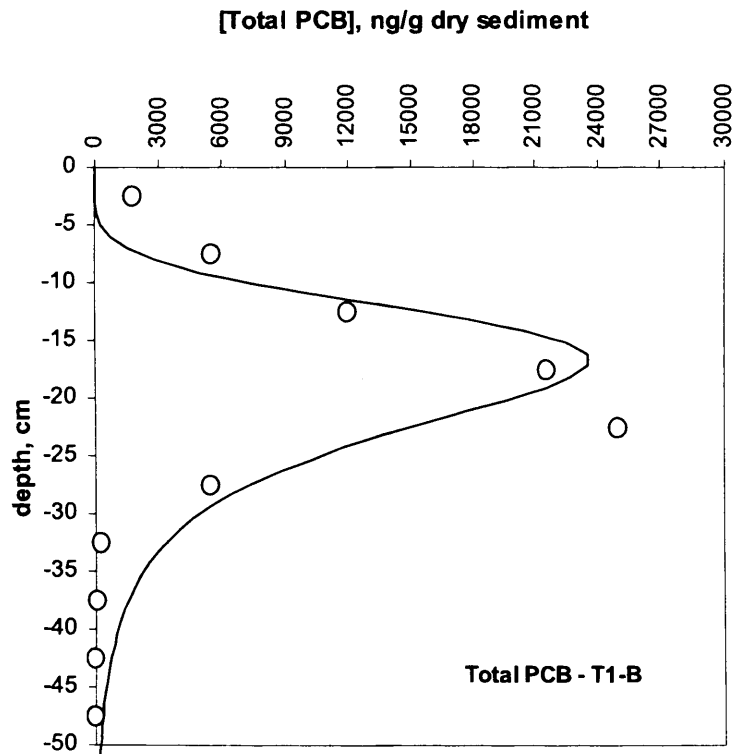
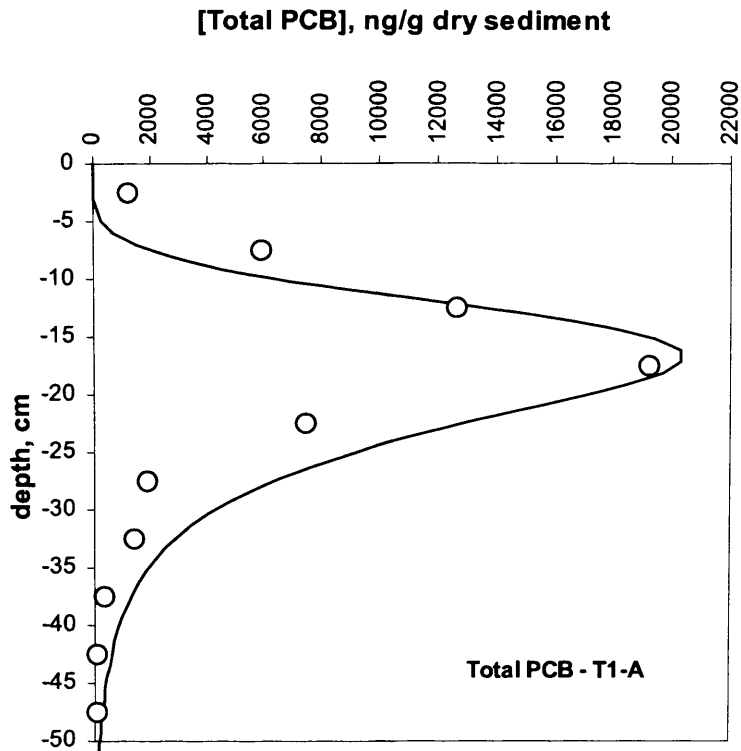


Figure 7-9. Predicted concentration-depth profiles for total PCB1 (-----) at transect T-IA and T-IB sites using $\tau = 33$ years and $w = 3 \text{ g}/(\text{cm}^2 \text{ y})$ in comparison with the actual data (o).

From Figures 7-8 and 7-9, the fit between the predicted and actual profiles was greatly improved, which supports the hypothesis that the contaminant distribution at sites T-1A and T-1B is explained by natural capping of clean sediment, contaminant diffusion in the pore water, and sorption onto the sediment matrix. The *RMS* values for the predicted profiles shown in Figure 7-9 were 0.18 for the total PCB at transect T-1A and 0.13 for the total PCB at transect T-1B. An improved overall agreement between the predicted and actual profiles was again shown with *r* values of 0.95 and 0.91 for the total PCB at transects T-1A and T-1B, respectively. Further, residual errors between the predicted and actual profiles using $\tau = 33$ years for the boundary conditions at the sediment-water interface and $w = 3 \text{ g}/(\text{cm}^2 \text{ y})$ were analysed. As shown in Figure 7-10, the tailings produced on residual error profiles may be attributed to an uncalibrated model parameter used in the simulation of the dataset.

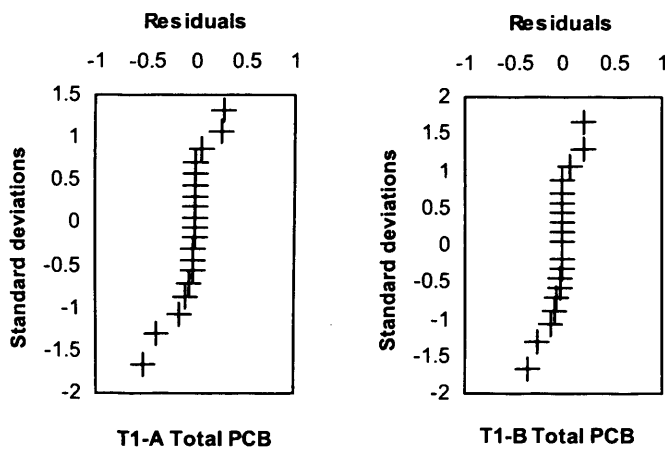


Figure 7-10. Analysis of residual errors between predicted and actual profiles for total PCB in both transect locations T-1A and T-1B using $\tau = 33$ years and $w = 3 \text{ g}/(\text{cm}^2 \text{ y})$

7.2.5 Model validation: Predicting natural recovery rates for PCB-contaminated sediments in Lake Hartwell

7.2.5.1 Approach. From the CoReTranS simulations done on Brenner's dataset, the natural recovery rates were predicted for PCB1 from T-1A and total PCB from T-1A and T-1B sites using time series predictions. Future PCB concentrations were predicted using an additional simulation time of 5, 10, 15 and 25 years, the results of which were fitted with best fit logarithmic regressions in order to approximate the contaminated sediment recovery rates. The recovery times were then calculated by setting the PCB concentration (*i.e.*, x-axis) to the EPA clean-up requirements of 1.0, 0.4 and 0.05 mg/kg.

7.2.5.2 Results. Figure 7-11 and 7-12 show the results of the time series analysis for estimating the recovery rates of PCB-contaminated sediments in Lake Hartwell. Excellent overall agreement between the predicted profiles and the fitted logarithmic regression profiles was shown with all r values equal to 1.0.

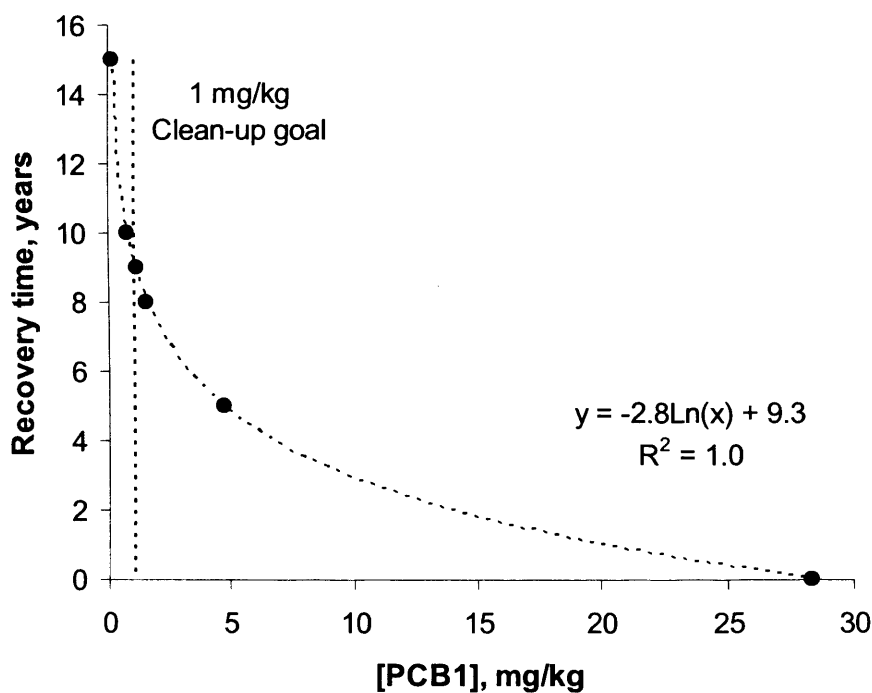


Figure 7-11. Time series predictions of natural recovery rates for PCB1 from T-1A, $\tau = 33$ years and $w = 3 \text{ g cm}^2/\text{y}$.

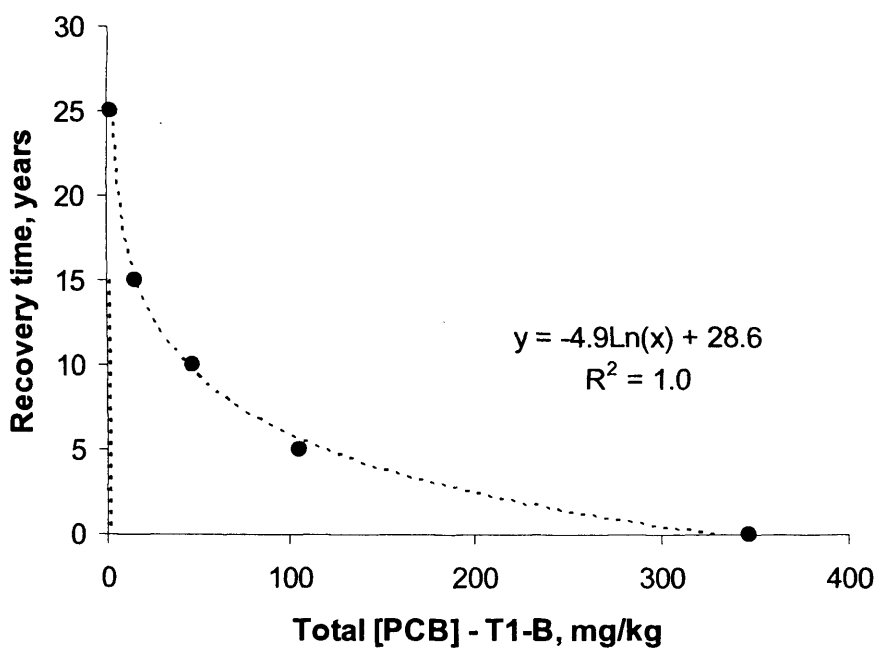
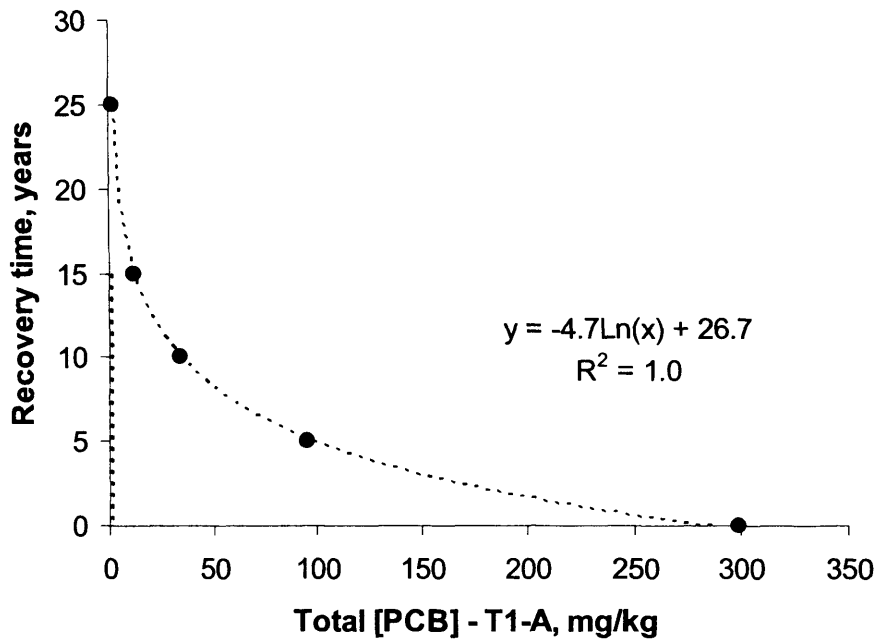


Figure 7-12. Time series predictions of natural recovery rates for Total PCB from T-1A and T-1B, $\tau = 33$ years and $w = 3 \text{ g cm}^2/\text{y}$.

7.2.5.3 Discussion. Using the time series trends presented in Figures 7-11 and 7-12, the recovery time to achieve the sediment clean-up goals are summarised in Table 7-5. The recovery time was determined by setting the contaminant value (i.e., x-axis) to 1.0, 0.4 and 0.05 mg/kg for PCB1 from transect T-IA and total PCB from transect T-IA and T-IB sites. From the time series trends, the 1.0 mg/kg clean-up goal for total PCB is predicted to be achieved by 2026 for transect T-1A and 2028 for transect T-1B. From these dates, another 4 years is needed to achieve the 0.4 mg/kg clean-up goal for total PCB in both transect locations. In comparison with the simulation results from CoReTranS, Brenner’s predictions for the time to achieve the specified sediment clean-up goals were significantly lower. This is presumably due to the fact that Brenner simply extrapolated past historical data from sediment cores using best fit logarithmic regressions and may be far too conservative estimates. It may also be possible that the trend may change for the next 10 – 20 years after the historical data has been collected and used due to in-bed PCB fate and transport processes, and thus the predicted sediment recovery time using this approach may significantly vary.

Table 7-5. Estimated time to achieve sediment clean-up goals set by the Superfund Record of Decision at Lake Hartwell (US Environmental Protection Agency, 1994)

	Site	Estimated time to achieve 1 mg/kg, years		Estimated time to achieve 0.4 mg/kg, years		Estimated time to achieve 0.05 mg/kg, years	
		CoReTranS	Brenner’s	CoReTranS	Brenner’s	CoReTranS	Brenner’s
PCB1	T-IA	10	-	12	-	18	-
Total PCB	T-IA	27	11 ^a	31	15 ^a	41	27 ^a
Total PCB	T-IB	29	11 ^a	33	16 ^a	43	28 ^a

^aBrenner’s prediction of sediment recovery time based on extrapolation of historical data using best fit regressions within the upper 95% prediction limits.

7.3 Conclusions for model predictions of PCB distribution and natural recovery in Lake Hartwell sediments and recommendations for future investigations

Monitored natural recovery of sediments is a remedial alternative in managing risks involved with contaminated sediments. It relies on natural in-bed fate and transport process (e.g., natural capping) to minimise or eliminate the risk to the environment. A dataset from a field monitoring study that evaluated the natural recovery of PCB-contaminated sediments at the Sangamo-Weston/Twelvemile Creek/Lake Hartwell Superfund Site (Lake Hartwell), Pickens County, SC was applied in CoReTranS to show that sediment deposition, diffusion, sorption and degradation were the prevailing processes that control the vertical distribution of PCBs at the contaminated site. Natural recovery rates were also predicted for PCB1 from T-IA and total PCB from T-IA and T-IB sites using time series predictions based on the calibrated model. The results of the time series trends were then compared with Brenner's approximation of sediment recovery times based on extrapolated historical data.

From the simulations done on the PCB distribution in sediments at Lake Hartwell site, the following may be potential areas for further research:

1. Determine accurate sediment accumulation rates using either ^{210}Pb or ^{137}Cs geochronological studies to examine the effect of sediment deposition to the vertical distribution of PCBs at the contaminated site.
2. Evaluate physico-chemical characteristics of the sediments to determine exact porosity values and anoxic/oxic conditions.
3. Investigate bioturbational activity of macro- and micro-benthos at the Lake Hartwell site and evaluate the mass transfer coefficient to critically examine the effect of contaminant loss due to bioturbation activity.

Chapter 7

4. Long-term monitoring programme should be in place to assess the efficacy of natural recovery of contaminated sediments and to determine if the clean-up goals were met at the predicted recovery times.

CHAPTER EIGHT

Predicting the effects of capping contaminated sediments using the CoReTranS model

8.1 Introduction

Sediments are the ultimate sink for many contaminants released to surface waters from a wide range of natural and anthropogenic activities. Once contaminated, these sediments subsequently become sources of contamination to surface and ground waters, thereby posing long-term ecological and human health risks. To date, remedial options for contaminated sediments are limited and include dredging, monitored natural attenuation and in situ capping. Dredging provides rapid removal of contaminated sediments from local areas but can be a cost-intensive operation due to widespread sediment removal, de-watering, treatment and disposal (Newell *et al.*, 1998; Palermo *et al.*, 1998; Sven-Olof, 1982). In addition, dredging may lead to contaminant remobilisation in the overlying water and impacts the benthic biological communities. Monitored natural attenuation is only an option if sediment deposition and contaminant degradation rates are sufficiently high to reduce the risk of contaminated sediment resuspension (Brenner *et al.*, 2004; US Environmental Protection Agency, 1998). In situ capping is a non-invasive remedial alternative to dredging and natural attenuation (Reible *et al.*, 2003). Well-designed caps, when properly placed, effectively isolate contaminated areas, stabilize contaminated sediments, and reduce contaminant flux into the water column.

By precluding direct contact of both the benthic diffusive boundary layer and the biologically active layer with the contaminated sediments, sediment caps prevent contaminant mobilisation and transport of contaminated sediments. Contaminant flux is reduced through sorption of contaminants to the sediment cap matrix and by increasing the diffusive and advective transport lengths. Further, engineered sediment caps can potentially provide new benthic habitat for the biological community on the sediment bed.

Sand caps have the advantage of relative ease of placement and stability, especially in sloped areas (Palermo *et al.*, 1998). In theory, finer-grained materials are more effective barriers because of their high sorption capacity and low permeability, but can be difficult to place atop submerged areas. Thus, to combine the sorptive capacity of fine-grained caps and logistic capabilities of sand-based caps, sorbent materials such as activated carbon, coke, coal and soil are used as amendments to sand caps (Accardi-Dey and Gschwend, 2002; Cornelissen *et al.*, 2005; Murphy *et al.*, 2006; Werner *et al.*, 2006; Werner *et al.*, 2005). Along with the chosen cap material, other engineering design criteria for an effective sediment cap include: thickness, breakthrough time, contaminant flux at the cap surface, steady state flux and time to approach steady state (Mohan *et al.*, 2000; Palermo *et al.*, 1998). Development and implementation of design criteria for an effective cap generally requires the use of fate and transport models. Simulation of contaminant migration within the sediment cap system using mathematical models enhances the fundamental understanding of contaminant behaviour within a sediment cap system and can be used to evaluate the longer-term effectiveness of in situ capping as a remedial option in managing contaminated sediments.

In this chapter, the CoReTranS model is used to predict the effects of sediment capping as a remedial option to manage contaminated sediments with examples of the application of each to simulation of different transport and reaction mechanisms in a sand cap and demonstration of numerical approach for modelling a sorptive cap. Simulation results from the CoReTranS model will also be compared with a steady state model developed by Lampert and Reible (2006), highlighting key points of each modelling approach as well as knowledge gaps.

8.2 Fate and transport models for sediment cap systems

A sediment cap system is typically modelled as three to four layers (Figure 1), comprising: the overlying water column, the sediment cap, which is further divided into a biologically active layer also known as the bioturbation layer with a depth of h_{bio} and the effective cap layer with a depth of h_{cap} , and the contaminated sediment bed. At the sediment-water interface, the magnitude of the contaminant flux is dictated by the benthic boundary layer mass transfer coefficient (k_{bl}).

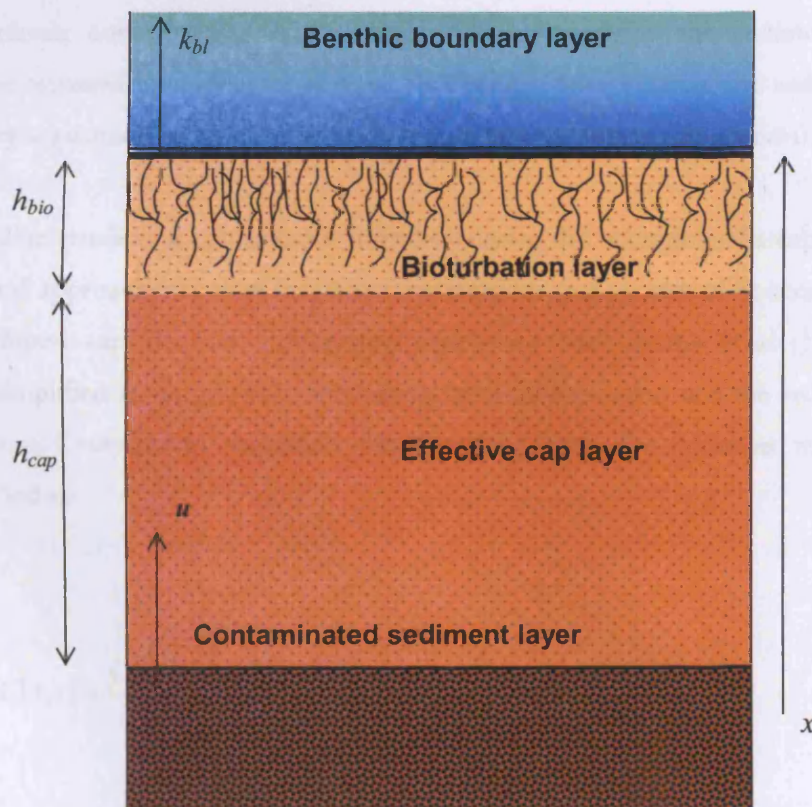


Figure 8-1. Depiction of a layered sediment cap system.

The vertical migration and distribution of a single chemical constituent within the cap system is typically described either by a single partial differential equation or systems of equations based on the diagenetic equation (Berner, 1980; Boudreau, 1997) given as,

$$R \frac{\partial C}{\partial t} = \frac{\partial}{\partial x} \left[\phi D_{eff} \frac{\partial C}{\partial x} \right] - \frac{\partial}{\partial x} [\phi u C] - \lambda \phi C \quad \text{Eq. 8-1}$$

where R is dependent on the sorption isotherm used in the model scenario.

It is typically assumed that the contaminant concentration in the sediment underneath the cap is uniformly distributed prior to the placement of the cap. The contaminant concentration in the water column overlying the sediment cap is likewise assumed homogenous. For this modelling demonstration, the sediment-bed porosity is assumed to be invariant with time (i.e., steady-state compaction).

To date, predicting contaminant migration during the operation of a cap using the analytical approach still uses simplified assumptions (e.g., constant concentration at the sediment-cap interface, infinite cap thickness model). Reible *et al.* (1998) used these simplified assumptions in estimating breakthrough time and the required cap thickness. Contaminant migration based on an advection-diffusion model was quantified as:

$$C(x,t) = \frac{C_o}{2} \left[\operatorname{erfc} \left(\frac{Rx - ut}{\sqrt{4RD_{eff}t}} \right) + \exp \left(\frac{ux}{D_{eff}} \right) \operatorname{erfc} \left(\frac{Rx + ut}{\sqrt{4RD_{eff}t}} \right) \right] \quad \text{Eq.8-2}$$

From equation 8-2, the breakthrough time and time to steady state were based upon the time to reach 5% and 95% of the steady state flux through cap thickness h , respectively. Though physically unrealistic, this modelling approach can approximate the finite-domain solutions for short transient times into relatively thick caps, when

the contaminant front is at some distance from the cap's upper boundary and advection dominates transport. This modelling approach however is not applicable when conditions at the top of the sediment cap (e.g., benthic activity, organic carbon fluctuations) significantly influence contaminant fate and transport.

An alternative approach is to use semi-analytical models. Fate and transport equations that are implicit necessitate complicated superposition techniques, or successive evaluations are frequently called semi-analytical. For example, Liu *et al.* (1998) successfully resolved this continuity requirement (i.e., flux and concentration) at the interface by using a more generalised integral transform method. The method essentially converts the given set of advection-diffusion equations to a set of ordinary differential equations subsequently solved as a linear system. A sign-count method was used to numerically evaluate the resulting eigenvalues.

Another approach in modelling sediment cap systems is by using numerical methods, whereby the grid or element representation of the system can effectively approximate variations in model parameters across multiple layers. This inherent capability enables the numerical model to assess a wide range of capping designs, including choice of capping materials, biodegradation rates and cap thickness. For example, the U.S. Army Corps of Engineers RECOVERY v3.0 model (Ruiz *et al.*, 2001; Ruiz and Schroeder, 2001) has demonstrated its capability to predict contaminant migration for cap operation at the Duwamish River dredged material disposal site in Seattle, Washington. The system was modelled as a well-mixed water column overlying a layered sediment bed. Vertical segmentation of the sediment layer using a combination of adaptive-size fourth-order Runge-Kutta (water column) and Crank-Nicholson (sediment layers) techniques afforded variations in thicknesses, porosities, and contaminant concentrations. Both monitored and simulated contaminant concentration profiles demonstrated the effectiveness of the designed cap. Murphy *et al.* (2006) also demonstrated the effectiveness of activated carbon-, coke-, and soil-amended sediment caps using a one-dimensional transport model including nonlinear sorption and first-order degradation. The model equations were simulated using MATLAB v6.5 and FEMLAB v3.0a, a commercial finite element solver.

8.3 Simulation of contaminant reactive transport in capped sediment systems

8.3.1 Model contaminant

Phenanthrene, a relatively soluble and mobile polyaromatic hydrocarbon, was chosen as test contaminant. PAHs due to their high sorption coefficients and legacy of use throughout the past century often represent the design-dictating contaminant. See Section 6.2.2 for a detailed description of the model contaminant.

8.3.2 Model simulations

8.3.2.1 Approach. To compare the analytical and numerical modelling approaches in predicting cap performance, four distinct one-dimensional fate and transport models are presented: diffusion, diffusion-degradation, diffusion-advection, and diffusion-advection-degradation models.

Parameter values for the contaminant's theoretical diffusivity in water, particle density, porosity, fraction organic carbon, organic carbon partition coefficient, and benthic boundary layer mass transfer coefficient were estimated *a priori*. Hydrodynamic dispersion was modelled as the product of the velocity through the cap and the dispersivity, α_D , estimated using a power function based on Neumann's (1990) analysis of 134 dispersivity values. That is,

$$\alpha_D = 0.0169h_{cap}^{1.53} \quad \text{Eq. 8-3}$$

The effective diffusivity of the system, D_{cap} , was estimated as a sum of D_{eff} and D_a . That is,

$$D_{cap} = D_{eff} + \alpha_D u \quad \text{Eq. 8-4}$$

The diffusion mechanism in the bioturbation layer takes into account bioturbation and bioirrigation mechanisms modelled as local biodiffusive processes (Reible *et al.*, 2006). Thus, D_{bio} was estimated as

$$D_{bio} = D_{cap} + D_{bio}^{pw} + \lambda R D_{bio}^p \quad \text{Eq. 8-5}$$

where D_{bio}^{pw} = pore water biodiffusion coefficient (i.e., for bioirrigation process), D_{bio}^p = particle biodiffusion coefficient (i.e., for bioturbation process) while the subscripts *bio* and *cap* denote parameters for the bioturbation layer and effective cap layer, respectively. It is important to note that the bioturbation layer thickness and biodiffusion coefficients are difficult parameters to evaluate and quantify. Thoms *et al.* (1995) presented a summary of observed bioturbation depths and biodiffusion coefficients from numerous studies with a variety of animals in both fresh and salt waters throughout the world. These data were separated into freshwater and estuarine categories and analyzed by Lampert and Reible (2006). The arithmetic mean values for biodiffusion coefficient were $1.23 \times 10^{-7} \text{ cm}^2/\text{s}$ and $3.95 \times 10^{-6} \text{ cm}^2/\text{s}$ for freshwater and estuarine environments, respectively. The mean values for bioturbation depth were 5.5 cm and 12.3 cm for freshwater and estuarine environments, respectively. Thus, for a freshwater system reasonable assumptions for bioturbation diffusion coefficient and depth are $1.23 \times 10^{-7} \text{ cm}^2/\text{s}$ and 5.5 cm.

Substantially less work has been done to quantify bioirrigation diffusion coefficients. Wood (1975) observed an irrigation rate in the upper 4 cm of sediment for oligochaetes of 1.46-1.48 μL water/worm/hr at 1°C and 9.5-15.0 μL water/worm/hr at 20°C. Cunningham (2002) found a similar rate of 6.3 μL water/worm/hr at 20°C in the oligochaete, *Limnodrilus hoffmeisteri*. In polluted sediment, oligochaete densities may be 10,000-100,000 worm/m². Assuming 50,000 worms/m² at 10°C whereby bioirrigation is directed randomly in the upper 5 cm of sediment, the bioirrigation diffusion coefficient is approximately $1 \times 10^{-5} \text{ cm}^2/\text{sec}$. Large marine organisms can process water at much higher rates although the organism density is much less. The pore water transport of the polychaete *Amphitrite*

Chapter 8

ornate, for example, was found to be 91 mL/hr (Aller and Yingst, 1978) but largely limited to the isolated tubes in which these species live. The effective bioirrigation diffusion coefficient for pore water transport by *Yoldia limatula* was found to be $\sim 1 \times 10^{-3}$ cm²/sec (Aller and Yingst, 1978). Thus, a reasonable estimate of a bioirrigation diffusion coefficient is 1×10^{-5} cm²/sec in fresh waters and 5×10^{-4} cm²/sec in estuarine waters. The pore water mixing rate tends to be much higher numerically than particle effective diffusion coefficients, but is generally of lesser importance than particle reworking due to the strongly sorbing nature of most sediment contaminants.

The rate of desorption at the cap-water interface is dictated by the benthic boundary layer mass transfer coefficient, which is a function of the turbulence and shear of the overlying water column. Thibodeaux (1996) presents a correlation for the benthic boundary layer mass transfer coefficient in a river:

$$k_{bl} = \frac{0.114 v_x n \sqrt{g h_{channel}}}{r_H^{2/3} Sc^{2/3}} \quad \text{Eq. 8-6}$$

where k_{bl} = benthic boundary layer mass transfer coefficient (m/s), v_x = velocity of the river (m/s), n = Manning's constant (from Manning's equation for open-channel flow in metric units), g = acceleration due to gravity (m/s²), $h_{channel}$ = depth of the channel (m), r_H = hydraulic radius (ratio of the channel cross-sectional area to the wetted perimeter, m), and Sc = Schmidt number, which is defined as the ratio of the kinematic viscosity of water, ν_w , and the molecular diffusion coefficient. If the width of the channel is much larger than the depth of the channel, the hydraulic radius can be approximated using

$$r_H = \frac{8}{9} h_{channel} \quad \text{Eq. 8-7}$$

Assuming a water temperature at the sediment-water interface of 10°C (i.e., $\nu_w = 1.306 \times 10^{-6}$ m²/s), the benthic boundary layer mass transfer coefficient correlation is reduced to:

$$k_{bl} = \frac{2.51 \times 10^6 v_x n D^{2/3}}{h_{channel}^{1/6}} \quad \text{Eq. 8-8}$$

For low-velocity systems, wind-driven circulation of water drives the mass transport. Thibodeaux (1996) presents the following relationship for the mass transfer coefficient:

$$k_{bl} = 0.031 \frac{\rho_a v_a^2 h_{channel}^2}{\rho_w MW^{1/2} L_{lake}} \quad \text{Eq. 8-9}$$

where ρ_a and ρ_w are the density of air and water, respectively, v_a is the wind velocity, MW is the molecular weight of the contaminant, and L_{lake} is the fetch of lake or water body in the direction of wind.

In this modelling demonstration, a 30 cm thick sand cap was considered where sediment depth is measured from the sediment-water interface. The biologically active layer (i.e., bioturbation layer) was assumed to be 5.6 cm deep measured from the sediment-water interface. Different values of K_{oc} for phenanthrene have been reported in the literature; a value of 4.3 log (L/kg) represents an approximate median value. The molecular diffusivity of phenanthrene in water was approximately 6×10^{-6} cm²/s. The fraction of organic carbon in the cap tends to be small, as sand is the material most commonly used for sediment capping. A value of 0.5% is a typical value that has been observed in many sands (e.g., Karapanagioti, 2000). At low f_{oc} values, sorption onto minerals can become the dominant mechanism; this mineral sorption served to provide a practical lower limit for K_D . The boundary layer mass transfer coefficient, k_{bl} , has a broad range of values as it depends on many different factors. Using equations 8-6 to 8-9 and the typical range of values for the parameters presented by Thibodeaux (1996), a reasonable range of values for k_{bl} is 1.5 to 80 cm/hr. Thus, a conservative estimate of this parameter assumed in the simulation is 15 cm/hr. Further, the advective velocity exhibits a high degree of variability at a site

Chapter 8

due to the heterogeneous nature of sediments and sediment pore structure. A high value for the advective velocity in sediment systems is 100 cm/yr. This results in a cap Peclet number greater than 1 for the proposed system, with advection being the dominant transport mechanism.

The contaminant degradation rate is a function of numerous parameters; it is possible to study this parameter in the laboratory although these studies can be costly both in terms of money and time. Numerous studies have examined decay rates of phenanthrene (Bossert and Bartha, 1986; Hyun *et al.*, 2006; Wang *et al.*, 1990). These studies indicate a half-life of approximately 30 days under aerobic conditions, which corresponds to a decay rate of about 3×10^{-7} /s. Scheunert *et al.* (1987) also reported degradation of phenanthrene concentrations under anaerobic conditions. A reasonable assumption is a decay rate an order of magnitude lower (3×10^{-8} /s). Table 8-1 presents a summary of the input parameters for the simulations.

Table 8-1. Parameters used in model simulations

Sediment Properties

Contaminant Pore water Concentration (C_0), ug/L	C_0
Fraction organic carbon at depth of interest (f_{oc})	0.005

Cap Properties

Organic carbon partition coefficient ($\log K_{oc}$), log L/kg	4.3
Contaminant theoretical diffusivity (D), cm^2/s	6.0×10^{-6}
Porosity	0.5
Particle density (ρ_p), g/cm^3	2.6
Boundary layer mass transfer coefficient (K_{bd}), cm/hr	15
Bioturbation layer depth (h_{bio}), cm	5.6
Pore water biodiffusion coefficient (D_{bio}^{pw}), cm^2/s	1×10^{-5}
Particle biodiffusion coefficient (D_{bio}^p), cm^2/s	1.2×10^{-7}
Darcy velocity (u), cm/yr	100
Effective cap degradation constant (γ_{cap}), 1/s	3.0×10^{-8}
Bioturbation layer degradation constant (γ_{bio}), 1/s	3.0×10^{-7}

Other Parameters

Number of grids	100
Retardation Factor (R)	260
Dispersivity (α_D)	0.27

Chapter 8

In CoReTranS, the reactive transport of phenanthrene through a 30 cm sand cap layer was simulated using equation 8-1 where D_{eff} and λ were modelled as discontinuous functions at depth h_{bio} . That is,

$$D_{eff} = \begin{cases} D_{bio} & 0 \leq x \leq h_{bio} \\ D_{cap} & h_{bio} < x < 30cm \end{cases} \quad \text{Eq. 8-10}$$

$$\lambda = \begin{cases} \lambda_{bio} & 0 \leq x \leq h_{bio} \\ \lambda_{cap} & h_{bio} < x < 30cm \end{cases} \quad \text{Eq. 8-11}$$

The initial and boundary conditions were:

$$\text{Initial condition:} \quad C(x, t)|_{t=0} = 0 \quad \text{Eq. 8-12}$$

$$\text{Boundary conditions:} \quad -D_{bio} \frac{\partial C_{bio}}{\partial x} = k_{bl} C_{bl} \quad \text{Eq. 8-13}$$

$$C(x, t)|_{x=30cm} = C_O \quad \text{Eq. 8-14}$$

In order to achieve steady-state condition, a series of simulations was done using various time periods ranging from 1 week to 100 years.

The sediment cap was assumed to consist of clean sand and thus the initial condition (equation 8-12) was assumed zero. The boundary condition at the sediment-water interface (equation 8-13) was derived using mass balance where the flux through the benthic boundary layer must equal the flux from the bioturbation layer. Since the advective fluxes out of the bioturbation layer and into the benthic boundary layer are equal, the diffusive flux must equal the flux due to mass transfer through the benthic boundary layer.

For the analytical approach, a steady-state design tool developed by Lampert and Reible (Lampert and Reible, 2006) was used to predict cap performance for containment treatment of contaminated sediments. The steady-state model was

formulated using two distinct ODEs for the effective cap layer and the bioturbation layer:

$$D_{bio} \frac{\partial^2 C_{bio}}{\partial x^2} = u \frac{\partial C_{bio}}{\partial x} + \lambda_{bio} \phi C_{bio} \quad \text{Eq. 8-15}$$

$$D_{cap} \frac{\partial^2 C_{cap}}{\partial x^2} = u \frac{\partial C_{cap}}{\partial x} + \lambda_{cap} \phi C_{cap} \quad \text{Eq. 8-16}$$

The concentrations at the boundaries were assumed constant at steady-state, where concentrations at the bioturbation layer-effective cap layer interface (C_b) and cap-water interface (C_w) were held as unknowns. A continuity equation based on constant contaminant flux at the bioturbation layer-effective cap layer interface was also introduced:

$$D_{bio} \frac{\partial C_{bio}}{\partial x} = D_{cap} \frac{\partial C_{cap}}{\partial x} \quad \text{Eq. 8-17}$$

Pore water concentration profiles of each layer are then calculated using equations 8-15 to 8-17, using simple ODE analysis.

8.3.2.2 Results. Results of the modelling simulation are shown in Figure 8-2. Goodness of fit between pore water concentration profiles from CoReTranS simulation and analytical solution were evaluated. An r value of 1.0 and RMS value of 0.0 normalised concentration unit was obtained for all four model scenarios showing excellent correlation between the numerical and analytical results.

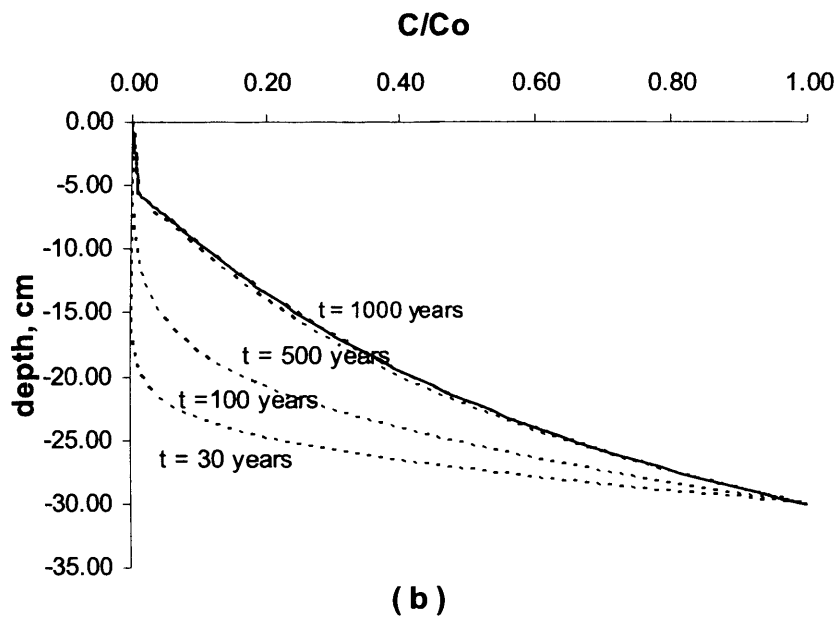
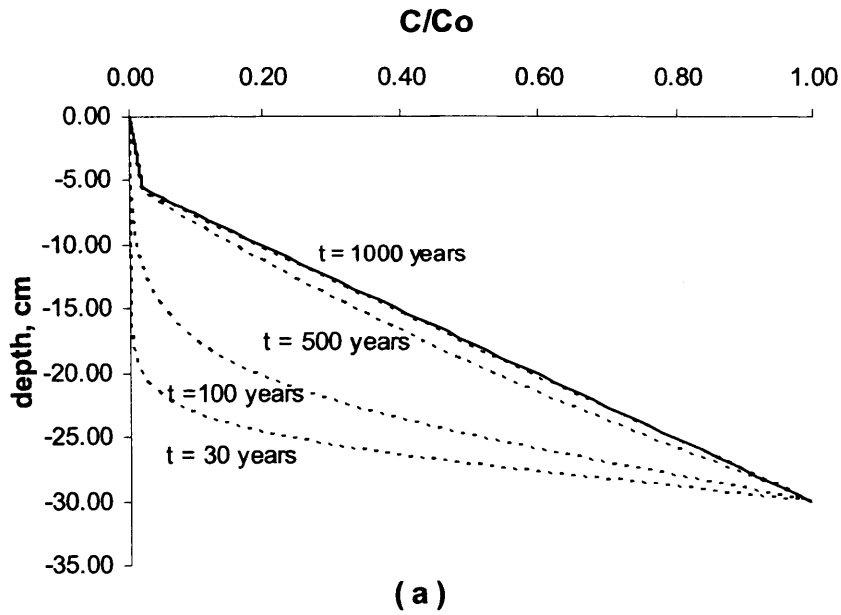


Figure 8-2a. Pore water concentration profiles of phenanthrene over a 30 cm sediment cap based on (a) Diffusion model, (b) Diffusion - Degradation model, modelled using an analytical approach (—) and a numerical approach (---).

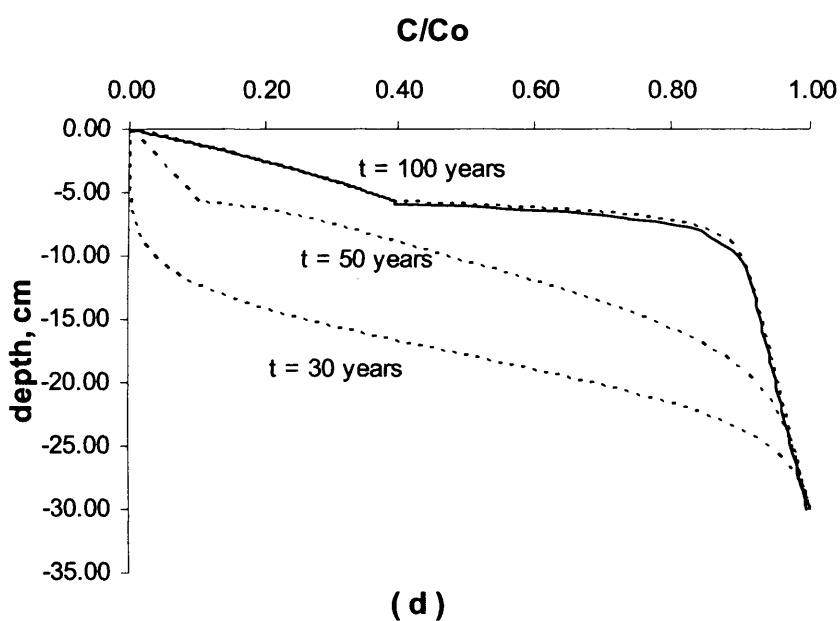
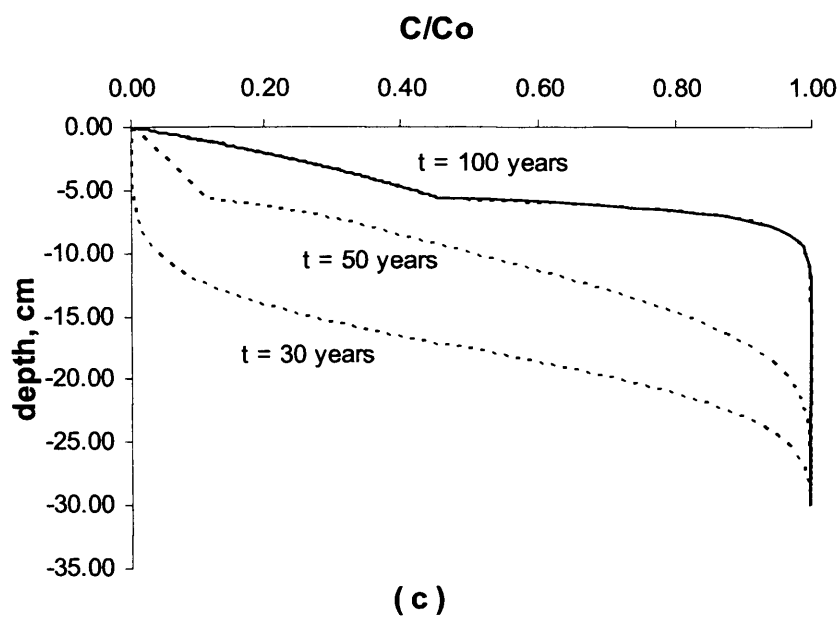


Figure 8-2b. Pore water concentration profiles of phenanthrene over a 30 cm sediment cap based on (c) Diffusion - Advection model, and (d) Diffusion - Advection - Degradation model, modelled using an analytical approach (—) and a numerical approach (---).

8.3.2.3 Discussion. Predicted pore water concentration profiles from the analytical approach show sharp transitions between the effective cap layer and bioturbation layer as expected from what essentially is a two-layer finite system. An excellent agreement ($r = 1.0$) between the simulation results and analytical solution was shown suggesting that the CoReTranS model can solve finite-layered systems with discontinuities in between sediment layers.

As shown in Figure 8-2, the time to reach steady-state for the diffusion-controlled contaminant transport scenario is ~ 1000 years. For the scenario where groundwater infiltration is significant (i.e., diffusion-advection) however, the time to reach steady-state is reduced to ~ 100 years. Further, phenanthrene concentration at the sediment-water interface is 2-3 orders of magnitude higher than that in scenarios without groundwater infiltration. This indicates that the advective velocity assumed in the simulation scenarios is a critical parameter in the analysis of cap performance in managing contaminated sediments. It is important to note that there is a lack of experimental or field data for capped systems at steady-state conditions to validate either modelling approach.

The effect of contaminant degradation to the distribution of phenanthrene in the cap layer is observed at simulation times higher than 500 years for the diffusion-controlled scenarios (Figure 8-2a) and 100 years when groundwater infiltration is significant (Figure 8-2b). This suggests that estimating cap degradation rates for cap monitoring studies is feasible when the Darcy velocity is higher.

The analytical approach evidently offers a relatively quick method of evaluating sediment cap design and performance at steady-state conditions. However, transient analysis required to evaluate pore water concentration-depth profiles over the design lifetime as well as cap breakthrough times is impossible to implement using the steady-state tool. Further, examining other assumptions for fate and transport of contaminants in capped systems may be difficult for an analytical approach as this would require a completely different analytical solution for every model equation formulated. For example, bioturbation can alternatively be modelled as a non-local exchange mechanism (Meysman *et al.*, 2003; Thibodeaux *et al.*, 2001).

8.4 Predicting contaminant fate and transport in sand capped systems amended with sorbent materials

8.4.1 Approach

The fate and transport of phenanthrene is simulated in a 30 cm sand cap amended with a 1 cm sorbent layer placed between the contaminated sediment and the effective cap layer (i.e., sand cap layer) as shown in Figure 8-3. Activated carbon and coke were chosen as sorbent materials for this modelling demonstration as these materials were found to highly influence the sorptive uptake of phenanthrene in soil and sediments (Kleineidam *et al.*, 1999; Karapanagioti *et al.*, 2000). In predicting the performance of the amended sand cap, the fate and transport model scenarios, model parameters and boundary conditions simulated in the preceding section were used.

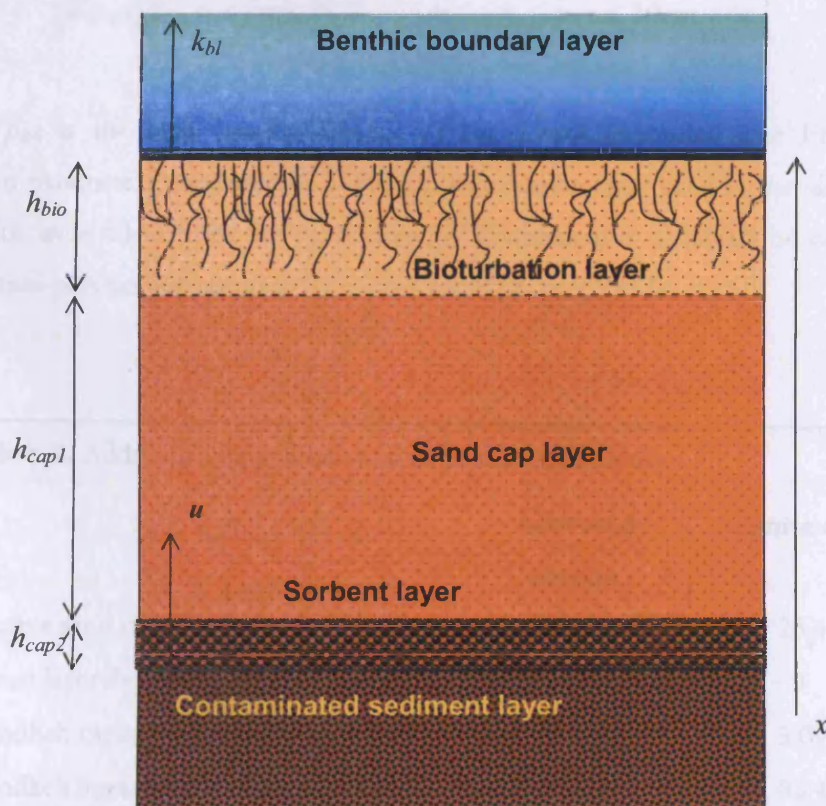


Figure 8-3. Depiction of a sand cap system amended with a sorbent layer.

Contaminant sorption onto sorbent materials is modelled using superposition of various sorption isotherms (i.e., linear and non-linear) (See for example, Weber *et al.*, 1992; Huang and Weber Jr., 1997; Xing and Pignatello, 1997; Xia and Ball, 1999). Thus, for this particular modelling demonstration, a conservative prediction of contaminant distribution within the cap was done using Weber's (1992) DRM equation to approximate contaminant sorption, specifically in the sorbent layer, over a period of 100 years for the diffusion and diffusion-advection models. The simulation period for the model scenarios were based on the predicted time to reach steady state condition for the diffusion models from the preceding section. For the non-linear sorption mechanism, the Freundlich sorption isotherm was used to account for the contaminant adsorption to these sorbent materials. Thus, the retardation factor was modelled as a discontinuous function at depth $h_{bio} + h_{cap1}$. That is,

$$R = \begin{cases} \varphi + \rho_B K_D & 0 < x \leq h_{bio} + h_{cap1} \\ \varphi + \rho_B K_D + \rho_{BS} n K_F C^{n-1} & h_{bio} + h_{cap1} < x \leq 30cm \end{cases} \quad \text{Eq. 8-18}$$

where ρ_{BS} is the bulk density (g/cm^3) of the sorbent material. The Freundlich sorption parameters presented in Table 8-2 and subsequently used in the simulation scenarios were taken from the study done by Kleineidam *et al.* (2002) on combined adsorption-partitioning sorption isotherms for PCBs and PAHs.

Table 8-2. Additional parameters used in model simulations

	Activated carbon	Lignite coke
Effective sand cap depth (h_{cap1}), cm	23.4	23.4
Sorbent layer depth (h_{cap2}), cm	1	1
Freundlich capacity factor ($\text{Log } K_F$), L/kg	6.18	5.09
Freundlich linearity parameter (n)	0.51	0.24
Bulk density (ρ_{BS}), g/cm^3	0.66	0.50

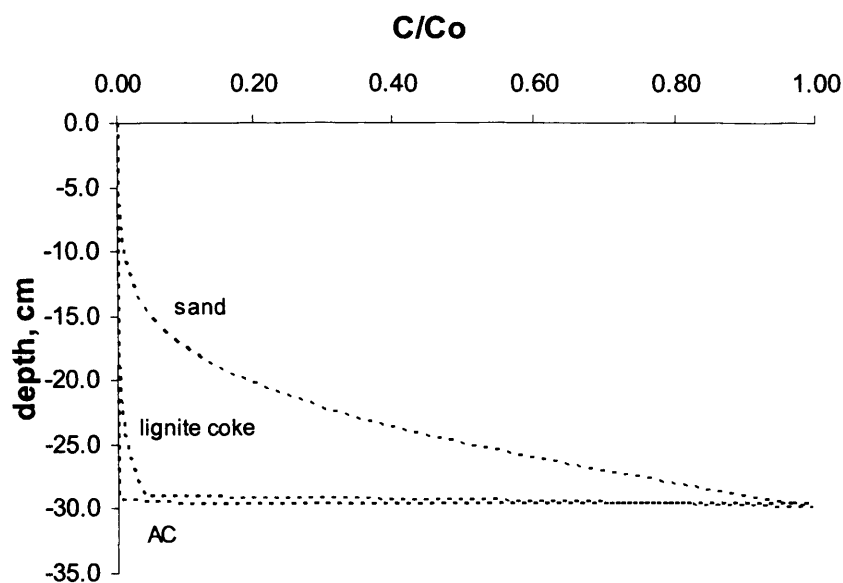
As there is no available analytical solution for the resulting highly non-linear PDE, the efficacy of the capped system is evaluated numerically on the basis of the simulation results.

8.4.2. Results and Discussion

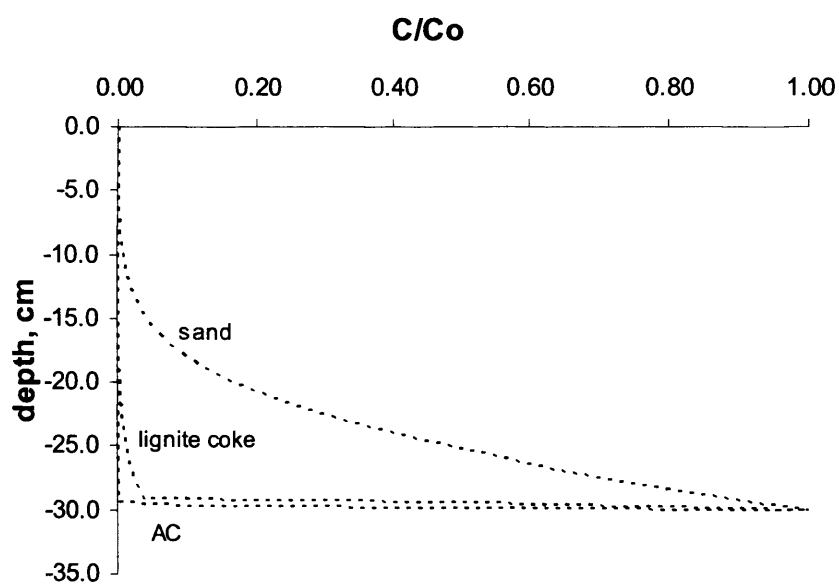
From the simulation results of the four model scenarios shown in Figure 8-4, phenanthrene was predicted to be mostly distributed within the sorbent layer primarily due to the strong sorption of the contaminant to the sorbent materials. Using the dual mode model for sorption, the increased retardation factor resulted in a much decreased contaminant diffusivity, advective velocity and degradation rates. The tendency of phenanthrene to strongly sorb to sorbent materials such as activated carbon and coke is well documented (e.g., Accardi-Dey and Gschwend, 2002; Grathwohl, 1990; Huang *et al.*, 2003; Kleineidam *et al.*, 2002).

Further, phenanthrene was effectively isolated within the sorbent layer comprising of AC for all model scenarios considered as shown in Figure 8-4. This suggests that sand caps amended with a thin layer (1 cm) of activated carbon can be applied to sites even with high groundwater infiltration (~100 cm/yr). Contaminant breakthrough beyond the 1 cm sorbent layer, however, occurred for the coke-amended sediment cap. This is reflective of the higher K_F and sorption capacity of activated carbon in comparison with lignite coke and sand.

In scenarios where groundwater infiltration is significant, phenanthrene concentration at the interface between the sand cap layer and the lignite coke layer was twice as much as the concentration for the diffusion-controlled scenario (see Table 8-3). Thus, the presence of groundwater infiltration must be factored in the design of coke-amended sand caps.



(a)



(b)

Figure 8-4a. Pore water concentration-depth profiles of phenanthrene over a 30 cm sediment cap amended with activated carbon (AC) and coke based on (a) Diffusion model, (b) Diffusion – Degradation model, over 100 years simulation time.

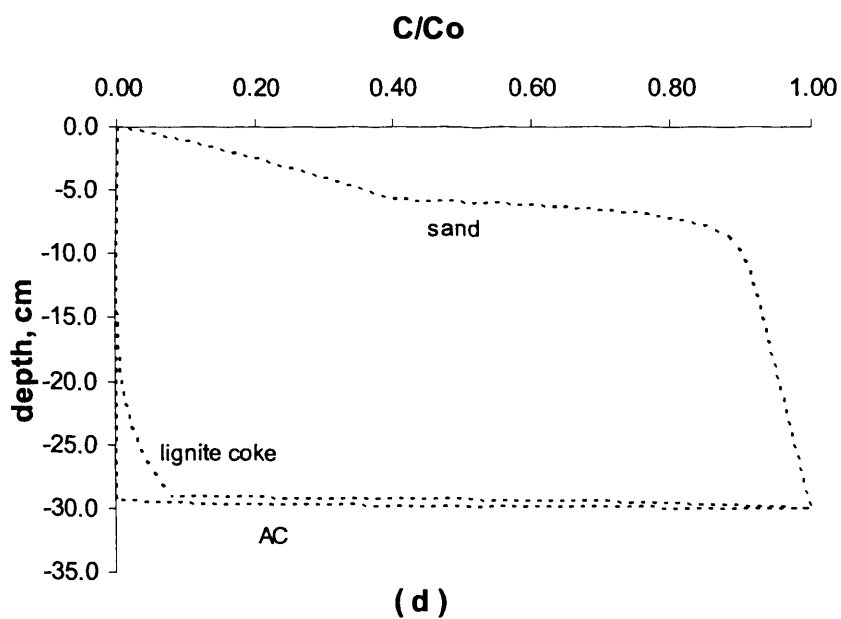
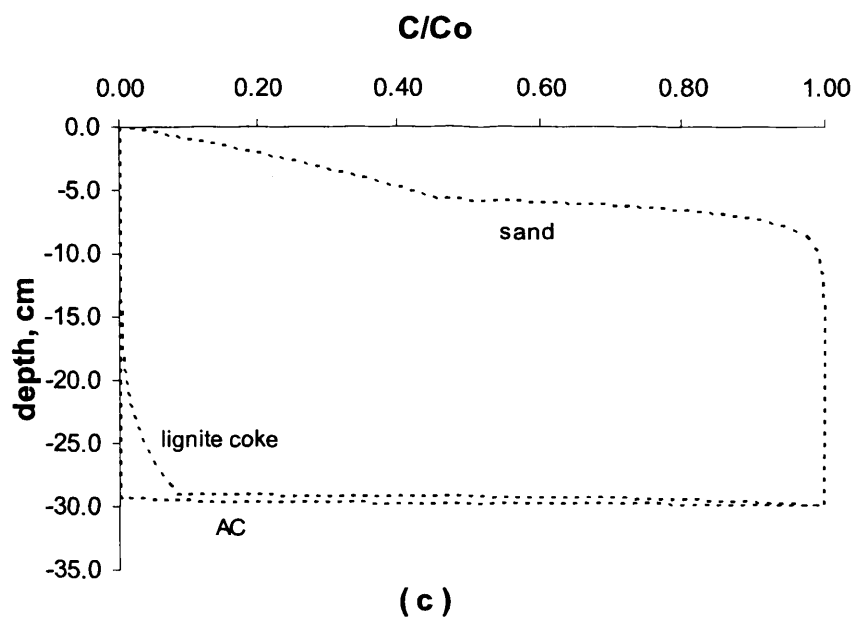


Figure 8-4b. Pore water concentration-depth profiles of phenanthrene over a 30 cm sediment cap amended with activated carbon (AC) and coke based on (c) Diffusion - Advection model, (d) Diffusion - Advection - Degradation model, over 100 years simulation time.

Table 8-3. Phenanthrene concentration at the sand cap-sorbent layer interface

	<i>C/Co (t = 100 yrs)</i>	
	<i>u = 0 cm/year</i>	<i>u = 100 cm/year</i>
<i>Without contaminant degradation</i>		
AC	1.0×10^{-5}	1.0×10^{-5}
Lignite coke	0.04	0.08
Sand	0.91	1.0
<i>With contaminant degradation</i>		
AC	8.6×10^{-6}	9.1×10^{-6}
Lignite coke	0.04	0.08
Sand	0.89	1.0

As shown in Figure 8-5, the steady-state concentration of phenanthrene at the interface between the sand cap layer and the activated carbon layer was an order of magnitude greater than that for the coke-amended sediment cap. The time to reach steady-state for the diffusion-controlled contaminant transport scenario in the coke-amended sediment cap is ~5000 years, which is five times more than the steady-state time for the sand cap. In the activated carbon-amended sediment cap, the time to reach steady state (diffusion-controlled scenario) is ~8000 years. For the scenario where groundwater infiltration is significant, the time to reach steady-state is reduced to ~2800 years for the coke-amended sediment cap and ~4000 years for the activated carbon-amended cap.

From the simulation results presented, adding a thin layer of sorbent material in sand caps can drastically improve the performance of the cap primarily due to the increased sorption capacity sorbent materials provide.

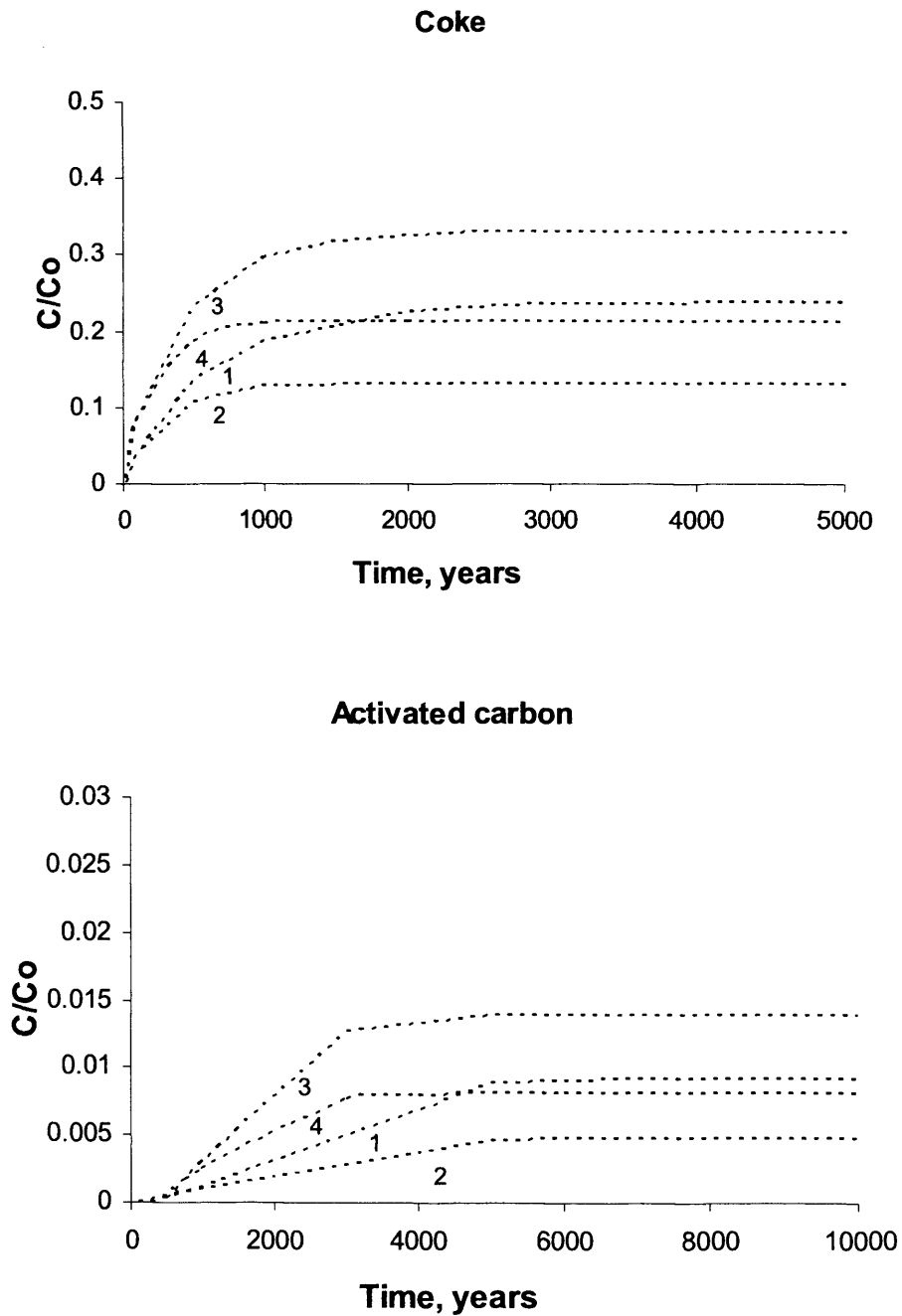


Figure 8-5. Pore water concentration of phenanthrene at the interface between the sand cap and the sorbent amended layer for the all four scenarios: (1) Diffusion model, (2) Diffusion – Degradation model, (3) Diffusion – Advection model, and (4) Diffusion – Advection – Degradation model over time.

8.6 Conclusions for model prediction of the effects of capping in contaminated sediments

In situ capping provides a relatively non-invasive remedial option for managing contaminated sediments. In order to evaluate cap performance and its impact on biota and water quality, as well as compare its effectiveness to that of other remedial strategies such as dredging, contaminant distribution over the capped system needs to be predicted. This chapter presented two modelling approaches in predicting contaminant fate and transport through a sediment cap. The analytical modelling approach offers a relatively quick method of evaluating cap performance at steady-state, but has a limited ability to accommodate complex transport mechanisms expressed by nonlinear governing equations over transient times. Numerical models can offer a wide range of model complexities including discontinuities at sediment interfaces. Both approaches have demonstrated their applicability in evaluating sediment capping scenarios and cap performance.

For the 30 cm thick sand cap that was considered for the hypothetical capped system presented in this chapter, the numerical results of the assumed modelling scenarios showed that the CoReTranS model can predict the effects of sediment capping by quantifying contaminant pore water concentration-depth profiles over transient times and time to reach steady-state conditions for a specified cap thickness. For the prevailing scenarios where contaminant transport is diffusion controlled, the predicted time to reach steady-state conditions is around a millennium. In cases where the groundwater infiltration is significant (~ 100 cm/yr), the time to reach steady-state conditions is reduced to a century. Further, the presence of an active bioturbated layer ($h_{bio} = 5$ cm) enhances the release of contaminants to the overlying water as evidenced by reduced contaminant distribution at the upper layer of the cap.

For the sand cap amended with sorbent materials (AC and coke), phenanthrene was predicted to be mostly distributed within the sorbent layer primarily due to the strong sorption of the contaminant to the sorbent materials. The AC-amended sand cap was more effective in isolating the contaminant within the sorbent layer for a sustained period of time (~ 100 years). Further, the presence of groundwater infiltration must be factored in the design of coke-amended sand caps. As shown

Chapter 8

from the results of the model predictions, adding a thin layer of sorbent material in sand caps can drastically improve the performance of the cap primarily due to the increased sorption capacity sorbent materials provide.

Results from the various simulation scenarios presented in this chapter using the CoReTranS model showed that sediment capping as a remedial strategy in managing contaminated sediments can effectively reduce contaminant flux to the overlying water through interaction with the sediment cap matrix and by increasing the dissolved contaminants' transport lengths (i.e., cap thickness) and increasing sorption uptake capacity of the cap by amending the cap material with sorbents such as AC and coke.

CHAPTER NINE

Summary, Conclusions and Recommendations

9.1 Summary

Surface water sediments from oceans, estuaries, lakes and rivers are highly complex biogeochemical environments. The fate and behaviour of organic contaminants that find their way into bed-sediments are essentially controlled by the various reaction and transport processes occurring in these environments. To date, bed-sediments in industrialised nations carry a worrying burden of sediment contamination (Power, 2002; US Environmental Protection Agency, 1997a), prompting environmental regulatory agencies in several countries to focus on the elimination or reduction of ecological and human health risks associated with contaminated sediments (Chapman and Wang, 2001; Environmental Agency Wales, 2004; SEDNET (European Sediment Research Network), 2005; US Environmental Protection Agency, 1998a). Since both ecological effects and risks are related to contaminant concentrations, understanding the in-bed fate and transport processes is therefore important not only in quantifying contaminant concentrations in bed-sediments but also in evaluating different remedial options in managing contaminated sediments (Apitz *et al.*, 2005).

Reactive transport modelling is an effective tool in critically examining the fate and transport of contaminants in soils and sediments. When applied together with laboratory experiments or field monitoring studies, reactive transport models can guide laboratory and field studies by identifying areas that needs further study. Development of reactive transport models particularly for layered bed-sediments,

however, has been limited compared to that of models in other reactive transport disciplines such as contaminant hydrogeology and early diagenesis.

This study has developed CoReTranS, a predictive modelling environment that can quantify one-dimensional organic contaminant reaction and transport in bed-sediments, using an object-oriented modelling approach. CoReTranS can facilitate selection of processing elements (i.e., contaminant species, reactive transport mechanisms) from a smart-menu graphical user interface thereby effectively building customised models that will suit site-specific applications.

The CoReTranS model has been verified and benchmarked by comparing pore water concentration profiles of simplified reactive transport problems simulated in CoReTranS with their corresponding analytical solutions. Goodness of fit between the predicted profile and the profile quantified from the analytical solution of all model scenarios was evaluated using *RMS* and *r*. The *RMS* values obtained from all scenarios ranged from 4.14×10^{-4} to 1.60×10^{-2} , which could be attributed to the assumption that was made in deriving the exact solution of the model equation for each scenario (i.e., predicted contaminant concentrations approaches zero as sediment depth approaches 30 cm, while for the analytical solution, the contaminant concentration will only approach zero as sediment depth approaches infinity). Thus, the residual error mostly lies on the base of the considered sediment column.

The following modelling studies were undertaken using the CoReTranS model:

Reactive transport and distribution of selected trace level organic contaminants in a riverine environment from a diffusion-controlled laboratory experiment as reported in Allan *et al.* (2002b; 2004).

Scope:

- Allan's study (2002; 2004) was aimed at understanding and modelling the various processes that determined the depth distribution of micro-organic contaminants.
- Changes in contaminant concentration in the overlying water, pore water and whole sediment were measured

Conceptual model

- The transport of contaminants was assumed to be mainly diffusion-controlled.
- Diffusion, sorption, degradation and bioturbation mechanisms may potentially predict the contaminant distribution in sediments.

Reactive transport model formulation

- Four model scenarios were considered and simulated in CoReTranS: (1) transport by molecular diffusion only, (2) sorption-retarded diffusive transport using linear partitioning coefficient, K_D , as a function of depth; modelled using a power law equation, (3) sorption-retarded diffusive transport with degradation, and (4) sorption-retarded diffusive transport with degradation and bioturbation.
- For the initial concentration, the bed-sediment was assumed clean prior to spiking of the model contaminants, and C_0 was thus set to zero.
- The measured overlying water concentration was considered as a boundary condition at the sediment-water interface, and modelled with an exponential correlation.
- Zero contaminant flux was assumed at the bottom of the two channels.

Model validation

- Concentration gradient (i.e., molecular diffusion) alone is not sufficient to predict the actual contaminant levels in the bed-sediment.
- Modelling contaminant partitioning using K_D as a function of depth did not improve the agreement between the predicted and actual profiles.
- Both contaminant degradation and bioturbational activity in the experimental channels were not predicted to impact the fate and transport of lindane in the bed-sediment.
- The diffusion-sorption model gave a good agreement after adjusting the sorption capacity (i.e., $K_D = 3 \text{ L/kg}$).

- No conclusive explanation of the reduced sorption capacity was presented due to lack of data regarding colloidal concentration in the experimental bed-sediment.

Vertical transport of petroleum-derived hydrocarbons in marsh sediments from a field study in Wild Harbour, West Falmouth, MA as reported in White *et al.* (2005).

Scope:

- White *et al.* (2005) investigated the abundance and persistence of PAHs in the Wild Harbour marsh sediments in order to assess whether diffusion and sorption are the prevailing processes that control the vertical distribution of PAHs at the contaminated site.
- Changes in total contaminant concentration in the bulk sediment were measured

Conceptual model

- A simple post-depositional transport model was developed to assess the effects of sediment-water partitioning and molecular diffusion on the post-depositional transport of PAHs.

Reactive transport model formulation

- Using the CoReTranS modelling environment, the dataset was simulated as a diffusion-sorption-advection (DSA) model.
- Degradation was assumed as a non-controlling mechanism in the downcore vertical distribution of PAHs at the site.
- Bioturbational effects was also assumed negligible, considering the probable decimation of the macrobenthic population as an after-effect of the oil spill.
- The contaminant was assumed to penetrate approximately 6 cm of the sediment bed when the oil was spilled based on the measured peak width of the contaminant profile at its highest concentration.

Model validation

- The predicted concentrations of C1- and C2-naphthalene in the upper 5 cm was attributed to the contaminant's diffusivities (i.e., 0.81 and 0.47 cm²/yr, respectively) exceeding the burial velocity (0.35 cm/yr).
- For C3-naphthalene, the predicted profile was narrower and more symmetric as compared to the profiles for C1- and C2-naphthalene, and was better approximated by the model. The profile, thus, showed to be a result of a more diffusion-controlled scenario.
- For the phenanthrene species, much narrower peaks resulted in the predicted profiles due to their relatively higher diffusion coefficients and more hydrophobic nature.

The CoReTranS model was also used to interpret results from the following field studies in order to explain key processes that controlled the fate and transport of PAHs and PCBs in bed-sediments:

Transport and distribution of PAHs purported to be derived from atmospheric particle emissions, wastewater discharges and accidental spillages from a nearby aluminium smelter, in sediments from Kitimat fjord system near Kitimat, British Columbia (Simpson *et al.*, 1998).

Scope:

- From Simpson's study (1998), a reactive transport model scenario was constructed and simulated in CoReTranS to determine the key processes that controlled the vertical distribution of PAHs at the Kitimat fjord site.
- No previous numerical model was developed for these studies, and thus the findings shown in the preceding sections were mostly presumptive.
- Changes in total contaminant concentration in the bulk sediment were measured

Conceptual model

- The key processes controlling the post-depositional distribution of aluminium smelter-derived PAHs in the marine sediments were deduced from the sediment core samples collected on site.
- The downcore profiles of PAH suggest diffusive transport of contaminants from a continuous contamination source at the sediment water interface, i.e., presumably there is an ongoing local input.
- The dramatic decrease of PAH concentration with depth implies retarded diffusive movement due to low diffusion coefficients and partitioning to the sediment matrix.
- The vertical movement of the contaminant front at the top segments of the sediment core (i.e., 0 – 10 cm depth) indicates inclusion of an advective process to the model scenario.

Reactive transport model formulation

- The model was developed in CoReTranS as a DSA scenario.
- The velocity of burial of particles below the sediment-water interface (i.e., sediment accumulation rate) was given values ranging from 0.25 to 0.5 cm/y by Simpson *et al.* (1998).
- The sediment porosity was given a value of 0.86 based on the study done on the collected sediments cores at the British Columbia fjords by Bornhold and Prior (1989).

Model validation

- the CoReTranS model predicted the dramatic decrease of the selected PAH concentrations with depth (due to low diffusion coefficients and partitioning of the contaminants to the sediment matrix) and the vertical movement of the contaminant front at 0 – 10 cm depth (due to an assumed advective mechanism in place).
- The relatively high PAH concentration near the sediment surface was indicative of the downward migration pattern of the contaminant front through episodic sediment deposition.

- The absence of subsurface maxima in the downcore PAH concentration profiles show that sediment contamination is still controlled by ongoing local inputs, presumably from the nearby aluminium smelter.
- Adding a degradation mechanism to the reactive transport model overly predicted contaminant loss particularly in the top layer of the bed-sediment

Reactive transport, distribution and natural recovery of PCB in contaminated sediments at the Sangamo-Weston/Twelvemile Creek/Lake Hartwell Superfund Site in the US (Brenner *et al.*, 2004).

Scope:

- PCB contamination of Lake Hartwell sediments was primarily due to discharges from the nearby capacitor plant.
- Changes in total contaminant concentration in the bulk sediment were measured.

Conceptual model

- The migration of PCB to the bed-sediment was hypothesized to be a result of the following individual (or combination of) mechanisms: contaminant diffusion from the overlying water; and contaminant sorption to suspended sediments that will eventually deposit at the sediment-water interface.

Reactive transport model formulation

- The governing model equation was simulated in CoReTranS as a diffusion-sorption-advection-degradation (DSAD) model.
- The velocity of burial of particles below the sediment-water interface (i.e., sediment accumulation rate) estimated using the ^{210}Pb and ^{137}Cs profiles from the study done by Brenner *et al.* (2004).
- The parameters used for the simulation of total PCB were based on average values of parameters for the 107 PCB congeners analysed.
- The contaminant concentration at the sediment-water was estimated using the contaminant's solubility S on the assumption that Lake Hartwell was heavily contaminated, and thus fully saturated with PCB discharged from the

nearby capacitor manufacturing plant at Sangamo-Weston, SC from 1955 until 1977 (US Environmental Protection Agency - Region 4, 2005).

- Future PCB concentrations were predicted using an additional simulation time of 5, 10, 15 and 25 years, the results of which were fitted with best fit logarithmic regressions in order to approximate the contaminated sediment recovery rates. The recovery times were then calculated by setting the PCB concentration (*i.e.*, x-axis) to the EPA clean-up requirements of 1.0, 0.4 and 0.05 mg/kg.

Model validation

- The predicted profiles showed narrow peak widths similar to the actual profiles, suggesting that a retarded diffusion mechanism was one of the controlling mechanisms.
- The predicted contaminant peaks did not match the contaminant peaks from the actual profiles, which suggests that sedimentation rates estimated by Brenner *et al.* (2004) did not fully capture the non-uniform historical sediment deposition at Lake Hartwell based on sediment dating, possibly due to sediment heterogeneity on site.
- PCB flux onto the bed-sediments at the site may have continued well beyond 22 years after PCB use was terminated at the Sangamo-Weston, SC plant in 1977.
- The predicted contaminant peak concentrations of PCB1 and total PCB at both transect locations fell within the τ range of 32 – 34 years, which is about 10 – 12 years of continuous contamination after PCB use at the site was terminated concomitant with the closure of the plant in 1987.
- In comparison with the simulation results from CoReTranS, Brenner's predictions for the time to achieve the specified sediment clean-up goals were significantly lower presumably due to the fact that Brenner simply extrapolated past historical data from sediment cores using best fit logarithmic regressions.

The CoReTrans model was also used to predict the effect of capping contaminated sediments as a remedial strategy.

- Prediction of cap performance using the CoReTrans model is defined by the contaminant's concentration-depth profiles in pore water over transient times and the length of time to reach steady-state conditions for a specified cap thickness.
- In predicting cap performance using CoReTranS, the reactive transport of phenanthrene through a 30 cm sand cap layer was simulated using four distinct model scenarios: diffusion, diffusion-degradation, diffusion-advection, and diffusion-advection-degradation models, where parameters D_{eff} and λ were modelled as discontinuous functions at depth h_{dis} .
- An excellent agreement ($RMS = 0.0 \text{ g/m}^3$ and $r = 1.0$) between the simulation results and analytical solution was shown, suggesting that the CoReTranS model can solve finite-layered systems with discontinuities in between sediment layers.
- The advective velocity is a critical parameter as it may increase or reduce the time to reach steady-state conditions within the capped system.
- Results from the various simulation scenarios presented in this chapter using the CoReTranS model showed that sediment capping as a remedial strategy in managing contaminated sediments can effectively reduce contaminant flux to the overlying water through interaction with the sediment cap matrix, and by increasing the dissolved contaminants' transport lengths (i.e., cap thickness).
- Sand caps amended with a thin layer (1 cm) of activated carbon can be applied to sites even with high groundwater infiltration ($\sim 100 \text{ cm/yr}$). Contaminant breakthrough beyond the 1 cm sorbent layer, however, occurred for the coke-amended sediment cap. This is reflective of the higher K_F and sorption capacity of activated carbon in comparison with lignite coke and sand.
- In scenarios where groundwater infiltration is significant, phenanthrene concentration at the interface between the sand cap layer and the lignite coke layer was twice as much as the concentration for the diffusion-controlled scenario.

- The steady-state concentration of phenanthrene at the interface between the sand cap layer and the activated carbon layer was an order of magnitude greater than that for the coke-amended sediment cap.
- The time to reach steady-state for the diffusion-controlled contaminant transport scenario in the coke-amended sediment cap is ~5000 years, which is five times more than the steady-state time for the sand cap. In the activated carbon-amended sediment cap, the time to reach steady state (diffusion-controlled scenario) is ~8000 years.
- For the scenario where groundwater infiltration is significant, the time to reach steady-state is reduced to ~2800 years for the coke-amended sediment cap and ~4000 years for the activated carbon-amended cap.

9.2 Conclusions

Comparing the results obtained from laboratory experiments or field monitoring studies of bed-sediment systems with different accumulation, degradation and release mechanisms, with the results from the CoReTranS model was critical in identifying the key processes that drive the fate and transport of organic contaminants in bed-sediments. All of these simulations were done on the CoReTranS modelling environment which allowed multiple hypotheses testing in developing comprehensive reactive transport model scenarios for each datasets. From these simulations the following conclusions can be drawn:

1. A numerical model for organic contaminant reaction and transport in layered bed-sediments (CoReTranS) that will enable prediction of concentration-depth profiles of organic contaminants in bed-sediments on the basis of input information about contaminant concentration in the overlying water, and vice versa is presented.

2. The use of the validated CoReTranS model in interpreting laboratory experiment and field study results has identified the following critical model parameters that govern fate and transport in bed-sediments:
 - a. **Effective diffusion coefficient.** D_{eff} is typically a magnitude or two less than the molecular diffusion coefficient D due to sediment porosity and tortuosity. If sorption is significant, D_{eff} is further reduced by the retardation factor R . If bioturbation activity is present in the system, D_{eff} is increased by adding a biodiffusion term. To date, substantially less work has been done to quantify biodiffusion coefficients. In chapter eight, the biodiffusion coefficient used in predicting cap performance was estimated from a summary of observed biodiffusion coefficients from numerous studies. Calibration of D_{eff} is therefore dependent on how well sediment porosity and tortuosity are characterised, as well as whether sorption and/or bioturbation are evident in the system.
 - b. **Advective velocity.** u can either be quantified as sediment accumulation rates due to sediment burial or seepage velocities as a result of hydrological flows. Advection essentially results in vertical movement of the contaminant front. For example, the PAH concentration-depth profiles from Kitimat, British Columbia as discussed in chapter six showed that the vertical movement of the contaminant front at 1 – 10 cm depth was predicted using an assumed advective mechanism in place. Further, the calibration of sediment accumulation rates was identified to be critical in predicting contaminant peaks from the actual PCB concentration-depth profiles as discussed in chapter seven. In predicting the effects of sediment capping as discussed in chapter eight, it is the advective flow that can mostly move the dissolved contaminants from the bed-sediment through the overlying sediment cap, thus impacting cap performance.
 - c. **Mass transfer coefficient.** In CoReTranS, η is either supplied as a user-defined parameter, or estimated using an empirical correlation by

Thibodeaux and Bierman (2003), if bioturbation is modelled as a non-local transport process as oppose to a simple biodiffusive process. The use of the empirical correlation, however, requires that the bioturbation depth h_{bio} should be given *a priori*. Both h_{bio} and biodiffusion coefficients are presently estimated from a summary of observed values from numerous studies, which may or may not accurately represent the system being studied. However, the inclusion of a non-local transport scenario in modelling systems where there is evidence of bioturbation activity is still critical in predicting contaminant fate and transport. For example, in Allan's experiment as discussed in chapter five, *oligochaete* worms were observed in the experimental bed-sediment, and may have influenced the distribution of lindane in the sediment. Evaluation of η using the native *oligochaete* worms in Allan's experiment set-up was thus recommended as future work. This parameter becomes negligible if bioturbation activity is not evident in the contaminated area.

- d. **Retardation factor.** If sorption is significant (e.g., $f_{oc} > 0$), R effectively reduces both advective and diffusive transport parameters. The contaminants dissolved in the sediment pore water moves at a retarded advective velocity and reduced diffusion coefficient as a result of the time contaminants spent on the sediment matrix. In chapters six and seven, contaminant concentration-depth profiles were predicted using D_{eff} corrected by a linear retardation factor based on K_{OC} values and given organic carbon fractions.
- e. **Degradation rate.** λ is typically estimated using the contaminant's half-life. The effect of the degradation process is essentially to reduce contaminant concentration in sediments, corresponding to a shift of the contaminant front to the left of the predicted profiles. This parameter becomes negligible if bacterial activity is not evident in the contaminated area, or the contaminant is too resistant from bacterial degradation. For example, degradation was not included in the model scenario presented in chapter six due to the assumptions that

chemical or biological degradation was not occurring today, or may have ceased 25 years ago as shown in White's study (2005b).

3. The use of the validated CoReTranS model in interpreting laboratory experiment and field study results has identified the following limitations of the CoReTranS model:
 - a. Predicting the reactive transport of organic contaminants in bed-sediments using CoReTranS is currently limited to the constituent equations embedded in the CoReTranS model.
 - b. In chapter 8, where bioturbation is modelled as biodiffusive transport, D_{eff} was plugged in as a user-defined parameter as there is currently no equation that can estimate biodiffusion coefficients.
 - c. Modelling of contaminant sorption is limited to equations based on sorption-desorption equilibrium. Rate-limited reaction processes that involve quantifying fractions of contaminants undergoing slow and fast sorption, as well as sorption-desorption hysteresis can not be simulated in CoReTranS.
 - d. Modelling of colloid-enhanced contaminant transport is currently not possible as this requires judicious differentiation between colloidal organic matter and dissolved organic carbon.
 - e. Reactive transport of organic contaminants due to sediment deposition is modelled in CoReTranS as an advective transport mechanism.

9.3 Recommendations

At present, the CoReTranS model can predict the vertical distribution of organic contaminant in bed-sediments by using measured parameters on-site, and by intuitively selecting individual or combinations of available, scientifically defensible fate and transport mechanisms integrated in the CoReTranS modelling environment. The CoReTranS model is therefore recommended to be used in contaminated sediment management projects to complement environmental monitoring plans.

Given the enormous expense of sediment remediation, regulators and industry/consultants can use the CoReTranS model to evaluate different management options by virtually testing and comparing the effectiveness of remediation alternatives for organic contaminants. For example, natural recovery rates can be predicted for an MNR project (as shown in Chapter 7), the efficacy of which can be compared against the use of a simple sand cap or a sorptive cap (as shown in Chapter 8) in achieving prescribed clean-up goals. Further, gaps within the site characterisation plan in its initial stages (e.g., full array of parameters to be measured *in situ*) can be identified at the start of the project by considering all the input parameters required by the CoReTranS model, and the probable fate and transport processes that control the spatial distribution of contaminants at the site.

The sediment research community can also benefit from the use of the CoReTranS model in interpreting historical contamination data (as shown in chapter 6). Critical parameters that affect the post-depositional transport of these contaminants in bed-sediments can be identified through modelling studies using the CoReTranS modelling environment. The CoReTranS model can therefore serve as a framework for data and knowledge concerning contaminant reaction and transport in bed-sediments.

The application of the CoReTranS model to the modelling studies presented in this thesis, however, highlighted the need to investigate other mechanisms (e.g., effect of colloids, biofilm formation) that evidently affected contaminant fate and transport in sediments. Thus, from the individual modelling studies presented in this thesis, the potential areas for further investigations identified from the use of the CoReTranS model may be as follows:

1. Chapter 5: CoReTranS model validation – Interpretation of laboratory experimental study results using the CoReTranS model
 - Evaluation of the mass transfer coefficient to critically examine the effect of bioturbation using the native *oligochaete* worms in Allan's experimental set-up;

- Analysis of the bioturbation flux of contaminant using a local bio-diffusion parameter;
 - Investigation of the effect of colloids present in different pore water concentrations; and
 - Investigation of slow/fast sorption phenomenon.
2. Chapter 6: CoReTranS model validation – Interpretation of field study results from PAH-contaminated sites using the CoReTranS model

PAHs in West Harbour, West Falmouth, MA

- Evaluation of the mass transfer coefficient to critically examine the effect of contaminant loss due to bioturbation activity of macrobenthic organisms on the marsh sediments;
- Analysis of colloidal concentrations along the marsh sediment cores to see if partitioning to a third phase can improve the prediction of contaminant distribution;
- Analysis of the intermittent effect of tides on the model parameters (i.e., functions of time); and
- Analysis of the effect of the marsh grass *Spartina alterniflora* that grow at the site and penetrate the upper sediment on the contaminant uptake loss (See, for example, Watts *et al.*, 2006).

PAHs in Kitimat Arm, Douglas Harbour, British Columbia

- Determine accurate sediment accumulation rates using either ^{210}Pb or ^{137}Cs geochronological studies to examine the effect of sediment deposition on the vertical distribution of PAHs at the contaminated site;
- Evaluate physico-chemical characteristics of the contaminated sediments to determine exact porosity values and anoxic/oxic conditions;
- Evaluate the mass transfer coefficient to critically examine the effect of contaminant loss due to bioturbation activity of macrobenthic organisms on the contaminated sediments; and

- Analyse colloidal concentrations in pore water to see if partitioning to a third phase can improve the prediction of contaminant distribution.
3. Chapter 7: Predicting PCB distribution in Lake Hartwell sediments and the effects of monitored natural recovery using the CoReTranS model
- Determine accurate sediment accumulation rates using either ^{210}Pb or ^{137}Cs geochronological studies to examine the effect of sediment deposition to the vertical distribution of PCBs at the contaminated site;
 - Evaluate physico-chemical characteristics of the sediments to determine exact porosity values and anoxic/oxic conditions;
 - Investigate bioturbational activity of macro- and micro-benthos at the Lake Hartwell site and evaluate the mass transfer coefficient to critically examine the effect of contaminant loss due to bioturbation activity; and
 - Long-term monitoring programme should be in place to assess the efficacy of natural recovery of contaminated sediments and to determine if the clean-up goals were met at the predicted recovery times.

For the CoReTranS model, the following future works may be pursued:

1. Inclusion of other relevant reactive transport mechanisms such as colloid-enhanced transport and rate-limited reaction processes to the CoReTranS model.
2. Extension of the CoReTranS model to include inorganic species.
3. Development of the CoReTranS model as a three-dimensional reactive transport model.
4. Development of the CoReTranS modelling environment's post-simulation functionalities such as: (a) statistical analyses for calibration of customised models; (b) optimisation procedures for selected environmental parameters, and; (c) a numerical sensitivity analysis component in order to understand the significance of each process, parameter and variable in the overall system, and the extent of their effects under realistic conditions.

References

- Abdel-Salam, A.; Chrysikopoulos, C.V. 1995. Analysis of a model for contaminant transport in fractured media in the presence of colloids. *Journal of Hydrology*. 165, 261-281.
- Abraham, W.R.; Nogales, B.; Golyshin, P.N.; Pieper, D.H.; Timmis, K.N. 2002. Polychlorinated biphenyl-degrading microbial communities in soils and sediments. *Current Opinion in Microbiology*. 5, 246-253.
- Accardi-Dey, A.; Gschwend, P.M. 2002. Assessing the Combined Roles of Natural Organic Matter and Black Carbon as Sorbents in Sediments. *Environmental Science and Technology*. 36, 21-29.
- Adamson, A.W. 1976. *The Physical Chemistry of Surfaces*. Wiley & Sons, Inc: New York.
- Agency for Toxic Substances and Disease Registry. 1995. Toxicological profile for polychlorinated biphenyls.
- Agency for Toxic Substances and Disease Registry. 2005. Toxicology profile for polyaromatic hydrocarbons - ATSDR's Toxicological Profiles on CD-ROM CRC Press
- Agency for Toxic Substances and Disease Registry (ATSDR). 1990. Public Health Statement, Polycyclic Aromatic Hydrocarbons
- Al-Niami, A.N.S.; Rushton, K.R. 1979. Dispersion in stratified porous media: Analytical solutions. *Water Resources Research*. 15, 1044-1048.
- Alexander, M. 2000. Aging, Bioavailability, and Overestimation of Risk from Environmental Pollutants. *Environmental Science and Technology*. 34, 4259-4265.
- Allan, I.J.; Stegemann, J.A. 2007. Chapter 7: Modelling of Pollutant Fate and Behaviour in Bed-sediments. In *Sediment Quality and Impact Assessment of Pollutants*; Barcelo, D., Petrovic, M., Eds.; Elsevier.
- Allan I.J. 2002. Transport and distribution of selected micro-organic contaminants in a riverine environment. *PhD Thesis*. University of Reading, UK.

Allan, I.J.; House, W.A.; Parker, A.; Carter, J.E. 2004. Transport and distribution of lindane and simazine in a riverine environment: measurements in bed sediments and modelling. *Pesticide Management Science*. 60, 417-433.

Allan, I.J.; House, W.A.; Parker, A.; Carter, J.E. 2005. Diffusion of the Synthetic Pyrethroid Permethrin into Bed-Sediments. *Environmental Science and Technology*. 39, 523-530.

Aller, R.C. 1980. Quantifying solute distributions in the bioturbated zone of marine sediments by defining an average microenvironment. *Geochimica et Cosmochimica Acta*. 44, 1955-1965.

Aller, R.C. 1982. The effects of macrobenthos on chemical properties of marine sediment and overlying water. In *Animal-sediment relations*; McCall, P.L., Tevesz, M.J.S., Eds.; Plenum Press: New York.

Aller, R.C. 2001. Transport and Reactions in the Bioirrigated Zone. In *The Benthic Boundary Layer, Transport Processes and Biogeochemistry*; Boudreau, B.P., Jørgensen, B.B., Eds.; Oxford University Press, Inc.: New York, pp 269-301.

Aller, R.C.; Aller, J.Y. 1992. Meiofauna and solute transport in marine muds. *Limnology and Oceanography*. 37, 1018-1033.

Aller, R.C.; Aller, J.Y. 1998. The effect of biogenic irrigation intensity and solute exchange on diagenetic reaction rates in marine sediments. *Journal of Marine Research*. 56, 905-936.

Aller, R.C.; Yingst, J.Y. 1978. Biogeochemistry of tube-dwellings: A study of the sedentary polychaete *Amphitrite ornata* (Leidy). *Journal of Marine Research*. 36, 201-254.

Aller, R.C.; Yingst, J.Y. 1985. Effects of the Marine Deposit-feeders *Heteromastus filiformis* (Polychaeta), *Macoma Balthica* (Bivalvia), and *Tellina texana* (Bivalvia) on Averaged Sediment Solute Transport, Reaction Rates, and Microbial Distribution. *Journal of Marine Research*. 43, 615-645.

Apitz, S.E.; Davis, J.W.; Finkelstein, K.; Hohreiter, D.W.; Hoke, R.; Jensen, R.H.; Jersak, J.; Kirtay, V.J.; Mack, E.E.; Magar, V.S.; Reible, D.D.; Stahl, R.G. 2005. Assessing and Managing Contaminated Sediments: Part II, Evaluating Risk and Monitoring Sediment Remedy Effectiveness. *Integrated Environmental Assessment and Management*. 1, 1-14.

Argent, R.M. 2004. An overview of model integration for environmental applications--components, frameworks and semantics. *Environmental Modelling & Software*. 19, 219-234.

Assinder, D.J.; Mudge, S.M.; Bourne, G.S. 1997. Radiological assessment of the ribble estuary--I. Distribution of radionuclides in surface sediments. *Journal of Environmental Radioactivity*. 36, 1-19.

az-Cruz, M.S.; Lopez de Alda, M.J.; Barcelo, D. 2003. Environmental behavior and analysis of veterinary and human drugs in soils, sediments and sludge. *TrAC Trends in Analytical Chemistry*. 22, 340-351.

- Bachmat, Y.; Bear, J. 1986. Macroscopic modelling of transport phenomena in porous media. 1: The continuum approach. *Transport in Porous Media*. 1, 213-240.
- Bahr, J.M. 1989. Analysis of nonequilibrium desorption of volatile organics during field test of aquifer decontamination. *Journal of Contaminant Hydrology*. 4, 205-222.
- Balci, O. Principles and techniques of simulation validation, verification, and testing. In *Proceedings of 1995 Winter Simulation Conference*; Alexopoulos, C.; Kang, K.; Lilegdon, W. R.; and Goldsman, D., Eds. December 3, 1995, pp 147-154.
- Ball, W.P.; Roberts, P.V. 1991. Long-term sorption of halogenated organic chemicals by aquifer material. 2. Intraparticle diffusion. *Environmental Science and Technology*. 25, 1237-1249.
- Barcelo, D.; Petrovic, M. 2007. *Sediment Quality and Impact Assessment of Pollutants*. Elsevier:
- Barnthouse, L.W.; Glaser, D.; Young, J. 2003. Effects of Historic PCB Exposures on the Reproductive Success of the Hudson River Striped Bass Population. *Environmental Science and Technology*. 37, 223-228.
- Bear, J. 1972. *Dynamics of Fluids in Porous Media*. Elsevier: New York.
- Bear, J.; Bachmat, Y. 1986. Macroscopic modelling of transport phenomena in porous media. 2: Applications to mass, momentum and energy transport. *Transport in Porous Media*. 1, 241-269.
- Bekhit, H.M.; Hassan, A.E. 2005. Two-dimensional modeling of contaminant transport in porous media in the presence of colloids. *Advances in Water Resources*. 28, 1320-1335.
- Benjamin, J.R.; Cornell, C.A. 1970. *Probability, Statistics, and Decisions for Civil Engineers*. McGraw-Hill: New York.
- Berens, A.R. 1978. Analysis of transport behavior in polymer powders. *Journal of Membrane Science*. 3, 247-264.
- Berner, R.A. 1980. *Early Diagenesis: A Theoretical Approach*. Princeton University Press: Princeton.
- Berner, R.A. 1964. An idealized model of dissolved sulfate distribution in recent sediments. *Geochimica et Cosmochimica Acta*. 28, 1497-1503.
- Bhosle, N.B.; Garg, A.; Jadhav, S.; Harjee, R.; Sawant, S.S.; Venkat, K.; Anil, A.C. 2004. Butyltins in water, biofilm, animals and sediments of the west coast of India. *Chemosphere*. 57, 897-907.
- Bian, L. 2007. Object-Oriented Representation of Environmental Phenomena: Is Everything Best Represented as an Object? *Annals of the Association of American Geographers*. 97, 267-281.
- Blumer, M. 1976. Polycyclic aromatic hydrocarbons in nature. *Scientific American*. 234, 34-45.

- Boeije, G.M.; Schowanek, D.R.; Vanrolleghem, P.A. 2000. Incorporation of biofilm activity in river biodegradation modeling: a case study for linear alkylbenzene sulphonate (LAS). *Water Research*. 34, 1479-1486.
- Boisvert, R.F.; Moreira, J.; Philippsen, M.; Pozo, R. 2001. Java and numerical computing. *Computing in Science & Engineering*. 3, 18-24.
- Bornhold, B.D.; Prior, D.B. 1989. Sediment Blocks on the Sea Floor in British Columbia Fjords. *Geo-Marine Letters*. 9, 135-144.
- Bornick, H.; Eppinger, P.; Grischek, T.; Worch, E. 2001. Simulation of Biological Degradation of Aromatic Amines in River Bed Sediments. *Water Research*. 35, 619-624.
- Bosma, T.N.P.; Middeldorp, P.J.M.; Schraa, G.; Zehnder, A.J.B. 1997. Mass Transfer Limitation of Biotransformation: Quantifying Bioavailability. *Environmental Science and Technology*. 31, 248-252.
- Bossert, I.D.; Bartha, R. 1986. Structure-biodegradability relationships of polycyclic aromatic hydrocarbons in soil. *Bulletin of Environmental Contamination and Toxicology*. 37, 490-495.
- Bouchard, D.C.; Wood, A.L.; Campbell, M.L.; Nkedi-Kizza, P.; Rao, P.S.C. 1988. Sorption nonequilibrium during solute transport. *Journal of Contaminant Hydrology*. 2, 209-223.
- Boudreau, B.P. 1984. On the equivalence of nonlocal and radial-diffusion models for porewater irrigation. *Journal of Marine Research*. 42, 731-735.
- Boudreau, B.P. 1986a. Mathematics of tracer mixing in sediments. 1. Spatially-dependent diffusive mixing. *American Journal of Science*. 286, 161-198.
- Boudreau, B.P. 1986b. Mathematics of tracer mixing in sediments. 2. Nonlocal mixing and biological conveyor-belt phenomena. *American Journal of Science*. 286, 199-238.
- Boudreau, B.P. 1997. *Diagenetic Models and their Implementation*. Springer: Berlin.
- Boudreau, B.P.; Bennett, R.H. 1999. New Rheological and Porosity Equations for Steady-state Compaction. *American Journal of Science*. 299, 517-528.
- Boudreau, B.P.; Imboden, D.M. 1987. Mathematics of tracer mixing in sediments. 3. The theory of nonlocal mixing within sediments. *American Journal of Science*. 287, 693-719.
- Boudreau, B.P.; Westrich, J.T. 1984. The dependence of bacterial sulfate reduction on sulfate concentration in marine sediments. *Geochimica et Cosmochimica Acta*. 48, 2503-2516.
- Boudreau, B.P. 1996a. A method-of-lines code for carbon and nutrient diagenesis in aquatic sediments. *Computers & Geosciences*. 22, 479-496.

- Boudreau, B.P. 1996b. The diffusive tortuosity of fine-grained unlithified sediments. *Geochimica et Cosmochimica Acta*. 60, 3139-3142.
- Boudreau, B.P. 1997b. A one-dimensional model for bed-boundary layer particle exchange. *Journal of Marine System*. 11, 279-303.
- Bradley, P.M.; Chapelle, F.H.; Landmeyer, J.E. 2001. Effect of redox conditions on MTBE biodegradation in surface water sediments. *Environmental Science and Technology*. 35, 4643-4647.
- Braida, W.J.; Pignatello, J.J.; Lu, Y.; Ravikovitch, P.I.; Neimark, A.V.; Xing, B. 2003. Sorption Hysteresis of Benzene in Charcoal Particles. *Environmental Science and Technology*. 37, 409-417.
- Brenner, R.C.; Magar, V.S.; Ickes, J.A.; Abbott, J.E.; Stout, S.A.; Crecelius, E.A.; Bingler, L.S. 2002. Characterization and FATE of PAH-Contaminated Sediments at the Wyckoff/Eagle Harbor Superfund Site. *Environmental Science and Technology*. 36, 2605-2613.
- Brenner, R.C.; Magar, V.S.; Ickes, J.A.; Foote, E.A.; Abbott, J.E.; Bingler, L.S.; Crecelius, E.A. 2004. Long-Term Recovery of PCB-Contaminated Surface Sediments at the Sangamo-Weston/Twelvemile Creek/Lake Hartwell Superfund Site. *Environmental Science and Technology*. 38, 2328-2337.
- Brusseau, M.L.; Jessup, R.E.; Rao, S.C. 1991. Nonequilibrium Sorption of Organic Chemicals: Elucidation of Rate-Limiting Processes. *Environmental Science and Technology*. 25, 134-142.
- Byrne, G.D.; Hindmarsh, A.C. 1987. Stiff ODE solvers: A review of current and coming attractions. *Journal of Computational Physics*. 70, 1-62.
- Calmano, W.; Ahlf, W.; Forstner, U. 1996. Sediment quality assessment: chemical and biological approaches. In *Sediments and Toxic Substances: Environmental Effects and Toxicity*; Calmano, W., Forstner, U., Eds.; Springer: Germany, pp 1-29.
- Calvillo, Y.M.; Alexander, M. 1996. Mechanism of microbial utilization of biphenyl sorbed to polyacrylic beads. *Applied Microbiology and Biotechnology*. 45, 383-390.
- Carlsson, C.; Johansson, A.K.; Alvan, G.; Bergman, K.; Kuhler, T. 2006. Are pharmaceuticals potent environmental pollutants?: Part II: Environmental risk assessments of selected pharmaceutical excipients. *Science of The Total Environment*. 364, 88-95.
- Carmo, A.M.; Hundal, L.S.; Thompson, M.L. 2000. Sorption of Hydrophobic Organic Compounds by Soil Materials: Application of Unit Equivalent Freundlich Coefficients. *Environmental Science and Technology*. 34, 4363-4369.
- Caromel, D.; Klauser, W.; Vayssière, J. 1998. Towards seamless computing and metacomputing in Java. *Concurrency: Practice and Experience*. 10, 1043-1064.
- Carroll, K.M.; Harkness, M.R.; Bracco, A.A.; Balcarcel, R.R. 1994. Application of a permeant/polymer diffusional model to the desorption of polychlorinated biphenyls from Hudson River sediments. *Environmental Science and Technology*. 28, 253-258.

- Carslaw, H.S.; Jaeger, J.C. 1959. *Conduction of Heat in Solids*. Clarendon Press: Oxford.
- Chandra, S.S.; Chandra, K. 2005. A comparison of Java and C#. *Journal of Computing Science in College*. 20, 238-254.
- Chang, P.; Wilke, C.R. 1955. Some Measurements of Diffusion in Liquids. *Journal of Physical Chemistry*. 59, 592-596.
- Chapman, P.M.; Wang, F. 2001. Assessing sediment contamination in estuaries. *Environmental Toxicology and Chemistry*. 20, 3-22.
- Charlesworth, S.M.; Foster, I.D.L. 1999. Sediment budgets and metal fluxes in two contrasting urban lake catchments in Coventry, UK. *Applied Geography*. 19, 199-210.
- Cheng, H.C.; Fen, C.S. 2006. A web-based distributed problem-solving environment for engineering applications. *Advances in Engineering Software*. 37, 112-128.
- Chiou, C.T.; Kile, D.E. 1998. Deviations from Sorption Linearity on Soils of Polar and Nonpolar Organic Compounds at Low Relative Concentrations. *Environmental Science and Technology*. 32, 338-343.
- Chiou, C.T.; Kile, D.E.; Rutherford, D.W.; Sheng, G.; Boyd, S.A. 2000. Sorption of Selected Organic Compounds from Water to a Peat Soil and Its Humic-Acid and Humin Fractions: Potential Sources of the Sorption Nonlinearity. *Environmental Science and Technology*. 34, 1254-1258.
- Chiou, C.T.; McGroddy, S.E.; Kile, D.E. 1998. Partition Characteristics of Polycyclic Aromatic Hydrocarbons on Soils and Sediments. *Environmental Science and Technology*. 32, 264-269.
- Chiou, C.T.; Peters, L.J.; Freed, V.H. 1979. A physical concept of soil-water equilibria for non-ionic organic compounds. *Science*. 206, 831-832.
- Chiou, C.T.; Malcolm, R.L.; Brinton, T.I.; Kile, D.E. 1986. Water solubility enhancement of some organic pollutants and pesticides by dissolved humic and fulvic acids. *Environmental Science and Technology*. 20, 502-508.
- Choi, J.; Francois-Carcaillet, F.; Boudreau, B.P. 2002. Lattice-automaton bioturbation simulator (LABS): implementation for small deposit feeders. *Computers & Geosciences*. 28, 213-222.
- Choy, B.; Reible, D.D. 2000. *Diffusion Models of Environmental Transport*. CRC Press LLC: Boca Raton, Florida.
- Cichota, R.; Elias, E.A.; de Jong van Lier, Q. 2004. Testing a finite-difference model for soil heat transfer by comparing numerical and analytical solutions. *Environmental Modelling & Software*. 19, 495-506.
- Cierniak, M.; Li, W. 1997. Optimizing Java bytecodes. *Concurrency: Practice and Experience*. 9, 427-444.

- Cooley, R. 1979. A method of estimating parameters and assessing reliability for models of steady state groundwater flow, 2: application of statistical analysis. *Water Resources Research*. 15, 603-617.
- Cornelissen, G.; Gustafsson, Ö. 2005. Importance of Unburned Coal Carbon, Black Carbon, and Amorphous Organic Carbon to Phenanthrene Sorption in Sediments. *Environmental Science and Technology*. 39, 764-769.
- Cornelissen, G.; Gustafsson, O.; Bucheli, T.D.; Jonker, M.T.O.; Koelmans, A.A.; vanNoort, P.C.M. 2005. Extensive Sorption of Organic Compounds to Black Carbon, Coal, and Kerogen in Sediments and Soils: Mechanisms and Consequences for Distribution, Bioaccumulation, and Biodegradation. *Environmental Science and Technology*. 39, 6881-6895.
- Crank, J. 1975. *The Mathematics of Diffusion*. Clarendon Press: Oxford, England.
- Cretney, W.J.; Wong, C.S.; MacDonald, R.W.; Erickson, P.E.; Fowler, B.R. Polycyclic aromatic hydrocarbons in surface sediments and age-dated cores from Kitimat Arm, Douglas Channel and adjoining waterways. In *Proceedings of a Workshop on the Kitimat Marine Environment, Canadian Technical Reports in Hydrography and Ocean Science*; MacDonald, R. W., Eds. 1983, pp 162-195.
- Crittenden, J.C.; Sanongraj, S.; Bulloch, J.L.; Hand, D.W.; Rogers, T.N.; Speth, T.F.; Ulmer, M. 1999. Correlation of Aqueous-Phase Adsorption Isotherms. *Environmental Science and Technology*. 33, 2926-2933.
- Cunningham B.P. 2002. Influence of tubificid oligochaetes on the fate of pyrene in contaminated sediment. *PhD Thesis*. Louisiana State University, Baton Rouge, Louisiana, USA.
- Cunningham, V.L.; Buzby, M.; Hutchinson, T.H.; Mastrocco, F.; Parke, N.; Roden, N. 2006. Effects of Human Pharmaceuticals on Aquatic Life: Next Steps. *Environmental Science and Technology*. 40, 3456-3462.
- Danckwerts, P.V. 1950. Absorption by simultaneous diffusion and chemical reaction. *Transaction of the Faraday Society*. 46, 300-304.
- Daniels, W.M.; House, W.A.; Zhmud, B.V.; Rae, J.E.; Parker, A. 1998. Diffusive movement of simazine and lindane in river-bed sediments. *Pest Management Science*. 54, 212-222.
- Darcy, H. 1856. *Les Publiques de la Ville de Dijon*. Dalmont, Paris.
- Davey, M.E.; O'toole, G.A. 2000. Microbial Biofilms: from Ecology to Molecular Genetics. *Microbiology and Molecular Biology Reviews*. 64, 847-867.
- de Beer, D.; Kuhl, M. 2001. Interfacial microbial mats and biofilms. In *The Benthic Boundary Layer, Transport Processes and Biogeochemistry*; Boudreau, B.P., Jørgensen, B.B., Eds.; Oxford University Press, Inc.: New York, pp 374-394.
- de Beer, D.; Stoodley, P.; Lewandowski, Z. 1994a. Liquid flow in heterogeneous biofilms. *Biotechnology and Bioengineering*. 44, 636-641.

- de Beer, D.; Stoodley, P.; Roe, F.; Lewandowski, Z. 1994b. Effects of biofilm structures on oxygen distribution and mass transport. *Biotechnology and Bioengineering*. 43, 1131-1138.
- de Brouwer, J.F.C.; Ruddy, G.K.; Jones, T.E.R.; Stal, L.J. 2002. Sorption of EPS to sediment particles and the effect on the rheology of sediment slurries. *Biogeochemistry*. 61, 57-71.
- Decho, A.W. 1990. Microbial exopolymer secretions in ocean environments: Their role(s) in food webs and marine processes. *Oceanography & Marine Biology Annual Reviews*. 28, 73-154.
- Devlin, M.; Best, M.; Haynes, D. 2007. Implementation of the Water Framework Directive in European marine waters. *Marine Pollution Bulletin*. 55, 1-2.
- Devol, A.H.; Christensen, J.P. 1993. Benthic fluxes and nitrogen cycling in sediments of the continental margin of the eastern North Pacific. *Journal of Marine Research*. 51, 345-372.
- Domenico, P.A.; Palciauskas, V.V. 1979. The volume-averaged mass-transport equation for chemical diagenetic models. *Journal of Hydrology*. 43, 427-438.
- Dowson, P.H.; Bubb, J.M.; Lester, J.N. 1996. Persistence and Degradation Pathways of Tributyltin in Freshwater and Estuarine Sediments. *Estuarine, Coastal and Shelf Science*. 42, 551-562.
- Dunnivant, F.M.; Polansky, A.L.; Elzerman, A.W. 1989. Persistence and distribution of PCBs in the sediments of a reservoir (Lake Hartwell, South Carolina). *Bulletin of Environmental Contamination and Toxicology*. 43, 870-878.
- Edgar, P.J.; Hursthouse, A.S.; Matthews, J.E.; Davies, I.M. 2003. An investigation of geochemical factors controlling the distribution of PCBs in intertidal sediments at a contamination hot spot, the Clyde Estuary, UK. *Applied Geochemistry*. 18, 327-338.
- Eggleton, J.; Thomas, K.V. 2004. A review of factors affecting the release and bioavailability of contaminants during sediment disturbance events. *Environment International*. 30, 973-980.
- Ehlers, L.J.; Luthy, R.G. 2003. Contaminant bioavailability in soil and sediment. *Environmental Science and Technology*. 37, 295A-302A.
- Emerson, S.; Jahnke, R.; Heggie, D. 1984. Sediment-Water Exchange in Shallow-Water Estuarine Sediments. *Journal of Marine Research*. 42, 709-730.
- Environmental Agency. 2001a. Environment Agency Framework for Groundwater Resources Modelling R&D Technical Report W214.
- Environmental Agency. 2001b. Guidance on Assigning Values to Uncertain Parameters in Subsurface Analytical Contaminant Fate and Transport Models NGWCLC Report No. NC/99/38/3.
- Environmental Agency Wales. 2004. Human Pharmaceuticals and their Impact on the Aquatic Environment.

- Erickson, M.J.; Turner, C.L.; Thibodeaux, L.J. 2005. Field Observation and Modeling of Dissolved Fraction Sediment-Water Exchange Coefficients for PCBs in the Hudson River. *Environmental Science and Technology*. 39, 549-556.
- European Center for Ecotoxicology and Toxicology of Chemicals (ECETOC). 2002. Scientific principles of soil hazard assessment of substances Technical Report No. 84.
- Ewald, G.; Berglund, O.; Svensson, J.M. 1997. Effect of Oligochaete Bioturbation on Sediment Accumulation of 2,2',4,4'-Tetrachlorobiphenyl. *Ecotoxicology and Environmental Safety*. 36, 66-71.
- Faraj, I.; Alshawi, M.; Aouad, G.; Child, T.; Underwood, J. 1999. Distributed Object Environment: Using International Standards for Data Exchange in the Construction Industry. *Computer-Aided Civil and Infrastructure Engineering*. 14, 395-405.
- Farley, K.J.; Germann, G.G.; Elzerman, A.W. 1994. Differential weathering of PCB congeners in Lake Hartwell, South Carolina. In *Environmental Chemistry of Lakes and Reservoirs*; Baker, L.A., Ed.; American Chemical Society: Washington, DC, pp 575-600.
- Farrell, J.; Reinhard, M. 1994. Desorption of halogenated organics from model solids, sediments, and soil under unsaturated conditions. 2. Kinetics. *Environmental Science and Technology*. 28, 63-72.
- Fasani, E.; Mella, M.; Monti, S.; Albini, A. 2001. Unexpected photoreactions of some 7-amino-6-fluoroquinolones in phosphate buffer. *European Journal of Organic Chemistry*. 2, 391-397.
- Fenner, K.; Scheringer, M.; MacLeod, M.; Matthies, M.; McKone, T.; Stroebe, M.; Beyer, A.; Bonnell, M.; LeGall, A.C.; Klasmeier, J.; Mackay, D.; vandeMeent, D.; Pennington, D.; Scharenberg, B.; Suzuki, N.; Wania, F. 2005. Comparing Estimates of Persistence and Long-Range Transport Potential among Multimedia Models. *Environmental Science and Technology*. 39, 1932-1942.
- Filippi, J.B.; Bisgambiglia, P. 2004. JDEVS: an implementation of a DEVS based formal framework for environmental modelling. *Environmental Modelling & Software*. 19, 261-274.
- Fisher, J.B.; Lick, W.J.; McCall, P.L.; Robbins, J.A. 1980. Vertical Mixing of Lake-Sediments by Tubificid Oligochaetes. *Journal of Geophysical Research-Oceans and Atmospheres*. 85, 3997-4006.
- Fleming, L.E.; Broad, K.; Clement, A.; Dewailly, E.; Elmir, S.; Knap, A.; Pomponi, S.A.; Smith, S.; Solo Gabriele, H.; Walsh, P. 2006. Oceans and human health: Emerging public health risks in the marine environment. *Marine Pollution Bulletin*. 53, 545-560.
- Flemming, H.C. 1995. Sorption sites in biofilms. *Water Science and Technology*. 32, 27-33.
- Forster, S.; Graf, G.; Kitlar, J.; Powilleit, M. 1995. Effects of bioturbation in oxic and hypoxic conditions: a microcosm experiment with a North Sea sediment community. *Marine Ecology Progress Series*. 116, 153-161.

- Foster, D.L.; Charlesworth, S.M.; Keen, D.H. 1991. A comparative study of heavy metal contamination and pollution in four reservoirs in the English Midlands, UK. *Hydrobiologia*. V214, 155-162.
- Francois, F.; Poggiale, J.C.; Durbec, J.P.; Stora, G. 1997. A New Approach for the Modelling of Sediment Reworking Induced by a Macrobenthic Community. *Acta Biotheoretica*. 45, 295-319.
- Francois, F.; Poggiale, J.C.; Durbec, J.P.; Stora, G. 2001. A new model of bioturbation for a functional approach to sediment reworking resulting from macrobenthic communities. In *Organism-Sediment Interactions*; Aller, J.Y., Woodin, S.A., Aller, R.C., Eds.; University of South Carolina Press: pp 75-88.
- Friedrich, J.; Karslioglu, M.O. 2003. Updating Fortran programs and other legacy code to an interactive window platform. *Computers & Geosciences*. 29, 1091-1100.
- Galle, T.; Gregoire, C.; Wagner, M.; Bierl, R. 2005. Bioavailability of HOC depending on the colloidal state of humic substances: A case study with PCB-77 and *Daphnia magna*. *Chemosphere*. 61, 2, 282-292.
- Gardiner, C.W. 1985. *Handbook of Stochastic Methods for Physics, Chemistry and Natural Sciences*. Springer-Verlag: Berlin Heidelberg.
- Glud, R.N.; Fenchel, T. 1999. The Importance of Ciliates for Interstitial Solute Transport in Benthic Communities. *Marine Ecology Progress Series*. 186, 93.
- Go, J.; Stegemann, J.A.; Allan, I.J.; Graham, R. Modelling and simulation framework for reactive transport of organic contaminants in bed-sediments using a pure Java object-oriented paradigm. In *9th International Conference on Computer Modelling and Simulation*; Al-Begain, K.; Orsoni, A.; and Al-Dabass, D., Eds. United Kingdom Simulation Society, Oriel College, Oxford, April 4, 2006, pp 102-108.
- Goldberg, E.D.; Koide, M. 1962. Geochronological studies of deep-sea sediments by the Io/Th method. *Geochimica et Cosmochimica Acta*. 26, 417-450.
- Golding, C.J.; Smernik, R.J.; Birch, G.F. 2005. Investigation of the Role of Structural Domains Identified in Sedimentary Organic Matter in the Sorption of Hydrophobic Organic Compounds. *Environmental Science and Technology*. 39, 3925-3932.
- Gonzales, J.J.; Magrans, J.O.; Alonso-Prados, J.L.; Garcia-Baudin, J.M. 2001. An analytically solved kinetic model for pesticide degradation in single compartment systems. *Chemosphere*. 44, 765-770.
- Grathwohl, P. 1990. Influence of organic matter from soils and sediments from various origins on the sorption of some chlorinated aliphatic hydrocarbons: implications on Koc correlations. *Environmental Science and Technology*. 24, 1687-1693.
- Gu, W.; Burns, N.; Collins, M.; Wong, W. 2000. The evolution of a high-performing Java virtual machine. *IBM Systems Journal*. 39, 135-150.

- Gueguen, C.; Dominik, J. 2003. Partitioning of trace metals between particulate, colloidal and truly dissolved fractions in a polluted river: the Upper Vistula River (Poland). *Applied Geochemistry*. 18, 457-470.
- Guinasso, N.L.; Schink, D.R. 1975. Quantitative estimates of biological mixing rates in abyssal sediments. *Journal of Geophysical Research - Oceans and Atmospheres*. 88, 7617-7622.
- Gustafsson, Ö.; Gschwend, P.M. 1998. The flux of black carbon to surface sediments on the New England continental shelf. *Geochimica et Cosmochimica Acta*. 62, 465-472.
- Haack, S.K.; Bekins, B.A. 2000. Microbial populations in contaminant plumes. *Hydrogeology Journal*. 8, 63-76.
- Hammond, D.E.; Fuller, C.; Harmon, D.; Hartman, B.; Korosec, M.; Miller, L.G.; Rea, R.; Warren, S.; Berelson, W.; Hager, S.W. 1985. Benthic fluxes in San Francisco Bay. *Hydrobiologia (Historical Archive)*. 129, 69-90.
- Harino, H.; O'Hara, S.C.M.; Burt, G.R.; Chesman, B.S.; Pope, N.D.; Langston, W.J. 2003. Organotin compounds in Mersey and Thames Estuaries a decade after UK TBT legislation. *Journal of Marine Biological Association UK*. 83, 11-22.
- Harper, M.P.; Davison, W.; Tych, W. 1999. One-Dimensional Views of Three-Dimensional Sediments. *Environmental Science and Technology*. 33, 2611-2616.
- Harrad, S.J.; Sewart, A.P.; Alcock, R.; Boumphrey, R.; Burnett, V.; Duarte-Davidson, R.; Halsall, C.; Sanders, G.; Waterhouse, K.; Wild, S.R.; Jones, K.C. 1994. Polychlorinated biphenyls (PCBs) in the British environment: Sinks, sources and temporal trends. *Environmental Pollution*. 85, 131-146.
- Hassanizadeh, M.; Gray, W.G. 1979. General conservation equations for multi-phase systems: 2. Mass, momenta, energy, and entropy equations. *Advances in Water Resources*. 2, 191-203.
- Hassanizadeh, S.M.; Gray, W.G. 1989a. Boundary and interface conditions in porous media. *Water Resources Research*. 25, 1705-1715.
- Hassanizadeh, S.M.; Gray, W.G. 1989b. Derivations of conditions describing transport across zones of reduced dynamics within multiphase systems. *Water Resources Research*. 25, 529-539.
- Hay M. 2005. Reconstitution des conditions océanographiques et climatiques de l'holocène supérieur à Effingham Inlet, Île de Vancouver, Colombie-Britannique. *PhD Thesis*. Université Laval, Vancouver, Canada.
- Hayduk, W.; Laurie, H. 1974. Prediction of diffusion coefficients for nonelectrolytes in dilute aqueous solutions. *American Institute of Chemical Engineering Journal*. 20, 611-615.
- Headley, J.V.; Gandrass, J.; Kuballa, J.; Peru, K.M.; Gong, Y. 1998. Rates of Sorption and Partitioning of Contaminants in River Biofilm. *Environmental Science and Technology*. 32, 3968-3973.

- Helsgaun, K. 2001. jDisco - a Java framework for combined discrete and continuous simulation. *DATALOGISKE SKRIFTER (Writings on Computer Science)*, Roskilde University - *unpublished*.
- Hernando, M.D.; Mezcuca, M.; Fernandez-Alba, A.R.; Barcelo, D. 2006. Environmental risk assessment of pharmaceutical residues in wastewater effluents, surface waters and sediments. *Talanta*. *69*, 334-342.
- Hites, R.A.; LAFLAMME, R.E.; Farrington, J.W. 1977. Sedimentary Polycyclic Aromatic Hydrocarbons: The Historical Record. *Science*. *198*, 829-831.
- Holthaus, K.I.E.; Johnson, A.C.; Jurgens, M.D.; Williams, R.J.; Smith, J.J.L.; Carter, J.E. 2002. The potential for estradiol and ethinylestradiol to sorb to suspended and bed sediments in some english rivers. *Environmental Toxicology and Chemistry*. *21*, 2526-2535.
- Hornsby, A.G.; Wauchope, R.D.; Herner, A.E. 1995. *Pesticide Properties in the Environment*. Springer: New York.
- Huang, W.; Peng, P.; Yu, Z.; Fu, J. 2003. Effects of organic matter heterogeneity on sorption and desorption of organic contaminants by soils and sediments. *Applied Geochemistry*. *18*, 955-972.
- Huang, W.; Weber Jr., W.J. 1997. A Distributed Reactivity Model for Sorption by Soils and Sediments. 10. Relationships between Desorption, Hysteresis, and the Chemical Characteristics of Organic Domains. *Environmental Science and Technology*. *31*, 2562-2569.
- Huang, W.; Weber Jr., W.J. 1998. A Distributed Reactivity Model for Sorption by Soils and Sediments. 11. Slow Concentration-Dependent Sorption Rates. *Environmental Science and Technology*. *32*, 3549-3555.
- Hudson-Edwards, K.; Macklin, M.; Taylor, M. 1997. Historic metal mining inputs to Tees river sediment. *Science of The Total Environment*. *194-195*, 437-445.
- Huettel, M.; Webster, I.T. 2001. Porewater Flow in Permeable Sediments. In *The Benthic Boundary Layer, Transport Processes and Biogeochemistry*; Boudreau, B.P., Jørgensen, B.B., Eds.; Oxford University Press, Inc.: New York, pp 144-179.
- Huettel, M.; Ziebis, W.; Forster, S.; Luther III, G.W. 1998. Advective Transport Affecting Metal and Nutrient Distributions and Interfacial Fluxes in Permeable Sediments. *Geochimica et Cosmochimica Acta*. *62*, 613-631.
- Huettel, M.; Roy, H.; Precht, E.; Ehrenhauss, S. 2003. Hydrodynamical impact on biogeochemical processes in aquatic sediments. *Hydrobiologia*. *494*, 231-236.
- Hylland, K. 2006. Biological effects in the management of chemicals in the marine environment. *Marine Pollution Bulletin*. *53*, 614-619.
- Hyun, S.; Jafvert, C.; Lee, L.; Rao, P. 2006. Laboratory studies to characterize the efficacy of sand capping a coal tar-contaminated sediment. *Chemosphere*. *63*, 1621-1631.

Imai, R.; Nagata, Y.; Fukuda, M.; Takagi, M.; Yano, K. 1991. Molecular cloning of a *Pseudomonas paucimobilis* gene encoding a 17-kilodalton polypeptide that eliminates HCl molecules from gamma-hexachlorocyclohexane. *The Journal of Bacteriology*. 173, 6811-6819.

International Agency for Research on Cancer (IARC). *Monographs on the evaluation of carcinogenic risks to humans: some traditional herbal medicines, some mycotoxins, naphthalene and styrene*. 2002.

Jennifer, M.B.; John, N.L. 1994. Anthropogenic heavy metal inputs to lowland river systems, a case study. The River Stour, U.K. *Water, Air, & Soil Pollution*. V78, 279-296.

Johnson, A.C.; White, C.; Besien, T.J.; Jurgens, M.D. 1998. The sorption potential of octylphenol, a xenobiotic oestrogen, to suspended and bed-sediments collected from industrial and rural reaches of three English rivers. *Science of The Total Environment*. 210-211, 271-282.

Jones, K.C.; Duarte-Davidson, R.; Cawse, P.A. 1995. Changes in the PCB Concentration of United Kingdom air between 1972 and 1992. *Environmental Science and Technology*. 29, 272-275.

Jonkers, N.; Laane, R.W.P.M.; de Graaf, C.; de Voogt, P. 2005. Fate modeling of nonylphenol ethoxylates and their metabolites in the Dutch Scheldt and Rhine estuaries: validation with new field data. *Estuarine, Coastal and Shelf Science*. 62, 141-160.

Jönsson, A.; Carman, R. 2000. Distribution of PCBs in Sediment from Different Bottom Types and Water Depths in Stockholm Archipelago, Baltic Sea. *AMBIO: A Journal of the Human Environment*. 29, 277-281.

Jørgensen, B.B.; Boudreau, B.P. 2001. Diagenesis and sediment-water exchange. In *The Benthic Boundary Layer, Transport Processes and Biogeochemistry*; Boudreau, B.P., Jørgensen, B.B., Eds.; Oxford University Press, Inc.: New York, pp 211-244.

Kalsch, W.; Knacker, T.; Robertz, M.; Studinger, G.; Franke, C. 1998. Partitioning and mineralization of [C14] Lindane in laboratory sediment-water system. *Environmental Toxicology and Chemistry*. 17, 662-669.

Karapanagioti, H.K.; Kleinedam, S.E.; Sabatini, D.A.; Grathwohl, P.; Ligouis, B.D. 2000. Impacts of Heterogeneous Organic Matter on Phenanthrene Sorption: Equilibrium and Kinetic Studies with Aquifer Material. *Environmental Science and Technology*. 34, 406-414.

Karickhoff, S.W.; Brown, O.S.; Scott, T.H. 1979. Sorption of hydrophobic pollutants on natural sediments. *Water Research*. 13, 241-248.

Kenaga, E.E.; Goring, C.A.I. 1980. Relationship between water solubility, soil sorption, octanol-water partitioning, and concentration of chemicals in biota. In *Aquatic Toxicology*; Parrish, P.R., Hendricks, A.C., Eds.; ASTM: Philadelphia, PA, pp 78-115.

- Kim, H.S.; Weber Jr., W.J. 2003. Preferential Surfactant Utilization by a PAH-Degrading Strain: Effects on Micellar Solubilization Phenomena. *Environmental Science and Technology*. 37, 3574-3580.
- King, A.J.; Readman, J.W.; Zhou, J.L. 2004. Dynamic behaviour of polycyclic aromatic hydrocarbons in Brighton marina, UK. *Marine Pollution Bulletin*. 48, 229-239.
- Kleineidam, S.E.; Rogner, K.N.; Ligouis, B.D.; Grathwohl, P. 1999. Organic Matter Facies and Equilibrium Sorption of Phenanthrene. *Environmental Science and Technology*. 33, 1637-1644.
- Kleineidam, S.E.; Schüth, C.; Grathwohl, P. 2002. Solubility-Normalized Combined Adsorption-Partitioning Sorption Isotherms for Organic Pollutants. *Environmental Science and Technology*. 36, 4689-4697.
- Klupinski, T.P.; Chin, Y.-P.; Traina, S.J. 2004. Abiotic Degradation of Pentachloronitrobenzene by Fe(II): Reactions on Goethite and Iron Oxide Nanoparticles. *Environmental Science and Technology*. 38, 4353-4360.
- Ko, F.C.; Baker, J.E. 1995. Partitioning of hydrophobic organic contaminants to resuspended sediments and plankton in the mesohaline Chesapeake Bay. *Marine Chemistry*. 49, 171-188.
- Koelmans, A.A.; Hubert, E.; Koopman, H.W.; Portelje, R.; Crum, S.J.H. 2000. Modeling the vertical distribution of carbendazim in sediments. *Environmental Toxicology and Chemistry*. 19, 793-800.
- Kokkonen, T.; Jolma, A.; Koivusalo, H. 2003. Interfacing environmental simulation models and databases using XML. *Environmental Modelling & Software*. 18, 463-471.
- Koretsky, C.M.; Meile, C.; Van Cappellen, P. 2002. Quantifying bioirrigation using ecological parameters: a stochastic approach. *Geochemical Transactions*. 3, 17-30.
- Krebs, C.T.; Burns, K.A. 1977. Long-term effects of an oil spill on populations of the salt-marsh crab *Uca pugnax*. *Science*. 197, 484-487.
- Kreft, A. 1981. On the boundary conditions of flow through porous media and conversion of chemical flow reactors. *Bulletin De L'Academie Polonaise Des Sciences-Serie Des Sciences Techniques*. 29, 521-529.
- Kuhrts, C.; Fennel, W.; Seifert, T. 2004. Model studies of transport of sedimentary material in the western Baltic. *Journal of Marine Systems*. 52, 167-190.
- Kujawinski, E.B.; Farrington, J.W.; Moffett, J.W. 2001. Marine protozoa produce organic matter with a high affinity for PCBs during grazing. *Environmental Science and Technology*. 35, 4060-4065.
- Kummerer, K. 2004. *Pharmaceuticals in the Environment. Sources, Fate, Effect and Risks*. Springer:
- la Penna, G.; Intrigila, B.; Laurenzi, A.R.; Orefice, S. 2006. An XML environment for scenario based requirements engineering. *Journal of Systems and Software*. 79, 379-403.

- Lampert, D.L.; Reible, D.D. Steady-state design model of concentrations and fluxes in a sediment cap. In *AIChE Annual Meeting*, San Francisco, California, November 12, 2006.
- Latimer, J.S.; Davis, W.R.; Keith, D.J. 1999. Mobilization of PAHs and PCBs from In-Place Contaminated Marine Sediments During Simulated Resuspension Events. *Estuarine, Coastal and Shelf Science*. 49, 577-595.
- Law, R.J.; Kelly, C.A.; Baker, K.L.; Langford, K.H.; Bartlett, T. 2002. Polycyclic aromatic hydrocarbons in sediments, mussels and crustacea around a former gasworks site in Shoreham-by-Sea, UK. *Marine Pollution Bulletin*. 44, 903-911.
- Lawrence, J.R.; Korber, D.R.; Hoyle, B.D.; Costerton, J.W.; Caldwell, D.E. 1991. Optical sectioning of microbial biofilms. *Journal of Bacteriology*. 173, 6558-6567.
- Leavesley, G.H.; Markstrom, S.L.; Brewer, M.S.; Viger, R.J. 1996. The modular modeling system (MMS) – The physical process modeling component of a database-centered decision support system for water and power management. *Water, Air, & Soil Pollution (Historical Archive)*. 90, 303-311.
- Leavesley, G.H.; Markstrom, S.L.; Restrepo, P.J.; Viger, R.J. 2002. A modular approach to addressing model design, scale, and parameter estimation issues in distributed hydrological modelling. *Hydrological Processes*. 16, 173-187.
- LeBas, G. *The Molecular Volumes of Liquid Chemical Compounds*. Monograph Longmans, Green: 1915.
- LeBouef, E.J.; Weber Jr., W.J. 1997. A Distributed Reactivity Model for Sorption by Soils and Sediments. 8. Sorbent Organic Domains: Discovery of a Humic Acid Glass Transition and an Argument for a Polymer-Based Model. *Environmental Science and Technology*. 31, 1697-1702.
- LeBouef, E.J.; Weber Jr., W.J. 2000a. Macromolecular Characteristics of Natural Organic Matter. 1. Insights from Glass Transition and Enthalpic Relaxation Behavior. *Environmental Science and Technology*. 34, 3623-3631.
- LeBouef, E.J.; Weber Jr., W.J. 2000b. Macromolecular Characteristics of Natural Organic Matter. 2. Sorption and Desorption Behavior. *Environmental Science and Technology*. 34, 3632-3640.
- Leenheer, J.A. 1991. Organic substance structure that facilitate contaminant transport and transformation in aquatic sediments. In *Organic substances in sediments and water, Vol. 1, Humics and soils*, Baker, R.A., Ed.; Lewis Publishers: Michigan.
- Legates, D.R.; McCabe Jr., G.J. 1999. Evaluating the use of "goodness-of-fit" measures in hydrologic and hydroclimatic model validation. *Water Resources Research*. 35, 233-242.
- Leij, F.J.; Genuchten, M.T. 1995. Approximate analytical solutions for solute transport in two-layer porous media. *Transport in Porous Media*. 18, 65-85.
- Li, J.; Carr, P.W. 1997. Accuracy of Empirical Correlations for Estimating Diffusion Coefficients in Aqueous Organic Mixtures. *Analytical Chemistry*. 69, 2530-2536.

- Li, S.-G.; Liu, Q. 2003. Interactive Groundwater (IGW): An innovative digital laboratory for groundwater education and research. *Computer Applications in Engineering Education*. 11, 179-202.
- Lick, W. 2006. The Sediment-Water Flux of HOCs Due to "Diffusion" or Is There a Well-Mixed Layer? If There Is, Does It Matter? *Environmental Science and Technology*. 40, 5610-5617.
- Lin, C.-H.M.; Pedersen, J.A.; Suffet, I.H. 2003. Influence of aeration on hydrophobic organic contaminant distribution and diffusive flux in estuarine sediments. *Environmental Science and Technology*. 37, 3547-3554.
- Liu, C.; Ball, W.P. 1998. Analytical modeling of diffusion-limited contamination and decontamination in a two-layer porous medium. *Advances in Water Resources*. 21, 297-313.
- Liu, C.; Ball, W.P.; Ellis, J.H. 1998. An Analytical Solution to the One-Dimensional Solute Advection-Dispersion Equation in Multi-Layer Porous Media. *Transport in Porous Media*. 30, 25-43.
- Liu, G.Q.; Zhang, G.; Li, X.D.; Li, J.; Peng, X.Z.; Qi, S.H. 2005. Sedimentary record of polycyclic aromatic hydrocarbons in a sediment core from the Pearl River Estuary, South China. *Marine Pollution Bulletin*. 51, 912-921.
- Ljung, L. 1987. *System Identification: Theory for the User*. Prentice Hall, Inc.: Englewood Cliffs, NJ.
- Loague, K.; Green, R.E. 1991. Statistical and graphical methods for evaluating solute transport models: Overview and application. *Journal of Contaminant Hydrology*. 7, 51-73.
- Loffler, D.; Rombke, J.; Meller, M.; Ternes, T.A. 2005. Environmental Fate of Pharmaceuticals in Water/Sediment Systems. *Environmental Science and Technology*. 39, 5209-5218.
- Lohmann, R.; MacFarlane, J.K.; Gschwend, P.M. 2005. Importance of Black Carbon to Sorption of Native PAHs, PCBs, and PCDDs in Boston and New York Harbor Sediments. *Environmental Science and Technology*. 39, 141-148.
- Long, J.L.A.; House, W.A.; Parker, A.; Rae, J.E. 1998. Micro-organic compounds associated with sediments in the Humber rivers. *Science of The Total Environment*. 210-211, 229-253.
- Lord, R.A.; Morgan, P.A. 2003. Metal Contamination of Active Stream Sediments in Upper Weardale, Northern Pennine Orefield, UK. *Environmental Geochemistry and Health*. V25, 95-104.
- Lyman, W.J.; Reehl, W.F.; Rosenblatt, D.H. 1990. *Handbook of chemical Property Estimation Methods: Environmental Behavior of Organic Compounds*. American Chemical Society: Washington D.C.
- Mackay, D.; Shiu, W.Y.; Ma, K.C. 1997. *Illustrated handbook of physical-chemical properties and environmental fate for organic chemicals V. Pesticide chemicals*. Lewis: London.

- MacKenzie, A.B.; Cook, G.T.; McDonald, P. 1999. Radionuclide distributions and particle size associations in Irish Sea surface sediments: implications for actinide dispersion. *Journal of Environmental Radioactivity*. 44, 275-296.
- Madsen, E.L.; Mann, C.L.; Bilotta, S.E. 1996. Oxygen limitations and ageing as explanation for the field persistence of naphthalene in coal tar-contaminated surface sediments. *Environmental Toxicology and Chemistry*. 15, 1876-1882.
- Manes, M. 1998. *Encyclopedia of Environmental Analysis and Remediation*. John Wiley: New York.
- Manilal, V.B.; Alexander, M. 1991. Factors affecting the microbial degradation of phenanthrene in soil. *Applied Microbiology and Biotechnology*. 35, 401-405.
- Marshall, W.L.; Slusher, R. 1966. Thermodynamics of calcium sulfate dehydrate in aqueous sodium chloride solutions, 0 – 110 °C. *Journal of Physical Chemistry*. 70, 4015-4027.
- Massias, D.; Grossi, V.; Bertrand, J.-C. 2003. In situ anaerobic degradation of petroleum alkanes in marine sediments: preliminary results. *Comptes Rendus Geoscience*. 335, 435-439.
- Matisoff, G.; Wang, X. 1998. Solute transport in sediments by freshwater infaunal bioirrigators. *Limnology and Oceanography*. 43, 1487-1499.
- McCarthy, J.F.; Zachara, J.M. 1989. Subsurface transport of contaminants. *Environmental Science and Technology*. 23, 496-502.
- McClung, R.E.D.; Kivelson, D. 1968. ESR Linewidths in Solution. V. Studies of Spin-Rotational Effects Not Described by Rotational Diffusion Theory. *The Journal of Chemical Physics*. 49, 3380-3391.
- McGinley, P.M.; Katz, L.E.; Weber Jr., W.J. 1993. A distributed reactivity model for sorption by soils and sediments. 2. Multicomponent systems and competitive effects. *Environmental Science and Technology*. 27, 1524-1531.
- Mermillod-Blondin, F.; Nogaro, G.; Datry, T.; Malard, F.; Gibert, J. 2005. Do tubicifid worms influence the fate of organic matter and pollutants in stormwater sediments? *Environmental Pollution*. 134, 57-69.
- Merrington, G.; Alloway, B.J. 1994. The transfer and fate of Cd, Cu, Pb and Zn from two historic metalliferous mine sites in the U.K. *Applied Geochemistry*. 9, 677-687.
- Meysman, F.J.R.; Boudreau, B.P.; Middelburg, J.J. 2003a. Relations Between Local, Nonlocal, Discrete and Continuous Models of Bioturbation. *Journal of Marine Research*. 61, 391-410.
- Meysman, F.J.R.; Middelburg, J.J.; Herman, P.M.J.; Heip, C.H.R. 2003b. Reactive transport in surface sediments. I. Model complexity and software quality. *Computers & Geosciences*. 29, 291-300.

- Meysman, F.J.R.; Middelburg, J.J.; Herman, P.M.J.; Heip, C.H.R. 2003c. Reactive transport in surface sediments. II. Media: an object-oriented problem-solving environment for early diagenesis. *Computers & Geosciences*. 29, 301-318.
- Meysman, F.J.R.; Boudreau, B.P.; Middelburg, J.J. 2005. Modeling reactive transport in sediments subject to bioturbation and compaction. *Geochimica et Cosmochimica Acta*. 69, 3601-3617.
- Middeldorp, P.J.M.; Jaspers, M.; Zehnder, A.J.B.; Schraa, G. 1996. Biotransformation of α -, β -, γ -, and δ -Hexachlorocyclohexane under Methanogenic Conditions. *Environmental Science and Technology*. 30, 2345-2349.
- Mikhailov, M.D.; Özisik, M.N. 1984. *Unified Analysis and Solutions of Heat and Mass Diffusion*. John Wiley: New York.
- Miller, C.T.; Pedit, J.A. 1992. Use of reactive surface-diffusion model to describe apparent sorption-desorption hysteresis and abiotic degradation of lindane in a subsurface material. *Environmental Science and Technology*. 26, 1417-1427.
- Miller, C.T.; Weber Jr., W.J. 1988. Modeling the sorption of hydrophobic contaminants by aquifer materials: II - Column reactor series. *Water Research*. 22, 465-474.
- Millington, R.J.; Quirk, J.M. 1961. Permeability of porous solids. *Transaction of the Society*. 57, 1200-1207.
- Mitra, S.; Dickhut, R.M. 1999. Three-phase modeling of polycyclic aromatic hydrocarbon association with pore-water-dissolved organic carbon. *Environmental Toxicology and Chemistry*. 18, 1144-1148.
- Mitra, S.; Klerks, P.L.; Bianchi, T.S.; Means, J.; Carman, K.R. 2000. Effects of estuarine organic matter biogeochemistry on the bioaccumulation of PAHs by two epibenthic species. *Estuaries and Coasts*. 23, 864-876.
- Mohan, R.K.; Brown, M.P.; Barnes, C.R. 2000. Design criteria and theoretical basis for capping contaminated marine sediments. *Applied Ocean Research*. 22, 85-93.
- Moreira, J.; Midkiff, S.P.; Gupta, M. 1998. A comparison of Java, C/C++, and FORTRAN for numerical computing. *Antennas and Propagation Magazine, IEEE*. 40, 102-105.
- Moreira, J.; Midkiff, S.P.; Gupta, M.; Artigas, P.V.; Snir, M.; Lawrence, R.D. 2000. Java programming for high-performance numerical computing. *IBM Systems Journal*. 39, 1-36.
- Murphy, P.; Marquette, A.; Reible, D.D.; Lowry, G.V. 2006. Predicting the performance of activated carbon- coke-, and soil-amended thin layer sediment caps. *Journal of Environmental Engineering*. 132, 787-794.
- Muslow, S.; Boudreau, B.P.; Smith, J.N. 1998. Bioturbation and porosity gradients. *Limnology and Oceanography*. 43, 1-9.

- Naf, C.; Broman, D.; Axelman, J. 1994. Characterisation of the PAH load outside an aluminium smelter on the Swedish Baltic coast. *Science of The Total Environment*. 156, 109-118.
- Nagasawa, S.; Kikuchi, R.; Nagata, Y.; Takagi, M.; Matsuo, M. 1993. Aerobic mineralization of [gamma]-HCH by *Pseudomonas paucimobilis* UT26. *Chemosphere*. 26, 1719-1728.
- Nam, K.; Alexander, M. 1998. Role of nanoporosity and hydrophobicity in sequestration and bioavailability: tests with model solids. *Environmental Science and Technology*. 32, 71-74.
- National Research Council. 2002. *Bioavailability of contaminated soils and sediments: processes, tools, and applications*. National Academic Press: Washinton, DC.
- Neuman, S. 1990. Universal scaling of hydraulic conductivities and dispersivities in geologic media. *Water Resources Research*. 26, 1749-1758.
- Newell, R.C.; Seiderer, L.J.; Hitchcock, D.R. 1998. The impact of dredging works in coastal waters: a review of the sensitivity to disturbance and subsequent recovery of biological resources on the sea bed. *Oceanography & Marine Biology Annual Reviews*. 136, 127-178.
- Nguyen, L.K.; Schiller, N.L. 1989. Identification of a slime exopolysaccharide depolymerase in mucoid strains of *Pseudomonas aeruginosa*. *Current Microbiology*. 18, 323-329.
- Nguyen, V.V.; Gray, W.G.; Pinder, G.F.; otha, J.F.; rerar, D.A. 1982. A theoretical investigation on the transport of chemicals in reactive porous media. *Water Resources Research*. 18, 1149-1156.
- Niesner, R.; Heintz, A. 2000. Diffusion coefficients for aromatics in aqueous solution. *Journal of Chemical & Engineering Data*. 45, 1121-1124.
- Nkedi-Kizza, P.; Brusseau, M.L.; Rao, S.C.; Hornsby, A.G. 1989. Nonequilibrium sorption during displacement of hydrophobic organic chemicals and calcium-45 through soil columns with aqueous and mixed solvents. *Environmental Science and Technology*. 23, 814-820.
- Nogotov, E.F. 1978. *Applications of numerical heat transfer*. UNESCO Hemisphere Publishing Corp.:
- NRC. 1997. *Contaminated Sediments in Ports and Waterways: Cleanup Strategies and Technologies*. National Academy Press: Washington, D.C.
- O'Loughlin, E.M.; Bowmer, K.H. 1975. Dilution and decay of aquatic herbicides in flowing channels. *Journal of Hydrology*. 26, 217-235.
- Oetken, M.; Nentwig, G.; Loffler, D.; Ternes, T.A.; Oehlmann, J. 2005. Effects of Pharmaceuticals on Aquatic Invertebrates. Part I. The Antiepileptic Drug Carbamazepine. *Archives of Environmental Contamination and Toxicology*. 49, 353-361.

- Ogata, A., Banks, R.B. 1961. A solution of the differential equation of longitudinal dispersion in porous media Professional Paper No. 411-A. US Geological Survey
- Oreskes, N.; Shrader-Frechette, K.; Belitz, K. 1994. Verification, Validation, and Confirmation of Numerical Models in the Earth Sciences. *Science*. 263, 641-646.
- Orvos, D.R.; Versteeg, D.J.; Inauen, J.; Capdevielle, M.; Rothenstein, A.; Cunningham, V. 2002. Aquatic toxicity of Triclosan. *Environmental Toxicology and Chemistry*. 21, 1338-1349.
- Owens, P.N.; Walling, D.E.; Carton, J.; Meharg, A.A.; Wright, J.; Leeks, G.J.L. 2001. Downstream changes in the transport and storage of sediment-associated contaminants (P, Cr and PCBs) in agricultural and industrialized drainage basins. *Science of The Total Environment*. 266, 177-186.
- Page-Jones, M. 2000. *Fundamentals of Object-Oriented Design in UML*. Dorset House Publishing: New York, NY.
- Palermo, M., Maynard, S., Miller, J., Reible, D.D. 1998. Guidance for in situ subaqueous capping of contaminated sediments EPA 905-B96-004.
- Peacock, E.E.; Hampson, G.R.; Nelson, R.K.; Xu, L.; Frysinger, G.S.; Gaines, R.B.; Farrington, J.W.; Tripp, B.W.; Reddy, C.M. 2007. The 1974 spill of the Bouchard 65 oil barge: Petroleum hydrocarbons persist in Winsor Cove salt marsh sediments. *Marine Pollution Bulletin*. 54, 214-225.
- Pedit, J.A.; Miller, C.T. 1994. Heterogeneous sorption processes in subsurface systems. 1. Model formulations and applications. *Environmental Science and Technology*. 28, 2094-2104.
- Pignatello, J.J.; Ferrandino, F.J.; Huang, L.Q. 1993. Elution of aged and freshly added herbicides from a soil. *Environmental Science and Technology*. 27, 1553-1567.
- Pignatello, J.J.; Xing, B. 1996. Mechanisms of Slow Sorption of Organic Chemicals to Natural Particles. *Environmental Science and Technology*. 30, 1-11.
- Pirrie, D.; Power, M.R.; Rollinson, G.; Camm, G.S.; Hughes, S.H.; Butcher, A.R.; Hughes, P. 2003. The spatial distribution and source of arsenic, copper, tin and zinc within the surface sediments of the Fal Estuary, Cornwall, UK. *Sedimentology*. 50, 579-595.
- Power, B. 2002. Scoping Study - Sediments in England and Wales: Nature and Extent of the Issues, Final Report Environment Agency, Bristol, UK
- Pressman, R.S. 2001. *Software Engineering: A Practitioner's Approach*. McGraw Hill: New York.
- Pretty, J.N.; Mason, C.F.; Nedwell, D.B.; Hine, R.E.; Leaf, S.; Dils, R. 2003. Environmental Costs of Freshwater Eutrophication in England and Wales. *Environmental Science and Technology*. 37, 201-208.

Ran, Y.; Xing, B.; Rao, P.S.C.; Fu, J. 2004. Importance of Adsorption (Hole-Filling) Mechanism for Hydrophobic Organic Contaminants on an Aquifer Kerogen Isolate. *Environmental Science & Technology*. 38, 4340-4348.

Ratola, N.; Santos, L.; Herbert, P.; Alves, A. Uncertainty associated to the analysis of organochlorine pesticides in water by solid-phase microextraction/gas chromatography–electron capture detection—Evaluation using two different approaches. *Analytica Chimica Acta*. 573-574, 202-208.

Reddy, C.M.; Eglinton, T.I.; Hounshell, A.; White, H.K.; Xu, L.; Gaines, R.B.; Frysiner, G.S. 2002a. The West Falmouth Oil Spill after Thirty Years: The Persistence of Petroleum Hydrocarbons in Marsh Sediments. *Environmental Science and Technology*. 36, 4754-4760.

Reddy, C.M.; Eglinton, T.I.; Hounshell, A.; White, H.K.; Xu, L.; Gaines, R.B.; Frysiner, G.S. 2002b. The West Falmouth Oil Spill after Thirty Years: The Persistence of Petroleum Hydrocarbons in Marsh Sediments. *Environmental Science and Technology*. 36, 4754-4760.

Reddy, C.M.; Quinn, J.G. 2001. The North Cape oil spill: hydrocarbons in Rhode Island coastal waters and Point Judith Pond. *Marine Environmental Research*. 52, 445-461.

Reddy, K.A.; Doraiswamy, L.K. 1967. Estimating Liquid Diffusivity. *Industrial & Engineering Chemistry Fundamentals*. 6, 77-79.

Reed, M.; Cuddy, S.M.; Rizzoli, A.E. 1999. A framework for modelling multiple resource management issues—an open modelling approach. *Environmental Modelling and Software*. 14, 503-509.

Reible, D.D. 1998. Guidance for in-situ subaqueous capping of contaminated sediments: Appendix B- Model for chemical containment by a cap US Environmental Protection Agency.

Reible, D.D.; Hayes, D.; Lue-Hing, C.; Patterson, J.; Bhowmik, N.; Johnson, M.; Teal, J. 2003. Comparison of the long-term risks of removal and in-situ management of contaminated sediments in the Fox River. *Soil and Sediment Contamination*. 12, 325-344.

Reible, D.D.; Popov, V.; Valsaraj, K.T.; Thibodeaux, L.J.; Lin, F.; Dikshit, M.; Todaro, M.A.; Fleeger, J.W. 1996. Contaminant fluxes from sediment due to tubificid oligochaete bioturbation. *Water Research*. 30, 704-714.

Reible, D.D.; Simpson-Kiehl, C.; Marquette, A. 2006. Contaminant Processes in Sediments. In *Sedimentation Engineering: Theory, Measurements, Modeling, and Practice*; Vanoni, V.A., Ed.; American Society of Civil Engineers: Reston, Virginia.

Reiser, R.; Toljander, H.; Albrecht, A.; Giger, W. 1997. Alkylbenzenesulfonates in recent lake sediments as molecular markers for the environmental behavior of detergent-derived chemicals. In *Molecular markers in environmental geochemistry*; Eganhouse, R.P., Ed.; American Chemical Society: Washington DC, pp 196-212.

- Rhoads, D.C. 1974. Organism sediment relations on the muddy sea floor. *Oceanography & Marine Biology Annual Reviews*. 12, 263.
- Rocher, V.; Azimi, S.; Moilleron, R.; Chebbo, G. 2004. Hydrocarbons and heavy metals in the different sewer deposits in the 'Le Marais' catchment (Paris, France): stocks, distributions and origins. *Science of The Total Environment*. 323, 107-122.
- Romani, A.M.; Sabater, S. 2000. Variability of heterotrophic activity in Mediterranean stream biofilms: A multivariate analysis of physical-chemical and biological factors. *Aquatic Sciences - Research Across Boundaries*. 62, 205-215.
- Roper, J.M.; Cherry, D.S.; Simmers, J.W.; Tatem, H.E. 1997. Bioaccumulation of PAHs in the Zebra Mussel at Times Beach, Buffalo, New York. *Environmental Monitoring and Assessment*. 46, 267-277.
- Rubin, J. 1983. Transport of reacting solutes in porous media; relation between mathematical nature of problem formulation and chemical nature of reactions. *Water Resources Research*. 19, 1231-1252.
- Ruiz, C.E.; Aziz, N.M.; Schroeder, P.R. 2001. RECOVERY: A contaminated sediment-water interaction model. *Environmental Modeling and Assessment*. 6, 151-158.
- Ruiz, C.E.; Schroeder, P.R. 2001. Assessment of contaminant isolation at Duwamish, Wash., capping site verifies RECOVERY prediction strength. *Dredging Research*. 4, 1-4.
- Rutgers van der Loeff, M.M. 1981. Wave effects on sediment water exchange in a submerged sand bed. *Netherlands Journal of Sea Research*. 15, 100-112.
- Ryan, J.N.; Elimelech, M. 1996. Colloid mobilization and transport in groundwater. *Colloids and Surfaces A: Physicochemical and Engineering Aspects*. 107, 1-56.
- Sabljić, A.; Gusten, H.; Verhaar, H.; Hermens, J. 1995. QSAR modelling of soil sorption. Improvements and systematics of log KOC vs. log KOW correlations. *Chemosphere*. 31, 4489-4514.
- Sancho, E.; Ferrando, M.D.; Lleo, C.; Andreu-Moliner, E. 1998. Pesticide Toxicokinetics in Fish: Accumulation and Elimination. *Ecotoxicology and Environmental Safety*. 41, 245-250.
- Sandi J. Formica; Julie A. Baron; Louis J. Thibodeaux; Kallat T. Valsaraj. 1988. PCB Transport Into Lake Sediments. Conceptual Model and Laboratory Simulation. *Environmental Science and Technology*. 22, 1435-1440.
- Sandnes, J.; Forbes, T.; Hansen, R.; Sandnes, B. 2000. Influence of particle type and faunal activity on mixing of di(2-ethylhexyl)phthalate (DEHP) in natural sediments. *Marine Ecology Progress Series*. 197, 151-167.
- Santschi, P.H.; Anderson, R.; Fleishier, M.Q. 1991. Measurement of diffusive sublayer thicknesses in the ocean by Alabaster dissolution, and their implications for the measurements of benthic fluxes. *Journal of Geophysical Research*. 96(C6), 641-657.

- Sastri, S.; Mohanti, S.; Rao, K. 1996. Liquid volume at normal boiling point. *The Canadian Journal of Chemical Engineering*. 74, 170-172.
- Schaffner, L.C.; Dickhut, R.M.; Mitra, S.; Lay, P.W.; Brouwer-Riel, C. 1997. Effects of Physical Chemistry and Bioturbation by Estuarine Macrofauna on the Transport of Hydrophobic Organic Contaminants in the Benthos. *Environmental Science and Technology*. 31, 3120-3125.
- Scheidegger, A.E. 1954. Statistical hydrodynamics in porous media. *Journal of Applied Physics*. 25, 994-1001.
- Scheunert, I.; Vockel, D.; Schmitzer, J.; Korte, F. 1987. Biomineralization rates of ¹⁴C-labelled organic chemicals in aerobic and anaerobic suspended soil. *Chemosphere*. 16, 1031-1041.
- Schiesser, W.E. 1991. *The Numerical Method of Lines: Integration of Partial Differential Equations*. Academic Press: San Diego, CA.
- Schmitt, T.M. 1992. *Analysis of Surfactants*. Marcel Dekker: New York.
- Schorer, M.; Eisele, M. 1997. Accumulation of inorganic and organic pollutants by biofilms in the aquatic environment. *Water, Air, & Soil Pollution*. 99, 651-659.
- Schwarzenbach, R.P.; Gschwend, P.M.; Imboden, D.M. 1993. *Environmental Organic Chemistry*. John Wiley & Sons: New York.
- Scrimshaw, M.D.; Wahlen, R.; Catterick, T.; Lester, J.N. 2005. Butyltin compounds in a sediment core from the old Tilbury basin, London, UK. *Marine Pollution Bulletin*. 50, 1500-1507.
- SEDNET (European Sediment Research Network). Contaminated Sediments in European River Basins. 2005.
- Shamir, U.Y.; Harleman, D.R.F. 1967. Dispersion in layered porous media. *Journal of Hydraulic Engineering - ASCE*. 93, 237-260.
- Shampine, L.F.; Gear, C.W. 1979. A user's view of solving stiff ordinary differential equations. *SIAM Review*. 21, 1-17.
- Sherwood, C.R.; Drake, D.E.; Wiberg, P.L.; Wheatcroft, R.A. 2002. Prediction of the fate of p,p'-DDE in sediment on the Palos Verdes shelf, California, USA. *Continental Shelf Research*. 22, 1025-1058.
- Shimizu, Y.; Sogabe, H.; Terashima, Y. 1998. The effects of colloidal humic substances on the movement of non-ionic hydrophobic organic contaminants in groundwater. *Water Science and Technology*. 38, 159-167.
- Shor, L.M.; Liang, W.; Rockne, K.J.; Young, L.Y.; Taghon, G.L.; Kosson, D.S. 2003a. Intra-Aggregate Mass Transport-Limited Bioavailability of Polycyclic Aromatic Hydrocarbons to *Mycobacterium* Strain PC01. *Environmental Science and Technology*. 37, 1545-1552.

- Shor, L.M.; Rockne, K.J.; Taghon, G.L.; Young, L.Y.; Kosson, D.S. 2003b. Desorption Kinetics for Field-Aged Polycyclic Aromatic Hydrocarbons from Sediments. *Environmental Science and Technology*. 37, 1535-1544.
- Shull, D. 2001. Transition-matrix model of bioturbation and radionuclide diagenesis. *Limnology and Oceanography*. 46, 905-916.
- Simpson, C.D.; Harrington, C.F.; Cullen, W.R.; Bright, D.A.; Reimer, K.J. 1998a. Polycyclic Aromatic Hydrocarbon Contamination in Marine Sediments near Kitimat, British Columbia. *Environmental Science and Technology*. 32, 3266-3272.
- Simpson, C.D.; Mosi, A.A.; Cullen, W.R.; Reimer, K.J. 1996. Composition and distribution of polycyclic aromatic hydrocarbon contamination in surficial marine sediments from Kitimat Harbor, Canada. *Science of The Total Environment*. 181, 265-278.
- Simpson, S.L.; Apte, S.C.; Batley, G.E. 1998b. Effect of Short-Term Resuspension Events on Trace Metal Speciation in Polluted Anoxic Sediments. *Environmental Science and Technology*. 32, 620-625.
- Sincovec, R.F.; Madsen, N.K. 1975. Software for nonlinear partial differential equations. *ACM Transactions on Mathematical Software*. 1, 232-260.
- Singh, B.K.; Kuhad, R.C.; Singh, A.; Tripathi, K.K.; Ghosh, P.K. 2000. Microbial degradation of the pesticide lindane ([gamma]-hexachlorocyclohexane). In *Advances in Applied Microbiology*; Academic Press: pp 269-298.
- Sivey, J.D.; Lee, C.M. 2007. Polychlorinated biphenyl contamination trends in Lake Hartwell, South Carolina (USA): Sediment recovery profiles spanning two decades. *Chemosphere*. 66, 1821-1828.
- Slater, G.F.; White, H.K.; Eglinton, T.I.; Reddy, C.M. 2005. Determination of Microbial Carbon Sources in Petroleum Contaminated Sediments Using Molecular ¹⁴C Analysis. *Environmental Science and Technology*. 39, 2552-2558.
- Slattery, J.C. 1967. General Balance Equation for a Phase Interface. *Industrial & Engineering Chemistry Fundamentals*. 6, 108-115.
- Soderstrom, T.; Stoica, P. 1989. *System Identification*. Prentice Hall, Inc.: Engelwood Cliffs, NJ.
- Soetaert, K.; Herman, P.M.J.; Middelburg, J.J.; Heip, C.H.R.; deStigter, H.S.; van Weering, T.C.E.; Epping, E.; Helder, W. 1996a. Modeling ²¹⁰Pb-derived mixing activity in ocean margin sediments: Diffusive versus nonlocal mixing. *Journal of Marine Research*. 54, 1207-1227.
- Soetaert, K.; Herman, P.M.J.; Middelburg, J.J. 1996b. A model of early diagenetic processes from the shelf to abyssal depths. *Geochimica et Cosmochimica Acta*. 60, 1019-1040.
- Song, J.; Peng, P.; Huang, W. 2002. Black Carbon and Kerogen in Soils and Sediments. 1. Quantification and Characterization. *Environmental Science and Technology*. 36, 3960-3967.

- Stevenson, F.J. 1994. *Humus Chemistry: Genesis, Composition, Reaction*. John Wiley & Sons: New York.
- Sugai, S.F. 1990. Transport and Sediment Accumulation of 210-Pb and 137-Cs in Two Southeast Alaskan Fjords. *Estuaries*. 13, 380-392.
- Sumpter, J.P.; Johnson, A.C. 2005. Lessons from Endocrine Disruption and Their Application to Other Issues Concerning Trace Organics in the Aquatic Environment. *Environmental Science and Technology*. 39, 4321-4332.
- Sven-Olof, R. 1982. Lake Trehörningen restoration project. Changes in water quality after sediment dredging. *Hydrobiologia*. 91-92, 549-558.
- Syvitski, J.P.M.; Burrell, D.C.; Skei, J.M. 1987. *Fjords: processes and products*. Springer-Verlag: New York.
- Syvitski, J.P.M.; Shaw, J. 1995. Sedimentology and geomorphology of fjords. In *Geomorphology and sedimentology of estuaries*; Perillo, G.M.E., Ed.; Elsevier Science: pp 113-178.
- Tahey, T.M.; Duineveld, G.C.A.; Berghuis, E.M.; Helder, W. 1994. Relation between sediment-water fluxes of oxygen and silicate and faunal abundance at continental shelf, slope and deep-water stations in the northwest Mediterranean. *Marine Ecology Progress Series*. 104, 119-130.
- Tang, Y.J.; Carpenter, S.; Deming, J.; Krieger-Brockett, B. 2005. Controlled Release of Nitrate and Sulfate to Enhance Anaerobic Bioremediation of Phenanthrene in Marine Sediments. *Environmental Science and Technology*. 39, 3368-3373.
- Ternes, T.A. 1998. Occurrence of drugs in German sewage treatment plants and rivers. *Water Research*. 32, 3245-3260.
- Thibodeaux, L.J. 1996. *Environmental Chemodynamics*. John Wiley & Sons, Inc.: New York.
- Thibodeaux, L.J.; Bierman, V.J. 2003. The Bioturbation-Driven Chemical Release Process. *Environmental Science and Technology*. 37, 252A-258A.
- Thibodeaux, L.J.; Valsaraj, K.T.; Reible, D.D. 2001. Bioturbation-Driven Transport of Hydrophobic Organic Contaminants from Bed Sediment. *Environmental Engineering Science*. 18, 215-223.
- Thomas, K.V.; Hurst, M.R.; Mathiessen, P.; Waldock, M.J. 2001. Characterization of estrogenic compounds in water samples collected from United Kingdom. *Environmental Toxicology and Chemistry*. 20, 2165-2170.
- Thoms, S.R., Matisoff, G., McCall, P.L., Wang, X. 1995. Models for alteration of sediments by benthic organisms Project 92-NPS-2. Water Environment Research Foundation
- Thrane, K.E. 1987. Deposition of polycyclic aromatic hydrocarbons (PAH) in the surroundings of primary aluminium industry. *Water, Air, & Soil Pollution*. 33, 385-393.

Tixier, C.; Singer, H.P.; Oellers, S.; Muller, S.R. 2003. Occurrence and Fate of Carbamazepine, Clofibrac Acid, Diclofenac, Ibuprofen, Ketoprofen, and Naproxen in Surface Waters. *Environmental Science and Technology*. 37, 1061-1068.

Torang, L.; Nyholm, N.; Albrechtsen, H.-J. 2003. Shifts in Biodegradation Kinetics of the Herbicides MCPP and 2,4-D at Low Concentrations in Aerobic Aquifer Materials. *Environmental Science and Technology*. 37, 3095-3103.

Trauth, M.H. 1998. TURBO: a dynamic-probabilistic simulation to study the effects of bioturbation on paleoceanographic time series. *Computers & Geosciences*. 24, 433-441.

Triebkorn, R.; Casper, H.; Heyd, A.; Eikemper, R.; Kohler, H.-R.; Schwaiger, J. 2004. Toxic effects of the non-steroidal anti-inflammatory drug diclofenac: Part II. Cytological effects in liver, kidney, gills and intestine of rainbow trout (*Oncorhynchus mykiss*). *Aquatic Toxicology*. 68, 151-166.

Tye, R.; Jepsen, R.; Lick, W. 1996. Effect of colloids, flocculation, particle size, and organic matter on the adsorption of hexachlorobenzene to sediments. *Environmental Toxicology and Chemistry*. 15, 643-651.

Tyler, A.O.; Millward, G.E. 1996. Distribution and partitioning of polychlorinated dibenzo-p-dioxins, polychlorinated dibenzofurans and polychlorinated biphenyls in the Humber Estuary, UK. *Marine Pollution Bulletin*. 32, 397-403.

Tzur, Y. 1971. Interstitial Diffusion and Advection of solutes in Accumulating Sediments. *Journal of Geophysical Research - Oceans and Atmospheres*. 76, 4208-4211.

UNEP Persistent Organic Pollutants Review Committee. *Consideration of chemicals proposed for inclusion in Annexes A, B and C of the Convention: Lindane*.

UNEP/POPS/POPRC.1/INF/8 Geneva, Switzerland: 2005.

US Environmental Protection Agency. 1983. Environmental Transport and Transformation of Polychlorinated Biphenyls EPA 560/5-83-025.

US Environmental Protection Agency. 1985. National Perspective on Sediment Quality EPA Contract No. 68-01-6986.

US Environmental Protection Agency. 1988. An Overview of Sediment Quality in the United States EPA 905/9-88/002.

US Environmental Protection Agency. 1994. Superfund Record of Decision: Sangamo-Weston/Twelvemile Creek/Lake Hartwell Site, Pickens, SC: Operable Unit 2 EPA/ROD/RO4-94/178.

US Environmental Protection Agency. 1996. PCBs: Cancer Dose-Response Assessment and Application to Environmental Mixtures EPA/600/P-96/001F.

US Environmental Protection Agency. 1997a. National Sediment Quality Survey: Assesses the probability of associated adverse human or ecological effects with contaminated sediment based on a weight-of-evidence evaluation EPA 823-R-97-006.

US Environmental Protection Agency. 1997b. The Incidence and Severity of Sediment Contamination in Surface Waters of the United States: Volume 1: National Sediment Quality Survey EPA 823-R-97-006.

US Environmental Protection Agency. 1998a. EPA's contaminated sediment management strategy EPA-823-R-98-001.

US Environmental Protection Agency. 1998b. EPA's monitored natural attenuation policy 308.

US Environmental Protection Agency. 2000. Waste Minimization Prioritization Tool: Background Document For The Tier III PBT Chemical List. Appendix A: WMPT Summary Spreadsheet.

US Environmental Protection Agency. 2005a. Contaminated Sediment Remediation Guidance for Hazardous Waste Sites EPA 540-R-05-012.

US Environmental Protection Agency. 2005b. Fiscal Year Annual Report: Goal 3 - Land Preservation and Restoration

US Environmental Protection Agency - Region 4. 2005. Five-year review report for the Sangamo Weston/Twelve Mile Creek/Lake Hartwell PCB Contamination Superfund Site - Operable Unit One Pickens, Pickens County, South Carolina EPA ID: SCD003354412.

US Geological Survey. 2007. Pesticides in the Nation's Streams and Ground Water, 1992–2001

Usländer, T. 2005. Trends of environmental information systems in the context of the European Water Framework Directive. *Environmental Modelling & Software*. 20, 1532-1542.

Valocchi, A.J. 1988. Theoretical analysis of deviations from local equilibrium during sorbing solute transport through idealized stratified aquifers. *Journal of Contaminant Hydrology*. 2, 191-207.

Valsaraj, K.T.; Sojitra, I. 1997. Transport of hydrophobic organic compounds by colloids through porous media 3. Diffusion from sediment porewater to overlying water in laboratory microcosms. *Colloids and Surfaces A: Physicochemical and Engineering Aspects*. 121, 125-133.

van der Wielen, L.; Zomerdijk, M.; Houwers, J.; Luyben, K. 1997. Diffusivities of organic electrolytes in water. *Chemical Engineering Journal*. 66, 111-121.

van Genuchten, M.; Alves, W.J. 1982. Analytical solutions of the one-dimensional convective-dispersive solute transport equation. *U. S. Department of Agriculture Technical Bulletin*. 1661, 1-151.

Vivanco, R.A.; Pizzi, N.J. 2005. Scientific computing with Java and C++: a case study using functional magnetic resonance neuroimages. *Software - Practice and Experience*. 35, 237-254.

- Voinov, A.; Costanza, R.; Wainger, L.; Boumans, R.; Villa, F.; Maxwell, T.; Voinov, H. 1999. Patuxent landscape model: integrated ecological economic modeling of a watershed. *Environmental Modelling and Software*. 14, 473-491.
- Volkering, F.; Breure, A.M.; Sterkenburg, A.; van Andel, J.G. 1992. Microbial degradation of PAHs: effect of substrate availability on bacterial growth kinetics. *Applied Microbiology and Biotechnology*. 36, 548-552.
- Wainright, S.C.; Hopkinson, J. 1997. Effects of sediment resuspension on organic matter processing in coastal environments: A simulation model. *Journal of Marine Systems*. 11, 353-368.
- Wang, X.; Matisoff, G. 1997. Solute Transport in Sediments by a Large Freshwater Oligochaete, *Branchiura sowerbyi*. *Environmental Science and Technology*. 31, 1926-1933.
- Wang, X.; Yu, X.; Bartha, R. 1990. Effect of bioremediation on polycyclic hydrocarbon residues in soil. *Environmental Science and Technology*. 24, 1086-1089.
- Wang, X.H.; Byun, D.S.; Wang, X.L.; Cho, Y.K. 2005. Modelling tidal currents in a sediment stratified idealized estuary. *Continental Shelf Research*. 25, 655-665.
- Wang, Y.; Van Cappellen, P. 1996. A multicomponent reactive transport model of early diagenesis: Application to redox cycling in coastal marine sediments. *Geochimica et Cosmochimica Acta*. 60, 2993-3014.
- Warren, N.; Allan, I.J.; Carter, J.E.; House, W.A.; Parker, A. 2003. Pesticides and other micro-organic contaminants in freshwater sedimentary environments--a review. *Applied Geochemistry*. 18, 159-194.
- Watts, A.W.; Ballester, T.P.; Gardner, K.H. 2006. Uptake of polycyclic aromatic hydrocarbons (PAHs) in salt marsh plants *Spartina alterniflora* grown in contaminated sediments. *Chemosphere*. 62, 1253-1260.
- Weber Jr., W.J.; DiGiano, F.A. 1996. *Process Dynamics in Environmental Systems*. Wiley-Interscience: New York.
- Weber Jr., W.J.; Huang, W. 1996. A Distributed Reactivity Model for Sorption by Soils and Sediments. 4. Intraparticle Heterogeneity and Phase-Distribution Relationships under Nonequilibrium Conditions. *Environmental Science and Technology*. 30, 881-888.
- Weber Jr., W.J.; Miller, C.T. 1988. Modeling the sorption of hydrophobic contaminants by aquifer materials - I. Rates and equilibria. *Water Research*. 22, 457-464.
- Weber, J.; Huang, W.; Yu, H. 1998. Hysteresis in the sorption and desorption of hydrophobic organic contaminants by soils and sediments: 2. Effects of soil organic matter heterogeneity. *Journal of Contaminant Hydrology*. 31, 149-165.
- Weber, W.J.; McGinley, P.M.; Katz, L.E. 1992. A distributed reactivity model for sorption by soils and sediments. 1. Conceptual basis and equilibrium assessments. *Environmental Science and Technology*. 26, 1955-1962.

- Weber, W.J.; McGinley, P.M.; Katz, L.E. 1991. Sorption phenomena in subsurface systems: Concepts, models and effects on contaminant fate and transport. *Water Research*. 25, 499-528.
- Webster, I.T.; Taylor, J.H. 1992. Rotational dispersion in porous media due to fluctuating flow. *Water Resources Research*. 28, 109-119.
- Wells, M.L.; Smith, G.J.; Bruland, K.W. 2000. The distribution of colloidal and particulate bioactive metals in Narragansett Bay, RI. *Marine Chemistry*. 71, 143-163.
- Wen, L.-S.; Santschi, P.H.; Gill, G.; Paternostro, C. 1999. Estuarine trace metal distributions in Galveston Bay: importance of colloidal forms in the speciation of the dissolved phase. *Marine Chemistry*. 63, 185-212.
- Wenderholm, E. 2005. Eclpss: a Java-based framework for parallel ecosystem simulation and modeling. *Environmental Modelling & Software*. 20, 1081-1100.
- Werner, D.; Ghosh, U.; Luthy, R.G. 2006. Modeling Polychlorinated Biphenyl Mass Transfer after Amendment of Contaminated Sediment with Activated Carbon. *Environmental Science and Technology*. 40, 4211-4218.
- Werner, D.; Higgins, C.P.; Luthy, R.G. 2005. The sequestration of PCBs in Lake Hartwell sediment with activated carbon. *Water Research*. 39, 2105-2113.
- Wheatcroft, R.A.; Jumars, P.A.; Smith, C.R.; Nowell, A.R.M. 1990. A mechanistic view of the particulate biodiffusion coefficient - step lengths, rest periods and transport directions. *Journal of Marine Research*. 48, 177-207.
- Wheatcroft, R.A.; Martin, W.R. 1996. Spatial variation in short-term (^{234}Th) sediment bioturbation intensity along an organic-carbon gradient. *Journal of Marine Research*. 54, 763-792.
- White, F. 1995. Multiple interactions in riverine biofilms -- surfactant adsorption, bacterial attachment and biodegradation. *Water Science and Technology*. 31, 61-70.
- White, H.K.; Li, X.; Lima, A.L.C.; Eglinton, T.I.; Reddy, C.M. 2005. Abundance, Composition, and Vertical Transport of PAHs in Marsh Sediments. *Environmental Science and Technology*. 39, 8273-8280.
- White, K.L. 1986. An overview of immunotoxicology and carcinogenic polycyclic aromatic hydrocarbons. *Environmental Carcinogenesis Reviews*. C4, 163-202.
- Wild, S.R.; Jones, K.C. 1995. Polynuclear aromatic hydrocarbons in the United Kingdom environment: A preliminary source inventory and budget. *Environmental Pollution*. 88, 91-108.
- Willmott, C.J. 1981. On the validation of models. *Physical Geography*. 2, 184-194.
- Woo, S.H.; Park, J.M.; Rittmann, B.E. 2001. Evaluation of the interaction between biodegradation and sorption of phenanthrene in soil-slurry systems. *Biotechnology and Bioengineering*. 73, 12-24.

- Wood, L.W. 1975. Role of oligochaetes in the circulation of water and solute across the mud-water interface. *Verhandlungen der Internationalen Vereinigung für Theoretische und Angewandte Limnologie*. 19, 1530-1533.
- Woodhead, R.J.; Law, R.J.; Matthiessen, P. 1999. Polycyclic Aromatic Hydrocarbons in Surface Sediments Around England and Wales, and Their Possible Biological Significance. *Marine Pollution Bulletin*. 38, 773-790.
- Wu, S.C.; Gschwend, P.M. 1986. Sorption kinetics of hydrophobic organic compounds to natural sediments and soils. *Environmental Science and Technology*. 20, 717-725.
- Wu, S.C.; Gschwend, P.M. 1988. Numerical modeling of sorption kinetics of organic compounds to soils and sediment particle. *Water Resources Research*. 24, 1373-1383.
- Xia, G.; Ball, W.P. 1999. Adsorption-Partitioning Uptake of Nine Low-Polarity Organic Chemicals on a Natural Sorbent. *Environmental Science and Technology*. 33, 262-269.
- Xia, G.; Ball, W.P. 2000. Polanyi-Based Models for the Competitive Sorption of Low-Polarity Organic Contaminants on a Natural Sorbent. *Environmental Science and Technology*. 34, 1246-1253.
- Xia, G.; Pignatello, J.P. 2001. Detailed Sorption Isotherms of Polar and Apolar Compounds in a High-Organic Soil. *Environmental Science and Technology*. 35, 84-94.
- Xing, B.; Pignatello, J.P. 1997. Dual-Mode Sorption of Low-Polarity Compounds in Glassy Poly(Vinyl Chloride) and Soil Organic Matter. *Environmental Science and Technology*. 31, 792-799.
- Yaws, C.L. 1999. *Chemical Properties Handbook*. McGraw Hill: New York.
- Ying, G.G.; Kookana, R.S.; Ru, Y.J. 2002. Occurrence and fate of hormone steroids in the environment. *Environment International*. 28, 545-551.
- Yong, R.; Xing, B.; Rao, S.C.; Fu, J. 2004. Importance of Adsorption (Hole-Filling) Mechanism for Hydrophobic Organic Contaminants on an Aquifer Kerogen Isolate. *Environmental Science and Technology*. 38, 4340-4348.
- Young, P.L. 1997. The longevity of minewater pollution: a basis for decision-making. *Science of The Total Environment*. 194-195, 457-466.
- Young, T.M.; Weber Jr., W.J. 1995. A Distributed Reactivity Model for Sorption by Soils and Sediments. 3. Effects of Diagenetic Processes on Sorption Energetics. *Environmental Science and Technology*. 29, 92-97.
- Youngblood, W.W.; Blumer, M. 1975. Polycyclic aromatic hydrocarbons in the environment: homologous series in soils and recent marine sediments. *Geochimica et Cosmochimica Acta*. 39, 1303-1314.
- Yu, W.; Cox, A. 1997. Java/DSM: A platform for heterogeneous computing. *Concurrency: Practice and Experience*. 9, 1213-1224.

Zhang, H.; Huang, C.-H. 2005. Oxidative Transformation of Fluoroquinolone Antibacterial Agents and Structurally Related Amines by Manganese Oxide. *Environmental Science and Technology*. 39, 4474-4483.

Zheng, C.; Bennett, G.D. 1995. *Applied Contaminant Transport Modeling: Theory and Practice*. Van Nostrand Reinhold:

Zhou, J.L.; Fileman, T.W.; House, W.A.; Long, J.L.A.; Mantoura, R.F.C.; Meharg, A.A.; Osborn, D.; Wright, J. 1999. Fluxes of Organic Contaminants from the River Catchment into, through and out of the Humber Estuary, UK. *Marine Pollution Bulletin*. 37, 330-342.

Zhou, J.L.; Fileman, T.W.; Evans, S.; Donkin, P.; Llewellyn, C.; Readman, J.W.; Mantoura, R.F.; Rowland, S.J. 1998. Fluoranthene and pyrene in the suspended particulate matter and surface sediments of the Humber Estuary, UK. *Marine Pollution Bulletin*. 36, 587-597.

Zhou, J.L.; Rowland, S.; Fauzi, R.; Mantoura, C.; Braven, J. 1994. The formation of humic coatings on mineral particles under simulated estuarine conditions--A mechanistic study. *Water Research*. 28, 571-579.

Appendix A. Program code for the CoReTranS numerical solver

```
/*
 * Created on 01-Nov-2006
 *
 * Jason Go
 */
package coretransProject2;

import jDisco.*;
import jDisco.Process;

public class CoretransNumericalSolver extends Process {

    PDEVariable thePorewaterConcentration;

    private double sedimentDepth;
    private double simulationTime;
    private double numberOfGrids;
    private double sedimentDensity;
    private double waterTemperature;
    private double foc;
    private double molarVolume;
    private double halfLife;
    private double logKow;
    private String porosityChoice;
    private double constantPorosity;
    private double porosityAtInterface;
    private double porosityAtInfinity;
    private double depthFactor;
    private double powerExponent;
    private double powerFactor;
    private boolean isDiffusivityUserDefined;
    private String diffusivityChoice;
    private double theDiffusivity;
    private boolean isSorptionSelected;
    private boolean isLinearPartitioningSelected;
    private boolean isLinearSorptionUserDefined;
    private double aPartitioningConstant;
    private double bPartitioningConstant;
    private boolean isFreundlichSelected;
    private double kf;
    private double n;
    private boolean isLangmuirSelected;
    private double s;
    private double b;
    private boolean isAdvectionSelected;
    private boolean isAdvectionUserDefined;
    private double pressureGradient;
    private double hydraulicConductivity;
    private double permeability;
    private boolean isBioturbationSelected;
    private boolean isBioturbationUserDefined;
    private double overlyingWaterConcentration;
    private double exchangeCoefficient;
    private double bioturbationDepth;
    private double waterVelocity;
    private boolean isDegradationSelected;
    private boolean isDegradationUserDefined;
    private double degradation;
    private boolean isDepositionSelected;
    private double deposition;
    private double r3ValueForLowerBoundary;
    private double r2ValueForLowerBoundary;
    private double r1ValueForLowerBoundary;
    private double r3ValueForUpperBoundary;
    private double r2ValueForUpperBoundary;
    private double r1ValueForUpperBoundary;
    private double lowerNeumannBoundaryValue;
    private double upperNeumannBoundaryValue;
    private double lowerDirichletBoundaryValue;
    private double upperDirichletBoundaryValue;
    private String boundaryType;
    private static double initialDepth;
```

```

private static double initialConcentrationAtInitialDepth;
private static double initialConcentration;
private static String initialConcentrationFunction;
private String contaminantDescription;

public CoretransNumericalSolver(double aDepth, double aGrid, double aTime,
                                double aDensity, double aTemperature, double
anOrganicFraction,
                                String aMolarVolume, String aHalfLife, String aLogKow,
String aDescription,
                                String aPorosityChoice, double aConstantPorosity, double
aPorosityAtInterface, double aPorosityAtInfinity, double anAttenuationFactor,
double aPowerFactor, double aPowerExponent,
                                boolean diffusivityIsUserDefined, String
diffusivityChoice, double aDiffusivity,
                                boolean sorptionIsSelected, boolean
linearSorptionIsSelected, boolean linearSorptionIsUserDefined, double
theAPartitioningConstant, double theBPartitioningConstant,
                                boolean freundlichIsSelected, double
aFreundlichConstant, double aFreundlichExponent,
                                boolean langmuirIsSelected, double
aLangmuirConcentration, double aLangmuirConstant,
                                boolean advectionIsSelected, boolean
advectionIsUserDefined, double aPressureGradient, double aHydraulicConductivity,
double aSedimentPermeability,
                                boolean bioturbationIsSelected, boolean
bioturbationIsUserDefined, double anOverlyingWaterConcentration, double
anExchangeCoefficient, double aBioturbationDepth, double anInterfaceWaterVelocity,
                                boolean degradationIsSelected, boolean
degradationIsUserDefined, double aDegradationConstant,
                                boolean depositionIsSelected, double aDepositionRate,
                                String theBoundaryConditionsType, double
theUpperDirichletBoundaryValue, double theLowerDirichletBoundaryValue, double
theUpperNeumannBoundaryValue, double theLowerNeumannBoundaryValue, double
theR1ValueForUpperBoundary, double theR2ValueForUpperBoundary,
                                double theR3ValueForUpperBoundary, double
theR1ValueForLowerBoundary, double theR2ValueForLowerBoundary, double
theR3ValueForLowerBoundary,
                                String theInitialConcentrationFunction, double
anInitialConcentration, double anInitialConcentrationAtInitialDepth, double
anInitialDepth){
    setSedimentDepth(aDepth);
    setNumberOfGrids(aGrid);
    setSimulationTime(aTime);
    setSedimentDensity(aDensity);
    setWaterTemperature(aTemperature);
    setOrganicFraction(anOrganicFraction);
    setMolarVolume(aMolarVolume);
    setHalfLife(aHalfLife);
    setLogKow(aLogKow);
    setDescription(aDescription);
    setPorosityChoice(aPorosityChoice);
    setConstantPorosity(aConstantPorosity);
    setPorosityAtInterface(aPorosityAtInterface);
    setPorosityAtInfinity(aPorosityAtInfinity);
    setAttenuationFactor(anAttenuationFactor);
    setPowerFactor(aPowerFactor);
    setPowerExponent(aPowerExponent);
    setDiffusivityIsUserDefined(diffusivityIsUserDefined);
    setDiffusivityChoice(diffusivityChoice);
    setDiffusivity(aDiffusivity);
    setIsSorptionSelected(sorptionIsSelected);
    setIsLinearPartitioningSelected(linearSorptionIsSelected);
    setIsLinearSorptionUserDefined(linearSorptionIsUserDefined);
    setAPartitioningConstant(theAPartitioningConstant);
    setBPartitioningConstant(theBPartitioningConstant);
    setIsFreundlichSelected(freundlichIsSelected);
    setFreundlichConstant(aFreundlichConstant);
    setFreundlichExponent(aFreundlichExponent);
    setIsLangmuirSelected(langmuirIsSelected);
    setLangmuirConcentration(aLangmuirConcentration);
    setLangmuirConstant(aLangmuirConstant);
    setIsAdvectionSelected(advectionIsSelected);
    setAdvectionIsUserDefined(advectionIsUserDefined);
    setPressureGradient(aPressureGradient);
    setHydraulicConductivity(aHydraulicConductivity);

```

```

setSedimentPermeability(aSedimentPermeability);
setIsBioturbationSelected(bioturbationIsSelected);
setBioturbationIsUserDefined(bioturbationIsUserDefined);
setOverlyingWaterConcentration(anOverlyingWaterConcentration);
setExchangeCoefficient(anExchangeCoefficient);
setBioturbationDepth(aBioturbationDepth);
setInterfaceWaterVelocity(anInterfaceWaterVelocity);
setIsDegradationSelected(degradationIsSelected);
setDegradationIsUserDefined(degradationIsUserDefined);
setDegradationConstant(aDegradationConstant);
setIsDepositionSelected(depositionIsSelected);
setDepositionRate(aDepositionRate);
setBoundaryConditionsType(theBoundaryConditionsType);
setUpperDirichletBoundaryValue(theUpperDirichletBoundaryValue);
setLowerDirichletBoundaryValue(theLowerDirichletBoundaryValue);
setUpperNeumannBoundaryValue(theUpperNeumannBoundaryValue);
setLowerNeumannBoundaryValue(theLowerNeumannBoundaryValue);
setR1ValueForLowerBoundary(theR1ValueForLowerBoundary);
setR2ValueForLowerBoundary(theR2ValueForLowerBoundary);
setR3ValueForLowerBoundary(theR3ValueForLowerBoundary);
setR1ValueForUpperBoundary(theR1ValueForUpperBoundary);
setR2ValueForUpperBoundary(theR2ValueForUpperBoundary);
setR3ValueForUpperBoundary(theR3ValueForUpperBoundary);
setInitialConcentrationFunction(theInitialConcentrationFunction);
setInitialConcentration(anInitialConcentration);
setInitialConcentrationAtInitialDepth(anInitialConcentrationAtInitialDepth);
setInitialDepth(anInitialDepth);
}

private void setDescription(String aDescription) {
    contaminantDescription = aDescription;
}

private void setInitialConcentrationFunction(String
newInitialConcentrationFunction) {
    initialConcentrationFunction = newInitialConcentrationFunction;
}
private void setInitialConcentration(double newInitialConcentration) {
    initialConcentration = newInitialConcentration;
}
private void setInitialConcentrationAtInitialDepth(double
newInitialConcentrationAtInitialDepth) {
    initialConcentrationAtInitialDepth = newInitialConcentrationAtInitialDepth;
}
private void setInitialDepth(double newInitialDepth) {
    initialDepth = newInitialDepth;
}

private void setBoundaryConditionsType(String newBoundaryConditionsType) {
    boundaryType = newBoundaryConditionsType;
}
private void setUpperDirichletBoundaryValue(double
newUpperDirichletBoundaryValue) {
    upperDirichletBoundaryValue = newUpperDirichletBoundaryValue;
}
private void setLowerDirichletBoundaryValue(double
newLowerDirichletBoundaryValue) {
    lowerDirichletBoundaryValue = newLowerDirichletBoundaryValue;
}
private void setUpperNeumannBoundaryValue(double newUpperNeumannBoundaryValue) {
    upperNeumannBoundaryValue = newUpperNeumannBoundaryValue;
}
private void setLowerNeumannBoundaryValue(double newLowerNeumannBoundaryValue) {
    lowerNeumannBoundaryValue = newLowerNeumannBoundaryValue;
}
private void setR1ValueForUpperBoundary(double newR1ValueForUpperBoundary) {
    r1ValueForUpperBoundary = newR1ValueForUpperBoundary;
}
private void setR2ValueForUpperBoundary(double newR2ValueForUpperBoundary) {
    r2ValueForUpperBoundary = newR2ValueForUpperBoundary;
}
private void setR3ValueForUpperBoundary(double newR3ValueForUpperBoundary) {
    r3ValueForUpperBoundary = newR3ValueForUpperBoundary;
}
private void setR1ValueForLowerBoundary(double newR1ValueForLowerBoundary) {
    r1ValueForLowerBoundary = newR1ValueForLowerBoundary;
}

```

```

}
private void setR2ValueForLowerBoundary(double newR2ValueForLowerBoundary) {
    r2ValueForLowerBoundary = newR2ValueForLowerBoundary;
}
private void setR3ValueForLowerBoundary(double newR3ValueForLowerBoundary) {
    r3ValueForLowerBoundary = newR3ValueForLowerBoundary;
}

private void setDepositionRate(double aDepositionRate) {
    deposition = aDepositionRate;
}

private void setIsDepositionSelected(boolean depositionIsSelected) {
    isDepositionSelected = depositionIsSelected;
}

private void setDegradationConstant(double degradationConstant) {
    degradation = degradationConstant;
}

private void setDegradationIsUserDefined(boolean degradationIsUserDefined) {
    isDegradationUserDefined = degradationIsUserDefined;
}

private void setIsDegradationSelected(boolean degradationIsSelected) {
    isDegradationSelected = degradationIsSelected;
}

private void setInterfaceWaterVelocity(double anInterfaceWaterVelocity) {
    waterVelocity = anInterfaceWaterVelocity;
}

private void setBioturbationDepth(double aBioturbationDepth) {
    bioturbationDepth = aBioturbationDepth;
}

private void setExchangeCoefficient(double anExchangeCoefficient) {
    exchangeCoefficient = anExchangeCoefficient;
}

private void setOverlyingWaterConcentration(double
anOverlyingWaterConcentration) {
    overlyingWaterConcentration = anOverlyingWaterConcentration;
}

private void setBioturbationIsUserDefined(boolean bioturbationIsUserDefined) {
    isBioturbationUserDefined = bioturbationIsUserDefined;
}

private void setIsBioturbationSelected(boolean bioturbationIsSelected) {
    isBioturbationSelected = bioturbationIsSelected;
}

private void setSedimentPermeability(double sedimentPermeability) {
    permeability = sedimentPermeability;
}

private void setHydraulicConductivity(double aHydraulicConductivity) {
    hydraulicConductivity = aHydraulicConductivity;
}

private void setPressureGradient(double aPressureGradient) {
    pressureGradient = aPressureGradient;
}

private void setAdvectionIsUserDefined(boolean advectionIsUserDefined) {
    isAdvectionUserDefined = advectionIsUserDefined;
}

private void setIsAdvectionSelected(boolean advectionIsSelected) {
    isAdvectionSelected = advectionIsSelected;
}

private void setLangmuirConstant(double langmuirConstant) {
    b = langmuirConstant;
}

```

```

private void setLangmuirConcentration(double langmuirConcentration) {
    s = langmuirConcentration;
}

private void setIsLangmuirSelected(boolean langmuirIsSelected) {
    isLangmuirSelected = langmuirIsSelected;
}

private void setFreundlichExponent(double freundlichExponent) {
    n = freundlichExponent;
}

private void setFreundlichConstant(double freundlichConstant) {
    kf = freundlichConstant;
}

private void setIsFreundlichSelected(boolean freundlichIsSelected) {
    isFreundlichSelected = freundlichIsSelected;
}

private void setBPartitioningConstant(double theBPartitioningConstant) {
    bPartitioningConstant = theBPartitioningConstant;
}

private void setAPartitioningConstant(double theAPartitioningConstant) {
    aPartitioningConstant = theAPartitioningConstant;
}

private void setIsLinearSorptionUserDefined(boolean
linearSorptionIsUserDefined) {
    isLinearSorptionUserDefined = linearSorptionIsUserDefined;
}

private void setIsLinearPartitioningSelected(boolean linearSelected) {
    isLinearPartitioningSelected = linearSelected;
}

private void setIsSorptionSelected(boolean sorptionIsSelected) {
    isSorptionSelected = sorptionIsSelected;
}

private void setDiffusivity(double aDiffusivity) {
    theDiffusivity = aDiffusivity;
}

private void setDiffusivityChoice(String aDiffusivityChoice) {
    diffusivityChoice = aDiffusivityChoice;
}

private void setDiffusivityIsUserDefined(boolean diffusivityIsUserDefined) {
    isDiffusivityUserDefined = diffusivityIsUserDefined;
}

private void setPowerExponent(double aPowerExponent) {
    powerExponent = aPowerExponent;
}

private void setPowerFactor(double aPowerFactor) {
    powerFactor = aPowerFactor;
}

private void setAttenuationFactor(double anAttenuationFactor) {
    depthFactor = anAttenuationFactor;
}

private void setPorosityAtInfinity(double aPorosityAtInfinity) {
    porosityAtInfinity = aPorosityAtInfinity;
}

private void setPorosityAtInterface(double aPorosityAtInterface) {
    porosityAtInterface = aPorosityAtInterface;
}

private void setConstantPorosity(double aConstantPorosity) {
    constantPorosity = aConstantPorosity;
}

```

```

private void setPorosityChoice(String aPorosityChoice) {
    porosityChoice = aPorosityChoice;
}

private void setLogKow(String aLogKow) {
    logKow = Double.parseDouble(aLogKow);
}

private void setHalfLife(String aHalfLife) {
    halfLife = Double.parseDouble(aHalfLife);
}

private void setMolarVolume(String aMolarVolume) {
    molarVolume = Double.parseDouble(aMolarVolume);
}

private void setOrganicFraction(double anOrganicFraction) {
    foc = anOrganicFraction;
}

private void setWaterTemperature(double temperature) {
    waterTemperature = temperature;
}

private void setSedimentDensity(double density) {
    sedimentDensity = density;
}

private void setSimulationTime(double time) {
    simulationTime = time;
}

private void setNumberOfGrids(double grid) {
    numberOfGrids = grid;
}

public void setSedimentDepth(double depth) {
    sedimentDepth = depth;
}

class PorewaterConcentration extends PDEVariable {

    PorewaterConcentration(double xLeft, double xRight, int nPoints) {
        super(xLeft, xRight, nPoints);
    }

    public double rate() {
        return (ddx()/retardationFactor()) - ((advection()*
porosityValue()/retardationFactor()) * dx()) - (degradation() * state()) -
((bioturbation()*porosityValue()/retardationFactor()) * state()) +
(bioturbationConstantTerm()*porosityValue()/retardationFactor()) + (deposition() *
dx());
    }

    public double D() {

        return diffusivity()* porosityValue(); }

    public double initialState() {
        double initial = 0;
        if (initialConcentrationFunction.equals("constant")){
            initial = initialConcentration;
        } else if (initialConcentrationFunction.equals("step")){
            if (x() <= initialDepth/100.0){
                initial = initialConcentrationAtInitialDepth;
            } else initial = 0;
        }
        return initial;
    }
}

```

```

}

public double b1Left() {

double b1Left = 0;
if (boundaryType.equals("dirichlet")){
    b1Left = 1;
} else if (boundaryType.equals("neumann")){
    b1Left = 0;
} else if (boundaryType.equals("robin")){
    b1Left = r1ValueForLowerBoundary;
}
return b1Left; }

public double b2Left() {

double b2Left = 0;
if (boundaryType.equals("dirichlet")){
    b2Left = 0;
} else if (boundaryType.equals("neumann")){
    b2Left = 1;
} else if (boundaryType.equals("robin")){
    b2Left = r2ValueForLowerBoundary;
}
return b2Left; }

public double b3Left() {

double b3Left = 0;
if (boundaryType.equals("dirichlet")){
    b3Left = lowerDirichletBoundaryValue;
} else if (boundaryType.equals("neumann")){
    b3Left = lowerNeumannBoundaryValue;
} else if (boundaryType.equals("robin")){
    b3Left = r3ValueForLowerBoundary;
}
return b3Left; }

public double b1Right() {

double b1Right = 0;
if (boundaryType.equals("dirichlet")){
    b1Right = 1;
} else if (boundaryType.equals("neumann")){
    b1Right = 0;
} else if (boundaryType.equals("robin")){
    b1Right = r1ValueForUpperBoundary;
}
return b1Right; }

public double b2Right() {

double b2Right = 0;
if (boundaryType.equals("dirichlet")){
    b2Right = 0;
} else if (boundaryType.equals("neumann")){
    b2Right = 1;
} else if (boundaryType.equals("robin")){
    b2Right = r2ValueForUpperBoundary;
}
return b2Right;}

public double b3Right() {

double b3Right = 0;
if (boundaryType.equals("dirichlet")){
    b3Right = upperDirichletBoundaryValue;
} else if (boundaryType.equals("neumann")){
    b3Right = upperNeumannBoundaryValue;
} else if (boundaryType.equals("robin")){
    b3Right = r3ValueForUpperBoundary;
}
return b3Right; }

private double porosityValue(){

double porosity = 1;

```

```

        if (porosityChoice.equals("constant")){
            porosity = constantPorosity;
        } else if (porosityChoice.equals("linear")){
            porosity = porosityAtInfinity + (porosityAtInterface -
porosityAtInfinity) * (1 - (x()/depthFactor));
        } else if (porosityChoice.equals("exponential")){
            porosity = porosityAtInfinity + (porosityAtInterface -
porosityAtInfinity) * Math.pow(Math.E, (-1*x()/depthFactor));
        } else if (porosityChoice.equals("inverse")){
            porosity = (porosityAtInfinity * porosityAtInterface)/
(Math.pow(Math.E, (-1*x()/depthFactor)));
        } else if (porosityChoice.equals("power")){
            porosity = powerFactor * Math.pow(x()*1000.0, -1*powerExponent);
        }
        return porosity;
    }

    private double viscosity(){

        double exponent = -10.2158 + (1792.5/waterTemperature) + (0.01773 *
waterTemperature) + (-1.2631E-5 * Math.pow(waterTemperature,2));
        double viscosity = Math.pow(10,exponent);
        return viscosity;
    }

    private double diffusivity(){

        double diffusivity = 0;
        double tortousity = 1-Math.log(Math.pow(porosityValue(),2.0));

        if (isDiffusivityUserDefined == true){

            diffusivity = theDiffusivity;
        } else {

            double theoreticalDiffusivity = 0;
            if (diffusivityChoice.equals("Wilke-Chang")){
                theoreticalDiffusivity = 5.06E-7 * waterTemperature / (viscosity() *
Math.pow(molarVolume,0.6));
            }
            if (diffusivityChoice.equals("Reddy-Doraiswamy")){
                theoreticalDiffusivity = 1.61E-7 * waterTemperature / (viscosity() *
Math.pow(molarVolume, (1.0/3)));
            }
            if (diffusivityChoice.equals("Hayduk-Laudie")){
                theoreticalDiffusivity = 13.26E-5 * Math.pow(viscosity(),-1.14) *
Math.pow(molarVolume,-0.589);
            }
            diffusivity = theoreticalDiffusivity / tortousity ;
        }

        return diffusivity * 60.48;
    }

    public double logKoc(){
        double logKoc = 0;
        if (contaminantDescription.equals("PAH")){
            logKoc = (0.98 * logKow) - 0.32;
        } else if (contaminantDescription.equals("PCB")){
            logKoc = (0.74* logKow) + 0.15;
        } else if (contaminantDescription.equals("pesticide")){
            logKoc = (0.904* logKow) - 0.542;
        }
        return logKoc;
    }

    private double isothermValue(){

        double linearIsotherm = 0;
        double freundlichIsotherm = 0;
        double langmuirIsotherm = 0;

```



```

if (isLinearPartitioningSelected == true){
    if (isLinearSorptionUserDefined == false){
        linearIsotherm = foc * Math.pow(10,logKoc());
    } else {
        linearIsotherm = aPartitioningConstant * Math.pow(x()*1000.0,-
1*bPartitioningConstant);
    }
}

if (isFreundlichSelected == true){
    freundlichIsotherm = n * kf * (Math.pow(state(),(n-1))); // *
Math.pow(0.000001,n)
}
if (isLangmuirSelected == true){
    langmuirIsotherm = -1*s*b/(Math.pow((1+b*state()),2));
}

return linearIsotherm + freundlichIsotherm + langmuirIsotherm;
}

public double retardationFactor(){
    double retardationFactor = porosityValue();

    if (isSorptionSelected == true){
        retardationFactor = porosityValue()+ (sedimentDensity *
isothermValue());
    }

    return retardationFactor;
}

public double advection(){
    double jAdv = 0;
    double advectionVelocity = 0;

    if (isAdvectionSelected == true){
        jAdv = 1;
        if (isAdvectionUserDefined == true){
            double advectionVelocityInPerSecond = permeability *
pressureGradient / (porosityValue()* viscosity() * 0.001); // 0.001 = cP to Pa.s
            advectionVelocity = advectionVelocityInPerSecond * 84600 * 7; // to
per week
        } else {
            double sedimentPermeability = hydraulicConductivity * viscosity()*
0.1 / 9800.0; // 0.1 = cP to Pa.s 9800 = (g) 9.8 x (density) 1000
            double advectionVelocityInPerSecond = sedimentPermeability *
pressureGradient / (porosityValue()* viscosity() * 0.001); // 0.001 = cP to Pa.s
            advectionVelocity = advectionVelocityInPerSecond * 84600 * 7; // to
per week
        }
    }

    return jAdv * advectionVelocity;
}

private double deposition(){
    double jDepo = 0;
    double depositionRate = 0;
    if (isDepositionSelected == true){
        jDepo = 1;

        depositionRate = deposition / (100 * 52 * 260); // 100 - cm to m, 52 -
year to weeks
    }
    return jDepo * depositionRate;
}

```

```

public double bioturbation(){
    double jBio = 0;
    double theExchangeCoefficient = 0;
    if (isBioturbationSelected == true){
        jBio = 1;
        if (isBioturbationUserDefined == true){
            theExchangeCoefficient = exchangeCoefficient;
        } else {
            // calculates the Koc * foc terms
            double KocFoc = foc * Math.pow(10,logKoc());
            double massTransferCoefficient = 0.036 *
Math.pow(bioturbationDepth/10.0, -0.2) * Math.pow(diffusivity(),2.0/3) *
Math.pow((waterVelocity*100),0.8) * Math.pow(viscosity()/1000.0,-0.466);
            double exchangeCoefficientInPerSecond = 1 / (
(bioturbationDepth/10.0) * ((1 / massTransferCoefficient) +
((bioturbationDepth/10.0) / (diffusivity()* KocFoc * sedimentDensity)))));
            theExchangeCoefficient = exchangeCoefficientInPerSecond * 86400 * 7;
        }
    }
    return jBio * theExchangeCoefficient;
}

private double bioturbationConstantTerm(){
    double constantTerm = 0;
    if (isBioturbationSelected == true){
        constantTerm = bioturbation() * b3Left()*
porosityValue()/retardationFactor();//overlyingWaterConcentration;
    }
    return constantTerm;
}

public double degradation(){
    double jDeg = 0;
    double degradationRate = 0;
    if (isDegradationSelected == true){
        jDeg = 1;
        if (isDegradationUserDefined == true){
            degradationRate = (degradation*7.0);
        } else {
            degradationRate = (Math.log(2) / (halfLife / 7));
        }
    }
    return jDeg * degradationRate;
}

}

public void actions() {
    dtMin = 1.0e-10; dtMax = 1.0;
    maxAbsError = maxRelError = 1.0e-10;
    thePorewaterConcentration = new PorewaterConcentration(0,
sedimentDepth/100.0, (int) numberOfGrids);
    thePorewaterConcentration.start();
    hold(simulationTime);
    double logKoc = thePorewaterConcentration.logKoc();
    thePorewaterConcentration.show("Porewater Concentration-Depth Profile");
    thePorewaterConcentration.showMore("Sediment-bound Concentration-Depth
Profile", isLinearPartitioningSelected, isLinearSorptionUserDefined,
aPartitioningConstant, bPartitioningConstant, foc, logKoc,
isFreundlichSelected, n, kf, isLangmuirSelected, s, b);
    thePorewaterConcentration.print("Porewater Concentration-Depth Profile");
    thePorewaterConcentration.printMore("Sediment-bound Concentration-Depth
Profile", isLinearPartitioningSelected, isLinearSorptionUserDefined,
aPartitioningConstant, bPartitioningConstant, foc, logKoc,
isFreundlichSelected, n, kf, isLangmuirSelected, s, b);
}
}
}

```

Appendix B. Program code for CoReTranS GUI

```
/*
 * Created on 29-Sep-2006
 *
 * Jason Go
 */
package coretransProject2;

import java.awt.event.ActionEvent;
import java.awt.event.ActionListener;
import java.awt.event.KeyEvent;

import javax.swing.BorderFactory;
import javax.swing.ButtonGroup;
import javax.swing.DefaultListModel;
import javax.swing.ImageIcon;
import javax.swing.JButton;
import javax.swing.JFileChooser;
import javax.swing.JFormattedTextField;
import javax.swing.JFrame;
import javax.swing.JLabel;
import javax.swing.JList;
import javax.swing.JMenu;
import javax.swing.JMenuBar;
import javax.swing.JOptionPane;
import javax.swing.JPanel;
import javax.swing.JRadioButton;
import javax.swing.JTextPane;
import javax.swing.ListSelectionModel;

import java.awt.BorderLayout;
import java.awt.Color;
import java.awt.FlowLayout;
import java.awt.Font;
import java.beans.PropertyChangeEvent;
import java.beans.PropertyChangeListener;

import java.io.File;
import java.io.IOException;

import java.text.DecimalFormat;
import java.text.NumberFormat;
import java.util.Calendar;
import java.util.GregorianCalendar;
import java.util.Vector;

import javax.swing.JTabbedPane;
import javax.swing.JScrollPane;
import javax.swing.SwingConstants;
import javax.swing.border.TitledBorder;

import javax.swing.JTextArea;
import javax.swing.KeyStroke;
import javax.swing.JTextField;
import javax.swing.JMenuItem;
import javax.swing.JSeparator;
import javax.swing.WindowConstants;
import javax.swing.border.BevelBorder;

import coretransProject2.CoretransNumericalSolver;

/**
 * This code was generated using CloudGarden's Jigloo
 * SWT/Swing GUI Builder, which is free for non-commercial
 * use. If Jigloo is being used commercially (ie, by a corporation,
 * company or business for any purpose whatever) then you
 * should purchase a license for each developer using Jigloo.
 * Please visit www.cloudgarden.com for details.
 * Use of Jigloo implies acceptance of these licensing terms.
 * *****
 * A COMMERCIAL LICENSE HAS NOT BEEN PURCHASED
 * for this machine, so Jigloo or this code cannot be used legally
 * for any corporate or commercial purpose.
 * *****
 */
```

```

*/
public class CoretransInterface extends JFrame implements ActionListener,
PropertyChangeListener {

    private JMenuBar menuBar;
    private JTabbedPane simulationParameters;
    private JPanel modelParameterPanel;
    private JButton sorptionButton;
    private JButton advectionButton;
    private JLabel organicFractionLabel;
    private JFormattedTextField waterTemperature;
    private JLabel waterTemperatureLabel;
    private JFormattedTextField sedimentDensity;
    private JLabel sedimentDensityLabel;
    private JFormattedTextField sedimentDepth;
    private JLabel sedimentDepthLabel;
    private JButton depositionButton;
    private JButton degradationButton;
    private JButton bioturbationButton;
    private JButton diffusionButton;
    private JScrollPane contaminantScrollPane;
    private JFormattedTextField organicFraction;
    private JPanel sedimentParameterPanel;
    private JPanel contaminantSelectionPanel;
    private JPanel modelSelectionPanel;
    private JPanel summaryPanel;
    private JTabbedPane selectionTabs;
    private JPanel advectionPanel;
    private JPanel depositionPanel;
    private JPanel degradationPanel;
    private JPanel bioturbationPanel;
    private JPanel sorptionPanel;
    private JPanel bannerPane;
    private JPanel entryPanel;
    private JMenuItem exit;
    private JSeparator menuSeparator;
    private JMenu menu;
    private JMenuItem open;
    private JMenuItem save;
    private JMenuItem help;
    private JLabel modelBanner;
    private JTextPane modelText;
    private JPanel buttonPane;
    private JButton readyButton;
    private JButton nextButton;
    private JButton exitButton;
    private JPanel integrationParameterPanel;
    private JPanel diffusionPanel;
    private ButtonGroup porosityProfile;
    private int diffusionIndex;
    private int sorptionIndex;
    private int advectionIndex;
    private int bioturbationIndex;
    private int degradationIndex;
    private int depositionIndex;
    private JFormattedTextField freundlichExponent;
    private JLabel freundlichExponentLabel;
    private JFormattedTextField freundlichConstant;
    private JLabel freundlichConstantLabel;
    private JFormattedTextField bConstantLinear;
    private JLabel bConstantLinearLabel;
    private JFormattedTextField aConstantLinear;
    private JLabel aConstantForLinearLabel;
    private JPanel langmuirDataPanel;
    private JPanel freundlichDataPanel;
    private JPanel linearPartitioningDataPanel;
    private JRadioButton langmuirButton;
    private JRadioButton freundlichButton;
    private JRadioButton linearPartitioningButton;
    private JPanel langmuirPanel;
    private JPanel freundlichPanel;
    private JPanel linearPartitioningPanel;
    private JButton haydukLaudieButton;
    private JButton reddyDoraiswamyButton;
    private JButton wilkeChangButton;
    private JPanel empiricalDiffusivityPanel;

```

```

private JRadioButton approximatedDiffusivityButton;
private JFormattedTextField userDefinedDiffusivity;
private JLabel userDefinedDiffusivityLabel;
private JRadioButton userDefinedDiffusivityButton;
private JPanel approximatedDiffusionPanel;
private JFormattedTextField exchangeCoefficient;
private JFormattedTextField depositionRate;
private JLabel depositionRateLabel;
private JFormattedTextField degradationConstant;
private JLabel degradationConstantLabel;
private JRadioButton userDefinedDegradationConstantButton;
private JRadioButton approximatedDegradationConstantButton;
private JFormattedTextField waterVelocity;
private JLabel waterVelocityButton;
private JFormattedTextField bioturbationDepth;
private JLabel bioturbationDepthLabel;
private JRadioButton approximatedBioturbationConstantButton;
private JLabel exchangeCoefficientLabel;
private JRadioButton userDefinedBioturbationConstantButton;
private JPanel bioturbationExchangeCoefficientPanel;
private JFormattedTextField overlyingWaterConcentration;
private JLabel overlyingWaterConcentrationButton;
private JFormattedTextField hydraulicConductivity;
private JLabel hydraulicConductivityLabel;
private JRadioButton approximatedVelocityButton;
private JFormattedTextField sedimentPermeability;
private JLabel sedimentPermeabilityLabel;
private JRadioButton userDefinedVelocityButton;
private JPanel advectiveVelocityPanel;
private JFormattedTextField pressureGradient;
private JLabel pressureGradientLabel;
private JFormattedTextField langmuirConstant;
private JLabel langmuirConstantLabel;
private JFormattedTextField langmuirConcentration;
private JLabel langmuirConcentrationLabel;
private JPanel userDefinedDiffusionPanel;
private ButtonGroup boundaryConditionsGroup;
private JPanel boundaryChoicesPanel;
private JFormattedTextField initialConcentration;
private JLabel initialConcentrationLabel;
private JFormattedTextField numberOfGrids;
private JLabel numberOfGridsLabel;
private JFormattedTextField simulationTime;
private JLabel simulationTimeLabel;
private JButton addContaminantButton;
private ButtonGroup diffusionGroup;
private ButtonGroup advectionGroup;
private ButtonGroup bioturbationGroup;
private ButtonGroup degradationGroup;
private ButtonGroup porosityGroup;
private ButtonGroup initialConditionsGroup;
private ButtonGroup boundaryGroup;
private NumberFormat valueFormat;
private double aSedimentDepth = 0;
private double aSedimentDensity = 0;
private double aWaterTemperature = 273;
private double anOrganicFractionContent = 0;
private double aSimulationTime = 0;
private double aNumberOfGrids = 0;
private double anInitialConcentration = 0;
private double aDiffusivity = 0;
private double anAConstant = 0;
private double aBConstant = 0;
private double aFreundlichConstant = 0;
private double aFreundlichExponent = 0;
private double aLangmuirConcentration = 0;
private double aLangmuirConstant = 0;
private double aPressureGradient = 0;
private double aSedimentPermeability = 0;
private double aHydraulicConductivity = 0;
private double anOverlyingWaterConcentration = 0;
private double anExchangeCoefficient = 0;
private double aBioturbationDepth = 0;
private double anInterfaceWaterVelocity = 0;
private double aDegradationConstant = 0;
private double aDepositionRate = 0;
private double aConstantPorosity = 0;

```

```

private double aPorosityAtInterface = 0;
private double aPorosityAtInfinity = 0;
private double anAttenuationFactor = 0;
private double aPowerFactor = 0;
private double aPowerExponent = 0;
private double anInitialDepth = 0;
private double anInitialConcentrationAtInitialDepth = 0;
private double aDirichletLowerBoundary = 0;
private double aDirichletUpperBoundary = 0;
private double aNeumannLowerBoundary = 0;
private double aNeumannUpperBoundary = 0;
private double aLowerConcentrationCoefficient = 0;
private double anUpperConcentrationCoefficient = 0;
private double aLowerFluxCoefficient = 0;
private double anUpperFluxCoefficient = 0;
private double aRobinLowerCondition = 0;
private double aRobinUpperCondition = 0;
private JList contaminantList;
private ContaminantDataAccess access;
private JButton cancelUpdateButton;
private JButton updateDatabaseButton;
private JTextField logKow;
private JLabel logKowLabel;
private JTextField halfLife;
private JLabel halfLifeLabel;
private JTextField molarVolume;
private JLabel molarVolumeLabel;
private JTextField molecularWeight;
private JLabel molecularWeightLabel;
private JTextField description;
private JLabel descriptionLabel;
private JTextField molecularFormula;
private JLabel molecularFormulaLabel;
private JTextField casRegistryNum;
private JLabel casRegistryNumLabel;
private JLabel contaminantLabel;
private JPanel updateDatabasePanel;
private JTextArea modelSummaryText;
private JButton linearUserButton;
private JButton linearDatabaseButton;
private JPanel linearPanel;
private JFormattedTextField robinUpperBoundary;
private JFormattedTextField robinLowerBoundary;
private JLabel robinGap2;
private JFormattedTextField robinUpperFluxCoefficient;
private JFormattedTextField robinLowerFluxCoefficient;
private JLabel robinGap;
private JFormattedTextField robinUpperConcentrationCoefficient;
private JFormattedTextField robinLowerConcentrationCoefficient;
private JRadioButton robinButton;
private JPanel robinPanel;
private JFormattedTextField neumannUpperBoundary;
private JLabel neumannUpperBoundaryLabel;
private JLabel neumannGap;
private JFormattedTextField neumannLowerBoundary;
private JLabel neumannLowerBoundaryLabel;
private JRadioButton neumannButton;
private JPanel neumannPanel;
private JFormattedTextField dirichletUpperBoundary;
private JLabel dirichletUpperBoundaryLabel;
private JLabel dirichletGap;
private JFormattedTextField dirichletLowerBoundary;
private JLabel dirichletLowerConditionLabel;
private JRadioButton dirichletButton;
private JPanel dirichletPanel;
private JFormattedTextField initialConcentrationAtInitialDepth;
private JLabel initialConcentrationAtInitialDepthLabel;
private JFormattedTextField initialDepthPenetration;
private JLabel initialDepthPenetrationLabel;
private JRadioButton stepFunctionInitialButton;
private JPanel stepInitialPanel;
private JRadioButton constantInitialConcentrationButton;
private JPanel constantInitialPanel;
private JFormattedTextField powerExponent;
private JLabel powerExponentLabel;
private JLabel gapLabel;
private JFormattedTextField powerFactor;

```

```

private JLabel powerFactorLabel;
private JRadioButton powerPorosityButton;
private JPanel powerPorosityPanel;
private JFormattedTextField attenuationFactor;
private JLabel attenuationFactorLabel;
private JRadioButton inverseExponentialButton;
private JFormattedTextField porosityAtInfinity;
private JLabel porosityAtInfinityLabel;
private JRadioButton exponentialPorosityButton;
private JFormattedTextField porosityAtInterface;
private JLabel porosityAtInterfaceLabel;
private JRadioButton linearPorosityButton;
private JPanel otherPorosityPanel;
private JFormattedTextField constantPorosity;
private JLabel constantPorosityLabel;
private JRadioButton constantPorosityButton;
private JPanel constantPorosityPanel;
private JPanel initialConditionsPanel;
private JPanel boundaryPanel;
private JPanel porosityPanel;
private Vector data;
DefaultListModel contaminantNames;
private ContaminantData contaminantData;
private String contaminantName;
private String contaminantMolarVolume;
private String contaminantHalfLife;
private String contaminantLogKow;
private boolean diffusionIsSelected = false;
private boolean sorptionIsSelected = false;
private boolean advectionIsSelected = false;
private boolean bioturbationIsSelected = false;
private boolean degradationIsSelected = false;
private boolean depositionIsSelected = false;
private boolean diffusivityIsUserDefined = false;
private boolean linearPartitioningIsSelected = false;
private boolean freundlichIsSelected = false;
private boolean langmuirIsSelected = false;
private boolean advectionIsUserDefined = false;
private boolean bioturbationIsUserDefined = false;
private boolean degradationIsUserDefined = false;
private String diffusivityChoice;
private String porosityChoice;
private String initialConcentrationFunction;
private String boundaryChoice;
private final static String newline = "\n";
private final static String newtab = "\t";
private boolean linearParameterIsUserDefined = false;
private JScrollPane modelSummaryScrollPane;
private GregorianCalendar c;
private String mechanisms;
private Vector parameters;
private String conditions;
private Vector model = new Vector();
private String contaminantCAS;
private String contaminantMF;
private String contaminantMW;
private Vector modelParameters;
CoretransNumericalSolver solver;
private String porosity;
private Vector isotherm = new Vector();
private ImageIcon icon;
private final JFileChooser fc = new JFileChooser();
private double resetValue = 0;
private JMenuItem helpFile;
private String mechanism = "";
private String isotherms = "";
private String initial;
private String boundary;
private String points = "";
private String morePoints = "";
private JTextField newContaminantName;
private String contaminantDescription;

public static void main(String[] args){
    CoretransInterface mainGUI = new CoretransInterface();
}

```

```

public CoretransInterface() {
    super();
    valueFormat = NumberFormat.getNumberInstance();
    access = new ContaminantDataAccess();
    access.initialise("ucesjgo", "ortega");

    initGUI();
}

{
    //Set Look & Feel
    try {

javax.swing.UIManager.setLookAndFeel("javax.swing.plaf.metal.MetalLookAndFeel")
;
    } catch(Exception e) {
        e.printStackTrace();
    }
}

private void initGUI() {
    try {
        /*
         * Set menu bar at the top of the interface window
         * Contains two menu: File and Help
         * File menu contains three items: Load, Save and Exit
         */
        {
            menuBar = new JMenuBar();
            setJMenuBar(menuBar);
            menuBar.setBackground(new java.awt.Color(130,192,255));
            {
                menu = new JMenu("    File    ");
                menuBar.add(menu);
                menu.setMnemonic(KeyEvent.VK_F);
                menu.setPopupMenuVisible(true);
                menu.setBackground(new java.awt.Color(130,192,255));

                {

                    open = new JMenuItem("        Open");
                    menu.add(open);
                    open.setMnemonic(KeyEvent.VK_O);
                    open.setAccelerator(KeyStroke.getKeyStroke(KeyEvent.VK_O,
ActionEvent.CTRL_MASK));
                    open.addActionListener(this);
                }
                {

                    save = new JMenuItem("        Save");
                    menu.add(save);
                    save.setMnemonic(KeyEvent.VK_S);
                    save.setAccelerator(KeyStroke.getKeyStroke(KeyEvent.VK_S,
ActionEvent.CTRL_MASK));
                    save.addActionListener(this);
                }
                {

                    menuSeparator = new JSeparator();
                    menu.add(menuSeparator);
                }
                {

                    exit = new JMenuItem("        Exit");
                    menu.add(exit);
                    exit.setMnemonic(java.awt.event.KeyEvent.VK_X);
                    exit.setAccelerator(KeyStroke.getKeyStroke(KeyEvent.VK_X,
ActionEvent.CTRL_MASK));
                }
            }
            {

                help = new JMenu();
                menuBar.add(help);
                help.setText("    Help    ");
                help.setMnemonic(java.awt.event.KeyEvent.VK_H);
                help.setBackground(new java.awt.Color(130,192,255));
                {

```



```

        helpFile = new JMenuItem("    About CORETRANS 1.0");
        helpFile.setAccelerator(KeyStroke.getKeyStroke(KeyEvent.VK_C,
ActionEvent.CTRL_MASK));
        help.add(helpFile);
    }
}
setDefaultCloseOperation(WindowConstants.DISPOSE_ON_CLOSE);
this.setTitle("Welcome to CoReTranS 1.0!");
this.setName("mainFrame");
this.setVisible(false);
{
    bannerPane = new JPanel();
    this.getContentPane().add(bannerPane, BorderLayout.NORTH);
    {
        icon = new
ImageIcon(getClass().getResource("images/coretransLogo.JPG"));
        modelBanner = new JLabel("oReTranS", icon, JLabel.LEFT);
        bannerPane.add(modelBanner);
        modelBanner.setFont(new Font("Impact", Font.BOLD, 21));
        modelBanner.setForeground(Color.blue);
        modelBanner.setPreferredSize(new java.awt.Dimension(745, 101));

        modelBanner.setBorder(BorderFactory.createBevelBorder(BevelBorder.RAISED));
        {
            modelText = new JTextPane();
            modelBanner.add(modelText);
            modelText.setText("A numerical modelling environment for organic
contaminant " +
                "reaction and transport in layered bed sediments capable of
predicting: " +
                "contaminant profiles as a function of bed sediment depth,
on the basis " +
                "of input information about contaminant concentrations in
the water column; " +
                "or contaminant concentrations in the water column, on the
basis of input " +
                "information about the contaminant profile in the bed
sediments.");

            modelText.setBounds(206, 6, 531, 89);
            modelText.setOpaque(false);
            modelText.setEditable(false);
        }
    }
}
{
    entryPanel = new JPanel();
    this.getContentPane().add(entryPanel, BorderLayout.CENTER);
    entryPanel.setAutoscrolls(true);
    {
        selectionTabs = new JTabbedPane();
        entryPanel.add(selectionTabs);
        selectionTabs.setPreferredSize(new java.awt.Dimension(733, 484));
        selectionTabs.setTabPlacement(JTabbedPane.RIGHT);

        {
            modelParameterPanel = new JPanel();
            selectionTabs.addTab("Contaminant Model", null,
modelParameterPanel, null);
            {
                modelSelectionPanel = new JPanel();
                FlowLayout modelSelectionPanelLayout = new FlowLayout();
                modelSelectionPanelLayout.setHgap(10);

                modelSelectionPanel.setLayout(modelSelectionPanelLayout);
                modelParameterPanel.add(modelSelectionPanel);
                modelSelectionPanel.setPreferredSize(new
java.awt.Dimension(292, 250));

                modelSelectionPanel.setBorder(BorderFactory.createTitledBorder("Select
mechanisms to model"));
                {
                    diffusionButton = new JButton();
                    modelSelectionPanel.add(diffusionButton);
                    diffusionButton.setText("Diffusion");
                }
            }
        }
    }
}

```

```

        diffusionButton.setPreferredSize(new
java.awt.Dimension(200, 30));

        diffusionButton.setBorder(BorderFactory.createBevelBorder(BevelBorder.RAISED));
        diffusionButton.addActionListener(this);
    }
    {
        sorptionButton = new JButton();
        modelSelectionPanel.add(sorptionButton);
        sorptionButton.setText("Sorption");
        sorptionButton.setPreferredSize(new java.awt.Dimension(200,
30));

        sorptionButton.setBorder(BorderFactory.createBevelBorder(BevelBorder.RAISED));
        sorptionButton.addActionListener(this);
    }
    {
        advectionButton = new JButton();
        modelSelectionPanel.add(advectionButton);
        advectionButton.setText("Advection");
        advectionButton.setPreferredSize(new
java.awt.Dimension(200, 30));

        advectionButton.setBorder(BorderFactory.createBevelBorder(BevelBorder.RAISED));
        advectionButton.addActionListener(this);
    }
    {
        bioturbationButton = new JButton();
        modelSelectionPanel.add(bioturbationButton);
        bioturbationButton.setText("Bioturbation");
        bioturbationButton.setPreferredSize(new
java.awt.Dimension(200, 30));

        bioturbationButton.setBorder(BorderFactory.createBevelBorder(BevelBorder.RAISED
));
        bioturbationButton.addActionListener(this);
    }
    {
        degradationButton = new JButton();
        modelSelectionPanel.add(degradationButton);
        degradationButton.setText("Degradation");
        degradationButton.setPreferredSize(new
java.awt.Dimension(200, 30));

        degradationButton.setBorder(BorderFactory.createBevelBorder(BevelBorder.RAISED
));
        degradationButton.addActionListener(this);
    }
    {
        depositionButton = new JButton();
        modelSelectionPanel.add(depositionButton);
        depositionButton.setText("Deposition");
        depositionButton.setPreferredSize(new
java.awt.Dimension(200, 30));

        depositionButton.setBorder(BorderFactory.createBevelBorder(BevelBorder.RAISED))
;
        depositionButton.addActionListener(this);
    }
    {
        contaminantSelectionPanel = new JPanel();
        FlowLayout contaminantSelectionPanelLayout = new FlowLayout();
        contaminantSelectionPanelLayout.setVgap(10);

        contaminantSelectionPanel.setLayout(contaminantSelectionPanelLayout);
        modelParameterPanel.add(contaminantSelectionPanel);
        contaminantSelectionPanel.setPreferredSize(new
java.awt.Dimension(266, 250));

        contaminantSelectionPanel.setBorder(BorderFactory.createTitledBorder("Select
contaminant species"));
    }
    {
        contaminantNames = new DefaultListModel();
        data = new Vector();
        data = access.getAll();
        for (int i = 0; i < data.size(); i++){

```

```

        contaminantData = (ContaminantData)data.get(i);
        String name = contaminantData.getContaminant();
        contaminantNames.addElement(name);
    }

    contaminantList = new JList(contaminantNames);

    contaminantList.setSelectionMode(ListSelectionModel.SINGLE_SELECTION);
    contaminantList.setLayoutOrientation(JList.VERTICAL);

    contaminantScrollPane = new JScrollPane(contaminantList);

    contaminantSelectionPanel.add(contaminantScrollPane);
    contaminantScrollPane.setPreferredSize(new
java.awt.Dimension(208, 163));
    contaminantScrollPane.setOpaque(false);
    }
    {
        addContaminantButton = new JButton();
        contaminantSelectionPanel.add(addContaminantButton);
        addContaminantButton.setText("Add");

        addContaminantButton.setBorder(BorderFactory.createBevelBorder(BevelBorder.RAISED));
        addContaminantButton.setPreferredSize(new
java.awt.Dimension(73, 30));
        addContaminantButton.addActionListener(this);
    }
    {
        updateDatabaseButton = new JButton();
        contaminantSelectionPanel
            .add(updateDatabaseButton);
        updateDatabaseButton.setText("Ok");
        updateDatabaseButton.setPreferredSize(new
java.awt.Dimension(70, 30));

        updateDatabaseButton.setBorder(BorderFactory.createBevelBorder(BevelBorder.RAISED));
        updateDatabaseButton.setEnabled(false);
        updateDatabaseButton.addActionListener(this);
    }
    {
        cancelUpdateButton = new JButton();
        contaminantSelectionPanel
            .add(cancelUpdateButton);
        cancelUpdateButton.setText("Cancel");
        cancelUpdateButton.setPreferredSize(new
java.awt.Dimension(78, 30));

        cancelUpdateButton.setBorder(BorderFactory.createBevelBorder(BevelBorder.RAISED));
        cancelUpdateButton.addActionListener(this);
    }
    {
        updateDatabasePanel = new JPanel();
        modelParameterPanel.add(updateDatabasePanel);
        updateDatabasePanel.setPreferredSize(new
java.awt.Dimension(567, 210));

        updateDatabasePanel.setBorder(BorderFactory.createTitledBorder("Update Database
Entry"));
        {
            contaminantLabel = new JLabel();
            updateDatabasePanel.add(contaminantLabel);
            contaminantLabel.setText("Contaminant name");
            contaminantLabel.setPreferredSize(new
java.awt.Dimension(120, 27));
        }
        {
            newContaminantName = new JTextField();
            updateDatabasePanel.add(newContaminantName);
            newContaminantName.setPreferredSize(new
java.awt.Dimension(145, 35));

            newContaminantName.setBorder(BorderFactory.createBevelBorder(BevelBorder.LOWERED));

```

```

        newContaminantName.setEditable(false);
    }
    {
        casRegistryNumLabel = new JLabel();
        updateDatabasePanel.add(casRegistryNumLabel);
        casRegistryNumLabel.setText("CAS Registry Num");
        casRegistryNumLabel.setPreferredSize(new
java.awt.Dimension(120, 27));
    }
    {
        casRegistryNum = new JTextField();
        updateDatabasePanel.add(casRegistryNum);
        casRegistryNum.setPreferredSize(new java.awt.Dimension(145,
35));
        casRegistryNum.setBorder(BorderFactory.createBevelBorder(BevelBorder.LOWERED));
        casRegistryNum.setEditable(false);
    }
    {
        molecularFormulaLabel = new JLabel();
        updateDatabasePanel.add(molecularFormulaLabel);
        molecularFormulaLabel.setText("Molecular formula");
        molecularFormulaLabel.setPreferredSize(new
java.awt.Dimension(120, 27));
    }
    {
        molecularFormula = new JTextField();
        updateDatabasePanel.add(molecularFormula);
        molecularFormula.setPreferredSize(new
java.awt.Dimension(145, 35));
        molecularFormula.setBorder(BorderFactory.createBevelBorder(BevelBorder.LOWERED)
);
        molecularFormula.setEditable(false);
    }
    {
        descriptionLabel = new JLabel();
        updateDatabasePanel.add(descriptionLabel);
        descriptionLabel.setText("Contaminant type");
        descriptionLabel.setPreferredSize(new
java.awt.Dimension(120, 27));
    }
    {
        description = new JTextField();
        updateDatabasePanel.add(description);
        description.setPreferredSize(new java.awt.Dimension(145,
35));
        description.setBorder(BorderFactory.createBevelBorder(BevelBorder.LOWERED));
        description.setEditable(false);
    }
    {
        molecularWeightLabel = new JLabel();
        updateDatabasePanel.add(molecularWeightLabel);
        molecularWeightLabel.setText("Molecular weight");
        molecularWeightLabel.setPreferredSize(new
java.awt.Dimension(120, 27));
    }
    {
        molecularWeight = new JTextField();
        updateDatabasePanel.add(molecularWeight);
        molecularWeight.setPreferredSize(new
java.awt.Dimension(145, 35));
        molecularWeight.setBorder(BorderFactory.createBevelBorder(BevelBorder.LOWERED))
;
        molecularWeight.setEditable(false);
    }
    {
        molarVolumeLabel = new JLabel();
        updateDatabasePanel.add(molarVolumeLabel);
        molarVolumeLabel.setText("Molar volume");
        molarVolumeLabel.setPreferredSize(new
java.awt.Dimension(120, 27));
    }
    {
        molarVolume = new JTextField();

```

```

        updateDatabasePanel.add(molarVolume);
        molarVolume.setPreferredSize(new java.awt.Dimension(145,
35));

        molarVolume.setBorder(BorderFactory.createBevelBorder(BevelBorder.LOWERED));
        molarVolume.setEditable(false);
        {
            halfLifeLabel = new JLabel();
            updateDatabasePanel.add(halfLifeLabel);
            halfLifeLabel.setText("Half Life (/day)");
            halfLifeLabel.setPreferredSize(new java.awt.Dimension(120,
27));
        }
        {
            halfLife = new JTextField();
            updateDatabasePanel.add(halfLife);
            halfLife.setPreferredSize(new java.awt.Dimension(145, 35));

            halfLife.setBorder(BorderFactory.createBevelBorder(BevelBorder.LOWERED));
            halfLife.setEditable(false);
            {
                logKowLabel = new JLabel();
                updateDatabasePanel.add(logKowLabel);
                logKowLabel.setText("Log Kow");
                logKowLabel.setPreferredSize(new java.awt.Dimension(120,
27));
            }
            {
                logKow = new JTextField();
                updateDatabasePanel.add(logKow);
                logKow.setPreferredSize(new java.awt.Dimension(145, 35));

                logKow.setBorder(BorderFactory.createBevelBorder(BevelBorder.LOWERED));
                logKow.setEditable(false);
            }
        }
        {
            integrationParameterPanel = new JPanel();
            FlowLayout integrationParameterPanelLayout = new FlowLayout();
            integrationParameterPanelLayout.setVgap(15);

            integrationParameterPanel.setLayout(integrationParameterPanelLayout);
            selectionTabs.addTab("Parameters", null,
integrationParameterPanel, null);

            integrationParameterPanel.setBorder(BorderFactory.createTitledBorder(null,
"Model parameters", TitledBorder.LEADING, TitledBorder.TOP));
            {
                sedimentDepthLabel = new JLabel();
                integrationParameterPanel.add(sedimentDepthLabel);
                sedimentDepthLabel.setText("Sediment Depth, cm");
                sedimentDepthLabel.setPreferredSize(new
java.awt.Dimension(200, 50));
            }
            {
                sedimentDepth = new JFormattedTextField(valueFormat);
                sedimentDepth.setValue(new Double(aSedimentDepth));
                integrationParameterPanel.add(sedimentDepth);
                sedimentDepth.setPreferredSize(new java.awt.Dimension(220
, 35));

                sedimentDepth.setBorder(BorderFactory.createBevelBorder(BevelBorder.LOWERED));
                sedimentDepth.addPropertyChangeListener("value", this);
            }
            {
                sedimentDensityLabel = new JLabel();
                integrationParameterPanel.add(sedimentDensityLabel);
                sedimentDensityLabel
                .setText("Sediment Density, Kg/L");
                sedimentDensityLabel.setPreferredSize(new
java.awt.Dimension(200, 50));
            }
        }
    }
}

```

```

    }
    {
        sedimentDensity = new JFormattedTextField(valueFormat);
        sedimentDensity.setValue(new Double(aSedimentDensity));
        integrationParameterPanel.add(sedimentDensity);
        sedimentDensity.setPreferredSize(new java.awt.Dimension(220,
35));

        sedimentDensity.setBorder(BorderFactory.createBevelBorder(BevelBorder.LOWERED))
;
        sedimentDensity.addPropertyChangeListener("value", this);
    }
    {
        waterTemperatureLabel = new JLabel();
        integrationParameterPanel.add(waterTemperatureLabel);
        waterTemperatureLabel
            .setText("Water Temperature, K");
        waterTemperatureLabel.setPreferredSize(new
java.awt.Dimension(200, 50));
    }
    {
        waterTemperature = new JFormattedTextField(valueFormat);
        waterTemperature.setValue(new Double(aWaterTemperature));
        integrationParameterPanel.add(waterTemperature);
        waterTemperature.addPropertyChangeListener("value", this);
        waterTemperature.setPreferredSize(new java.awt.Dimension(220,
35));

        waterTemperature.setBorder(BorderFactory.createBevelBorder(BevelBorder.LOWERED)
);
    }
    {
        organicFractionLabel = new JLabel();
        integrationParameterPanel.add(organicFractionLabel);
        organicFractionLabel.setText("Organic Fraction Content");
        organicFractionLabel.setPreferredSize(new
java.awt.Dimension(200, 50));
    }
    {
        organicFraction = new JFormattedTextField(valueFormat);
        organicFraction.setValue(new
Double(anOrganicFractionContent));
        integrationParameterPanel.add(organicFraction);
        organicFraction.addPropertyChangeListener("value", this);
        organicFraction.setPreferredSize(new java.awt.Dimension(220,
35));

        organicFraction.setBorder(BorderFactory.createBevelBorder(BevelBorder.LOWERED))
;
    }
    {
        simulationTimeLabel = new JLabel();
        integrationParameterPanel.add(simulationTimeLabel);
        simulationTimeLabel.setText("Simulation Time, weeks");
        simulationTimeLabel.setPreferredSize(new
java.awt.Dimension(200, 50));
    }
    {
        simulationTime = new JFormattedTextField(valueFormat);
        simulationTime.setValue(new Double(aSimulationTime));
        integrationParameterPanel.add(simulationTime);
        simulationTime.addPropertyChangeListener("value", this);
        simulationTime.setPreferredSize(new java.awt.Dimension(220,
35));

        simulationTime.setBorder(BorderFactory.createBevelBorder(BevelBorder.LOWERED));
    }
    {
        numberOfGridsLabel = new JLabel();
        integrationParameterPanel.add(numberOfGridsLabel);
        numberOfGridsLabel.setText("Number of Grids");
        numberOfGridsLabel.setPreferredSize(new
java.awt.Dimension(200, 50));
    }
    {
        numberOfGrids = new JFormattedTextField(valueFormat);

```

```

        numberOfGrids.setValue(new Double(aNumberOfGrids));
        integrationParameterPanel.add(numberOfGrids);
        numberOfGrids.addPropertyChangeListener("value", this);
        numberOfGrids.setPreferredSize(new java.awt.Dimension(220,
35));

        numberOfGrids.setBorder(BorderFactory.createBevelBorder(BevelBorder.LOWERED));
    }

    {
        porosityPanel = new JPanel();
        selectionTabs.addTab("Porosity Profile", null, porosityPanel,
null);
        porosityPanel.setBorder(BorderFactory.createTitledBorder("Select
porosity profile and enter parameter values"));
        porosityGroup = new ButtonGroup();
        {
            constantPorosityPanel = new JPanel();
            porosityPanel.add(constantPorosityPanel);
            constantPorosityPanel.setPreferredSize(new
java.awt.Dimension(570, 53));
            {
                constantPorosityButton = new JRadioButton();
                constantPorosityPanel
                    .add(constantPorosityButton);
                constantPorosityButton.setText("Constant");
                porosityGroup.add(constantPorosityButton);
                constantPorosityButton.setPreferredSize(new
java.awt.Dimension(145, 40));
                constantPorosityButton.addActionListener(this);
            }
            {
                constantPorosityLabel = new JLabel();
                constantPorosityPanel.add(constantPorosityLabel);
                constantPorosityLabel.setText("Porosity");
                constantPorosityLabel.setPreferredSize(new
java.awt.Dimension(160, 40));
            }
            {
                constantPorosity = new JFormattedTextField(valueFormat);
                constantPorosity.setValue(new Double(aConstantPorosity));
                constantPorosityPanel.add(constantPorosity);
                constantPorosity.setPreferredSize(new
java.awt.Dimension(200, 40));
            }
            constantPorosity.setBorder(BorderFactory.createBevelBorder(BevelBorder.LOWERED)
);
            {
                constantPorosity.setEditable(false);
                constantPorosity
                    .addPropertyChangeListener(this);
            }
        }
        otherPorosityPanel = new JPanel();
        FlowLayout otherPorosityPanelLayout = new FlowLayout();
        otherPorosityPanelLayout.setVgap(30);
        otherPorosityPanel.setLayout(otherPorosityPanelLayout);
        porosityPanel.add(otherPorosityPanel);
        otherPorosityPanel.setPreferredSize(new
java.awt.Dimension(570, 224));
        {
            linearPorosityButton = new JRadioButton();
            otherPorosityPanel.add(linearPorosityButton);
            linearPorosityButton.setText("Linear");
            porosityGroup.add(linearPorosityButton);
            linearPorosityButton.setPreferredSize(new
java.awt.Dimension(145, 40));
            linearPorosityButton.addActionListener(this);
        }
        {
            porosityAtInterfaceLabel = new JLabel();
            otherPorosityPanel.add(porosityAtInterfaceLabel);
            porosityAtInterfaceLabel.setText("Porosity at interface");
            porosityAtInterfaceLabel.setPreferredSize(new
java.awt.Dimension(160, 40));
        }
    }
}

```

```

    }
    {
        porosityAtInterface = new JFormattedTextField(valueFormat);
        porosityAtInterface.setValue(new
Double(aPorosityAtInterface));
        otherPorosityPanel.add(porosityAtInterface);
        porosityAtInterface.setPreferredSize(new
java.awt.Dimension(200, 40));

        porosityAtInterface.setBorder(BorderFactory.createBevelBorder(BevelBorder.LOWER
ED));
        porosityAtInterface.setEditable(false);
        porosityAtInterface
            .addPropertyChangeListener(this);
    }
    {
        exponentialPorosityButton = new JRadioButton();
        otherPorosityPanel.add(exponentialPorosityButton);
        exponentialPorosityButton.setText("Exponential");
        porosityGroup.add(exponentialPorosityButton);
        exponentialPorosityButton.setPreferredSize(new
java.awt.Dimension(145, 40));
        exponentialPorosityButton
            .addActionListener(this);
    }
    {
        porosityAtInfinityLabel = new JLabel();
        otherPorosityPanel.add(porosityAtInfinityLabel);
        porosityAtInfinityLabel.setText("Porosity at infinite
depth");
        porosityAtInfinityLabel.setPreferredSize(new
java.awt.Dimension(160, 40));
    }
    {
        porosityAtInfinity = new JFormattedTextField(valueFormat);
        porosityAtInfinity.setValue(new
Double(aPorosityAtInfinity));
        otherPorosityPanel.add(porosityAtInfinity);
        porosityAtInfinity.setPreferredSize(new
java.awt.Dimension(200, 40));

        porosityAtInfinity.setBorder(BorderFactory.createBevelBorder(BevelBorder.LOWERE
D));
        porosityAtInfinity.setEditable(false);
        porosityAtInfinity
            .addPropertyChangeListener(this);
    }
    {
        inverseExponentialButton = new JRadioButton();
        otherPorosityPanel.add(inverseExponentialButton);
        inverseExponentialButton.setText("Inverse exponential");
        porosityGroup.add(inverseExponentialButton);
        inverseExponentialButton.setPreferredSize(new
java.awt.Dimension(145, 40));
        inverseExponentialButton
            .addActionListener(this);
    }
    {
        attenuationFactorLabel = new JLabel();
        otherPorosityPanel.add(attenuationFactorLabel);
        attenuationFactorLabel.setText("Attenuation factor");
        attenuationFactorLabel.setPreferredSize(new
java.awt.Dimension(160, 40));
    }
    {
        attenuationFactor = new JFormattedTextField(valueFormat);
        attenuationFactor.setValue(new
Double(anAttenuationFactor));
        otherPorosityPanel.add(attenuationFactor);
        attenuationFactor.setPreferredSize(new
java.awt.Dimension(200, 40));

        attenuationFactor.setBorder(BorderFactory.createBevelBorder(BevelBorder.LOWERED
));
        attenuationFactor.setEditable(false);
        attenuationFactor
            .addPropertyChangeListener(this);
    }

```



```

    }
    }
    {
        powerPorosityPanel = new JPanel();
        FlowLayout powerPorosityPanelLayout = new FlowLayout();
        powerPorosityPanelLayout.setVgap(30);
        powerPorosityPanel.setLayout(powerPorosityPanelLayout);
        porosityPanel.add(powerPorosityPanel);
        powerPorosityPanel.setPreferredSize(new
java.awt.Dimension(570, 151));
        {
            powerPorosityButton = new JRadioButton();
            powerPorosityPanel.add(powerPorosityButton);
            powerPorosityButton.setText("Power");
            porosityGroup.add(powerPorosityButton);
            powerPorosityButton.setPreferredSize(new
java.awt.Dimension(145, 40));
            powerPorosityButton.addActionListener(this);
        }
        {
            powerFactorLabel = new JLabel();
            powerPorosityPanel.add(powerFactorLabel);
            powerFactorLabel.setText("Power factor");
            powerFactorLabel.setPreferredSize(new
java.awt.Dimension(160, 40));
        }
        {
            powerFactor = new JFormattedTextField(valueFormat);
            powerFactor.setValue(new Double(aPowerFactor));
            powerPorosityPanel.add(powerFactor);
            powerFactor.setPreferredSize(new java.awt.Dimension(200,
40));

            powerFactor.setBorder(BorderFactory.createBevelBorder(BevelBorder.LOWERED));
            powerFactor.setEditable(false);
            powerFactor.addPropertyChangeListener(this);
        }
        {
            gapLabel = new JLabel();
            powerPorosityPanel.add(gapLabel);
            gapLabel.setPreferredSize(new java.awt.Dimension(145, 40));
        }
        {
            powerExponentLabel = new JLabel();
            powerPorosityPanel.add(powerExponentLabel);
            powerExponentLabel.setText("Power exponent");
            powerExponentLabel.setPreferredSize(new
java.awt.Dimension(160, 40));
        }
        {
            powerExponent = new JFormattedTextField(valueFormat);
            powerExponent.setValue(new Double(aPowerExponent));
            powerPorosityPanel.add(powerExponent);
            powerExponent.setPreferredSize(new java.awt.Dimension(200,
40));

            powerExponent.setBorder(BorderFactory.createBevelBorder(BevelBorder.LOWERED));
            powerExponent.setEditable(false);
            powerExponent.addPropertyChangeListener(this);
        }
    }
    {
        initialConditionsPanel = new JPanel();
        selectionTabs.addTab(
            "Initial Conditions",
            null,
            initialConditionsPanel,
            null);
        initialConditionsGroup = new ButtonGroup();
        {
            constantInitialPanel = new JPanel();
            initialConditionsPanel.add(constantInitialPanel);
            FlowLayout constantInitialPanelLayout = new FlowLayout();
            constantInitialPanelLayout.setVgap(10);
            constantInitialPanel.setLayout(constantInitialPanelLayout);

```

```

        constantInitialPanel.setPreferredSize(new
java.awt.Dimension(563, 177));

        constantInitialPanel.setBorder(BorderFactory.createTitledBorder("");
        {
            constantInitialConcentrationButton = new JRadioButton();

            initialConditionsGroup.add(constantInitialConcentrationButton);

            constantInitialPanel.add(constantInitialConcentrationButton);
            constantInitialConcentrationButton.setText("Constant ");
            constantInitialConcentrationButton.setPreferredSize(new
java.awt.Dimension(429, 87));
            constantInitialConcentrationButton
                .addActionListener(this);
        }
        {
            initialConcentrationLabel = new JLabel();
            constantInitialPanel.add(initialConcentrationLabel);
            initialConcentrationLabel.setText("Initial Concentration,
g/m3");
            initialConcentrationLabel.setPreferredSize(new
java.awt.Dimension(200, 50));
        }
        {
            initialConcentration = new
JFormattedTextField(valueFormat);
            initialConcentration.setValue(new
Double(anInitialConcentration));
            constantInitialPanel.add(initialConcentration);
            initialConcentration.addPropertyChangeListener("value",
this);
            initialConcentration.setPreferredSize(new
java.awt.Dimension(220, 35));

            initialConcentration.setBorder(BorderFactory.createBevelBorder(BevelBorder.LOWE
RED));
            initialConcentration.setEditable(false);
        }
    }
    {
        stepInitialPanel = new JPanel();
        initialConditionsPanel.add(stepInitialPanel);
        stepInitialPanel.setPreferredSize(new java.awt.Dimension(563,
241));

        stepInitialPanel.setBorder(BorderFactory.createTitledBorder(""));
        {
            stepFunctionInitialButton = new JRadioButton();
            initialConditionsGroup.add(stepFunctionInitialButton);
            stepInitialPanel.add(stepFunctionInitialButton);
            stepFunctionInitialButton.setText("Step function");
            stepFunctionInitialButton.setPreferredSize(new
java.awt.Dimension(429, 93));
            stepFunctionInitialButton
                .addActionListener(this);
        }
        {
            initialDepthPenetrationLabel = new JLabel();
            stepInitialPanel
                .add(initialDepthPenetrationLabel);
            initialDepthPenetrationLabel.setText("Initial depth
penetration, cm");
            initialDepthPenetrationLabel.setPreferredSize(new
java.awt.Dimension(200, 50));
        }
        {
            initialDepthPenetration = new
JFormattedTextField(valueFormat);
            initialDepthPenetration.setValue(new
Double(anInitialDepth));
            stepInitialPanel.add(initialDepthPenetration);
            initialDepthPenetration.setPreferredSize(new
java.awt.Dimension(220, 35));

```



```

    dirichletLowerBoundary.setBorder(BorderFactory.createBevelBorder(BevelBorder.LOWERED));
        dirichletLowerBoundary.setEditable(false);
        dirichletLowerBoundary
            .addPropertyChangeListener("value",this);
    }
    {
        dirichletGap = new JLabel();
        dirichletPanel.add(dirichletGap);
        dirichletGap.setPreferredSize(new java.awt.Dimension(145,
40));
    }
    {
        dirichletUpperBoundaryLabel = new JLabel();
        dirichletPanel.add(dirichletUpperBoundaryLabel);
        dirichletUpperBoundaryLabel.setText("Concentration at
infinite depth");
        dirichletUpperBoundaryLabel.setPreferredSize(new
java.awt.Dimension(190, 40));
    }
    {
        dirichletUpperBoundary = new
JFormattedTextField(valueFormat);
        dirichletUpperBoundary.setValue(new
Double(aDirichletLowerBoundary));
        dirichletPanel.add(dirichletUpperBoundary);
        dirichletUpperBoundary.setPreferredSize(new
java.awt.Dimension(190, 40));

        dirichletUpperBoundary.setBorder(BorderFactory.createBevelBorder(BevelBorder.LOWERED));
            dirichletUpperBoundary.setEditable(false);
            dirichletUpperBoundary
                .addPropertyChangeListener("value",this);
        }
    }
    {
        neumannPanel = new JPanel();
        FlowLayout neumannPanelLayout = new FlowLayout();
        neumannPanelLayout.setVgap(15);
        neumannPanel.setLayout(neumannPanelLayout);
        boundaryPanel.add(neumannPanel);
        neumannPanel.setPreferredSize(new java.awt.Dimension(570,
130));
        neumannPanel.setBorder(BorderFactory.createTitledBorder(""));
        {
            neumannButton = new JRadioButton();
            boundaryGroup.add(neumannButton);
            neumannPanel.add(neumannButton);
            neumannButton.setText("Neumann Conditions");
            neumannButton.setPreferredSize(new java.awt.Dimension(145,
40));
            neumannButton.addActionListener(this);
        }
        {
            neumannLowerBoundaryLabel = new JLabel();
            neumannPanel.add(neumannLowerBoundaryLabel);
            neumannLowerBoundaryLabel.setText("Flux at interface,
g/m2");
            neumannLowerBoundaryLabel.setPreferredSize(new
java.awt.Dimension(190, 40));
        }
        {
            neumannLowerBoundary = new
JFormattedTextField(valueFormat);
            neumannLowerBoundary.setValue(new
Double(aNeumannLowerBoundary));
            neumannPanel.add(neumannLowerBoundary);
            neumannLowerBoundary.setPreferredSize(new
java.awt.Dimension(190, 40));

            neumannLowerBoundary.setBorder(BorderFactory.createBevelBorder(BevelBorder.LOWERED));
                neumannLowerBoundary.setEditable(false);
                neumannLowerBoundary
                    .addPropertyChangeListener("value", this);
        }
    }

```

```

    }
    {
        neumannGap = new JLabel();
        neumannPanel.add(neumannGap);
        neumannGap.setPreferredSize(new java.awt.Dimension(145,
40));
    }
    {
        neumannUpperBoundaryLabel = new JLabel();
        neumannPanel.add(neumannUpperBoundaryLabel);
        neumannUpperBoundaryLabel.setText("Flux at infinite
depth");
        neumannUpperBoundaryLabel.setPreferredSize(new
java.awt.Dimension(190, 40));
    }
    {
        neumannUpperBoundary = new
JFormattedTextField(valueFormat);
        neumannUpperBoundary.setValue(new
Double(aNeumannUpperBoundary));
        neumannPanel.add(neumannUpperBoundary);
        neumannUpperBoundary.setPreferredSize(new
java.awt.Dimension(190, 40));

        neumannUpperBoundary.setBorder(BorderFactory.createBevelBorder(BevelBorder.LOWE
RED));
        neumannUpperBoundary.setEditable(false);
        neumannUpperBoundary
            .addChangeListener("value", this);
    }
}
{
    robinPanel = new JPanel();
    FlowLayout robinPanelLayout = new FlowLayout();
    robinPanelLayout.setVgap(10);
    robinPanel.setLayout(robinPanelLayout);
    boundaryPanel.add(robinPanel);
    robinPanel.setPreferredSize(new java.awt.Dimension(570, 197));
    robinPanel.setBorder(BorderFactory.createTitledBorder(""));
    {
        robinButton = new JRadioButton();
        boundaryGroup.add(robinButton);
        robinPanel.add(robinButton);
        robinButton.setText("Robin Conditions");
        robinButton.setPreferredSize(new java.awt.Dimension(145,
40));
        robinButton.addActionListener(this);
    }
    {
        robinLowerConcentrationCoefficient = new
JFormattedTextField(valueFormat);
        robinLowerConcentrationCoefficient.setValue(new
Double(aLowerConcentrationCoefficient));
        robinPanel.add(robinLowerConcentrationCoefficient);
        robinLowerConcentrationCoefficient.setPreferredSize(new
java.awt.Dimension(190, 50));

        robinLowerConcentrationCoefficient.setBorder(BorderFactory.createTitledBorder("
Lower concentration factor"));
        robinLowerConcentrationCoefficient.setEditable(false);
        robinLowerConcentrationCoefficient
            .addChangeListener("value", this);
    }
    {
        robinUpperConcentrationCoefficient = new
JFormattedTextField(valueFormat);
        robinUpperConcentrationCoefficient.setValue(new
Double(anUpperConcentrationCoefficient));
        robinPanel.add(robinUpperConcentrationCoefficient);
        robinUpperConcentrationCoefficient.setPreferredSize(new
java.awt.Dimension(190, 50));
        robinUpperConcentrationCoefficient.setEditable(false);

        robinUpperConcentrationCoefficient.setBorder(BorderFactory.createTitledBorder("
Upper concentration factor"));
        robinUpperConcentrationCoefficient
            .addChangeListener("value", this);
    }
}

```

```

    }
    {
        robinGap = new JLabel();
        robinPanel.add(robinGap);
        robinGap.setPreferredSize(new java.awt.Dimension(145, 40));
    }
    {
        robinLowerFluxCoefficient = new
JFormattedTextField(valueFormat);
        robinLowerFluxCoefficient.setValue(new
Double(aLowerFluxCoefficient));
        robinPanel.add(robinLowerFluxCoefficient);
        robinLowerFluxCoefficient.setPreferredSize(new
java.awt.Dimension(190, 50));
        robinLowerFluxCoefficient.setEditable(false);

        robinLowerFluxCoefficient.setBorder(BorderFactory.createTitledBorder("Lower
flux factor"));
        robinLowerFluxCoefficient
            .addChangeListener("value", this);
    }
    {
        robinUpperFluxCoefficient = new
JFormattedTextField(valueFormat);
        robinUpperFluxCoefficient.setValue(new
Double(anUpperFluxCoefficient));
        robinPanel.add(robinUpperFluxCoefficient);
        robinUpperFluxCoefficient.setPreferredSize(new
java.awt.Dimension(190, 50));
        robinUpperFluxCoefficient.setEditable(false);

        robinUpperFluxCoefficient.setBorder(BorderFactory.createTitledBorder("Upper
flux factor"));
        robinUpperFluxCoefficient
            .addChangeListener("value", this);
    }
    {
        robinGap2 = new JLabel();
        robinPanel.add(robinGap2);
        robinGap2.setPreferredSize(new java.awt.Dimension(145,
40));
    }
    {
        robinLowerBoundary = new JFormattedTextField(valueFormat);
        robinLowerBoundary.setValue(new
Double(aRobinLowerCondition));
        robinPanel.add(robinLowerBoundary);
        robinLowerBoundary.setPreferredSize(new
java.awt.Dimension(190, 50));

        robinLowerBoundary.setBorder(BorderFactory.createTitledBorder("Lower boundary
condition"));
        robinLowerBoundary.setEditable(false);
        robinLowerBoundary
            .addChangeListener("value", this);
    }
    {
        robinUpperBoundary = new JFormattedTextField(valueFormat);
        robinUpperBoundary.setValue(new
Double(aRobinUpperCondition));
        robinPanel.add(robinUpperBoundary);
        robinUpperBoundary.setPreferredSize(new
java.awt.Dimension(190, 50));

        robinUpperBoundary.setBorder(BorderFactory.createTitledBorder("Upper boundary
condition"));
        robinUpperBoundary.setEditable(false);
        robinUpperBoundary
            .addChangeListener("value", this);
    }
}
{
    diffusionPanel = new JPanel();
    selectionTabs.addTab("Diffusion", null, diffusionPanel, null);
    diffusionGroup = new ButtonGroup();
    {

```

```

        userDefinedDiffusionPanel = new JPanel();
        diffusionPanel.add(userDefinedDiffusionPanel);
        userDefinedDiffusionPanel.setPreferredSize(new
java.awt.Dimension(532, 155));

        userDefinedDiffusionPanel.setBorder(BorderFactory.createTitledBorder("Diffusivi
ty constant is taken from the user"));
        {
            userDefinedDiffusivityButton = new JRadioButton();
            userDefinedDiffusionPanel
                .add(userDefinedDiffusivityButton);
            userDefinedDiffusivityButton.setText("User Defined
Constant");
            userDefinedDiffusivityButton.setPreferredSize(new
java.awt.Dimension(180, 108));
            diffusionGroup.add(userDefinedDiffusivityButton);
            userDefinedDiffusivityButton
                .addActionListener(this);
        }
        {
            userDefinedDiffusivityLabel = new JLabel();
            userDefinedDiffusionPanel
                .add(userDefinedDiffusivityLabel);
            userDefinedDiffusivityLabel.setText("Diffusivity, cm2/s");
            userDefinedDiffusivityLabel.setPreferredSize(new
java.awt.Dimension(109, 48));

            userDefinedDiffusivityLabel.setHorizontalAlignment(SwingConstants.TRAILING);
        }
        {
            userDefinedDiffusivity = new
JFormattedTextField(valueFormat);
            userDefinedDiffusivity.setValue(new Double(aDiffusivity));
            userDefinedDiffusionPanel
                .add(userDefinedDiffusivity);
            userDefinedDiffusivity.addPropertyChangeListener("value",
this);
            userDefinedDiffusivity.setPreferredSize(new
java.awt.Dimension(193, 39));

            userDefinedDiffusivity.setBorder(BorderFactory.createBevelBorder(BevelBorder.LO
WERED));
        }
        {
            userDefinedDiffusivity.setEditable(false);
        }
        {
            approximatedDiffusionPanel = new JPanel();
            diffusionPanel.add(approximatedDiffusionPanel);
            approximatedDiffusionPanel.setPreferredSize(new
java.awt.Dimension(532, 297));

            approximatedDiffusionPanel.setBorder(BorderFactory.createTitledBorder("Diffusiv
ity constant is approximated using empirical correlations"));
            {
                approximatedDiffusivityButton = new JRadioButton();
                approximatedDiffusionPanel
                    .add(approximatedDiffusivityButton);
                approximatedDiffusivityButton
                    .setText("Approximated Constant");
                approximatedDiffusivityButton.setPreferredSize(new
java.awt.Dimension(172, 233));
                diffusionGroup.add(approximatedDiffusivityButton);
                approximatedDiffusivityButton
                    .addActionListener(this);
            }
            {
                empiricalDiffusivityPanel = new JPanel();
                FlowLayout empiricalDiffusivityPanelLayout = new
FlowLayout();
                empiricalDiffusivityPanelLayout.setVgap(20);

                empiricalDiffusivityPanel.setLayout(empiricalDiffusivityPanelLayout);
                approximatedDiffusionPanel
                    .add(empiricalDiffusivityPanel);
                empiricalDiffusivityPanel.setPreferredSize(new
java.awt.Dimension(234, 161));
            }
        }
    }
}

```

```

        wilkeChangButton = new JButton();
        empiricalDiffusivityPanel.add(wilkeChangButton);
        wilkeChangButton.setText("Wilke-Chang");
        wilkeChangButton.setPreferredSize(new
java.awt.Dimension(175, 30));

        wilkeChangButton.setBorder(BorderFactory.createBevelBorder(BevelBorder.RAISED))
;
        wilkeChangButton.setEnabled(false);
        wilkeChangButton.addActionListener(this);
    }
    {
        reddyDoraiswamyButton = new JButton();
        empiricalDiffusivityPanel.add(reddyDoraiswamyButton);
        reddyDoraiswamyButton.setText("Reddy-Doraiswamy");
        reddyDoraiswamyButton.setPreferredSize(new
java.awt.Dimension(175, 30));

        reddyDoraiswamyButton.setBorder(BorderFactory.createBevelBorder(BevelBorder.RAI
SED));
        reddyDoraiswamyButton.setEnabled(false);
        reddyDoraiswamyButton
            .addActionListener(this);
    }
    {
        haydukLaudieButton = new JButton();
        empiricalDiffusivityPanel.add(haydukLaudieButton);
        haydukLaudieButton.setText("Hayduk-Laudie");
        haydukLaudieButton.setPreferredSize(new
java.awt.Dimension(175, 30));

        haydukLaudieButton.setBorder(BorderFactory.createBevelBorder(BevelBorder.RAISED
));
        haydukLaudieButton.setEnabled(false);
        haydukLaudieButton.addActionListener(this);
    }
}
diffusionIndex = selectionTabs.getTabCount()-1;
boolean enabled = selectionTabs.isEnabledAt(diffusionIndex);
selectionTabs.setEnabledAt(diffusionIndex, false);
}
{
    sorptionPanel = new JPanel();
    selectionTabs.addTab("Sorption", null, sorptionPanel, null);
    sorptionPanel.setBorder(BorderFactory.createTitledBorder("Select
a single isotherm or combinations of these:"));
    {
        linearPartitioningPanel = new JPanel();
        sorptionPanel.add(linearPartitioningPanel);
        linearPartitioningPanel.setPreferredSize(new
java.awt.Dimension(540, 137));

        linearPartitioningPanel.setBorder(BorderFactory.createTitledBorder(""));
        {
            linearPanel = new JPanel();
            FlowLayout linearPanelLayout = new FlowLayout();
            linearPanelLayout.setVgap(8);
            linearPanel.setLayout(linearPanelLayout);
            linearPartitioningPanel.add(linearPanel);
            linearPanel.setPreferredSize(new java.awt.Dimension(148,
121));

            {
                linearPartitioningButton = new JRadioButton();
                linearPanel.add(linearPartitioningButton);
                linearPartitioningButton.setText("Linear Partitioning");
                linearPartitioningButton.setPreferredSize(new
java.awt.Dimension(145, 26));
                linearPartitioningButton
                    .addActionListener(this);
            }
            {
                linearDatabaseButton = new JButton();
                linearPanel.add(linearDatabaseButton);
                linearDatabaseButton.setText("Use Database");
                linearDatabaseButton.setPreferredSize(new
java.awt.Dimension(126, 32));
            }
        }
    }
}

```



```

linearDatabaseButton.setBorder(BorderFactory.createBevelBorder(BevelBorder.RAISED));
        linearDatabaseButton.setEnabled(false);
        linearDatabaseButton
            .addActionListener(this);
    }
    {
        linearUserButton = new JButton();
        linearPanel.add(linearUserButton);
        linearUserButton.setText("User Defined");
        linearUserButton.setPreferredSize(new
java.awt.Dimension(126, 32));

        linearUserButton.setBorder(BorderFactory.createBevelBorder(BevelBorder.RAISED))
;
            linearUserButton.setEnabled(false);
            linearUserButton.addActionListener(this);
        }
    }
    {
        linearPartitioningDataPanel = new JPanel();
        linearPartitioningPanel.add(linearPartitioningDataPanel);
        linearPartitioningDataPanel.setPreferredSize(new
java.awt.Dimension(362, 117));
    }
    {
        aConstantForLinearLabel = new JLabel();
        linearPartitioningDataPanel
            .add(aConstantForLinearLabel);
        aConstantForLinearLabel.setText("a constant (a x depth^
b)");
        aConstantForLinearLabel.setPreferredSize(new
java.awt.Dimension(180, 50));
    }
    {
        aConstantLinear = new JFormattedTextField(valueFormat);
        aConstantLinear.setValue(new Double(anAConstant));
        linearPartitioningDataPanel
            .add(aConstantLinear);
        aConstantLinear.addPropertyChangeListener("value",
this);
        aConstantLinear.setPreferredSize(new
java.awt.Dimension(165, 35));

        aConstantLinear.setBorder(BorderFactory.createBevelBorder(BevelBorder.LOWERED))
;
            aConstantLinear.setEditable(false);
        }
    }
    {
        bConstantLinearLabel = new JLabel();
        linearPartitioningDataPanel.add(bConstantLinearLabel);
        bConstantLinearLabel.setText("b constant (a x depth^
b)");
        bConstantLinearLabel.setPreferredSize(new
java.awt.Dimension(180, 50));
    }
    {
        bConstantLinear = new JFormattedTextField(valueFormat);
        bConstantLinear.setValue(new Double(aBConstant));
        linearPartitioningDataPanel.add(bConstantLinear);
        bConstantLinear.addPropertyChangeListener("value",
this);
        bConstantLinear.setPreferredSize(new
java.awt.Dimension(165, 35));

        bConstantLinear.setBorder(BorderFactory.createBevelBorder(BevelBorder.LOWERED))
;
            bConstantLinear.setEditable(false);
        }
    }
    {
        freundlichPanel = new JPanel();
        sorptionPanel.add(freundlichPanel);
        freundlichPanel.setPreferredSize(new java.awt.Dimension(540,
137));
    }

```

```

freundlichPanel.setBorder(BorderFactory.createTitledBorder(""));
    {
        freundlichButton = new JRadioButton();
        freundlichPanel.add(freundlichButton);
        freundlichButton.setText("Freundlich");
        freundlichButton.setPreferredSize(new
java.awt.Dimension(145, 115));
        freundlichButton.addActionListener(this);
    }
    {
        freundlichDataPanel = new JPanel();
        freundlichPanel.add(freundlichDataPanel);
        freundlichDataPanel.setPreferredSize(new
java.awt.Dimension(362, 117));
        {
            freundlichConstantLabel = new JLabel();
            freundlichDataPanel
                .add(freundlichConstantLabel);
            freundlichConstantLabel.setText("Freundlich Constant,
(m3/g)^n");
            freundlichConstantLabel.setPreferredSize(new
java.awt.Dimension(180, 50));
        }
        {
            freundlichConstant = new
JFormattedTextField(valueFormat);
            freundlichConstant.setValue(new
Double(aFreundlichConstant));
            freundlichDataPanel.add(freundlichConstant);
            freundlichConstant.addPropertyChangeListener("value",
this);
            freundlichConstant.setPreferredSize(new
java.awt.Dimension(165, 35));
            freundlichConstant.setEditable(false);

            freundlichConstant.setBorder(BorderFactory.createBevelBorder(BevelBorder.LOWERE
D));
        }
        {
            freundlichExponentLabel = new JLabel();
            freundlichDataPanel
                .add(freundlichExponentLabel);
            freundlichExponentLabel.setText("Freundlich Exponent,
n");
            freundlichExponentLabel.setPreferredSize(new
java.awt.Dimension(180, 50));
        }
        {
            freundlichExponent = new
JFormattedTextField(valueFormat);
            freundlichExponent.setValue(new
Double(aFreundlichExponent));
            freundlichDataPanel.add(freundlichExponent);
            freundlichExponent.addPropertyChangeListener("value",
this);
            freundlichExponent.setPreferredSize(new
java.awt.Dimension(165, 35));

            freundlichExponent.setBorder(BorderFactory.createBevelBorder(BevelBorder.LOWERE
D));
            freundlichExponent.setEditable(false);
        }
    }
    {
        langmuirPanel = new JPanel();
        sorptionPanel.add(langmuirPanel);
        langmuirPanel.setPreferredSize(new java.awt.Dimension(540,
137));
        langmuirPanel.setBorder(BorderFactory.createTitledBorder(""));
        {
            langmuirButton = new JRadioButton();
            langmuirPanel.add(langmuirButton);
            langmuirButton.setText("Langmuir");
            langmuirButton.setPreferredSize(new java.awt.Dimension(145,
115));

```

```

        langmuirButton.addActionListener(this);
    }
    {
        langmuirDataPanel = new JPanel();
        langmuirPanel.add(langmuirDataPanel);
        langmuirDataPanel.setPreferredSize(new
java.awt.Dimension(362, 117));
        {
            langmuirConcentrationLabel = new JLabel();
            langmuirDataPanel
                .add(langmuirConcentrationLabel);
            langmuirConcentrationLabel.setText("Saturated
Concentration, g/m3");
            langmuirConcentrationLabel.setPreferredSize(new
java.awt.Dimension(180, 50));
        }
        langmuirConcentration = new
JFormattedTextField(valueFormat);
        langmuirConcentration.setValue(new
Double(aLangmuirConcentration));
        langmuirDataPanel
            .add(langmuirConcentration);
        langmuirConcentration.addPropertyChangeListener("value",
this);
        langmuirConcentration.setPreferredSize(new
java.awt.Dimension(165, 35));

        langmuirConcentration.setBorder(BorderFactory.createBevelBorder(BevelBorder.LOWERED));
        {
            langmuirConcentration.setEditable(false);
        }
        {
            langmuirConstantLabel = new JLabel();
            langmuirDataPanel
                .add(langmuirConstantLabel);
            langmuirConstantLabel.setText("Langmuir Constant");
            langmuirConstantLabel.setPreferredSize(new
java.awt.Dimension(180, 50));
        }
        langmuirConstant = new JFormattedTextField(valueFormat);
        langmuirConstant.setValue(new
Double(aLangmuirConstant));
        langmuirDataPanel.add(langmuirConstant);
        langmuirConstant.addPropertyChangeListener("value",
this);
        langmuirConstant.setPreferredSize(new
java.awt.Dimension(165, 35));

        langmuirConstant.setBorder(BorderFactory.createBevelBorder(BevelBorder.LOWERED));
    };
        langmuirConstant.setEditable(false);
    }
}
sorptionIndex = selectionTabs.getTabCount()-1;
boolean enabled = selectionTabs.isEnabledAt(sorptionIndex);
selectionTabs.setEnabledAt(sorptionIndex, false);
}
{
    advectionPanel = new JPanel();
    selectionTabs.addTab("Advection", null, advectionPanel, null);
    {
        pressureGradientLabel = new JLabel();
        advectionPanel.add(pressureGradientLabel);
        pressureGradientLabel.setText("Pore Pressure Gradient, Pa/m");
        pressureGradientLabel.setPreferredSize(new
java.awt.Dimension(226, 105));
    }
    {
        pressureGradient = new JFormattedTextField(valueFormat);
        pressureGradient.setValue(new Double(aPressureGradient));
        advectionPanel.add(pressureGradient);
        pressureGradient.addPropertyChangeListener("value", this);
        pressureGradient.setPreferredSize(new java.awt.Dimension(180,
35));
    }
}

```

```

pressureGradient.setBorder(BorderFactory.createBevelBorder(BevelBorder.LOWERED
);
    }
    {
        advectiveVelocityPanel = new JPanel();
        advectionPanel.add(advectiveVelocityPanel);
        advectiveVelocityPanel.setPreferredSize(new
java.awt.Dimension(519, 284));

        advectiveVelocityPanel.setBorder(BorderFactory.createTitledBorder("Select a
parameter to approximate the advective velocity"));
        advectionGroup = new ButtonGroup();
        {
            userDefinedVelocityButton = new JRadioButton();
            advectiveVelocityPanel
                .add(userDefinedVelocityButton);
            userDefinedVelocityButton.setText("User defined
parameter");
            userDefinedVelocityButton.setPreferredSize(new
java.awt.Dimension(373, 55));
            advectionGroup.add(userDefinedVelocityButton);
            userDefinedVelocityButton
                .addActionListener(this);
        }
        {
            sedimentPermeabilityLabel = new JLabel();
            advectiveVelocityPanel
                .add(sedimentPermeabilityLabel);
            sedimentPermeabilityLabel.setText("Sediment Permeability,
m2");
            sedimentPermeabilityLabel.setPreferredSize(new
java.awt.Dimension(180, 35));
        }
        {
            sedimentPermeability = new
JFormattedTextField(valueFormat);
            sedimentPermeability.setValue(new
Double(aSedimentPermeability));
            advectiveVelocityPanel
                .add(sedimentPermeability);
            sedimentPermeability.addPropertyChangeListener("value",
this);
            sedimentPermeability.setPreferredSize(new
java.awt.Dimension(180, 35));

            sedimentPermeability.setBorder(BorderFactory.createBevelBorder(BevelBorder.LOWE
RED));
        }
        {
            sedimentPermeability.setEditable(false);
        }
        {
            approximatedVelocityButton = new JRadioButton();
            advectiveVelocityPanel
                .add(approximatedVelocityButton);
            approximatedVelocityButton.setText("Using Kaman-Cozeny
Equation");
            approximatedVelocityButton.setPreferredSize(new
java.awt.Dimension(373, 55));
            advectionGroup.add(approximatedVelocityButton);
            approximatedVelocityButton
                .addActionListener(this);
        }
        {
            hydraulicConductivityLabel = new JLabel();
            advectiveVelocityPanel
                .add(hydraulicConductivityLabel);
            hydraulicConductivityLabel.setText("Hydraulic Conductivity,
m/s");
            hydraulicConductivityLabel.setPreferredSize(new
java.awt.Dimension(180, 35));
        }
        {
            hydraulicConductivity = new
JFormattedTextField(valueFormat);
            hydraulicConductivity.setValue(new
Double(aHydraulicConductivity));
            advectiveVelocityPanel

```

```

        .add(hydraulicConductivity);
        hydraulicConductivity.addPropertyChangeListener("value",
this);
        hydraulicConductivity.setPreferredSize(new
java.awt.Dimension(180, 35));
        hydraulicConductivity.setBorder(BorderFactory.createBevelBorder(BevelBorder.LOWERED));
        hydraulicConductivity.setEditable(false);
    }
    }
    advectionIndex = selectionTabs.getTabCount()-1;
    boolean enabled = selectionTabs.isEnabledAt(advectionIndex);
    selectionTabs.setEnabledAt(advectionIndex, false);
}
{
    bioturbationPanel = new JPanel();
    selectionTabs.addTab("Bioturbation", null, bioturbationPanel,
null);
    {
        overlyingWaterConcentrationButton = new JLabel();
        bioturbationPanel
        .add(overlyingWaterConcentrationButton);
        overlyingWaterConcentrationButton.setText("Overlying Water
Concentration, g/m3");
        overlyingWaterConcentrationButton.setPreferredSize(new
java.awt.Dimension(254, 116));
    }
    {
        overlyingWaterConcentration = new
JFormattedTextField(valueFormat);
        overlyingWaterConcentration.setValue(new
Double(anOverlyingWaterConcentration));
        bioturbationPanel.add(overlyingWaterConcentration);
        overlyingWaterConcentration.addPropertyChangeListener("value",
this);
        overlyingWaterConcentration.setPreferredSize(new
java.awt.Dimension(180, 35));
        overlyingWaterConcentration.setBorder(BorderFactory.createBevelBorder(BevelBorder.LOWERED));
    }
    {
        bioturbationExchangeCoefficientPanel = new JPanel();
        bioturbationPanel.add(bioturbationExchangeCoefficientPanel);
        bioturbationExchangeCoefficientPanel.setPreferredSize(new
java.awt.Dimension(526, 314));
        bioturbationExchangeCoefficientPanel.setBorder(BorderFactory.createTitledBorder
("Select a parameter to approximate the exchange coefficient"));
        bioturbationGroup = new ButtonGroup();
        {
            userDefinedBioturbationConstantButton = new JRadioButton();
            bioturbationExchangeCoefficientPanel
            .add(userDefinedBioturbationConstantButton);
            userDefinedBioturbationConstantButton
            .setText("User Defined Parameter");
            userDefinedBioturbationConstantButton.setPreferredSize(new
java.awt.Dimension(380, 60));
            bioturbationGroup.add(userDefinedBioturbationConstantButton);
            userDefinedBioturbationConstantButton
            .addActionListener(this);
        }
        {
            exchangeCoefficientLabel = new JLabel();
            bioturbationExchangeCoefficientPanel
            .add(exchangeCoefficientLabel);
            exchangeCoefficientLabel.setText("Exchange Coefficient, per
week");
            exchangeCoefficientLabel.setPreferredSize(new
java.awt.Dimension(180, 35));
        }
        {
            exchangeCoefficient = new JFormattedTextField(valueFormat);
            exchangeCoefficient.setValue(new
Double(anExchangeCoefficient));

```

```

        bioturbationExchangeCoefficientPanel
            .add(exchangeCoefficient);
        exchangeCoefficient.addPropertyChangeListener("value",
this);
        exchangeCoefficient.setPreferredSize(new
java.awt.Dimension(180, 35));
        exchangeCoefficient.setBorder(BorderFactory.createBevelBorder(BevelBorder.LOWER
ED));
        exchangeCoefficient.setEditable(false);
    }
    {
        approximatedBioturbationConstantButton = new JRadioButton();
        bioturbationExchangeCoefficientPanel
            .add(approximatedBioturbationConstantButton);
        approximatedBioturbationConstantButton.setText("Thibodeaux -
Bierman Equation");
        approximatedBioturbationConstantButton.setPreferredSize(new
java.awt.Dimension(380, 60));
        bioturbationGroup.add(approximatedBioturbationConstantButton);
        approximatedBioturbationConstantButton
            .addActionListener(this);
    }
    {
        bioturbationDepthLabel = new JLabel();
        bioturbationExchangeCoefficientPanel
            .add(bioturbationDepthLabel);
        bioturbationDepthLabel.setText("Bioturbation Depth, mm");
        bioturbationDepthLabel.setPreferredSize(new
java.awt.Dimension(180, 35));
    }
    {
        bioturbationDepth = new JFormattedTextField(valueFormat);
        bioturbationDepth.setValue(new Double(aBioturbationDepth));
        bioturbationExchangeCoefficientPanel
            .add(bioturbationDepth);
        bioturbationDepth.addPropertyChangeListener("value", this);
        bioturbationDepth.setPreferredSize(new
java.awt.Dimension(180, 35));
        bioturbationDepth.setBorder(BorderFactory.createBevelBorder(BevelBorder.LOWERED
));
        bioturbationDepth.setEditable(false);
    }
    {
        waterVelocityButton = new JLabel();
        bioturbationExchangeCoefficientPanel
            .add(waterVelocityButton);
        waterVelocityButton.setText("Interface Water Velocity,
m/s");
        waterVelocityButton.setPreferredSize(new
java.awt.Dimension(180, 35));
    }
    {
        waterVelocity = new JFormattedTextField(valueFormat);
        waterVelocity.setValue(new
Double(anInterfaceWaterVelocity));
        bioturbationExchangeCoefficientPanel
            .add(waterVelocity);
        waterVelocity.addPropertyChangeListener("value", this);
        waterVelocity.setPreferredSize(new java.awt.Dimension(180,
35));
        waterVelocity.setBorder(BorderFactory.createBevelBorder(BevelBorder.LOWERED));
        waterVelocity.setEditable(false);
    }
    }
    bioturbationIndex = selectionTabs.getTabCount()-1;
    boolean enabled = selectionTabs.isEnabledAt(bioturbationIndex);
    selectionTabs.setEnabledAt(bioturbationIndex, false);
}
{
    degradationPanel = new JPanel();
    selectionTabs.addTab("Degradation", null, degradationPanel,
null);
    degradationGroup = new ButtonGroup();

```

```

    {
        approximatedDegradationConstantButton = new JRadioButton();
        degradationPanel
            .add(approximatedDegradationConstantButton);
        approximatedDegradationConstantButton.setText("Approximate the
degradation constant using theoretical half-lives");
        approximatedDegradationConstantButton.setPreferredSize(new
java.awt.Dimension(440, 150));

        approximatedDegradationConstantButton.setVerticalAlignment(SwingConstants.BOTTO
M);

        degradationGroup.add(approximatedDegradationConstantButton);
        approximatedDegradationConstantButton
            .addActionListener(this);
    }
    {
        userDefinedDegradationConstantButton = new JRadioButton();
        degradationPanel
            .add(userDefinedDegradationConstantButton);
        userDefinedDegradationConstantButton.setText("User Defined
Parameter");
        userDefinedDegradationConstantButton.setPreferredSize(new
java.awt.Dimension(440, 50));
        degradationGroup.add(userDefinedDegradationConstantButton);
        userDefinedDegradationConstantButton
            .addActionListener(this);
    }
    {
        degradationConstantLabel = new JLabel();
        degradationPanel.add(degradationConstantLabel);
        degradationConstantLabel.setText("Degradation constant, per
day");
        degradationConstantLabel.setPreferredSize(new
java.awt.Dimension(180, 35));
    }
    {
        degradationConstant = new JFormattedTextField(valueFormat);
        degradationConstant.setValue(new
Double(aDegradationConstant));
        degradationPanel.add(degradationConstant);
        degradationConstant.addPropertyChangeListener("value", this);
        degradationConstant.setPreferredSize(new
java.awt.Dimension(180, 35));

        degradationConstant.setBorder(BorderFactory.createBevelBorder(BevelBorder.LOWER
ED));

        degradationConstant.setEditable(false);
    }
    degradationIndex = selectionTabs.getTabCount()-1;
    boolean enabled = selectionTabs.isEnabledAt(degradationIndex);
    selectionTabs.setEnabledAt(degradationIndex, false);
}
{
    depositionPanel = new JPanel();
    selectionTabs.addTab("Deposition", null, depositionPanel, null);
    {
        depositionRateLabel = new JLabel();
        depositionPanel.add(depositionRateLabel);
        depositionRateLabel.setText("Deposition Rate, cm/yr");
        depositionRateLabel.setPreferredSize(new
java.awt.Dimension(180, 460));
    }
    {
        depositionRate = new JFormattedTextField(valueFormat);
        depositionRate.setValue(new Double(aDepositionRate));
        depositionPanel.add(depositionRate);
        depositionRate.addPropertyChangeListener("value", this);
        depositionRate.setPreferredSize(new java.awt.Dimension(180,
35));

        depositionRate.setBorder(BorderFactory.createBevelBorder(BevelBorder.LOWERED));
    }
    depositionIndex = selectionTabs.getTabCount()-1;
    boolean enabled = selectionTabs.isEnabledAt(depositionIndex);
    selectionTabs.setEnabledAt(depositionIndex, false);
}
}

```

```

        summaryPanel = new JPanel();
        selectionTabs.addTab("Model Summary", null, summaryPanel, null);
        {
            modelSummaryText = new JTextArea(280, 200);
            modelSummaryText.setPreferredSize(new java.awt.Dimension(537,
431));
            modelSummaryScrollPane = new JScrollPane(modelSummaryText,
JScrollPane.VERTICAL_SCROLLBAR_ALWAYS, JScrollPane.HORIZONTAL_SCROLLBAR_ALWAYS);
            summaryPanel.add(modelSummaryScrollPane);
            modelSummaryScrollPane.setPreferredSize(new
java.awt.Dimension(570, 462));
            modelSummaryText.setEditable(false);
        }
    }
}

{
    buttonPane = new JPanel();
    this.getContentPane().add(buttonPane, BorderLayout.SOUTH);
    FlowLayout buttonPanelLayout = new FlowLayout();
    buttonPanelLayout.setAlignment(FlowLayout.CENTER);
    buttonPane.setLayout(buttonPanelLayout);
    buttonPane.setPreferredSize(new java.awt.Dimension(517, 36));
    {
        readyButton = new JButton();
        buttonPane.add(readyButton);
        readyButton.setText("Ready");
        readyButton.setPreferredSize(new java.awt.Dimension(505, 26));
        readyButton.setBorder(BorderFactory
            .createBevelBorder(BevelBorder.RAISED));
        readyButton.addActionListener(this);
    }
    {
        nextButton = new JButton();
        buttonPane.add(nextButton);
        nextButton.setText("Next");
        nextButton
            .setPreferredSize(new java.awt.Dimension(113, 26));
        nextButton.setBorder(BorderFactory
            .createBevelBorder(BevelBorder.RAISED));
        nextButton.addActionListener(this);
    }
    {
        exitButton = new JButton();
        buttonPane.add(exitButton);
        exitButton.setText("Exit");
        exitButton.setPreferredSize(new java.awt.Dimension(113, 26));
        exitButton.setBorder(BorderFactory.createBevelBorder(BevelBorder.RAISED));
        exitButton.addActionListener(this);
    }
}
CoretransInterface.setDefaultLookAndFeelDecorated(true);

pack();
this.setVisible(true);
this.setLocation(10,10);
this.setSize(760, 700);
} catch (Exception e) {
    e.printStackTrace();
}
}

public void actionPerformed(ActionEvent e) {
    if (e.getSource() == diffusionButton){
        diffusionIsSelected = true;
        model.addElement("Diffusion");
        selectionTabs.setEnabledAt(diffusionIndex, true);
    } else if (e.getSource() == sorptionButton){

```



```

        sorptionIsSelected = true;
        model.addElement("Sorption");
        selectionTabs.setEnabledAt(sorptionIndex, true);
    } else if (e.getSource() == advectionButton){
        advectionIsSelected = true;
        model.addElement("Advection");
        selectionTabs.setEnabledAt(advectionIndex, true);
    } else if (e.getSource() == bioturbationButton){
        bioturbationIsSelected = true;
        model.addElement("Bioturbation");
        selectionTabs.setEnabledAt(bioturbationIndex, true);
    } else if (e.getSource() == degradationButton){
        degradationIsSelected = true;
        model.addElement("Degradation");
        selectionTabs.setEnabledAt(degradationIndex, true);
    } else if (e.getSource() == depositionButton){
        depositionIsSelected = true;
        model.addElement("Deposition");
        selectionTabs.setEnabledAt(depositionIndex, true);
    }
}

if (e.getSource() == addContaminantButton){
    newContaminantName.setEditable(true);
    casRegistryNum.setEditable(true);
    molecularFormula.setEditable(true);
    description.setEditable(true);
    molecularWeight.setEditable(true);
    molarVolume.setEditable(true);
    halfLife.setEditable(true);
    logKow.setEditable(true);
    updateDatabaseButton.setEnabled(true);
}
if (e.getSource() == cancelUpdateButton){
    newContaminantName.setEditable(false);
    casRegistryNum.setEditable(false);
    molecularFormula.setEditable(false);
    description.setEditable(false);
    molecularWeight.setEditable(false);
    molarVolume.setEditable(false);
    halfLife.setEditable(false);
    logKow.setEditable(false);
    updateDatabaseButton.setEnabled(false);
}
if (e.getSource() == updateDatabaseButton){

    String aContaminant = newContaminantName.getText();
    String aMolarVolume = molarVolume.getText();
    String aMolecularFormula = molecularFormula.getText();
    String aMolecularWeight = molecularWeight.getText();
    String aCASRegistryNum = casRegistryNum.getText();
    String aHalfLife = halfLife.getText();
    String aLogKow = logKow.getText();
    String aDescription = description.getText();

    ContaminantData newData = new ContaminantData(aContaminant, aMolarVolume,
aMolecularFormula, aMolecularWeight, aCASRegistryNum, aHalfLife, aLogKow,
aDescription);
    try {
        access.addContaminantData(newData);
    } catch (DuplicateException e1) {
        e1.printStackTrace();
    }
    contaminantNames.addElement(aContaminant);
}

if (e.getSource() == constantPorosityButton){
    porosityChoice = "constant";
    constantPorosity.setEditable(true);
    porosityAtInterface.setEditable(false);
    porosityAtInfinity.setEditable(false);
    attenuationFactor.setEditable(false);
    powerFactor.setEditable(false);
    powerExponent.setEditable(false);
    porosityAtInterface.setValue(new Double(resetValue));
    porosityAtInfinity.setValue(new Double(resetValue));
    attenuationFactor.setValue(new Double(resetValue));
}

```

```

    powerFactor.setValue(new Double(resetValue));
    powerExponent.setValue(new Double(resetValue));
} else if (e.getSource() == linearPorosityButton){
    porosityChoice = "linear";
    constantPorosity.setEditable(false);
    porosityAtInterface.setEditable(true);
    porosityAtInfinity.setEditable(true);
    attenuationFactor.setEditable(true);
    powerFactor.setEditable(false);
    powerExponent.setEditable(false);
    constantPorosity.setValue(new Double(resetValue));
    powerFactor.setValue(new Double(resetValue));
    powerExponent.setValue(new Double(resetValue));
} else if (e.getSource() == exponentialPorosityButton){
    porosityChoice = "exponential";
    constantPorosity.setEditable(false);
    porosityAtInterface.setEditable(true);
    porosityAtInfinity.setEditable(true);
    attenuationFactor.setEditable(true);
    powerFactor.setEditable(false);
    powerExponent.setEditable(false);
    constantPorosity.setValue(new Double(resetValue));
    powerFactor.setValue(new Double(resetValue));
    powerExponent.setValue(new Double(resetValue));
} else if (e.getSource() == inverseExponentialButton ){
    porosityChoice = "inverse";
    constantPorosity.setEditable(false);
    porosityAtInterface.setEditable(true);
    porosityAtInfinity.setEditable(true);
    attenuationFactor.setEditable(true);
    powerFactor.setEditable(false);
    powerExponent.setEditable(false);
    constantPorosity.setValue(new Double(resetValue));
    powerFactor.setValue(new Double(resetValue));
    powerExponent.setValue(new Double(resetValue));
} else if (e.getSource() == powerPorosityButton){
    porosityChoice = "power";
    constantPorosity.setEditable(false);
    porosityAtInterface.setEditable(false);
    porosityAtInfinity.setEditable(false);
    attenuationFactor.setEditable(false);
    powerFactor.setEditable(true);
    powerExponent.setEditable(true);
    constantPorosity.setValue(new Double(resetValue));
    porosityAtInterface.setValue(new Double(resetValue));
    porosityAtInfinity.setValue(new Double(resetValue));
    attenuationFactor.setValue(new Double(resetValue));
}

if (e.getSource() == constantInitialConcentrationButton){
    initialConcentrationFunction = "constant";
    initialConcentration.setEditable(true);
    initialDepthPenetration.setEditable(false);
    initialConcentrationAtInitialDepth.setEditable(false);
    initialDepthPenetration.setValue(new Double(resetValue));
    initialConcentrationAtInitialDepth.setValue(new Double(resetValue));
}

} else if (e.getSource() == stepFunctionInitialButton){
    initialConcentrationFunction = "step";
    initialConcentration.setEditable(false);
    initialDepthPenetration.setEditable(true);
    initialConcentrationAtInitialDepth.setEditable(true);
    initialConcentration.setValue(new Double(resetValue));
}

}

if (e.getSource() == dirichletButton){
    boundaryChoice = "dirichlet";
    dirichletLowerBoundary.setEditable(true);
    dirichletUpperBoundary.setEditable(true);
    neumannLowerBoundary.setEditable(false);
    neumannUpperBoundary.setEditable(false);
    robinLowerConcentrationCoefficient.setEditable(false);
    robinUpperConcentrationCoefficient.setEditable(false);
    robinLowerFluxCoefficient.setEditable(false);
    robinUpperFluxCoefficient.setEditable(false);
    robinLowerBoundary.setEditable(false);
    robinUpperBoundary.setEditable(false);
}

```

```

neumannLowerBoundary.setValue(new Double(resetValue));
neumannUpperBoundary.setValue(new Double(resetValue));
robinLowerConcentrationCoefficient.setValue(new Double(resetValue));
robinUpperConcentrationCoefficient.setValue(new Double(resetValue));
robinLowerFluxCoefficient.setValue(new Double(resetValue));
robinUpperFluxCoefficient.setValue(new Double(resetValue));
robinLowerBoundary.setValue(new Double(resetValue));
robinUpperBoundary.setValue(new Double(resetValue));

} else if (e.getSource() == neumannButton){
boundaryChoice = "neumann";
dirichletLowerBoundary.setEditable(false);
dirichletUpperBoundary.setEditable(false);
neumannLowerBoundary.setEditable(true);
neumannUpperBoundary.setEditable(true);
robinLowerConcentrationCoefficient.setEditable(false);
robinUpperConcentrationCoefficient.setEditable(false);
robinLowerFluxCoefficient.setEditable(false);
robinUpperFluxCoefficient.setEditable(false);
robinLowerBoundary.setEditable(false);
robinUpperBoundary.setEditable(false);
dirichletLowerBoundary.setValue(new Double(resetValue));
dirichletUpperBoundary.setValue(new Double(resetValue));
robinLowerConcentrationCoefficient.setValue(new Double(resetValue));
robinUpperConcentrationCoefficient.setValue(new Double(resetValue));
robinLowerFluxCoefficient.setValue(new Double(resetValue));
robinUpperFluxCoefficient.setValue(new Double(resetValue));
robinLowerBoundary.setValue(new Double(resetValue));
robinUpperBoundary.setValue(new Double(resetValue));
} else if (e.getSource() == robinButton){
boundaryChoice = "robin";
dirichletLowerBoundary.setEditable(false);
dirichletUpperBoundary.setEditable(false);
neumannLowerBoundary.setEditable(false);
neumannUpperBoundary.setEditable(false);
robinLowerConcentrationCoefficient.setEditable(true);
robinUpperConcentrationCoefficient.setEditable(true);
robinLowerFluxCoefficient.setEditable(true);
robinUpperFluxCoefficient.setEditable(true);
robinLowerBoundary.setEditable(true);
robinUpperBoundary.setEditable(true);
dirichletLowerBoundary.setValue(new Double(resetValue));
dirichletUpperBoundary.setValue(new Double(resetValue));
neumannLowerBoundary.setValue(new Double(resetValue));
neumannUpperBoundary.setValue(new Double(resetValue));
}

if (e.getSource() == userDefinedDiffusivityButton){
diffusivityIsUserDefined = true;
diffusivityChoice = "null";
userDefinedDiffusivity.setEditable(true);
wilkeChangButton.setEnabled(false);
reddyDoraiswamyButton.setEnabled(false);
haydukLaudieButton.setEnabled(false);
} else if (e.getSource() == approximatedDiffusivityButton){
diffusivityIsUserDefined = false;
userDefinedDiffusivity.setEditable(false);
userDefinedDiffusivity.setValue(new Double(resetValue));
wilkeChangButton.setEnabled(true);
reddyDoraiswamyButton.setEnabled(true);
haydukLaudieButton.setEnabled(true);
}

if (e.getSource() == wilkeChangButton){
diffusivityChoice = "Wilke-Chang";
reddyDoraiswamyButton.setEnabled(false);
haydukLaudieButton.setEnabled(false);
} else if (e.getSource() == reddyDoraiswamyButton){
diffusivityChoice = "Reddy-Doraiswamy";
reddyDoraiswamyButton.setEnabled(true);
wilkeChangButton.setEnabled(false);
haydukLaudieButton.setEnabled(false);
} else if (e.getSource() == haydukLaudieButton){
diffusivityChoice = "Hayduk-Laudie";
haydukLaudieButton.setEnabled(true);
wilkeChangButton.setEnabled(false);
reddyDoraiswamyButton.setEnabled(false);
}

```

```

}
if (e.getSource() == linearPartitioningButton){
    isotherm.addElement("Linear partitioning");
    linearPartitioningIsSelected = true;
    linearDatabaseButton.setEnabled(true);
    linearUserButton.setEnabled(true);
    aConstantLinear.setEditable(false);
    bConstantLinear.setEditable(false);

} else if (e.getSource() == freundlichButton){
    isotherm.addElement("Freundlich");
    freundlichIsSelected = true;
    freundlichConstant.setEditable(true);
    freundlichExponent.setEditable(true);
} else if (e.getSource() == langmuirButton){
    isotherm.addElement("Langmuir");
    langmuirIsSelected = true;
    langmuirConcentration.setEditable(true);
    langmuirConstant.setEditable(true);
}
if (e.getSource() == linearDatabaseButton){
    linearParameterIsUserDefined = false;
    linearUserButton.setEnabled(false);
    aConstantLinear.setEditable(false);
    bConstantLinear.setEditable(false);
}
if (e.getSource() == linearUserButton){
    linearParameterIsUserDefined = true;
    linearDatabaseButton.setEnabled(false);
    aConstantLinear.setEditable(true);
    bConstantLinear.setEditable(true);
}

if (e.getSource() == userDefinedVelocityButton){
    advectionIsUserDefined = true;
    sedimentPermeability.setEditable(true);
    hydraulicConductivity.setEditable(false);
    hydraulicConductivity.setValue(new Double(resetValue));
} else if (e.getSource() == approximatedVelocityButton){
    advectionIsUserDefined = false;
    sedimentPermeability.setEditable(false);
    hydraulicConductivity.setEditable(true);
    sedimentPermeability.setValue(new Double(resetValue));
}

if (e.getSource() == userDefinedBioturbationConstantButton){
    bioturbationIsUserDefined = true;
    exchangeCoefficient.setEditable(true);
    bioturbationDepth.setEditable(false);
    waterVelocity.setEditable(false);
    bioturbationDepth.setValue(new Double(resetValue));
    waterVelocity.setValue(new Double(resetValue));
} else if (e.getSource() == approximatedBioturbationConstantButton){
    bioturbationIsUserDefined = false;
    exchangeCoefficient.setEditable(false);
    bioturbationDepth.setEditable(true);
    waterVelocity.setEditable(true);
    exchangeCoefficient.setValue(new Double(resetValue));
}

if (e.getSource() == approximatedDegradationConstantButton){
    degradationIsUserDefined = false;
    degradationConstant.setEditable(false);
    degradationConstant.setValue(new Double(resetValue));
} else if (e.getSource() == userDefinedDegradationConstantButton){
    degradationIsUserDefined = true;
    degradationConstant.setEditable(true);
}

if (e.getSource() == open){
    int returnVal = fc.showOpenDialog(menuBar);
    if (returnVal == JFileChooser.APPROVE_OPTION){

        File file = fc.getSelectedFile();

        CoretransDataFileLoader fileLoader;

```

```

    try {
        fileLoader = new CoretransDataFileLoader(file.getName(),
"output.dat");
        sedimentDepth.setValue(new Double(fileLoader.getParamaters(1)));

        sedimentDensity.setValue(new Double(fileLoader.getParamaters(3)));
        waterTemperature.setValue(new Double(fileLoader.getParamaters(5)));
        organicFraction.setValue(new Double(fileLoader.getParamaters(7)));
        simulationTime.setValue(new Double(fileLoader.getParamaters(9)));
        numberOfGrids.setValue(new Double(fileLoader.getParamaters(11)));
        constantPorosity.setValue(new Double(fileLoader.getParamaters(13)));
        porosityAtInterface.setValue(new
Double(fileLoader.getParamaters(15)));
        porosityAtInfinity.setValue(new
Double(fileLoader.getParamaters(17)));
        attenuationFactor.setValue(new
Double(fileLoader.getParamaters(19)));
        powerFactor.setValue(new Double(fileLoader.getParamaters(21)));
        powerExponent.setValue(new Double(fileLoader.getParamaters(23)));
        initialConcentration.setValue(new
Double(fileLoader.getParamaters(25)));
        initialDepthPenetration.setValue(new
Double(fileLoader.getParamaters(27)));
        initialConcentrationAtInitialDepth.setValue(new
Double(fileLoader.getParamaters(29)));
        dirichletLowerBoundary.setValue(new
Double(fileLoader.getParamaters(31)));
        dirichletUpperBoundary.setValue(new
Double(fileLoader.getParamaters(33)));
        neumannLowerBoundary.setValue(new
Double(fileLoader.getParamaters(35)));
        neumannUpperBoundary.setValue(new
Double(fileLoader.getParamaters(37)));
        robinLowerConcentrationCoefficient.setValue(new
Double(fileLoader.getParamaters(39)));
        robinUpperConcentrationCoefficient.setValue(new
Double(fileLoader.getParamaters(41)));
        robinLowerFluxCoefficient.setValue(new
Double(fileLoader.getParamaters(43)));
        robinUpperFluxCoefficient.setValue(new
Double(fileLoader.getParamaters(45)));
        robinLowerBoundary.setValue(new
Double(fileLoader.getParamaters(47)));
        robinUpperBoundary.setValue(new
Double(fileLoader.getParamaters(49)));
        userDefinedDiffusivity.setValue(new
Double(fileLoader.getParamaters(51)));
        aConstantLinear.setValue(new Double(fileLoader.getParamaters(53)));
        bConstantLinear.setValue(new Double(fileLoader.getParamaters(55)));
        freundlichConstant.setValue(new
Double(fileLoader.getParamaters(57)));
        freundlichExponent.setValue(new
Double(fileLoader.getParamaters(59)));
        langmuirConcentration.setValue(new
Double(fileLoader.getParamaters(61)));
        langmuirConstant.setValue(new Double(fileLoader.getParamaters(63)));
        pressureGradient.setValue(new Double(fileLoader.getParamaters(65)));
        sedimentPermeability.setValue(new
Double(fileLoader.getParamaters(67)));
        hydraulicConductivity.setValue(new
Double(fileLoader.getParamaters(69)));
        overlyingWaterConcentration.setValue(new
Double(fileLoader.getParamaters(71)));
        exchangeCoefficient.setValue(new
Double(fileLoader.getParamaters(73)));
        bioturbationDepth.setValue(new
Double(fileLoader.getParamaters(75)));
        waterVelocity.setValue(new Double(fileLoader.getParamaters(77)));
        degradationConstant.setValue(new
Double(fileLoader.getParamaters(79)));
        depositionRate.setValue(new Double(fileLoader.getParamaters(81)));

    } catch (IOException e1) {
        // TODO Auto-generated catch block
        e1.printStackTrace();
    }
}

```

```

    }
}

if (e.getSource() == save){
    int returnVal = fc.showSaveDialog(menuBar);
    if (returnVal == JFileChooser.APPROVE_OPTION){
        File file = fc.getSelectedFile();
        System.out.println("File saved: " + file.getName());
        String report = "Sediment depth, mm" + newline + aSedimentDepth +
newline +
        "Sediment density, kg/L" + newline + aSedimentDensity +
newline +
        "Temperature, K" + newline + aWaterTemperature + newline +
        "Fraction of Organic Carbon" + newline +
anOrganicFractionContent + newline +
        "Simulation time, weeks" + newline + aSimulationTime +
newline +
        "Number of grids" + newline + aNumberOfGrids + newline +
        "Constant porosity" + newline + aConstantPorosity + newline
+
        "Porosity at interface" + newline + aPorosityAtInterface +
newline +
        "Porosity at infinite depth" + newline +
aPorosityAtInfinity + newline +
        "Attenuation factor" + newline + anAttenuationFactor +
newline +
        "Power constant porosity" + newline + aPowerFactor +
newline +
        "Power exponent porosity" + newline + aPowerExponent +
newline +
        "Initial concentration, g/m3" + newline +
anInitialConcentration + newline +
        "Initial depth, cm" + newline + anInitialDepth + newline +
        "Initial concentration at initial depth, g/m3" + newline +
anInitialConcentrationAtInitialDepth + newline +
        "Dirichlet lower boundary, g/m3" + newline +
aDirichletLowerBoundary + newline +
        "Dirichlet upper boundary, g/m3" + newline +
aDirichletUpperBoundary + newline +
        "Neumann lower boundary, g/m2" + newline +
aNeumannLowerBoundary + newline +
        "Neumann upper boundary, g/m2" + newline +
aNeumannUpperBoundary + newline +
        "Robin lower concentration coefficient" + newline +
aLowerConcentrationCoefficient + newline +
        "Robin upper concentration coefficient" + newline +
anUpperConcentrationCoefficient + newline +
        "Robin lower flux coefficient" + newline +
aLowerFluxCoefficient + newline +
        "Robin upper flux coefficient" + newline +
anUpperFluxCoefficient + newline +
        "Robin lower boundary, g/m3" + newline +
aRobinLowerCondition + newline +
        "Robin upper boundary, g/m3" + newline +
aRobinUpperCondition + newline +
        "User defined Diffusivity, cm/s" + newline + aDiffusivity +
newline +
        "constant a for Linear partitioning" + newline +
anAConstant + newline +
        "constant b for Linear partitioning" + newline + aBConstant
+ newline +
        "Freundlich constant, (m3/g)^n" + newline +
aFreundlichConstant + newline +
        "Freundlich exponent" + newline + aFreundlichExponent +
newline +
        "Langmuir saturation concentration, g/m3" + newline +
aLangmuirConcentration + newline +
        "Langmuir constant" + newline + aLangmuirConstant + newline
+
        "Porewater pressure gradient, Pa/m" + newline +
aPressureGradient + newline +
        "Sediment permeability, m2" + newline +
aSedimentPermeability + newline +
        "Hydraulic conductivity, m/s" + newline +
aHydraulicConductivity + newline +

```

```

                "Overlying water concentration, g/m3" + newline +
anOverlyingWaterConcentration + newline +
                "Bioturbation exchange coefficient, /week" + newline +
anExchangeCoefficient + newline +
                "Bioturbation depth, mm" + newline + aBioturbationDepth +
newline +
                "Water velocity at interface, m/s" + newline +
anInterfaceWaterVelocity + newline +
                "User defined degradation rate, /week" + newline +
aDegradationConstant + newline +
                "Deposition rate, cm/yr" + newline + aDepositionRate;

        try {
            CoretransDataFileSaver fileSaverfileSaver = new
CoretransDataFileSaver(file.getName(), report);
        } catch (IOException e1) {
            // TODO Auto-generated catch block
            e1.printStackTrace();
        }
    }
}

if (e.getSource() == readyButton){
    boolean noContaminantSelected = contaminantList.isSelectionEmpty();

    if (noContaminantSelected == true){
        JOptionPane.showMessageDialog(this, "You have to select a contaminant
to complete the transport model.");
        return;
    }
    findContaminant();
    if (diffusionIsSelected == false){
        JOptionPane.showMessageDialog(this, "You have to select the diffusion
process to complete the transport model.");
        return;
    }
    if (aSedimentDepth == 0){
        JOptionPane.showMessageDialog(this, "You have to supply the sediment
depth to complete the transport model.");
        return;
    }
    if (aSimulationTime == 0){
        JOptionPane.showMessageDialog(this, "You have to supply the simulation
time to complete the transport model.");
        return;
    }
    if (aNumberOfGrids == 0){
        JOptionPane.showMessageDialog(this, "You have to supply the number of
grids to complete the transport model.");
        return;
    }
}

    solver = new CoretransNumericalSolver(aSedimentDepth, aNumberOfGrids,
aSedimentDensity, aWaterTemperature,
anOrganicFractionContent,
contaminantMolarVolume, contaminantHalfLife,
contaminantLogKow, contaminantDescription,
porosityChoice, aConstantPorosity,
aPorosityAtInterface, aPorosityAtInfinity, anAttenuationFactor, aPowerFactor,
aPowerExponent,
diffusivityIsUserDefined, diffusivityChoice,
aDiffusivity,
sorptionIsSelected, linearPartitioningIsSelected, linearParameterIsUserDefined,
anAConstant, aBConstant,
freundlichIsSelected, aFreundlichConstant,
aFreundlichExponent,
langmuirIsSelected, aLangmuirConcentration,
aLangmuirConstant,
advectionIsSelected, advectionIsUserDefined,
aPressureGradient, aHydraulicConductivity, aSedimentPermeability,
bioturbationIsSelected,
bioturbationIsUserDefined, anOverlyingWaterConcentration, anExchangeCoefficient,
aBioturbationDepth, anInterfaceWaterVelocity,
degradationIsSelected,
degradationIsUserDefined, aDegradationConstant,

```

```

        depositionIsSelected, aDepositionRate,
        boundaryChoice, aDirichletUpperBoundary,
aDirichletLowerBoundary, aNeumannUpperBoundary, aNeumannLowerBoundary,
anUpperConcentrationCoefficient,
        anUpperFluxCoefficient,
aRobinUpperCondition, aLowerConcentrationCoefficient, aLowerFluxCoefficient,
aRobinLowerCondition,
        initialConcentrationFunction,
anInitialConcentration, anInitialConcentrationAtInitialDepth, anInitialDepth);
CoretransNumericalSolver.activate(solver);
System.out.println(contaminantDescription);

DecimalFormat formatter = new DecimalFormat("0.##E0");
DecimalFormat aFormat = new DecimalFormat("#,###.##");

modelSummaryText.append("CORETRANS 1.0" + newline);

c = (GregorianCalendar) GregorianCalendar.getInstance();
int hr = c.get(Calendar.HOUR_OF_DAY);
int mn = c.get(Calendar.MINUTE);
String time = hr + " : " + mn;

int dayOfTheWeek = c.get(Calendar.DAY_OF_WEEK);
String days = "";
switch (dayOfTheWeek) {
    case 1: days = "Sunday"; break;
    case 2: days = "Monday"; break;
    case 3: days = "Tuesday"; break;
    case 4: days = "Wednesday"; break;
    case 5: days = "Thursday"; break;
    case 6: days = "Friday"; break;
    case 7: days = "Saturday"; break;
}
int day = c.get(Calendar.DATE);
int month = c.get(Calendar.MONTH);
int year = c.get(Calendar.YEAR);
String date = days + " " + day + " / " + month + " / " + year;

modelSummaryText.append(time + " " + date + newline);
modelSummaryText.append(newline + "=====" +
newline);
modelSummaryText.append("  Model Simulation Summary" + newline);
modelSummaryText.append("=====" + newline);
modelSummaryText.append(newline + "Contaminant" + newtab + newtab + ": " +
+ contaminantName + newline);
modelSummaryText.append("CAS Registry Number" + newtab + ": " +
contaminantCAS + newline);
modelSummaryText.append("Molecular Formula" + newtab + ": " +
contaminantMF + newline);
modelSummaryText.append("Molecular Weight" + newtab + ": " +
contaminantMW + newline);
modelSummaryText.append("Molar Volume" + newtab + newtab + ": " +
contaminantMolarVolume + newline);
modelSummaryText.append("Log Kow" + newtab + newtab + ": " +
contaminantLogKow + newline);
modelSummaryText.append("Half Life (days)" + newtab + newtab + ": " +
contaminantHalfLife + newline);

modelSummaryText.append(newline + "I.  Mechanisms" + newline + newline);
for (int i = 0; i < model.size(); i++) {
    String process = (String)model.elementAt(i);
    modelSummaryText.append(process + newline);
    mechanism = mechanism + process + newline;
}
modelSummaryText.append(newline + "II.  Parameters" + newline);
modelSummaryText.append(newline + "Sediment depth" + newtab + newtab + ": "
+ aSedimentDepth + " cm" + newline);
modelSummaryText.append("Sediment density" + newtab + ": " +
aSedimentDensity + " Kg/L" + newline);
modelSummaryText.append("Water temperature" + newtab + ": " +
aWaterTemperature + " K" + newline);
modelSummaryText.append("Organic fraction" + newtab + newtab + ": " +
anOrganicFractionContent + newline);

if (porosityChoice == "constant") {
    porosity = "(constant) " + aConstantPorosity;
} else if (porosityChoice == "linear") {

```



```

        porosity = "(linear) " + aPorosityAtInfinity + " - " +
aFormat.format((aPorosityAtInterface - aPorosityAtInfinity)/anAttenuationFactor)
+ " x depth";
    } else if (porosityChoice == "exponential"){
        porosity = "(exponential) " + aPorosityAtInfinity + " + " +
aFormat.format(aPorosityAtInterface - aPorosityAtInfinity) + " x exp(" +
aFormat.format(-1/anAttenuationFactor) + " x depth)" ;
    } else if (porosityChoice == "inverse"){
        porosity = "(inverse exponential) " +
aFormat.format(aPorosityAtInfinity * aPorosityAtInterface) + " / (" +
aPorosityAtInterface + " + " + aFormat.format(aPorosityAtInfinity -
aPorosityAtInterface) + " x exp(" + (-1/anAttenuationFactor) + " x depth))" ;
    } else if (porosity == "power"){
        porosity = "(power) " + aPowerFactor + " x depth^ -" +
aPowerExponent;
    }
    modelSummaryText.append("Porosity" + newtab + newtab + ": " + porosity +
newline);
    modelSummaryText.append("Simulation time" + newtab + newtab + ": " +
aSimulationTime + " weeks" + newline);
    modelSummaryText.append("Number of grids" + newtab + ": " +
aNumberOfGrids + newline);

    modelSummaryText.append(newline + "Empirical correlation" + newtab + ":
" + diffusivityChoice + newline);
    modelSummaryText.append("Effective diffusivity" + newtab + ": " +
formatter.format(solver.thePorewaterConcentration.D()/60.48) + " cm2/s"+ newline);

    modelSummaryText.append(newline + "Sorption isotherms" + newtab + ": " +
newline);
    for (int i = 0; i < isotherm.size(); i++){
        String sorption = (String)isotherm.elementAt(i);
        modelSummaryText.append(sorption + newline);
        isotherms = isotherms + sorption + newline;
    }

    if (linearParameterIsUserDefined == true){
        modelSummaryText.append("Partitioning coefficient" + newtab + ": " +
anAConstant + " depth^-" + aBConstant);
    } else {
        modelSummaryText.append("Partitioning coefficient" + newtab + ": " +
aFormat.format(anOrganicFractionContent * Math.pow(10, (0.98 *
Double.parseDouble(contaminantLogKow) - 0.32))) + " L/Kg");
    }
    modelSummaryText.append(newline + "Freundlich constant" + newtab + ": " +
aFreundlichConstant);
    modelSummaryText.append(newline + "Freundlich exponent" + newtab + ": " +
aFreundlichExponent);
    modelSummaryText.append(newline + "Saturation concentration" + newtab +
": " + aLangmuirConcentration);
    modelSummaryText.append(newline + "Langmuir constant" + newtab + ": " +
aLangmuirConstant + newline);

    modelSummaryText.append(newline + "Advection velocity" + newtab + ": " +
aFormat.format(solver.thePorewaterConcentration.advection()/(84600 * 7)) + "
m/s");
    modelSummaryText.append(newline + "Mass exchange coefficient" + newtab +
": " + aFormat.format(solver.thePorewaterConcentration.bioturbation()/(84600 *
7)) + " /s");
    modelSummaryText.append(newline + "Degradation rate" + newtab + ": " +
formatter.format(solver.thePorewaterConcentration.degradation()/7) + " /day");
    modelSummaryText.append(newline + "Deposition rate" + newtab + newtab +
": " + aDepositionRate + " cm/yr");

    modelSummaryText.append(newline + newline + "III. Initial and Boundary
Conditions"+ newline);
    if (initialConcentrationFunction == "constant"){
        modelSummaryText.append(newline + "Initial Concentration" + newtab +
newtab + newtab + ": " + anInitialConcentration + " g/m3" + newline);
        initial = newline + "Initial Concentration" + newtab + ": " +
anInitialConcentration + " g/m3" + newline;
    } else if (initialConcentrationFunction == "step"){
        modelSummaryText.append(newline + "Initial Concentration" + newtab +
newtab + ": " + anInitialConcentrationAtInitialDepth + " g/m3 uniformly
distributed at " + anInitialDepth + " cm depth" + newline );
    }

```

```

        initial = newline + "Initial Concentration" + newtab + ": " +
anInitialConcentrationAtInitialDepth + " g/m3 uniformly distributed at " +
anInitialDepth + " cm depth" + newline;
    }

    modelSummaryText.append(newline + "Boundary Conditions" + newtab + newtab
+ ": " + boundaryChoice + newline);
    if (boundaryChoice == "dirichlet"){
        modelSummaryText.append("Concentration at interface" + newtab + newtab
+ ": " + aDirichletLowerBoundary + " g/m3" + newline);
        modelSummaryText.append("Concentration at " + aSedimentDepth + " mm
depth" + newtab + ": " + aDirichletUpperBoundary + " g/m3" + newline);
        boundary = "Concentration at interface" + newtab + newtab + ": " +
aDirichletLowerBoundary + " g/m3" + newline + "Concentration at " + aSedimentDepth
+ " mm depth" + newtab + ": " + aDirichletUpperBoundary + " g/m3" + newline;
    } else if (boundaryChoice == "neumann"){
        modelSummaryText.append("Flux at interface" + newtab + newtab + ": "
+ aNeumannLowerBoundary + " g/m2" + newline);
        modelSummaryText.append("Flux at " + aSedimentDepth + " mm depth" +
newtab + ": " + aNeumannUpperBoundary + " g/m2" + newline);
        boundary = "Flux at interface" + newtab + newtab + ": " +
aNeumannLowerBoundary + " g/m2" + newline + "Flux at " + aSedimentDepth + " mm
depth" + newtab + ": " + aNeumannUpperBoundary + " g/m2" + newline;
    } else if (boundaryChoice == "robin"){
        modelSummaryText.append("Conditions at interface" + newtab + ": " +
aLowerConcentrationCoefficient + "C(x,t) + " + aLowerFluxCoefficient + "dC(x,t) =
" + aRobinLowerCondition + newline);
        modelSummaryText.append("Conditions at " + aSedimentDepth + " mm
depth" + newtab + ": " + anUpperConcentrationCoefficient + "C(x,t) + " +
anUpperFluxCoefficient + "dC(x,t) = " + aRobinUpperCondition + newline);
        boundary = "Conditions at interface" + newtab + ": " +
aLowerConcentrationCoefficient + "C(x,t) + " + aLowerFluxCoefficient + "dC(x,t) =
" + aRobinLowerCondition + newline + "Conditions at " + aSedimentDepth + " mm
depth" + newtab + ": " + anUpperConcentrationCoefficient + "C(x,t) + " +
anUpperFluxCoefficient + "dC(x,t) = " + aRobinUpperCondition + newline;
    }
    modelSummaryText.append(newline + "Porewater Concentration-Depth profile"
+ newline);
    modelSummaryText.append(newline + newtab + "Depth" + newtab + newtab +
"Concentration" + newline);
    for (int i = 0; i <
solver.thePorewaterConcentration.printPoints().size(); i++){

        modelSummaryText.append(solver.thePorewaterConcentration.printPoints().elementA
t(i) + newline);
        String point =
solver.thePorewaterConcentration.printPoints().elementAt(i) + newline;
        points = points + point;
    }
    modelSummaryText.append(newline + newline + "Sediment-bound
Concentration-Depth profile" + newline);
    modelSummaryText.append(newline + newtab + "Depth" + newtab + newtab +
"Concentration" + newline);
    for (int i = 0; i <
solver.thePorewaterConcentration.printPoints().size(); i++){

        modelSummaryText.append(solver.thePorewaterConcentration.printMorePoints(linear
PartitioningIsSelected, linearParameterIsUserDefined, anAConstant, aBConstant,
anOrganicFractionContent, Double.parseDouble(contaminantLogKow),
freundlichIsSelected, aFreundlichConstant, aFreundlichExponent,
langmuirIsSelected, aLangmuirConcentration,
aLangmuirConstant).elementAt(i) + newline);
        String point =
solver.thePorewaterConcentration.printMorePoints(linearPartitioningIsSelected,
linearParameterIsUserDefined, anAConstant, aBConstant,
anOrganicFractionContent, Double.parseDouble(contaminantLogKow),
freundlichIsSelected, aFreundlichConstant, aFreundlichExponent,
langmuirIsSelected, aLangmuirConcentration,
aLangmuirConstant).elementAt(i) + newline;
        morePoints = morePoints + point;
    }

    modelSummaryText.append(newline + newline + "----- END -----" + newline);

    String report = "CORETRANS 1.0" + newline + time + " " + date + newline +
newline + "=====" + newline +
" Model Simulation Summary" + newline +

```

```

"=====" + newline +
newline + "Contaminant" + newtab + newtab + newtab + ": " +
contaminantName + newline +
"CAS Registry Number" + newtab + ": " + contaminantCAS + newline +
"Molecular Formula" + newtab + newtab + ": " + contaminantMF +
newline +
"Molecular Weight" + newtab + newtab + ": " + contaminantMW +
newline +
"Molar Volume" + newtab + newtab + ": " + contaminantMolarVolume +
newline +
"Log Kow" + newtab + newtab + newtab + ": " + contaminantLogKow +
newline +
"Half Life (days)" + newtab + newtab + ": " + contaminantHalfLife +
newline +
newline + "I. Mechanisms" + newline + newline + mechanism +
newline + "II. Parameters " + newline +
newline + "Sediment depth" + newtab + newtab + ": " +
aSedimentDepth + " mm" + newline +
"Sediment density" + newtab + newtab + ": " + aSedimentDensity + "
Kg/L" + newline +
"Water temperature" + newtab + newtab + ": " + aWaterTemperature +
" K" + newline +
"Organic fraction" + newtab + newtab + ": " +
anOrganicFractionContent + newline +
"Porosity" + newtab + newtab + newtab + ": " + porosity + newline +
"Simulation time" + newtab + newtab + ": " + aSimulationTime + "
weeks" + newline +
"Number of grids" + newtab + newtab + ": " + aNumberOfGrids +
newline +
newline + "Empirical correlation" + newtab + ": " +
diffusivityChoice + newline +
"Effective diffusivity" + newtab + ": " +
formatter.format(solver.thePorewaterConcentration.D()/60.48) + " cm2/s" + newline +
newline + "Sorption isotherms" + newtab + ": " + newline +
isotherms +
newline + "Freundlich constant" + newtab + newtab + ": " +
aFreundlichConstant +
newline + "Freundlich exponent" + newtab + newtab + ": " +
aFreundlichExponent +
newline + "Saturation concentration" + newtab + ": " +
aLangmuirConcentration +
newline + "Langmuir constant" + newtab + newtab + newtab + ": " +
aLangmuirConstant + newline +
newline + "Advection velocity" + newtab + newtab + ": " +
aFormat.format(solver.thePorewaterConcentration.advection()/(84600 * 7)) + " m/s"
+
newline + "Mass exchange coefficient" + newtab + ": " +
aFormat.format(solver.thePorewaterConcentration.bioturbation()/(84600 * 7)) + "
/s" +
newline + "Degradation rate" + newtab + newtab + newtab + ": " +
formatter.format(solver.thePorewaterConcentration.degradation()/7) + " /day" +
newline + "Deposition rate" + newtab + newtab + newtab + ": " +
aDepositionRate + " cm/yr" + newline +
newline + newtab + "III. Initial and Boundary Conditions" + newline
+ initial +
newline + "Boundary Conditions" + newtab + newtab + newtab + ": " +
boundaryChoice + newline + boundary +
newline + "Porewater Concentration-Depth profile" + newline +
newline + newtab + "Depth" + newtab + newtab + newtab +
newtab + "Concentration" + newline + points +
newline + "Sediment-bound Concentration-Depth profile" + newline +
newline + newtab + "Depth" + newtab + newtab + newtab +
newtab + "Concentration" + newline + morePoints +
newline + newtab + "----- END -----" + newline;

try {
CoretransDataFileSaver fileSaverfileSaver = new
CoretransDataFileSaver("summary.dat", report);
} catch (IOException e1) {
// TODO Auto-generated catch block
e1.printStackTrace();
}

access.terminate();
}
}

```

```

public void propertyChange(PropertyChangeEvent e) {

    if (e.getSource() == sedimentDepth){
        aSedimentDepth = ((Number)sedimentDepth.getValue()).doubleValue();
    }
    if (e.getSource() == sedimentDensity){
        aSedimentDensity = ((Number)sedimentDensity.getValue()).doubleValue();
    }
    if (e.getSource() == waterTemperature){
        aWaterTemperature = ((Number)waterTemperature.getValue()).doubleValue();
    }
    if (e.getSource() == organicFraction){
        anOrganicFractionContent =
((Number)organicFraction.getValue()).doubleValue();
    }
    if (e.getSource() == simulationTime){
        aSimulationTime = ((Number)simulationTime.getValue()).doubleValue();
    }
    if (e.getSource() == numberOfGrids){
        aNumberOfGrids = ((Number)numberOfGrids.getValue()).doubleValue();
    }
    if (e.getSource() == initialConcentration){
        anInitialConcentration =
((Number)initialConcentration.getValue()).doubleValue();
    }
    if (e.getSource() == initialDepthPenetration){
        anInitialDepth =
((Number)initialDepthPenetration.getValue()).doubleValue();
    }
    if (e.getSource() == initialConcentrationAtInitialDepth){
        anInitialConcentrationAtInitialDepth =
((Number)initialConcentrationAtInitialDepth.getValue()).doubleValue();
    }
    if (e.getSource() == constantPorosity){
        aConstantPorosity = ((Number)constantPorosity.getValue()).doubleValue();
    }
    if (e.getSource() == porosityAtInterface){
        aPorosityAtInterface =
((Number)porosityAtInterface.getValue()).doubleValue();
    }
    if (e.getSource() == porosityAtInfinity){
        aPorosityAtInfinity =
((Number)porosityAtInfinity.getValue()).doubleValue();
    }
    if (e.getSource() == attenuationFactor){
        anAttenuationFactor =
((Number)attenuationFactor.getValue()).doubleValue();
    }
    if (e.getSource() == powerFactor){
        aPowerFactor = ((Number)powerFactor.getValue()).doubleValue();
    }
    if (e.getSource() == powerExponent){
        aPowerExponent = ((Number)powerExponent.getValue()).doubleValue();
    }
    if (e.getSource() == userDefinedDiffusivity){
        aDiffusivity = ((Number)userDefinedDiffusivity.getValue()).doubleValue();
    }
    if (e.getSource() == aConstantLinear){
        anAConstant = ((Number)aConstantLinear.getValue()).doubleValue();
    }
    if (e.getSource() == bConstantLinear){
        aBConstant = ((Number)bConstantLinear.getValue()).doubleValue();
    }
    if (e.getSource() == freundlichConstant){
        aFreundlichConstant =
((Number)freundlichConstant.getValue()).doubleValue();
    }
    if (e.getSource() == freundlichExponent){
        aFreundlichExponent =
((Number)freundlichExponent.getValue()).doubleValue();
    }
    if (e.getSource() == langmuirConcentration){
        aLangmuirConcentration =
((Number)langmuirConcentration.getValue()).doubleValue();
    }
}

```

```

    }
    if (e.getSource() == langmuirConstant){
        aLangmuirConstant = ((Number)langmuirConstant.getValue()).doubleValue();
    }
    if (e.getSource() == pressureGradient){
        aPressureGradient = ((Number)pressureGradient.getValue()).doubleValue();
    }
    if (e.getSource() == sedimentPermeability){
        aSedimentPermeability =
((Number)sedimentPermeability.getValue()).doubleValue();
    }
    if (e.getSource() == hydraulicConductivity){
        aHydraulicConductivity =
((Number)hydraulicConductivity.getValue()).doubleValue();
    }
    if (e.getSource() == overlyingWaterConcentration){
        anOverlyingWaterConcentration =
((Number)overlyingWaterConcentration.getValue()).doubleValue();
    }
    if (e.getSource() == exchangeCoefficient){
        anExchangeCoefficient =
((Number)exchangeCoefficient.getValue()).doubleValue();
    }
    if (e.getSource() == bioturbationDepth){
        aBioturbationDepth =
((Number)bioturbationDepth.getValue()).doubleValue();
    }
    if (e.getSource() == waterVelocity){
        anInterfaceWaterVelocity =
((Number)waterVelocity.getValue()).doubleValue();
    }
    if (e.getSource() == degradationConstant){
        aDegradationConstant =
((Number)degradationConstant.getValue()).doubleValue();
    }
    if (e.getSource() == depositionRate){
        aDepositionRate = ((Number)depositionRate.getValue()).doubleValue();
    }
    if (e.getSource() == dirichletUpperBoundary){
        aDirichletUpperBoundary =
((Number)dirichletUpperBoundary.getValue()).doubleValue();
    }
    if (e.getSource() == dirichletLowerBoundary){
        aDirichletLowerBoundary =
((Number)dirichletLowerBoundary.getValue()).doubleValue();
    }
    if (e.getSource() == neumannUpperBoundary){
        aNeumannUpperBoundary =
((Number)neumannUpperBoundary.getValue()).doubleValue();
    }
    if (e.getSource() == neumannLowerBoundary){
        aNeumannLowerBoundary =
((Number)neumannLowerBoundary.getValue()).doubleValue();
    }
    if (e.getSource() == robinLowerConcentrationCoefficient){
        aLowerConcentrationCoefficient =
((Number)robinLowerConcentrationCoefficient.getValue()).doubleValue();
    }
    if (e.getSource() == robinUpperConcentrationCoefficient){
        anUpperConcentrationCoefficient =
((Number)robinUpperConcentrationCoefficient.getValue()).doubleValue();
    }
    if (e.getSource() == robinLowerFluxCoefficient){
        aLowerFluxCoefficient =
((Number)robinLowerFluxCoefficient.getValue()).doubleValue();
    }
    if (e.getSource() == robinUpperFluxCoefficient){
        anUpperFluxCoefficient =
((Number)robinUpperFluxCoefficient.getValue()).doubleValue();
    }
    if (e.getSource() == robinUpperBoundary){
        aRobinUpperCondition =
((Number)robinUpperBoundary.getValue()).doubleValue();
    }
    if (e.getSource() == robinLowerBoundary){
        aRobinLowerCondition =
((Number)robinLowerBoundary.getValue()).doubleValue();
    }

```